AD-A112 259 SRI INTERNATIONAL MENLO PARK CA F/G 4/1
PROCEEDINGS OF THE PLACES PRELIMINARY DATA REVIEW MEETING, 20 A--ETC(U)
JUL 81 D R MCDANIEL DNA001-78-C-0379
UNCLASSIFIED DNA-5848P NL

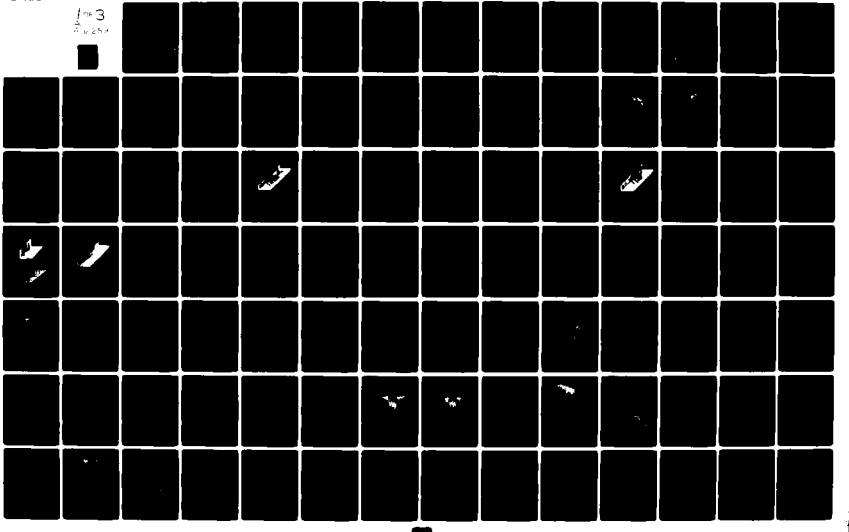

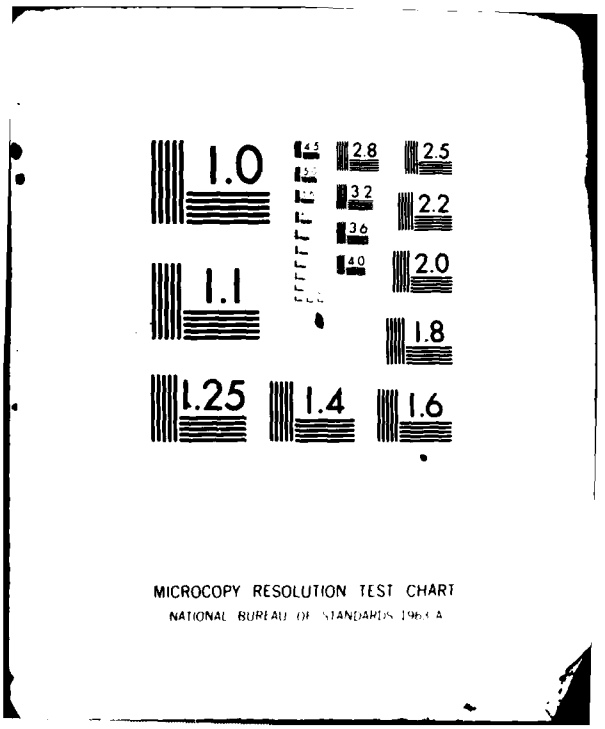
1.0
1.1
1.25
1.4
1.6
1.8
2.0
2.2
2.5
2.8
3.2
3.6
4.0
MICROCOPY RESOLUTION TEST CHART
NATIONAL BUREAU OF STANDARDS 1963 A

DNA 5848P

PROCEEDINGS OF THE PLACES PRELIMINARY DATA REVIEW MEETING, 20 AND 21 MAY 1981

Dan R. McDaniel, Compiler
SRI International
333 Ravenswood Avenue
Menlo Park, California 94025

1 July 1981

Proceedings

CONTRACT No. DNA 001-78-C-0379

THIS WORK SPONSORED BY THE DEFENSE NUCLEAR AGENCY
UNDER RDT&E RMSS CODE B322081466 I25AAXHX00011 H2590D.

Prepared for
Director
DEFENSE NUCLEAR AGENCY
Washington, D. C. 20305

Destroy this report when it is no longer needed. Do not return to sender.

PLEASE NOTIFY THE DEFENSE NUCLEAR AGENCY, ATTN: STTI, WASHINGTON, D.C. 20305, IF YOUR ADDRESS IS INCORRECT, IF YOU WISH TO BE DELETED FROM THE DISTRIBUTION LIST, OR IF THE ADDRESSEE IS NO LONGER EMPLOYED BY YOUR ORGANIZATION.

UNCLASSIFIED

SECURITY CLASSIFICATION OF THIS PAGE *(When Data Entered)*

REPORT DOCUMENTATION PAGE	READ INSTRUCTIONS BEFORE COMPLETING FORM
1. REPORT NUMBER: DNA 5848P	2. GOVT ACCESSION NO.: AD-A112 259
3. RECIPIENT'S CATALOG NUMBER:	
4. TITLE *(and Subtitle)*: PROCEEDINGS OF THE PLACES PRELIMINARY DATA REVIEW MEETING, 20 AND 21 MAY 1981	5. TYPE OF REPORT & PERIOD COVERED: Proceedings for Period 20-21 May 1981
	6. PERFORMING ORG. REPORT NUMBER: SRI Project 7745
7. AUTHOR(s): Dan R. McDaniel, Compiler	8. CONTRACT OR GRANT NUMBER(s): DNA 001-78-C-0379
9. PERFORMING ORGANIZATION NAME AND ADDRESS: SRI International, 333 Ravenswood Avenue, Menlo Park, California 94025	10. PROGRAM ELEMENT, PROJECT, TASK AREA & WORK UNIT NUMBERS: Subtask I25AAXHX000-11
11. CONTROLLING OFFICE NAME AND ADDRESS: Director, Defense Nuclear Agency, Washington, D.C. 20305	12. REPORT DATE: 1 July 1981
	13. NUMBER OF PAGES: 248
14. MONITORING AGENCY NAME & ADDRESS*(if different from Controlling Office)*:	15. SECURITY CLASS *(of this report)*: UNCLASSIFIED
	15a. DECLASSIFICATION DOWNGRADING SCHEDULE: N/A

16. DISTRIBUTION STATEMENT *(of this Report)*

Approved for public release; distribution unlimited.

17. DISTRIBUTION STATEMENT *(of the abstract entered in Block 20, if different from Report)*

18. SUPPLEMENTARY NOTES

This work sponsored by the Defense Nuclear Agency under RDT&E RMSS Code B322081466 I25AAXHX00011 H2590D.

19. KEY WORDS *(Continue on reverse side if necessary and identify by block number)*

Barium Releases	Incoherent Scatter
Ionospheric Plasmas	Field-Aligned Structure
Electron Density Probes	Mass Spectrometry
Satellite Communications	Scintillation

20. ABSTRACT *(Continue on reverse side if necessary and identify by block number)*

The Position, Location, and Communications Effects Simulation (PLACES) experiment was conducted at Eglin AFB, Florida, during the period of 4 to 12 December 1980. Four barium releases were made on four separate days. The primary experiment was to measure time-of-arrival fluctuation and spread in a signal passed through the barium cloud from a rocket-borne beacon to a ground receiving station. A secondary experiment was the measurement of phase and amplitude scintillation on a UHF signal (from the LES-8 satellite), passing through the barium cloud to a receiver in a C-135 Aircraft. In addition to

DD FORM 1 JAN 73 1473 EDITION OF 1 NOV 65 IS OBSOLETE

UNCLASSIFIED

SECURITY CLASSIFICATION OF THIS PAGE *(When Data Entered)*

20. ABSTRACT (Continued)

these two experiments, a rocket-borne electron density probe and mass spectrometer made in-situ measurements on the barium cloud. The ion cloud position was determined in real time by the FPS-85 radar operating in an incoherent scatter mode. Ground optics, an ionosonde, a magnetometer, and a low-light-level TV tracking system also supported the experiment.

TABLE OF CONTENTS

BLANK PAGE

INTRODUCTION

A. General

PLACES (Position Location And Communication Effects Simulations) is a field experiment sponsored by the Defense Nuclear Agency (DNA) to demonstrate and investigate the effect of structured ionospheric plasmas on satellite communication and navigation systems. The experiment was carried out in December 1980, at Eglin Air Force Base, Florida. The structured plasma environment was created by the release of barium vapor at an altitude of 185 km. Signals from the LES-8 satellite passed through the drifting plasma cloud and were received by an airborne receiving station. Also, signals from rocket-borne transmitters passed through the drifting plasma cloud and were received by ground receiving stations.

B. PLACES Test Description

The PLACES tests consisted of four 48-kg barium releases that were launched during the period 4 through 12 December 1980. Associated with the barium events were the launch of one in-situ probe rockets, and two RF beacon rockets. Event times were selected to optimize the visible window at the time the cloud was most sharply striated. During each of the four events, a C-135 aircraft from the Air Force Avionics Laboratory made multiple passes through the barium ion cloud shadow, recording signals from LES-8. The geometry of the experiment is depicted in Figure 1. The test elements of PLACES were as follows:

- 48-kg barium releases (4)
- Rocket-borne beacons (4 planned, 2 launched)
- Rocket-borne probes (2 planned, 1 launched)
- AFAL aircraft No. 662
- FPS-85 radar system
- Beacon receiver stations (2)

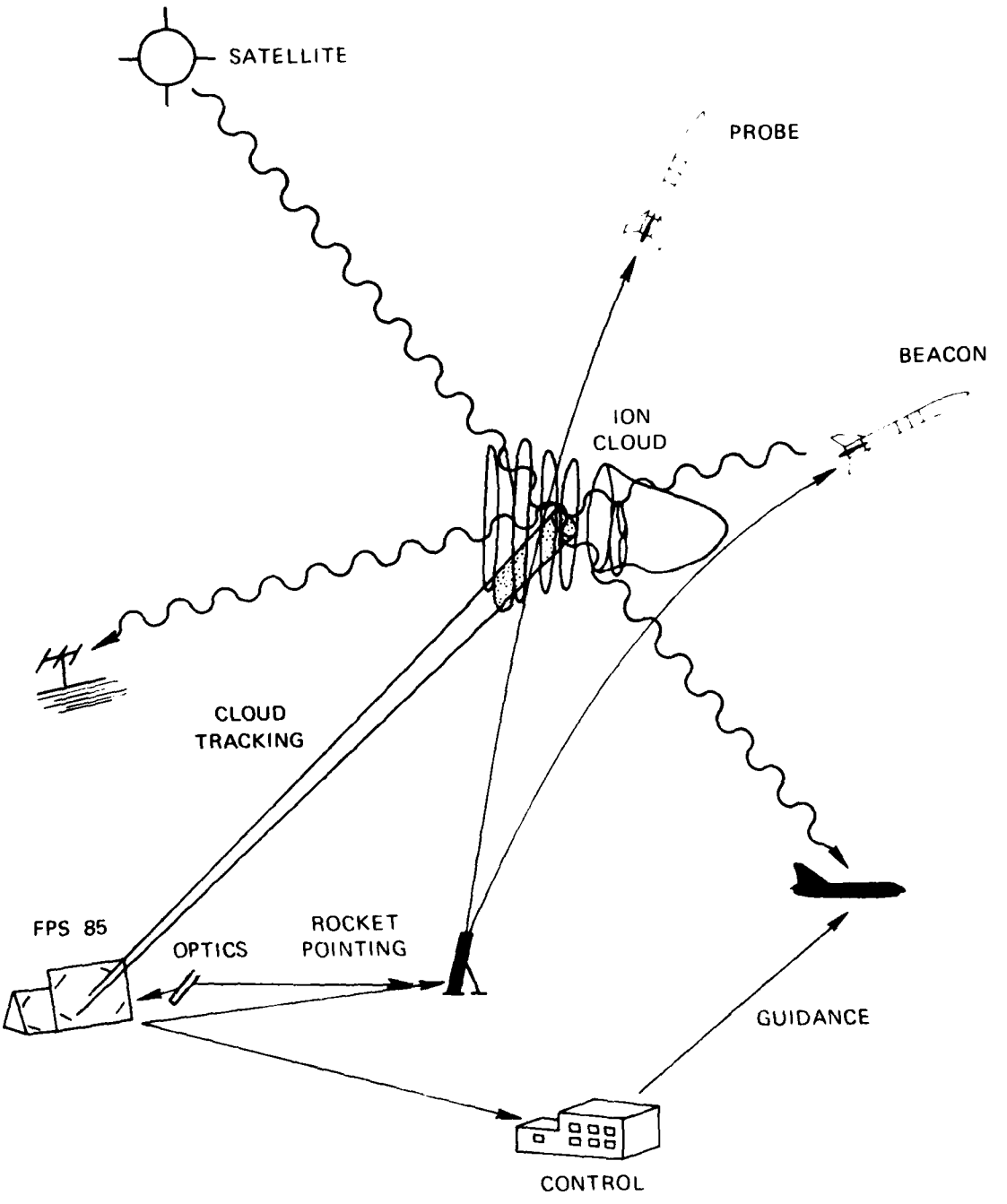

FIGURE 1 PLACES CONCEPT

- TV tracking stations (2)
- Ground optics (3 sites)
- Intensified optics (1 site)
- Magnetometer/ionosonde
- Range support systems.

The primary experiment was to measure RF signal time-of-arrival fluctuation and spread that are associated with a strong scatter environment, using a rocket-borne beacon.

The secondary experiment was to (1) measure the barium cloud fading channel in order to provide data for back propagation diagnostics, (2) generate real-time diagnostic information about the barium cloud, and (3) obtain fading data for the phase-locked modem hardware simulations.

A map depicting general locations for instrumentation, launch, and control sites is shown in Figure 2. Experiment control was at CCF.

C. Event Description

The events were designated GAIL, HOPE, IRIS, and JAN. Eglin Test Range authorized launch operations on every even day from 4 through 20 December. After three dry runs on 25 November, and 2 and 3 December, the first launch operation was scheduled for 4 December.

Event GAIL was counted down and launched at 2305Z on 4 December 1980. It was planned that a probe rocket and beacon rocket would be flown during this event. Because of range safety problems caused by an unexpected drift direction of the ion cloud, neither of the instrumented rockets could be launched.

Event HOPE was counted down and launched at 2305Z on 6 December 1980. It was again planned that a probe rocket and beacon rocket would be flown during this event. Again, anomalous behavior of the ion cloud prevented the launching of these rockets.

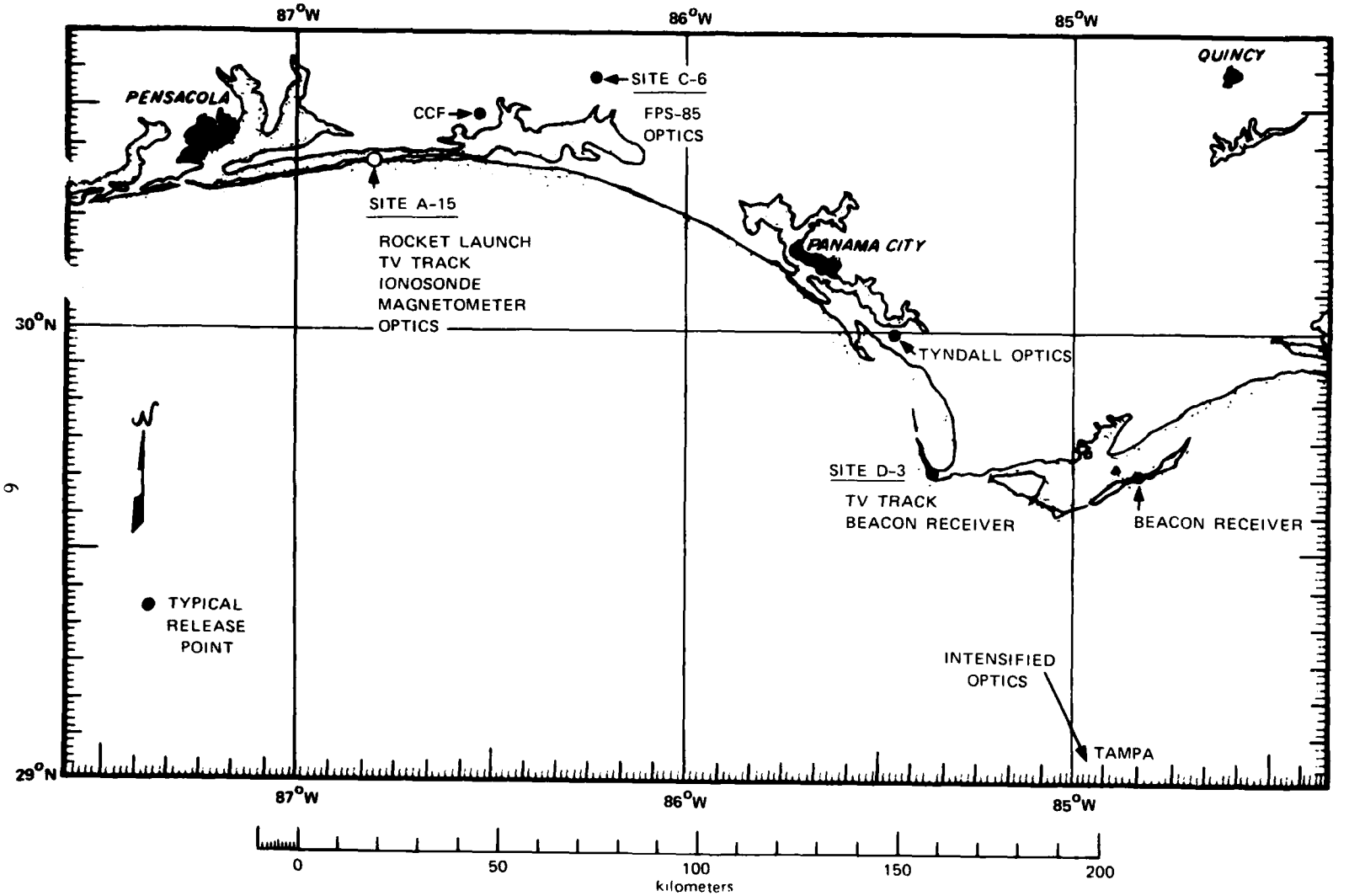

FIGURE 2 INSTRUMENT LOCATIONS

The decision was made to fly two beacon rockets during Event IRIS because they were the primary experiment and no data had as yet been gathered. Event IRIS was counted down and launched at 2310Z on 8 December 1980. Two beacon rockets were successfully launched and occulted by the ion cloud. Good quality data were gathered from both beacons.

Because of the success of Event IRIS, the test composition for Event JAN was revised to include one probe and one beacon rocket. Event JAN was counted down and launched at 2311Z on 12 December. One probe rocket was launched that successfully penetrated the ion cloud, but cloud drift again prevented launch of the beacon rocket.

No launch operations were attempted on 10 December because of inclement weather.

D. Organization

The PLACES field program is sponsored by the Defense Nuclear Agency and is planned and carried out by SRI International. The satellite and beacon experiments were conceived and are being implemented by ESL, Inc. The program participants and their areas of responsibility are as follows:

- DNA--Program sponsorship and management
- SRI--Test planning and direction, and operation of FPS-85, TV tracking system, ionosonde, and magnetometer
- ESL--Satellite and beacon measurements, beacon payloads, and operation of beacon ground stations
- SLA--Rocket operations, payload integration
- Thiokol--Barium payloads
- NRL--Pulsed plasma probes
- AFGL--Mass spectrometer
- TIC--Ground optics
- LASL--Intensified optics
- AFAL--Aircraft support
- ESD--Satellite support.

Figure 3 depicts the test organization.

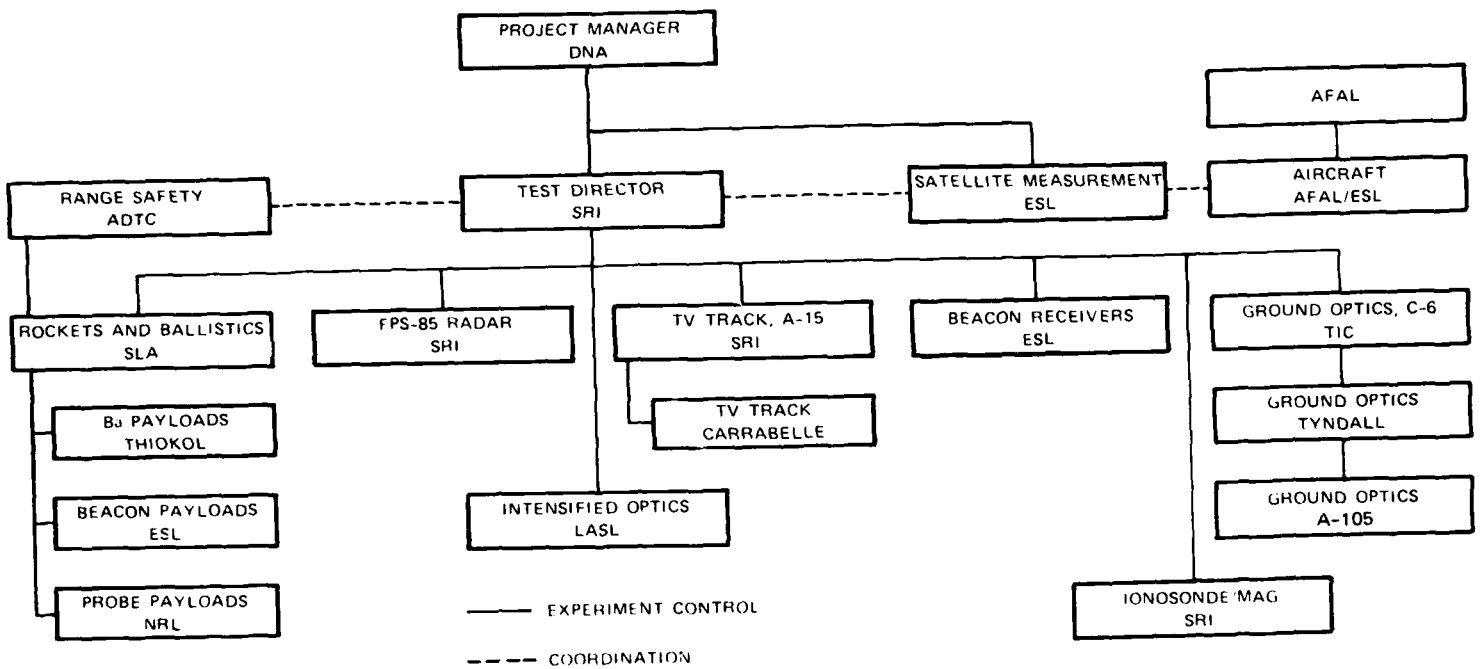

FIGURE 3 PLACES TEST OPERATIONS ORGANIZATION

BEACON EXPERIMENT MEASUREMENTS

J. M. Marshall
ESL Incorporated
Sunnvale, CA

I INTRODUCTION

Two beacon rockets were launched during Event IRIS of the PLACES Experiment. Successful data were recorded from each of these beacons at both ground receiving sites--Cape San Blas (D3A), and St. George Island. The ground receiving systems effectively measure the complex channel impulse response of the striated barium plasma. The technique used to recover the channel impulse response relies on the processing of the pseudorandom phase modulation of the rocket transmitted signal. The received signal inphase and quadrature components are hardware cross-correlated with a replica of the modulating PN sequence in the ground station receiver. Provided the PN sequence autocorrelation is sufficiently narrow compared to the time delay extent of the channel impulse response, an accurate representation of the channel impulse response is realized. No other beacon rockets were launched during the PLACES series of barium releases due to range safety and operational constraints. Strongly contributing to these launch difficulties was the unusual northward drift of the other three barium releases.

The beacon experiment uses two signals transmitted from the beacon rocket. A strong scatter striated plasma environment of interest is created at VHF by the barium environment. For this reason, a VHF link at 98 MHz is used. This VHF link is biphase modulated by a pseudonoise signal at a 9.8-megachip-per-second rate. The beacon receiver stations, by virtue of the high-rate PN modulation, perform high-resolution cross-correlation measurements of the propagation channel, and in particular, measurements of its time-of-arrival fluctuation and spread properties.

A C-band CW signal at 4116 MHz (98 MHz x 42) is also transmitted by the rocket in phase coherence with the 98-MHz VHF signal. This signal provides a phase and time reference to remove the effects of rocket motion induced on the VHF signal, thus leaving only propagation channel effects. The beacon rocket payload also carries a C-band transponder at 5 GHz, a telemetry transmitter at S-band, and three strobe lights to allow RF and optical tracking.

For the purposes of launching the beacon rocket and the probe rocket, the cloud tracking was performed by a TV tracking station at D3 near the Cape San Blas ground receiver site and by a TV tracking station at the A-15 launch complex. The beacon rocket was to have been aimed so that its trajectory would lie 100 km behind the barium cloud as viewed from a ground station. Due to the extreme southern occultation geometry achieved, it was necessary to use a 40-km occultation target distance. Two adequately separated ground stations were provided to better ensure occultation in spite of rocket inaccuracies. Useful occultation data were obtained at both sites on each flight, although propagation effects were generally better at one site than another, as expected.

The primary purpose of the PLACES experiment was to measure the time-of-arrival fluctuations and spread that are associated with radio wave propagation through a strong scatter striated plasma environment. The measurements of time-of-arrival spread and jitter are relevant to the strategic performance of wideband pseudonoise SHF communications and navigation systems including NAVSTAR GPS. The frequency domain manifestation of time-of-arrival spread is fading decorrelation with frequency, and thus the results of this configuration are also relevant to wideband frequency hopping systems. The beacon experiment provided these measurements of the time-of-arrival fluctuations and spread.

II OCCULTATION GEOMETRY

TV track data from Eglin AFB Sites D3 and A-15 were used for targeting the simultaneous beacon rocket occultation of the D3A and St. George Island receiving sites. The trajectories flown on Flight 1 and Flight 2

are shown on Figures 1 and 2. The time since launch is indicated on these trajectories. Also shown is the indicated FPS-85 radar location of the maximum density portion of the ion cloud at the occultation time. During the occultation the rocket velocity is approximately 1.44 km/s; thus the occultation times are short.

Table 1 provides a summary of the occultation geometries. The site geodetic locations are also provided for reference. The peak plasma density location from the FPS-85 radar at occultation time is shown, as is the peak density measured by the radar.[1] It is interesting to note that the indicated peak density values are somewhat less than for the STRESS Event ESTHER; the peak density for ESTHER[2] was approximately 7.3×10^{12} m^{-3} at 30 min. On the other hand, the radar data also indicated that the cloud is somewhat larger than ESTHER at this time. These estimates could change somewhat upon final calibration of the radar data. The aircraft data would imply that the scintillation effects are at least as strong as during ESTHER, perhaps indicative of a larger striation extent.

The elevation angles were lower than planned, due to the extreme southern occultation geometry, but were well within the design constraints of the VHF antenna. The occultation occurred nearly 60 km south of the southern boundary of the intended cloud drift region. When the cloud drifted too far to the north, a downleg beacon occultation could not successfully be conducted. Outside the southern boundary a 100-km occultation distance could not be achieved but a 40-km occultation distance was possible. As indicated, three of the four barium releases initially drifted northward. IRIS drifted southeast.

The magnetic aspect angle was also somewhat less than anticipated, due to the extreme southern occultation geometry. As summarized in Table 1, the aspect angles were approximately 42° and 36°, respectively, for the paths to the two receiving sites.

The beacon rocket on both these launches was targeted 40 km behind the TV optics cloud track point. On Flight 1 the beacon rocket flew 26.9 km behind the radar maximum density point. The raypath to St. George

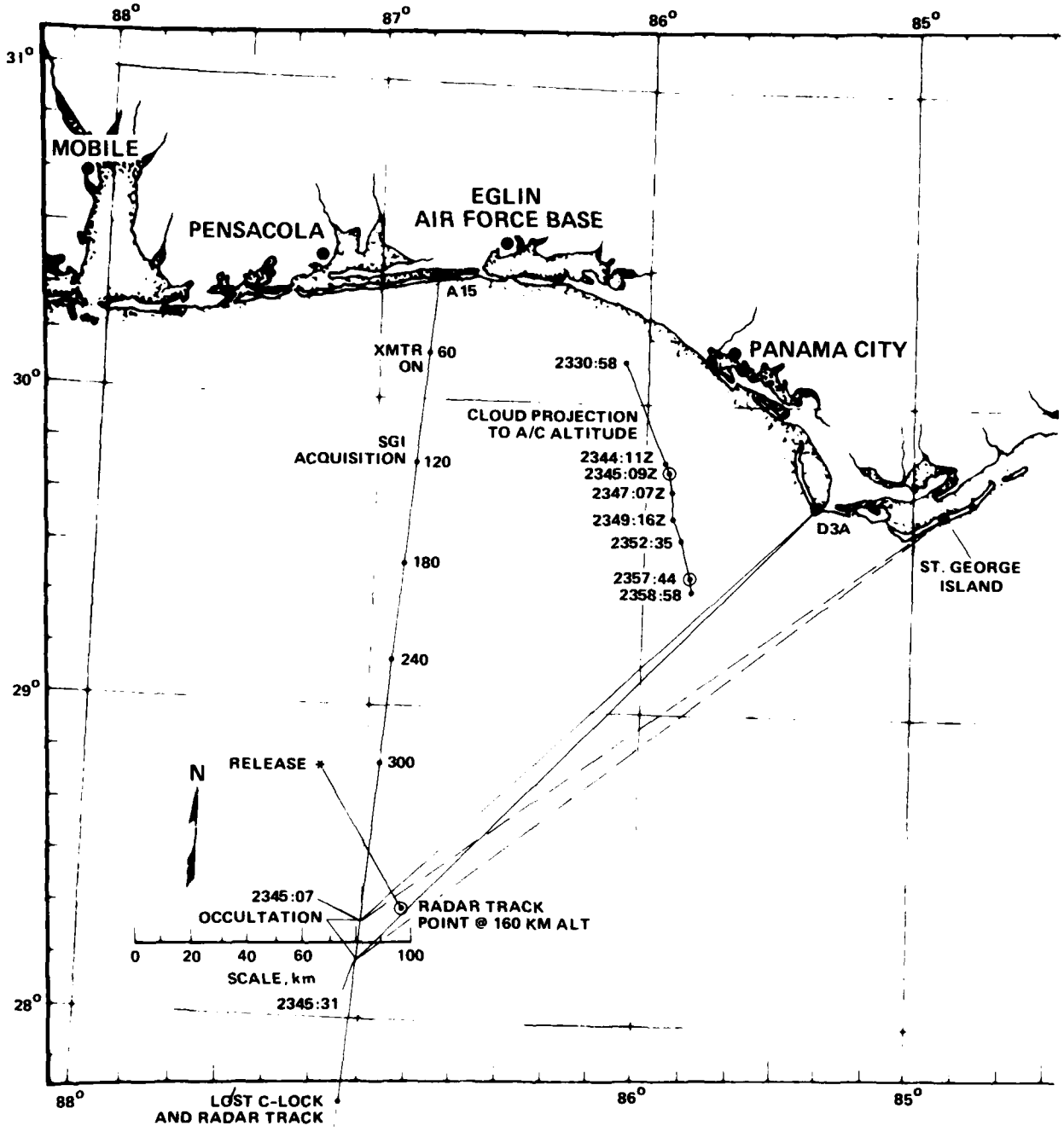

FIGURE 1 BEACON ROCKET TRAJECTORY FLIGHT 1

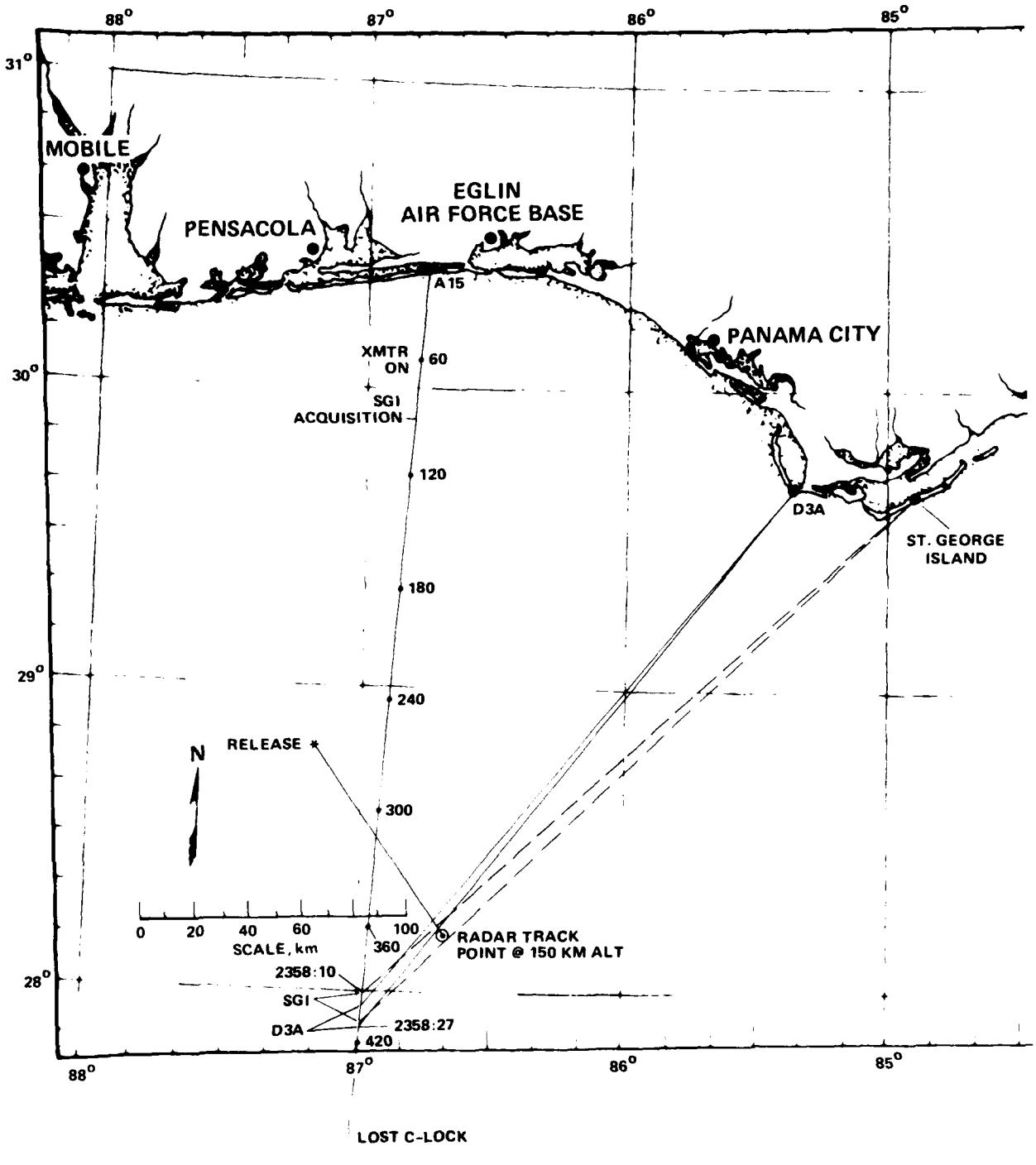

FIGURE 2 BEACON ROCKET TRAJECTORY FLIGHT 2

Table 1

OCCULTATION GEOMETRY SUMMARY

	Site	Occultation Time (Z)	Cloud* Location (Lat., Long., Alt.)	$N_{e_{max}}$ (m^{-3})+	Location of Rocket			Occultation Distance (km)	Magnetic Aspect (deg)
					Elevation (deg)	Azimuth (deg)	Slant Range (km)		
Flight 1	St. George Island (29°38'36", 84°54'07")	2345:07 to 2345:31	28.350°, 86.850°, 160 km at 2345:24Z	3.7×10^{12}	36.1	235.2	321.1	26.9	~42
	Cape San Blas (D3A) (29°40'00", 85°21'18")	2345:09 to 2345:30			38.2	230.1	303.3	--	~36
Flight 2	St. George Island	2358:10 to 2358:25	28.185°, 86.695°, 150 km at 2358:20 Z	2.6×10^{12}	32.6	228.4	331.1	46.0	~41
	Cape San Blas	2358:17 to 2358:27			32.9	222.6	313.6	--	~35

*Peak N_e point, per radar track.

+As measured by the radar.

Island missed slicing the cloud through this maximum density point by approximately 1.9 km. On Flight 2 the beacon rocket flew 46 km behind the radar-indicated maximum density point. The line of sight to St. George Island on this second shot appears to have passed through the maximum density point indicated by the radar. These distances behind the cloud appear within the predicted rocket trajectory dispersion anticipated.

Substantially less energy delay spread was noted on the second beacon occultation. While this is believed to be due to the geometry as described later in this section, it is interesting to note that the radar data indicated a 10-km drop in the peak density altitude from 160 km to approximately 150 km altitude between the first (2345:24Z) and the second (2358:20Z) beacon occultations. The aircraft data indicated a period of lesser scintillation activity around this time as well. However, the aircraft was transiting approximately 15 km north of the cloud center projection according to the real-time tracking displays. On the other hand, on the first occultation strong fading was noted by the aircraft at a 12-km northward miss distance. Aircraft passes approximately 20 min after the second occultation again show strong, long-lasting scintillation effects. It may be that during the time of the second occultation the indicated radar track point was somewhat north of the true cloud center; this needs to be investigated further. If such is the case, the lesser delay spread on the second beacon occultation would be much easier to explain.

The occultation geometry for St. George Island is shown in Figure 3 for Flight 1. Also shown are a few data points from the FPS-85 radar cloud track, from which a rough estimate for the 10^6 cm^{-3} electron density contour has been sketched. The contour is for the maximum density 160-km altitude plane. Note that the TV optics track point as obtained from the aircraft positioning data agrees well with the radar location of the cloud center. That is, the aircraft projection data reprojected to a 160-km altitude along the path to the LES-8 satellite closely matches the radar data. The actual TV track altitude was not available for comparison.

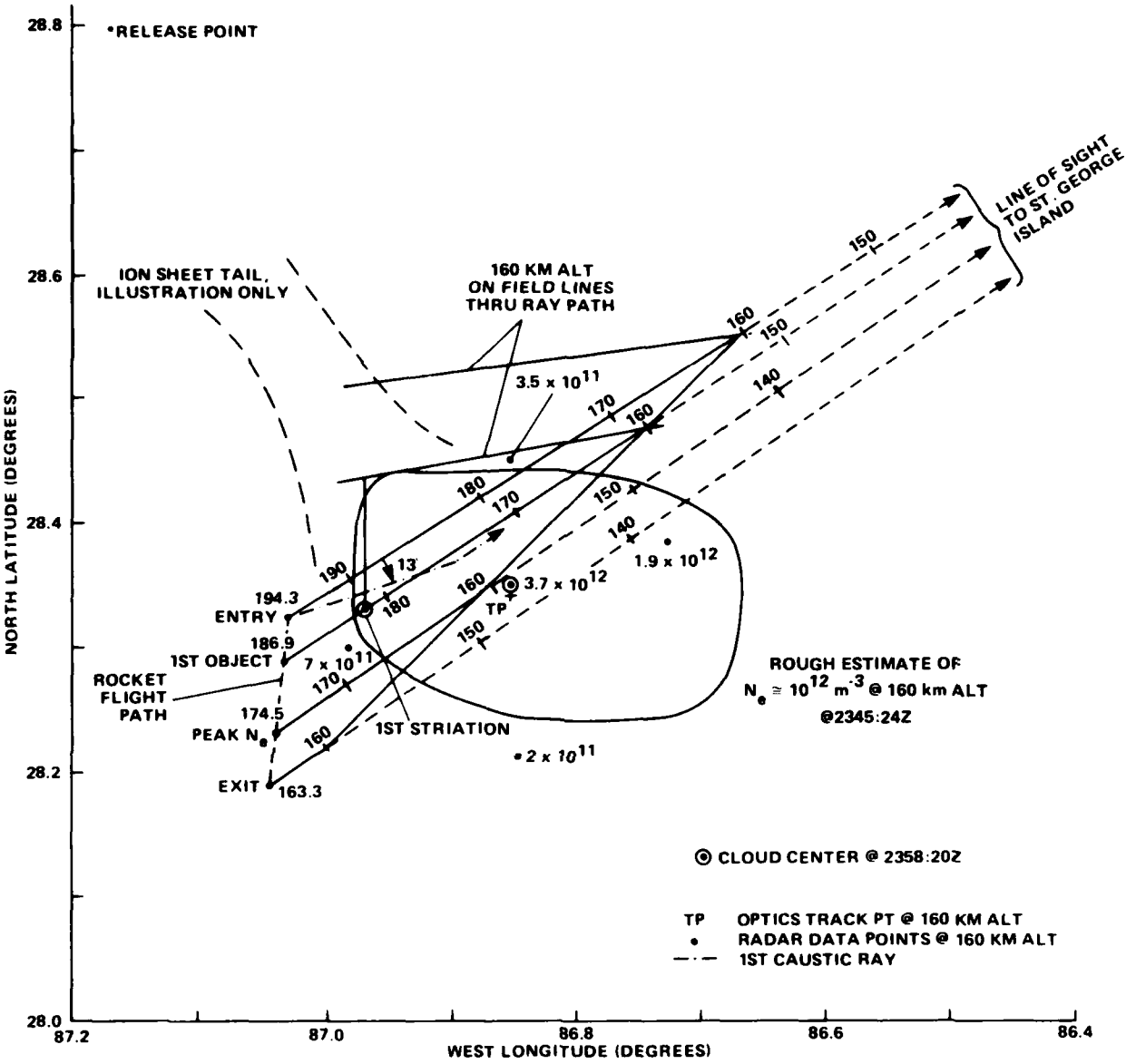

FIGURE 3 OCCULTATION GEOMETRY FOR ST. GEORGE ISLAND, BEACON FLIGHT 1

The line-of-sight to St. George Island is shown in Figure 3 at several times of interest. The intersection of the path with the 160-km altitude plane is indicated by the transition from the solid to the dashed line. The four paths show the time at which the maximum electron content (signal delay) is observed, and the time at which the signal exits the cloud. The rocket altitude at these times is also indicated. For instance, at the time the path enters the cloud, the rocket was at an

altitude of 194.3 km and when the path exited the cloud the altitude was 163.3 km. Various data were taken from the FPS-16 radar beacon tracking data. There were three FPS-16 radars tracking the beacon rocket. Two of these agree with 50 m while the third differs by no more than 500 m.

As a further aid to visualizing the manner in which the line-of-sight path clices through the cloud, a line is shown indicating the 160-km altitude point along the magnetic field lines that pass through the ray-path. This illustrates, for instance, that field lines through the $10^{12}{}_{m}{}^{-3}$ density contour are not cut until around the time the first object is traversed. It is also from this view that it can be seen that the line-of-sight path to St. George Island missed slicing the cloud at its maximum density point by approximately 1.9 km.

The occultation geometry for Cape San Blas (Site D3A) is shown in Figure 4. This figure shows that the path to Cape San Blas sliced the cloud somewhat more toward the tail, missing the radar track point by 3.5 to 4 km.

The position of the first object can be estimated from the first object crossing times and noting the point at which the paths to D3A and St. George Island cross. This is labeled on Figures 3 and 4 as the first striation. The field line through this point is sketched down to the 160-km altitude point. This first striation is traversed at approximately 181 km altitude along the path to St. George Island and approximately 176 km altitude along the path to D3A.

An interesting comparison of these geometry data with the aircraft experiment data can be made. The aircraft transited the ion cloud shadow approximately 5 min 33 s prior to the beacon occultation and again 2 min 37 s after the beacon occultation. From the real-time tracking display the relative positions of the FPS-85 cloud center track point and the aircraft position from the FPS-16 radar track can be determined. From these data the intersection of the path connecting the aircraft and the satellite with the cloud geometry can be determined. This is shown in Figure 5 for the pass prior to occultation, and in Figure 6 for the pass following occultation. The shape of the ion cloud contour shown is that roughly

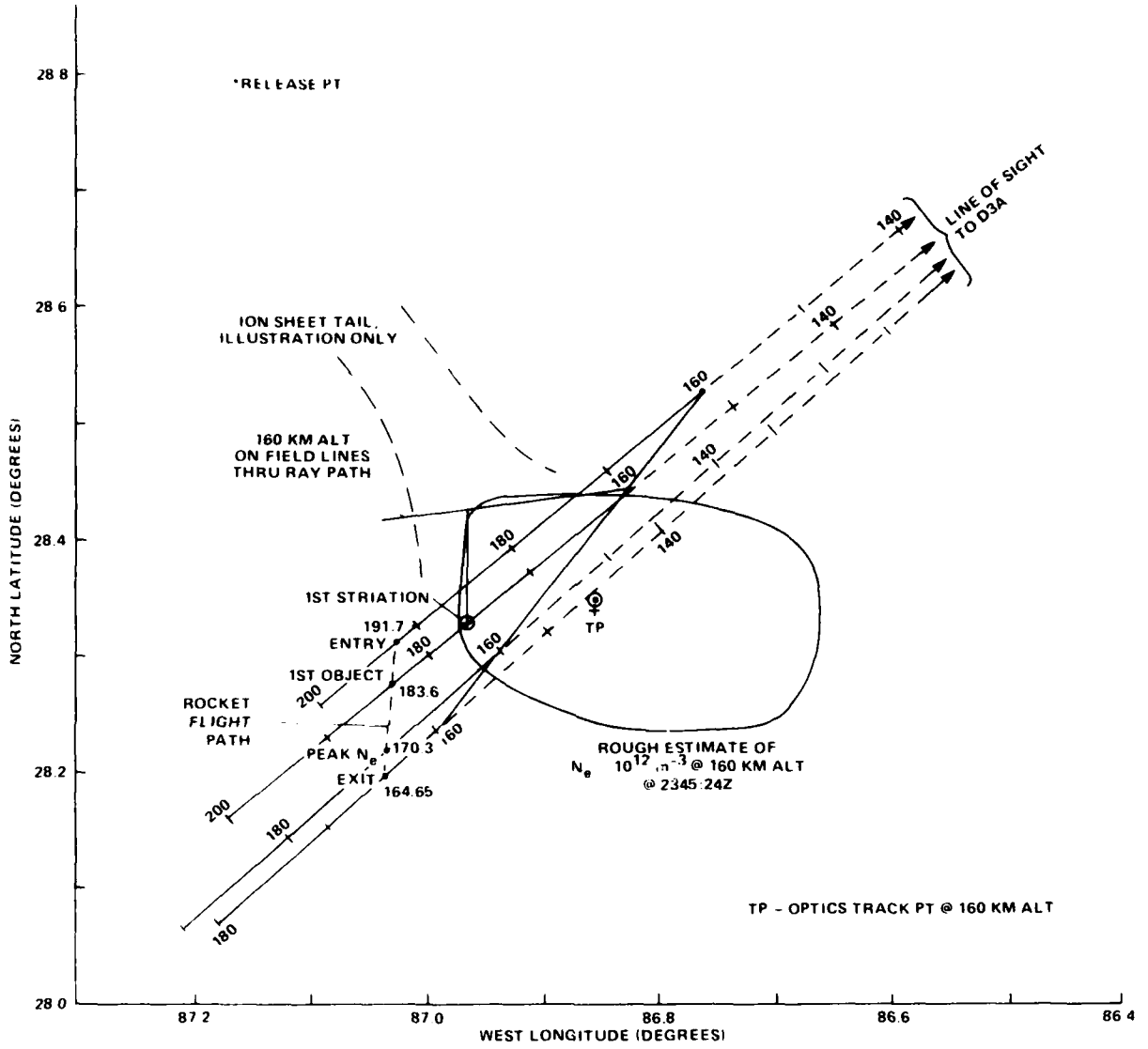

FIGURE 4 OCCULTATION GEOMETRY FOR CAPE SAN BLAS, BEACON FLIGHT 1

estimated from the radar data at the time of occultation. The center has been translated to correspond with the real-time display data at the time of the aircraft transit 5 min earlier and 2 min later. There is some room for error in that the radar track altitude may not be 160 km at these times, however.

The propagation path cut the field line through the cloud center approximately 173 km in altitude. The aircraft propagation path slice

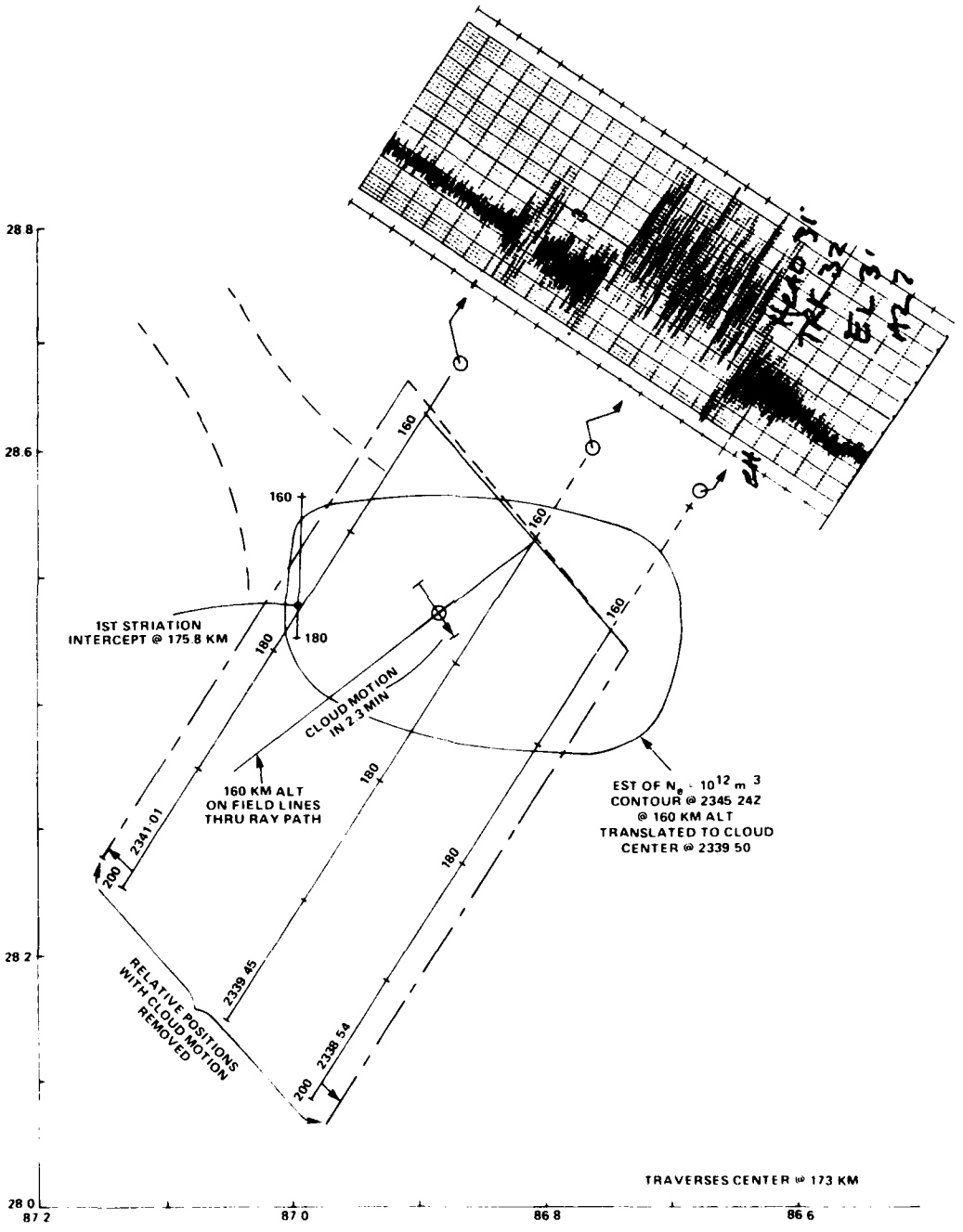

FIGURE 5 AIRCRAFT OCCULTATION GEOMETRY AT 2339:50Z, 5 min 33 s BEFORE OCCULTATION

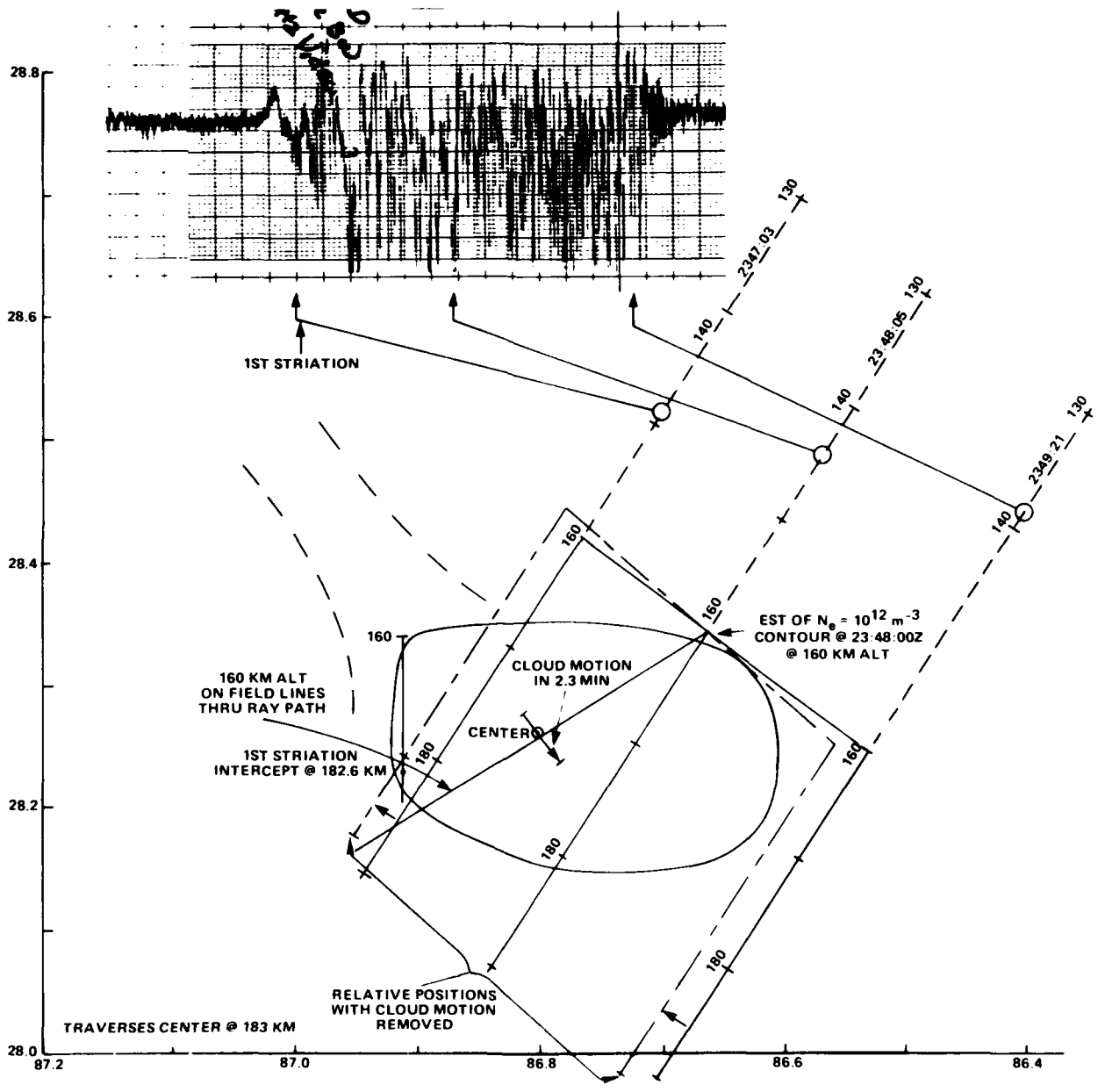

FIGURE 6 AIRCRAFT OCCULTATION GEOMETRY AT 2348Z, 2 min 37 s AFTER OCCULTATION

through the 160-km altitude plane is nearly orthogonal to the beacon slice because of the near vertical transit of the rocket as opposed to the constant altitude transit of the aircraft. Nonetheless, some of the same field lines are cut.

Because the aircraft takes approximately 2 min to traverse the fading region, the position of the cloud center will move appreciably with respect to the cloud contour shown. The motion of the cloud center during the transit is indicated by the arrow through the cloud center. The positions of the raypath at the beginning and of the pass corrected for the relative cloud motion are also shown. In effect, relative to the contour drawn, the fading begins somewhat further south (the cloud was further north) and the fading ends further north (the cloud has moved south). The aircraft was in level flight throughout the fading intervals shown.

There appears to be reasonable correlation between the contour drawn (appropriate to 5 min 33 s later) and the observed fading. Further, it appears that there is evidence that striation development is taking place. The aircraft in Figure 5 appears to traverse the first striation object seen by the beacon receivers at the northern end of its pass. The path cuts this field line approximately 175.8 km in altitude. Between this object and the main body of the striations there are no structure effects evident in the fading data. In Figure 6 fading is observed over the entire aircraft transit of the cloud.

In Figure 6 the path traverses the center field line at an altitude of 183 km, approximately 10 km higher than during the earlier transit. It would appear that the first striation object would have been traversed at approximately 183 km in altitude. This geometry can be refined, following a more detailed reduction of the radar data.

The strobe lights on the rocket were not observed in photographs, nor were they observed on the TV tracking system for either launch; thus it is difficult to tell exactly where the rocket trajectory cut the striations. Through triangulation techniques it is anticipated that the rocket path across the view from the ground stations can be determined at a later date. From St. George Island the rocket trajectory makes an angle of 59°

with the horizontal, going from the upper right to the lower left. As a rough guess, the trajectory probably cuts the receiving station view such that the lower part of the trajectory exits the cloud near the apparent bend or knee where the striations blend into the background ion cloud.

The occultation geometry for the second beacon is shown in Figures 7 and 8 for St. George Island and Cape San Blas, respectively. The cloud contour shown is that derived for the first occultation and is at 160 km altitude. As discussed earlier, the radar data indicated a drop in peak-density altitude from 160 to approximately 150 km between the first and second occultations. The peak-density point at 150 km altitude is shown as well as the intersection of the beacon line-of-sight path with the 150-km altitude plane.

Figure 7 shows that the beacon path cut the 150-km altitude center track point exactly on the path to St. George Island. However, the peak integrated electron content (peak signal delay) occurred somewhat after transiting the indicated center. In comparing Figure 3 with Figure 7, it would appear that the occultation geometry was not that dissimilar. However, the second occultation occurred approximately 6 km further back toward the release point. Additionally, the path cuts a slice of the cloud a few kilometers to the south of the first striation object identified on the first occultation. This occultation clearly does not result in as long a distance through the cloud as did the first occultation. If most of the striation development were to the northeast side, then this trajectory would have occulted fewer striations.

The occultation geometry for Cape San Blas, Flight 2, shown in Figure 8, shows that the striations were cut very low in altitude. This more than likely accounts for the weak fading and small delay spread observed on this path.

Figure 9 shows the measured electron content over the entire trajectory along the path to St. George Island for the first beacon. The contribution of the background ionosphere is small, as indicated. This plot was constructed in the field from the raw data and can be refined at a later date. The integrated electron content was calculated based on the time-of-arrival shift in the received signal at each instant in time.

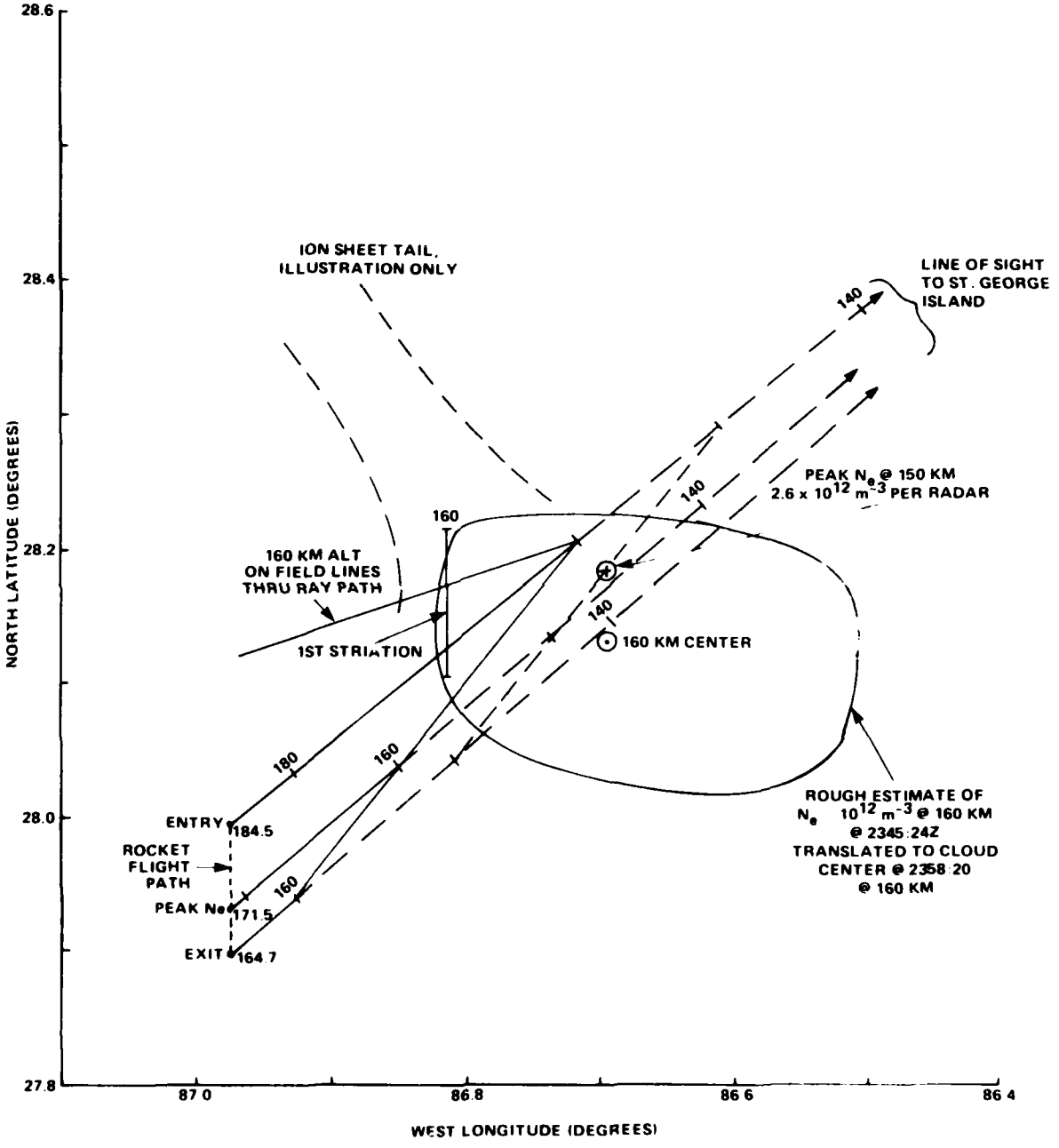

FIGURE 7 OCCULTATION GEOMETRY FOR ST. GEORGE ISLAND, BEACON FLIGHT 2

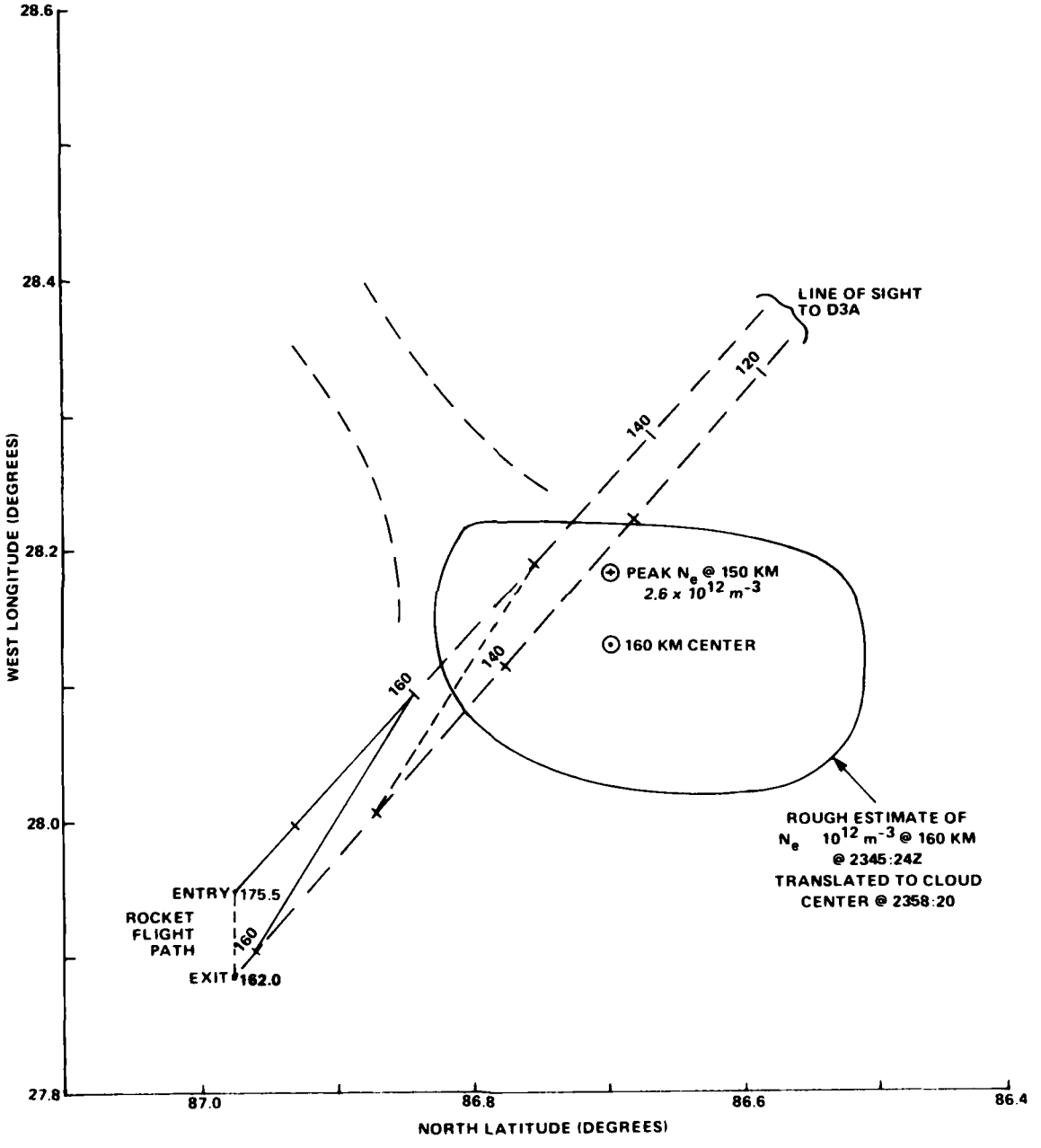

FIGURE 8 OCCULTATION GEOMETRY FOR CAPE SAN BLAS, BEACON FLIGHT 2

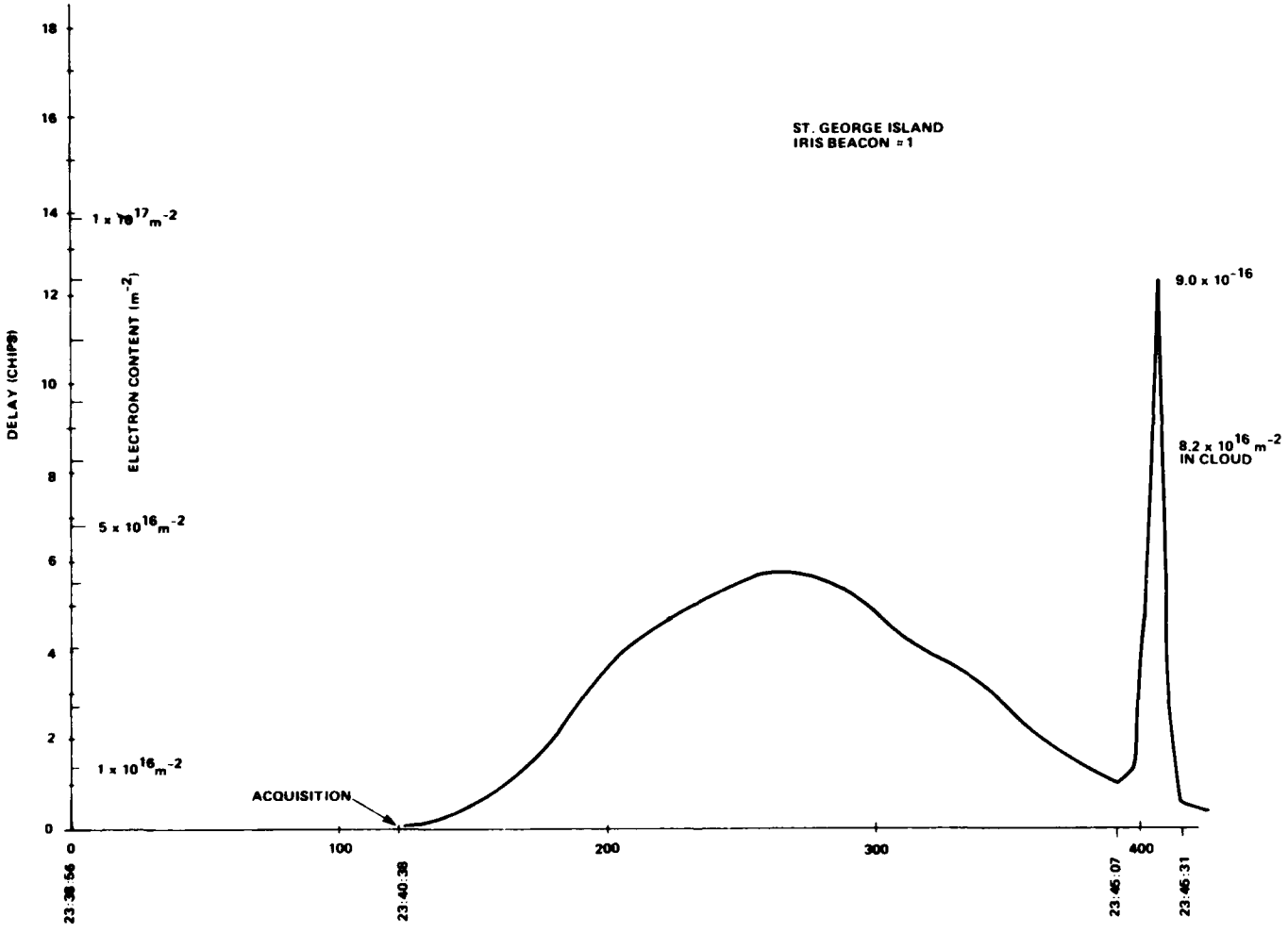

FIGURE 9 MEASURED ELECTRON CONTENT FOR ST. GEORGE ISLAND, BEACON 1

III BEACON EXPERIMENT DATA REVIEW

Two beacon rockets were launched during Event IRIS of the PLACES Experiment. Successful data were recorded from each of these beacons at both the Cape San Blas ground station and the receiving station located on St. George Island.

A. St. George Island Beacon 1

As anticipated, occultation of the first beacon was initially obtained at St. George Island. The magnitude of the impulse response recorded is graphically reproduced in Figure 10. This figure represents data collected over the time interval from 2345:01.8Z to 2345:34.2Z, where time is represented as the third dimension. During this time interval approximately 12,960 samples of the impulse response were taken by the receiving hardware. For plotting purposes, 32 of these responses were averaged to produce each of the 400 horizontal scans presented in the figure.

Beginning from early time, the immediate features evident in the recorded response are the refracted-ray caustic contributions appearing at late delays. From this first appearance in Figure 10 there appears to be significant energy in these components at delays even greater than the 30-chip measurement window. As expected, the relative delay of these caustics decreases as the transmitter approaches the cloud. This is a result of the decreasing difference in distance to the receiver between the beacon rocket direct path and the caustic raypaths refracting from the cloud. During occultation, when the rocket is behind the barium plasma, many caustic paths appear to merge, giving a more random appearance to the delay spread. As the rocket flight continues, identifiable caustics again appear, spreading energy to about 23 chips of delay on emergence from occultation.

Samples of the energy delay profile (magnitude of the channel impulse response) are shown in Figures 11 through 14 sampled approximately each 0.5 s. Near the time of maximum integrated electron content when the line-of-sight path to St. George Island passes through the center of the

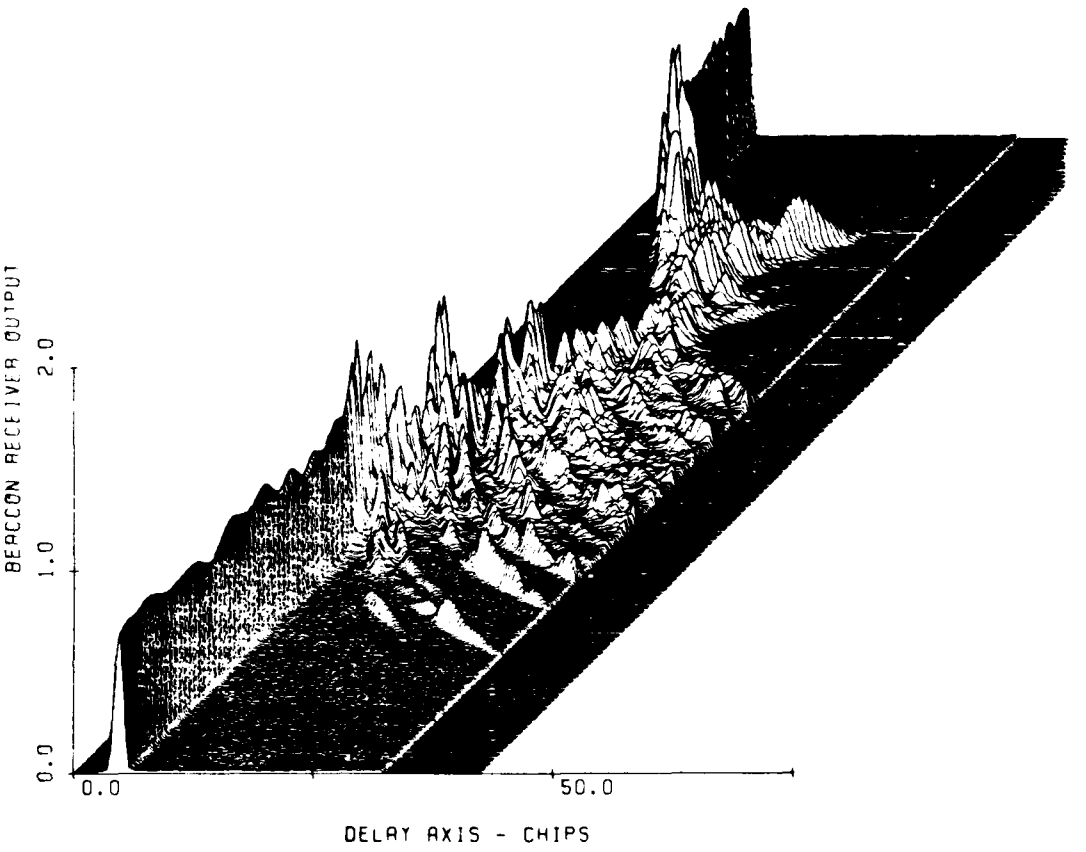

FIGURE 10 ENERGY DELAY PROFILE, ST. GEORGE ISLAND, FIRST BEACON, TIME SPAN FROM 2345:1.8Z TO 2345:34.2Z

striations (~2345:23Z), the signal exhibits a significant defocusing and delay spread. Near this time a delay spread of greater than 10 chips (~1 μs) occurs. This is probably a good initial estimate for the amount of spreading due to the random scattering imposed by the striations. In comparing this response with the unperturbed signal prior to occultation, it is apparent that a net time-of-arrival delay of about 13 chips (~1.3 μs) has been added by the gross electron content of the barium cloud. Most strikingly apparent in these figures is the large delay spread that occurs and the potential implications to PN code tracking system design. There is some broadening of the cross-correlation of the received signal due to

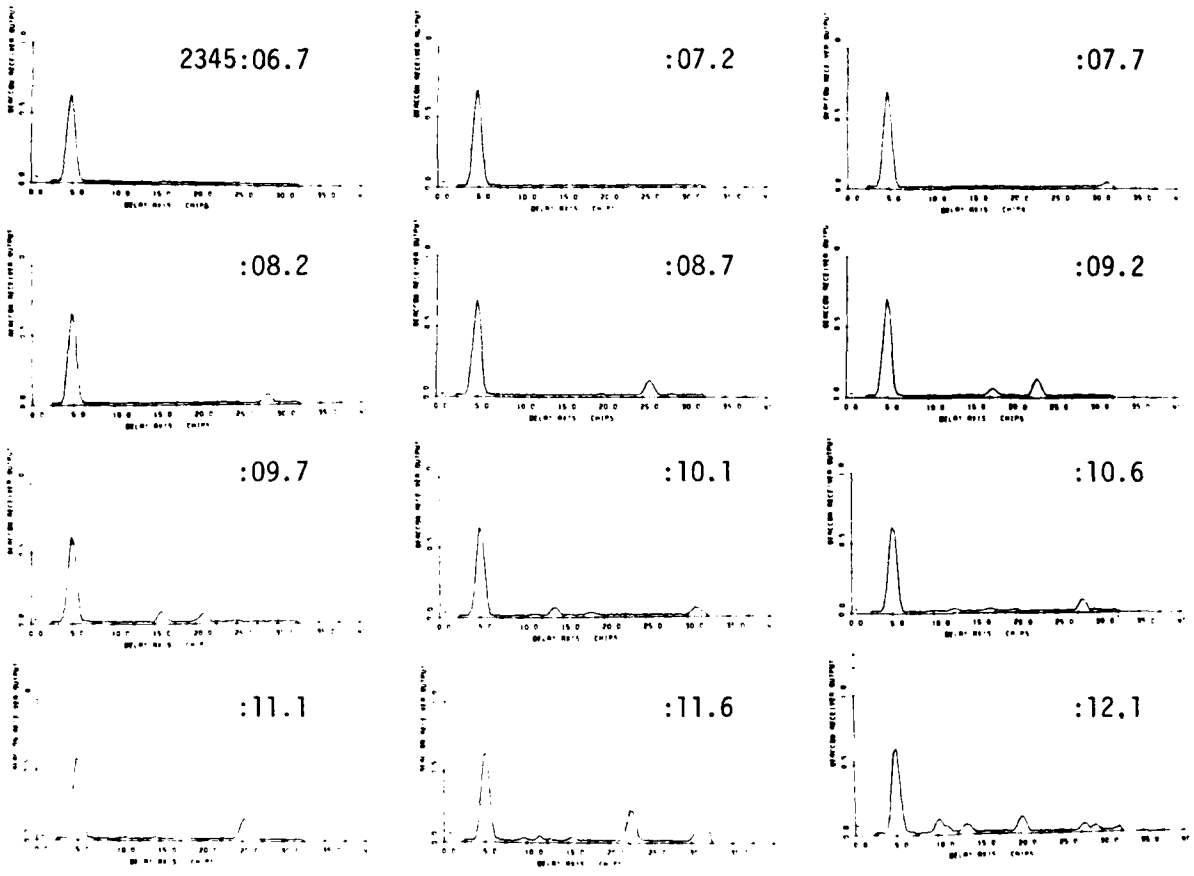

FIGURE 11 ENERGY DELAY PROFILE BETWEEN 2345:06.7Z AND 2345:12.1Z, ST. GEORGE ISLAND

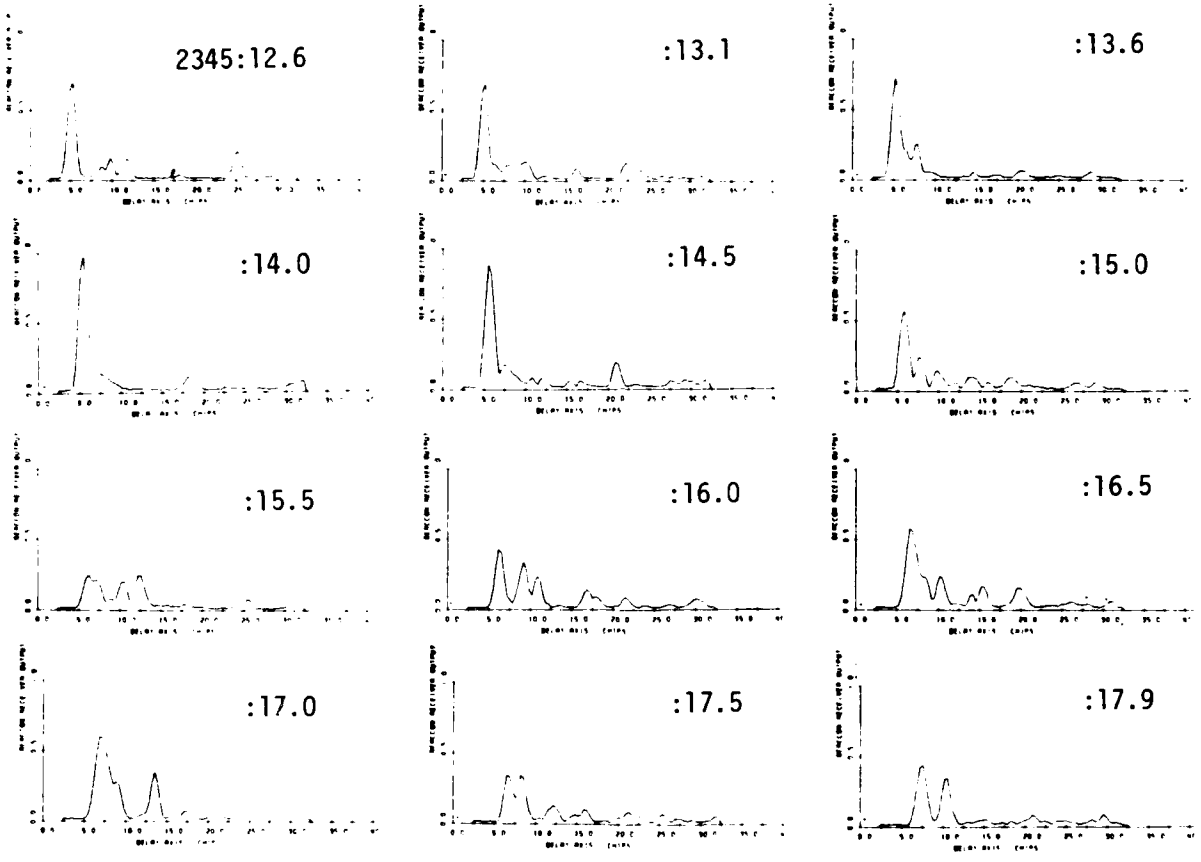

FIGURE 12 ENERGY DELAY PROFILE BETWEEN 2345:12.6Z AND 2345:17.9Z, ST. GEORGE ISLAND

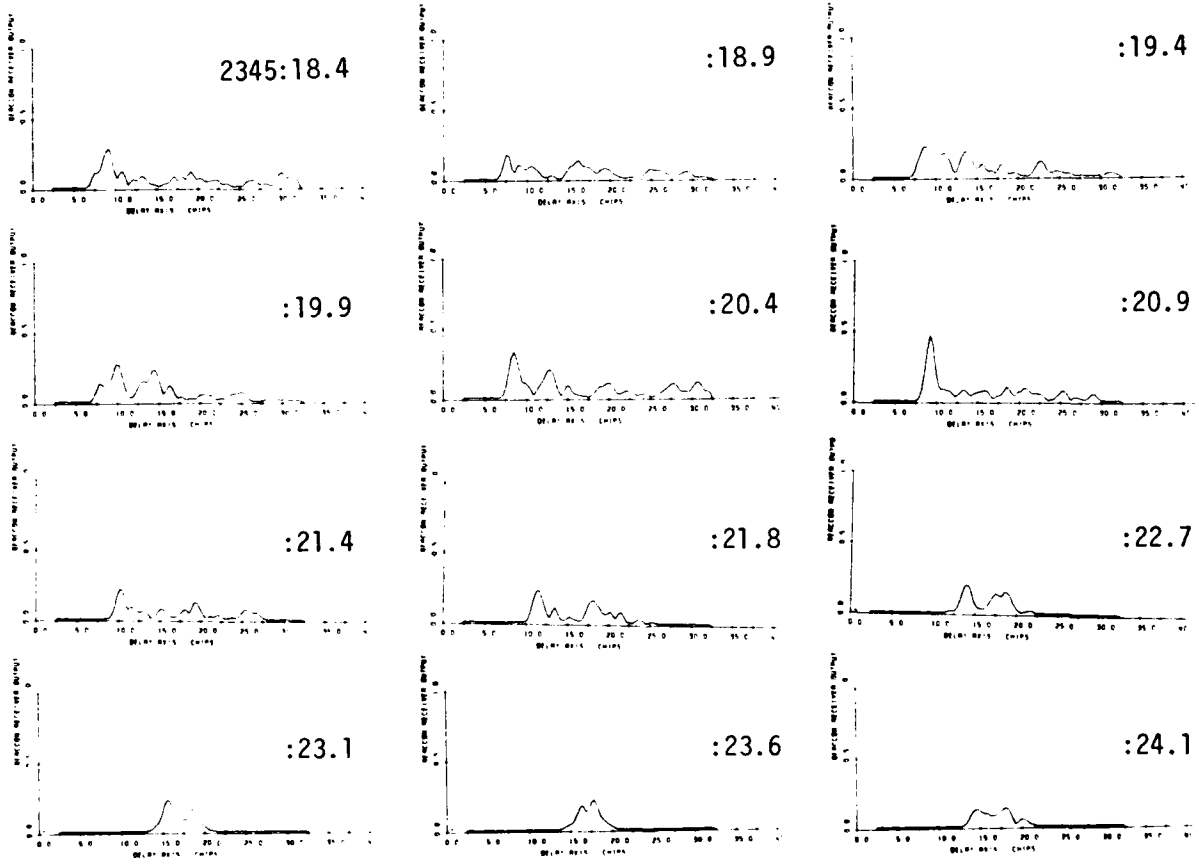

FIGURE 13 ENERGY DELAY PROFILE BETWEEN 2345:18.4Z AND 2345:24.1Z, ST. GEORGE ISLAND

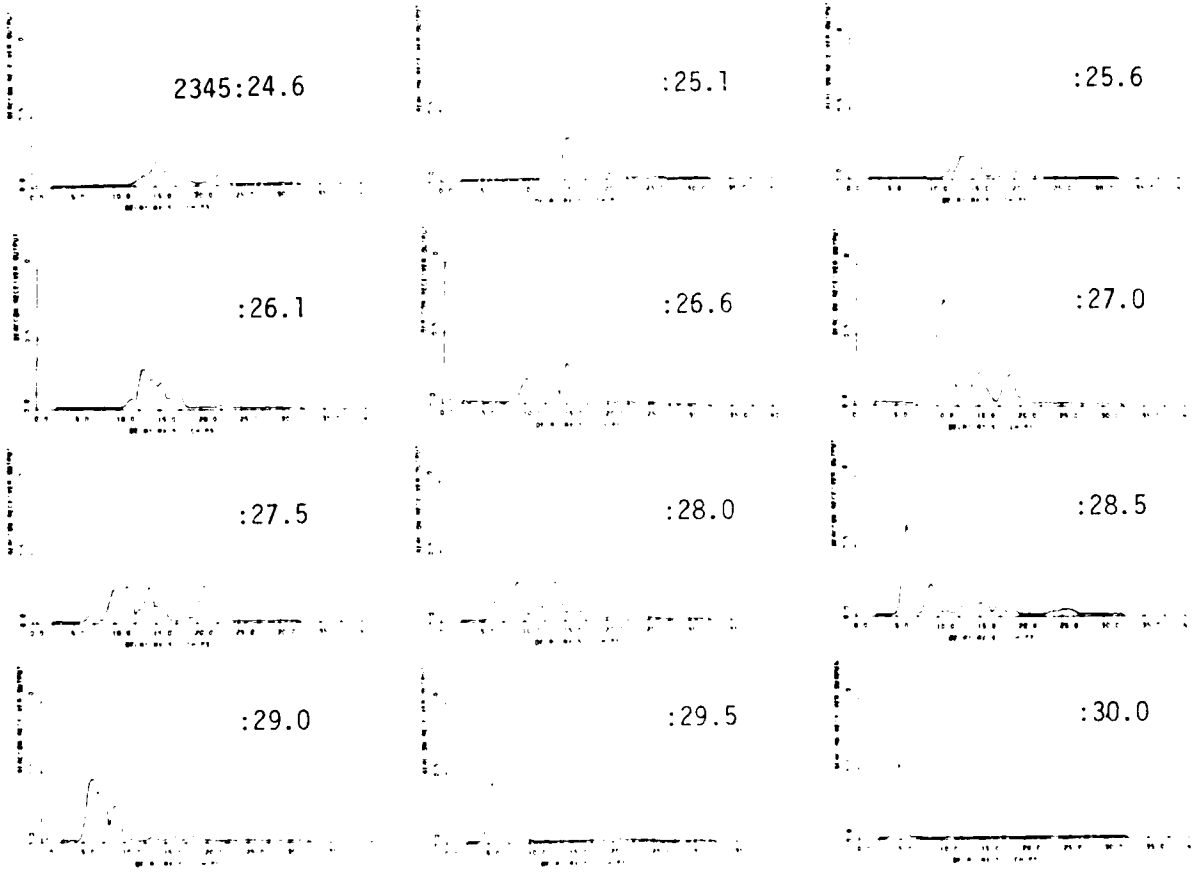

FIGURE 14 ENERGY DELAY PROFILE BETWEEN 2345:24.6Z AND 2345:30Z, ST. GEORGE ISLAND

hardware imperfections and due to the signal dispersion imposed by the ionosphere and barium plasma; this will be removed during planned future signal processing.

B. Cape San Blas Beacon 1

Figure 15 shows the impulse response recorded at Cape San Blas for the first beacon rocket. The time span for this figure is 2345:00.4Z to 0345:32.9Z, and it was plotted in the same manner as Figure 10. The SNR for these data was measured at 32.7 dB preceding occultation. Well defined caustics are apparent in these data on approach to the cloud, though none appear as the beacon rocket exits from the cloud. It is believed this is due to the manner in which the path exits the bottom of the cloud.

Selected snapshots of the channel measurements taken approximately every 0.5 s are provided in Figure 16 for the Cape San Blas receiving site. This sequence is interesting in that it initially shows a larger delayed path than a direct path component. The direct path grows in strength as the path exits the bottom of the cloud. Potentially this behavior can cause loss of lock or false lock in conventional code tracking circuits. At other times the signal displays significant energy spread over nearly 20 chips. A better measure of the random component of the delay spread is probably 8 to 10 chips as measured near the maximum of the integrated electron content along the path (near 2345:26Z).

C. St. George Island Beacon 2

The occultation was achieved for the second beacon rocket from St. George Island beginning at 2358:10Z. The impulse response recorded for this event is shown in Figure 17 over a time period from 2358:01.2Z to 2358:33.7Z. Again a slight symmetry is noted to the delay pattern for this receiver geometry. In this case the initial caustic energy does not show up at large delays as it did for the first beacon, nor is the delay spread as large. The maximum delay seen is approximately 26 chips for the caustics occurring on approach to the cloud. The defocusing that occurs behind the cloud center is also less (compare the amplitudes of

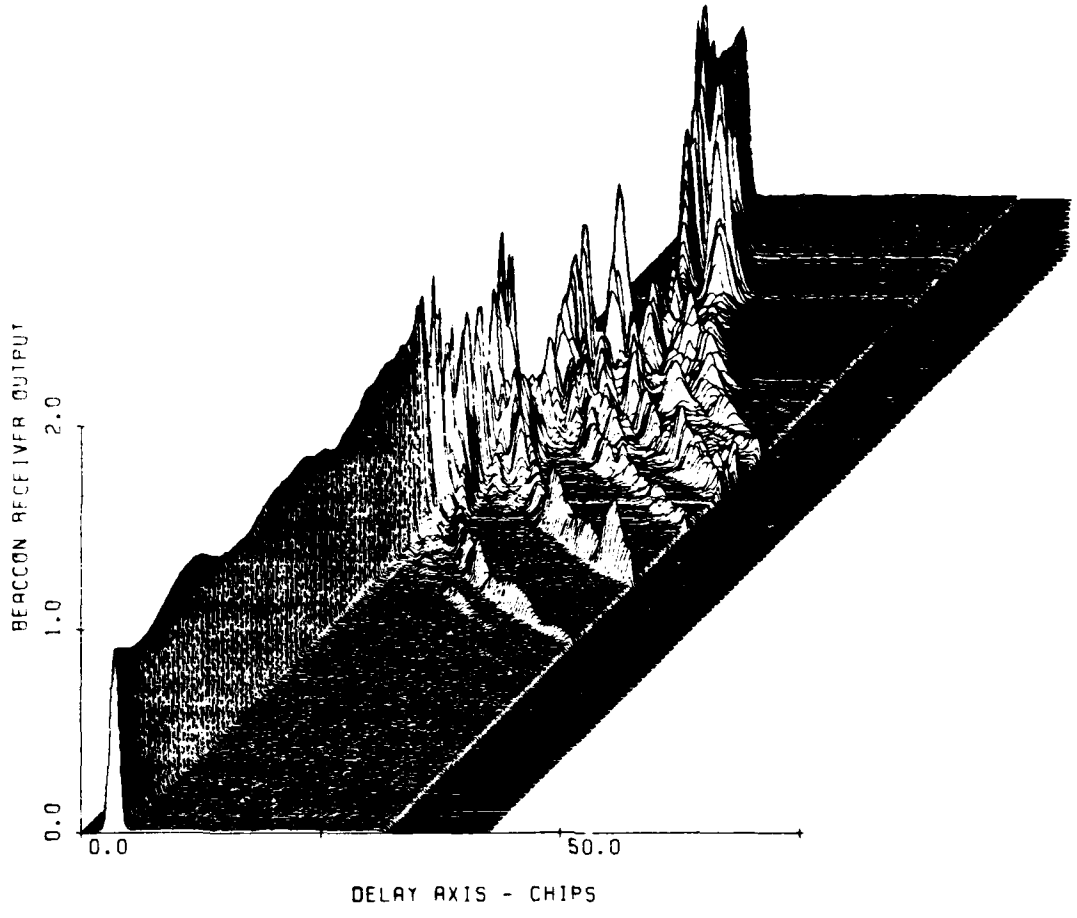

FIGURE 15 ENERGY DELAY PROFILE, CAPE SAN BLAS, FIRST BEACON, TIME SPAN FROM 2345:00.4Z TO 2345:32.9Z

Figure 10 to Figure 17). Because the two rockets reached the cloud only 13 minutes apart, it is doubtful that these differences are due to cloud aging. Rather, the weaker effects experienced for the second beacon seem to point to interaction with a weaker and/or less developed portion of the cloud. This perspective is consistent with the geometry interpretation given earlier.

The impulse response patterns presented here are difficult to describe or categorize due to the complexity of the real barium environment.

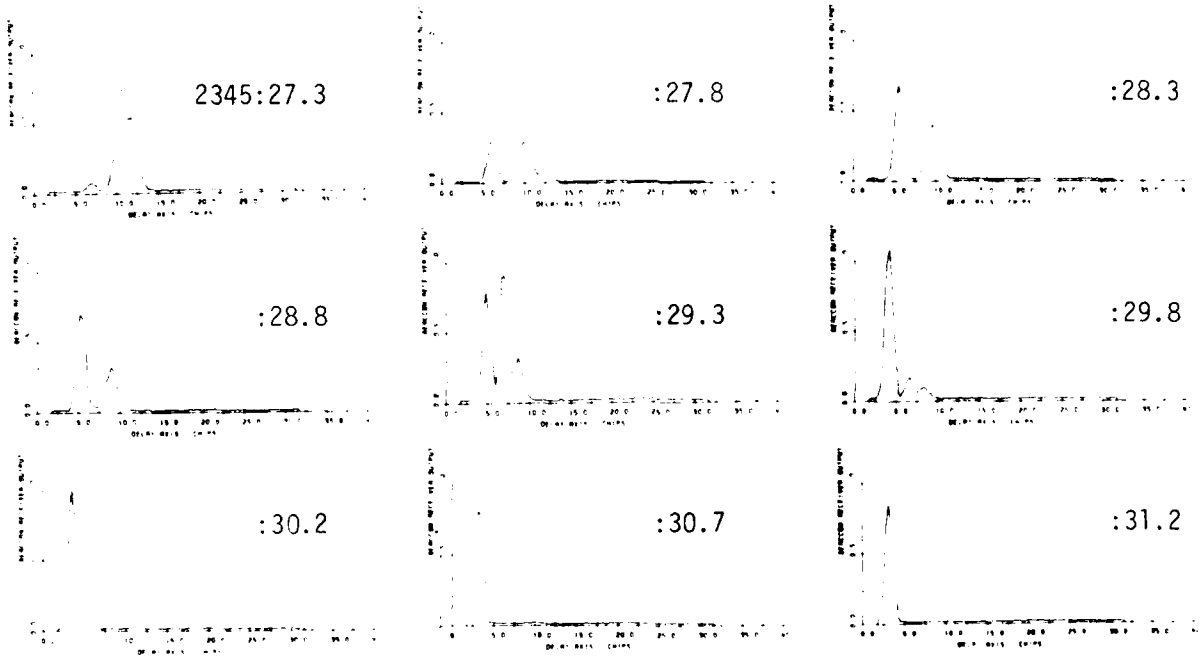

FIGURE 16 ENERGY DELAY PROFILE BETWEEN 2345:27.3Z AND 2345:31.2Z, CAPE SAN BLAS

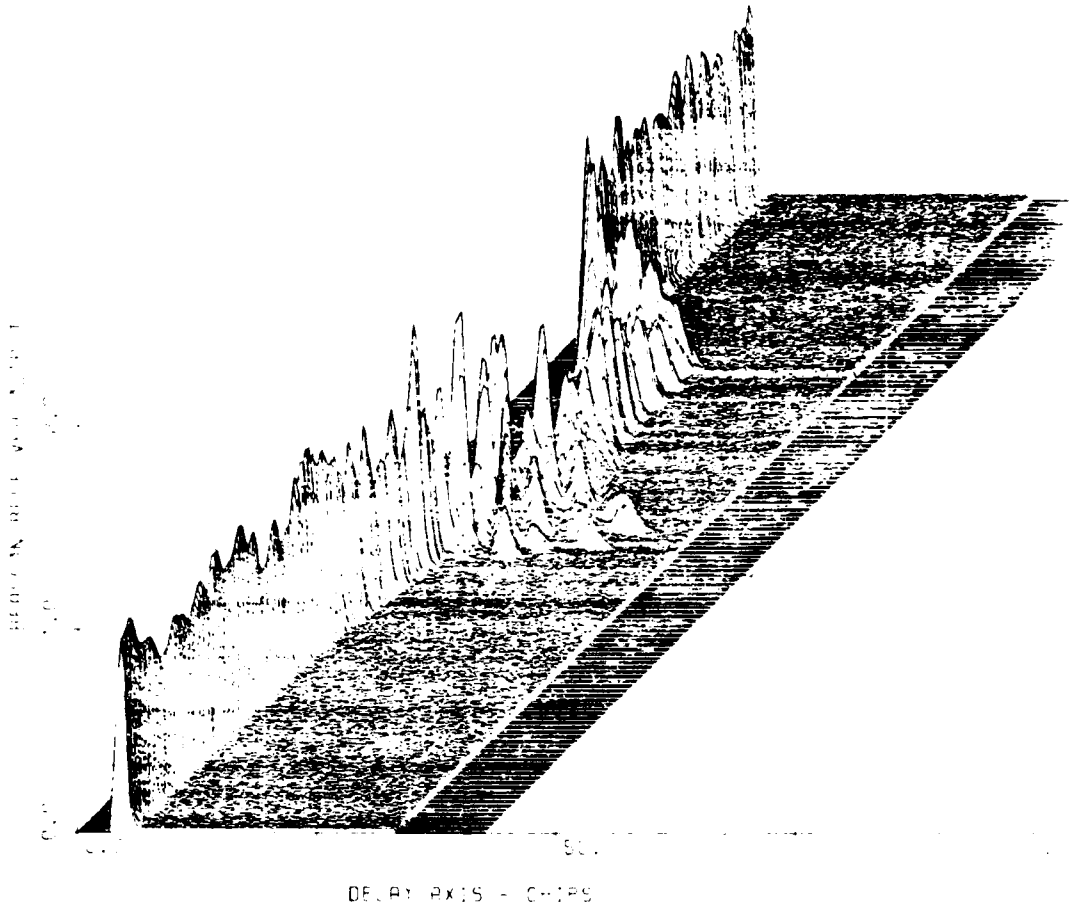

FIGURE 17 PULSE DELAY PROFILE, ST. GEORGE ISLAND, SECOND BEACON, TIME SPAN FROM 2358:01.2Z TO 2358:33.7Z

The primary effects are expected to arise from the striations themselves, but the gross plasma itself can also significantly disturb the channel impulse response.

In an effort to examine the contributions of the gross plasma to the measured signal characteristics, a quick effort was made to model the gross plasma along the path to St. George Island for this second occultation. To accomplish this the integrated content was approximated from the time-of-arrival delay of the main lobe of the impulse response. Numerical propagation calculations using the PATS code were performed across

a 20-MHz bandwidth with 98 MHz center frequency using this environment. The propagation geometry used was patterned after an estimate of that which existed for the second beacon at St. George Island. The results of these propagation calculations were then assembled to provide a prediction of the transfer characteristic of the environment. This transfer function was then Fourier transformed to yield the predicted impulse response. The results of this simulation appear on the top of Figure 18. Figure 18 also provides a detailed view of the response actually recorded (bottom), which includes the striation effects as well as the gross plasma effects.

The unsymmetric nature of the plasma in the plane cut by the raypath is apparent in the caustic components showing up on approach to the medium but not on exit. Apparent in Figure 18 are two distinct sets of caustics in the simulated environment where four are initially visible in the actual data. This seems to indicate that there was some structuring of the plasma occulted. It is also noted that the measured impulse response delay spread is considerably greater through the center of the occultation region than occurs for the unstructured plasma simulation. A separation of the random striation effects from the gross plasma effects is planned in future processing. It is also noted that the initial caustic rays arise differently than modeled. This may be due to the coarseness of the radio data used in this calculation. More exacting calculations will be performed at a later date.

D. Cape San Blas Beacon 2

The data from the second beacon rocket as recorded at Cape San Blas appear in Figure 19. The time span plotted extends from 2358:05.4Z to 2358:37.9Z. Because caustics were not evident as the path entered the cloud, an adjustment in the measurement window (time delay tracking of the signal) was made that resulted in a partial loss of signal upon exit of the ion cloud. As shown, the signal abruptly shifted back and largely out of the measurement window at 2358:25Z. A few seconds later (at 2358:30Z), the measurement window was shifted to again encompass the signal. Based on the time of occultation at St. George Island, the occultation at Cape San Blas should occur within several seconds of 2358:18Z.

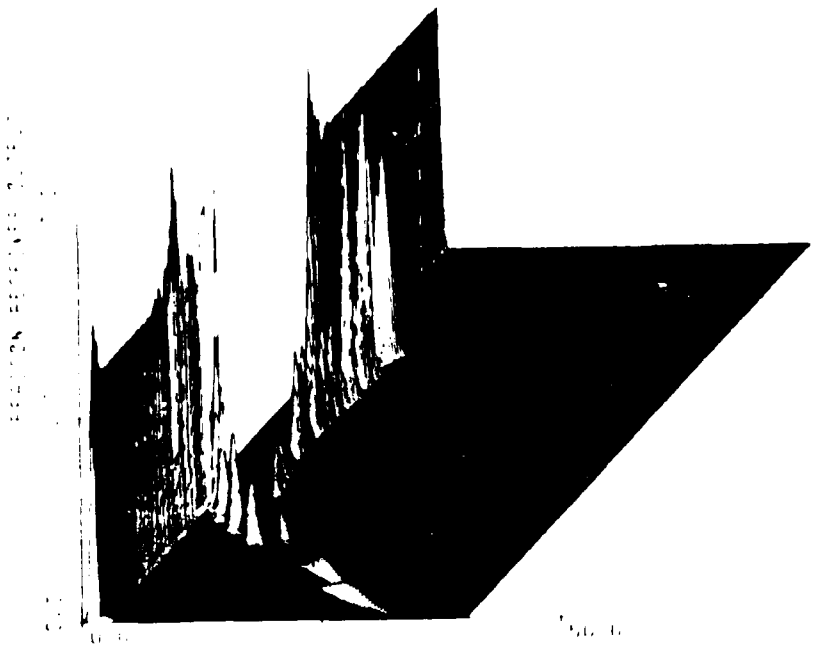

COMPUTED
GROSS
PLASMA
EFFECTS

DELAY AXIS - CHIPS

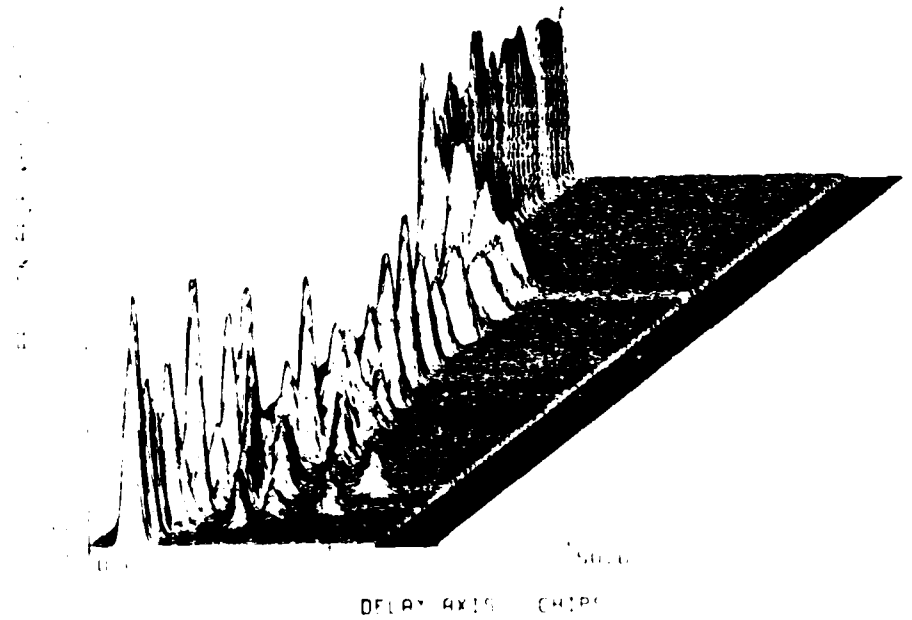

MEASURED
DATA

DELAY AXIS - CHIPS

FIGURE 18 AN ESTIMATED IMPULSE RESPONSE FOR THE GROSS BARIUM CLOUD AS SEEN AT ST. GEORGE ISLAND FOR THE SECOND ROCKET (TOP), AND THE ACTUAL DATA RECORDED (BOTTOM)

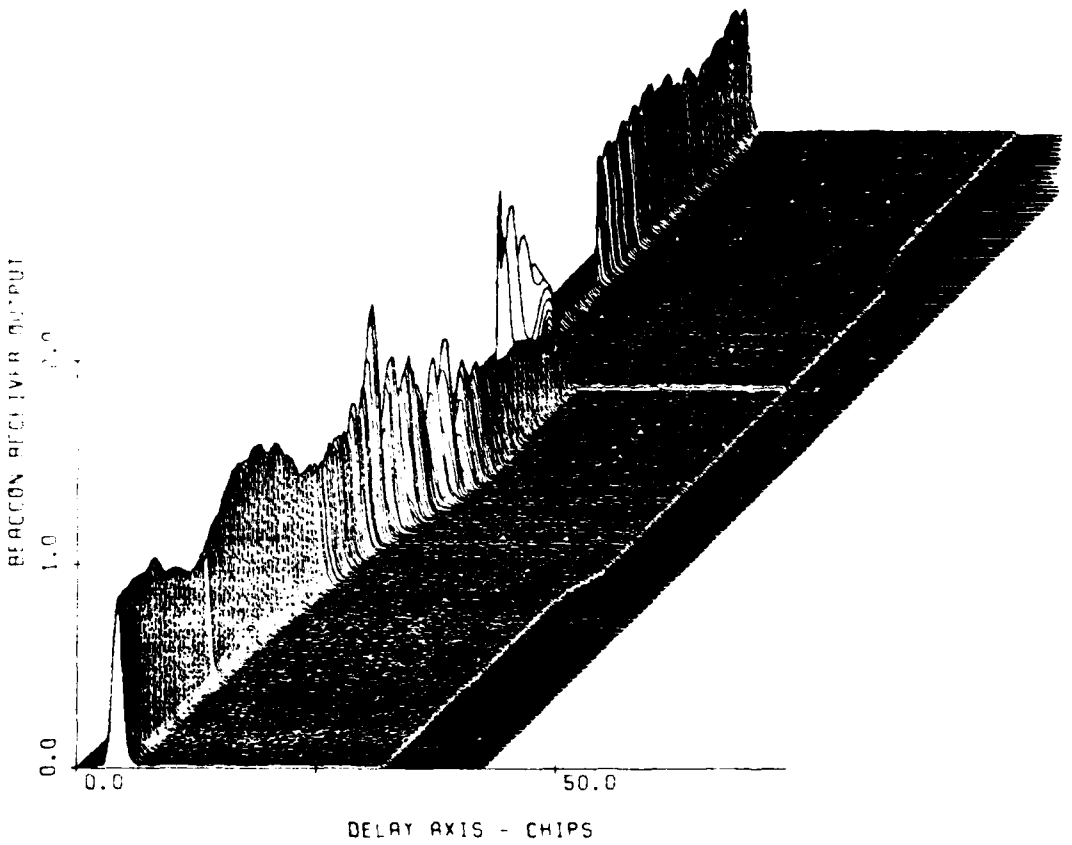

FIGURE 19 PULSE DELAY PROFILE, CAPE SAN BLAS, SECOND BEACON, TIME SPAN FROM 2358:05.4Z TO 2358:37.9Z

Notably absent at this time (or any other time) are the discrete caustic rays observed in the other occultation data. The evidence of the cloud is apparent, however, in the increasing time-of-arrival (chip) delay beginning at about 2358:18Z. These data indicate that only a marginal intersection of the beacon signal path with the barium plasma occurred. Some weak fading is evident, however. Thus, some weakly striated material may have been occulted.

IV CONCLUSIONS

The primary purpose of the beacon experiment was to measure the time-of-arrival jitter and spread (or frequency selective properties) produced by a striated plasma. In this regard the experiment has been highly successful. An accurate understanding of the relation between the plasma structure and these parameters is important to the understanding of the performance of spread-spectrum PSK systems and high-data-rate systems operating through a striated ionospheric plasma. Even without this detailed understanding, the data are directly relevant to system performance. The data indicate the potential for loss of code lock and false lock as well as the usual difficulties in operating through fading environments.

The agreement of the PLACES beacon experiment data with theoretical relations for the time-of-arrival jitter and spread remain to be tested. A cursory review of the data would suggest that a geometrical approach based on angular spectrum arguments will successfully account for the measured energy delay profile and as well as the spectrum of the signal at each component of delay. This geometrical interpretation would explain the basic cause of the signal time-of-arrival jitter and spread as the geometric increase in path length produced by the plasma angular scattering. The data taken are of high quality and should facilitate the theoretical interpretation of the measurements.

REFERENCES

1. V. H. Gonzalez, Private Communication, March 1981

2. V. H. Gonzalez, "Analysis of UHF Radar Data--STRESS Series," DNA 4823F, Final Report for Period May 1977 to September 1978, Contract DNA 001-76-C-0341, SRI International, Menlo Park, CA (1 December 1978).

BLANK PAGE

AIRCRAFT EXPERIMENT MEASUREMENTS

J. M. Marshall

ESL Incorporated
Sunnyvale, CA

I INTRODUCTION

The PLACES aircraft experiment used two UHF tone signals, one transmitted from the aircraft (Doppler precorrected) to LES-8/9 and one received (Doppler corrected) from LES-8/9 at the aircraft. Doppler correction is provided by a K-band reference signal generated at the satellite coherently with the UHF signal. These signals were used successfully during the STRESS experiment in 1977. The capability represented by the aircraft experiment is unique for two reasons: (1) it provides data on the evolution of plasma structure that satisfy the needs of the nuclear effects community, and (2) it enhances the volume and quality of results, not only from a communications perspective, but also from the perspective of plasma phenomenology and propagation. It was anticipated that better quality as well as quantity of data would be obtained during the PLACES experiment than during the STRESS experiment. This improvement was expected through improved real-time diagnostics and aircraft control procedures. A quick look at the data collected indicates that this improvement was achieved.

With some minor modifications, the aircraft positioning system that was used during STRESS was used during PLACES. This system consisted of radar (FPS-85) cloud tracking, aircraft position tracking, and two-way communication between the aircraft and the Central Control Facility (CCF). The aircraft was directed, via the communications link, to the regior of predicted scintillation effects. This region is the "shadow" of the barium ion cloud that has been calculated from the measured ion cloud position and the precomputed satellite position. A significant improvement in this system over that used during STRESS was the transmission of

real-time diagnostic data from the aircraft to the experiment control center at the CCF. At times, the real-time link was the only means available to position the aircraft because the FPS-85 radar, as a result of several unrelated problems, was unable to provide proper ion cloud track information on several occasions and optical tracking was available only as a backup during the 40-min twilight optical window.

II AIRCRAFT EXPERIMENT OVERVIEW

The aircraft experiment employed LES-8 throughout the experiment. LES-8 and LES-9 were in nearly identical orbital positions. The uplink and downlink tone processing equipment built by ESL under the STRESS program performed reliably. There was no apparent degradation over the past 3 years in the overall signal quality. In fact, 2 or 3 dB of SNR improvement appears to have been realized, possibly through a combination of more favorable geometry and hardware/antenna changes on the aircraft. A quick look at the downlink C/KT indicated approximately 51 dB-Hz compared to 46 to 47 dB-Hz measured during STRESS.

Table 1 summarizes the aircraft data recorded. The release coordinates shown are only approximate. The location given for IRIS and JAN is the rocket location as release was initiated. (Triangulation from optics can provide a better estimate of the geometric center of initial barium release.) Both uplink and downlink data are available except during periods when K-band phase lock was lost. Without K-lock the uplink tone data are lost. The real-time processing software generally worked reliably. Occasional computer crashes did occur, but were generally quickly corrected by the highly efficient CCF programming staff. Loss of K-lock would result in loss of phase lock in the real-time processing software, but again this only presented minor difficulties. The greatest difficulties were encountered with the FPS-85 radar tracking data. Only during Event IRIS was useful cloud data obtained consistently for positioning the aircraft. Without the real-time relay link through the FLTSATCOM and the associated aircraft position displays it would not have been possible to position the aircraft and obtain fading data on the other three events.

Table 1

A/C DATA SUMMARY

Release	Release Time (Z)	Release Altitude (km)	Release Location	No. of Passes	Data Period
GAIL 12/4/80	2307:36	178.1	~29.37°N ~87.37°W	32	2307:10 to 0148 0136 Last strong fading (R + 2:29)
HOPE 12/6/80	2307:37	179.4	~29.25°N ~87.0°W	33	2307:40 to 0206 0113 Last strong fading (R + 2:06)
IRIS 12/8/80	2313:07	179.6	28.799°N 87.166°W	31	2329 to 0205 0150 Last fading data (R + 2:37)
JAN 12/12/80	2313:42	184.3	29.166°N 86.993°W	35	2314:06 to 0200 0157 Last strong fading (R + 2:43)

III TEST RESULTS FOR GAIL

The barium cloud for the first experiment, GAIL, was released on 4 December 1980 at 2307:36Z. It was released at an altitude of 178.1 km approximately 87.37°W, 29.37°N. The projection at release of this cloud from the LES-8 satellite down to the 10.668-km aircraft altitude is 86°14'36"W, 31°at'43"N. This is slightly southwest of the planned projection of 86°11'31"W, 31°31'1"N. The cloud quickly moved northeast from this point, stopped for a few minutes, then moved southwest at a slower pace for the rest of the experiment. The apparent projection from the satellite to the aircraft operating altitude appears to follow a somewhat different pattern due to the satellite motion, as shown in Figure 1. The cloud projection was about 1° south and 1° west of the release point at R + 2 hr 28 min.

The early-time cloud drift was more northerly than previously observed. This northerly drift in conjunction with an optical tracking error resulted in the apparent cloud drifting outside the range safety firing limits for the beacon and the probe before striations were clearly evident.

The optical tracking system uses two ground sites to follow the cloud, and from these located the cloud position. During this release, the D3A ground site tracked the neutral cloud, not the striated ion cloud, causing the projection of the ion cloud position to be significantly northeast of its actual position. The FPS-85 radar was not working from Release (R) to R + 20 min, due to a cable failure. The tracking error is clearly evident in the large jump in the cloud projection point around 2347Z when the track was switched from optics to radar. The aircraft tracking radar was held for missile tracking for the first 21 min; thus, the aircraft position during this time must be derived from the less accurate onboard INS data. As a further complication, the radar provided the projection data using the LES-9 ephemeris rather than LES-8. These difficulties resulted in no useful data until approximately 1 hour after release. Figure 2 shows the aircraft ground track, which reflects the difficulty in obtaining good projection data.

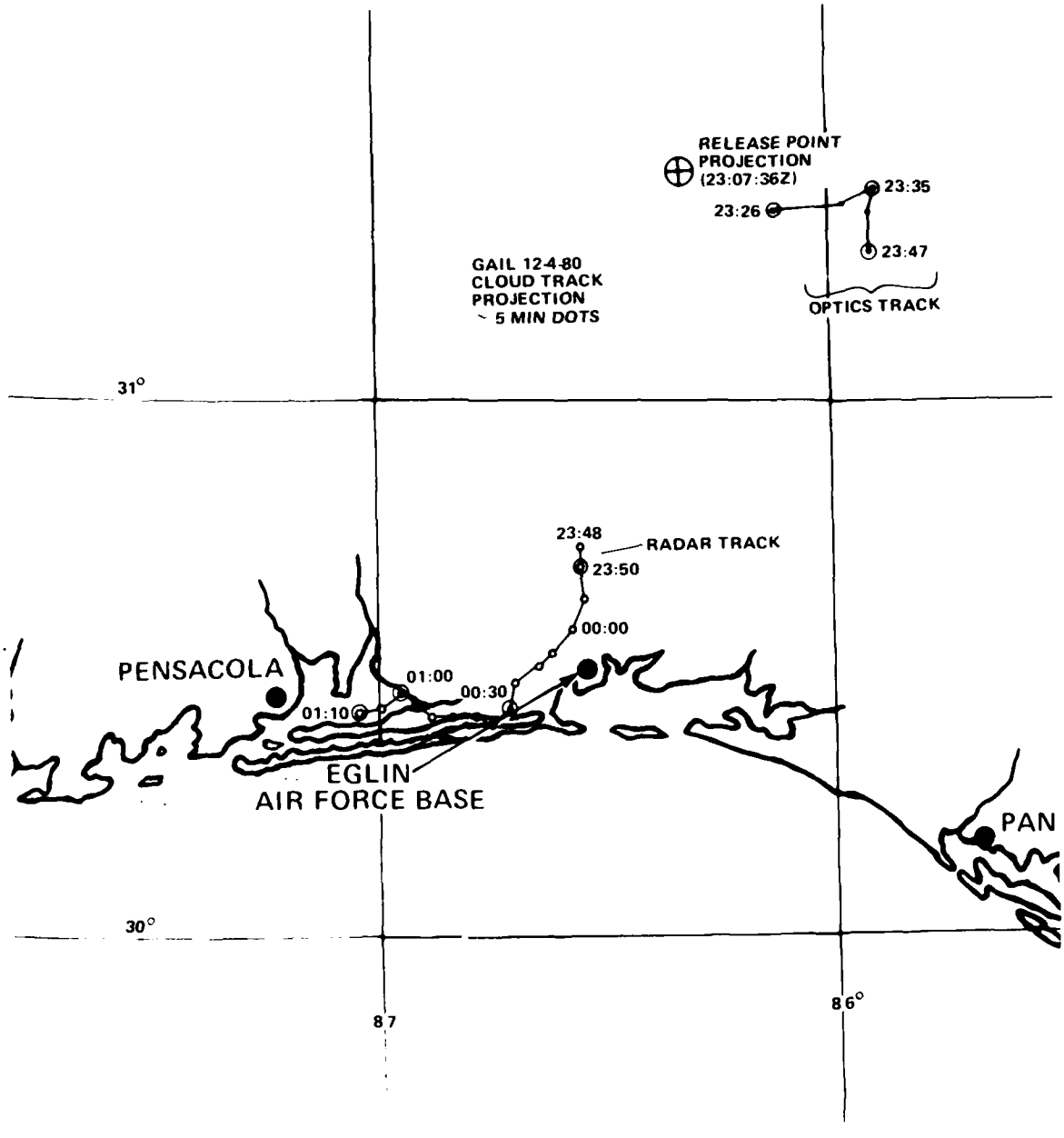

FIGURE 1 ION CLOUD TRACK PROJECTION FOR GAIL

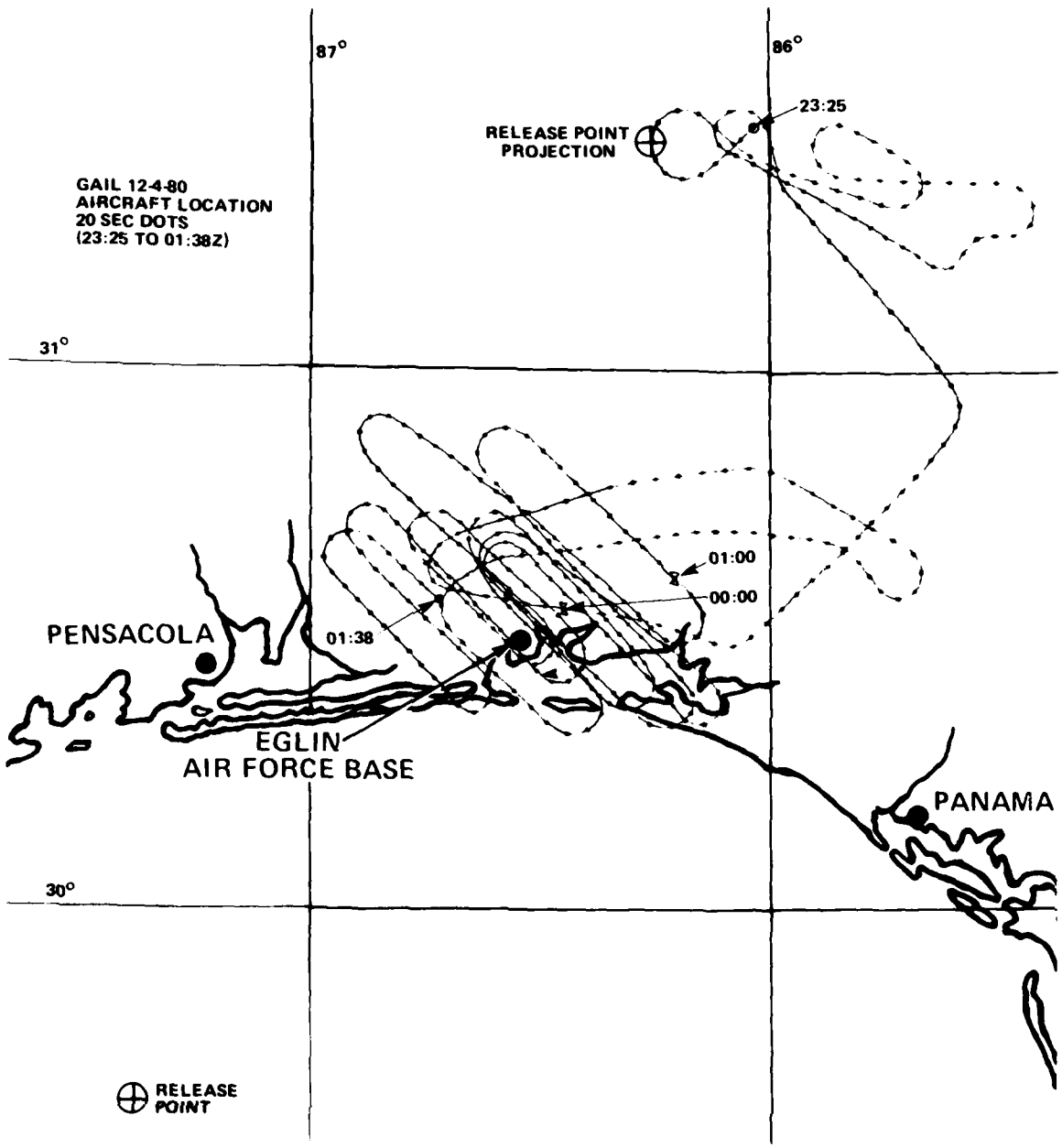

FIGURE 2 AIRCRAFT GROUND TRACK FOR GAIL

Figures 3, 4, and 5 show the aircraft ground track during each hour and also show the periods of strong (deep) fading. Since the radar projection was south of the true projection, the first pass of the aircraft through the radar track around 2400Z resulted in no fading and the aircraft was vectored north, back toward the last optics track data. It was along this flight path that strong fading was observed (see Figure 4). From that point on, the real-time aircraft track display and real-time fading display were used to position the aircraft.

A total of 32 passes were made with fading seen as late as R + 2 hr 45 min. Moderate-to-strong fading was seen during 18 of the 19 passes between R + 50 min and R + 1 hr 32 min. Weak fading and diffraction ringing were observed between R + 1 min and R + 50 min. During most of this first 50 min, the aircraft was following the incorrect optics track point projection data, causing it to traverse the high-altitude, low-ion-density part of the cloud northeast of the cloud center. Only weak fading was seen during the last two passes. Uplink data are available for 12 of the 32 passes, while downlink data are available for all 32 passes.

The data received from each of these releases show the expected progression of effects from diffraction ringing, large defocusing from the background ion cloud, large defocus with superimposed fading from developing striations, and eventually random fading at late times. Representative data are described below.

Examples of early-time passes are given in Figures 6 and 7. These passes show early-time diffraction or multipath ringing characterized by oscillating amplitude fluctuations. This diffraction ringing was noted almost immediately following each release. This can be contrasted with the strong, deep fading seen in Figure 8 for Pass 11, which shows what we term strong fading characteristic of well developed striations. The last strong fading of the night for GAIL is shown in Figure 9. It is interesting to note the coarseness or slower fading that results at late time.

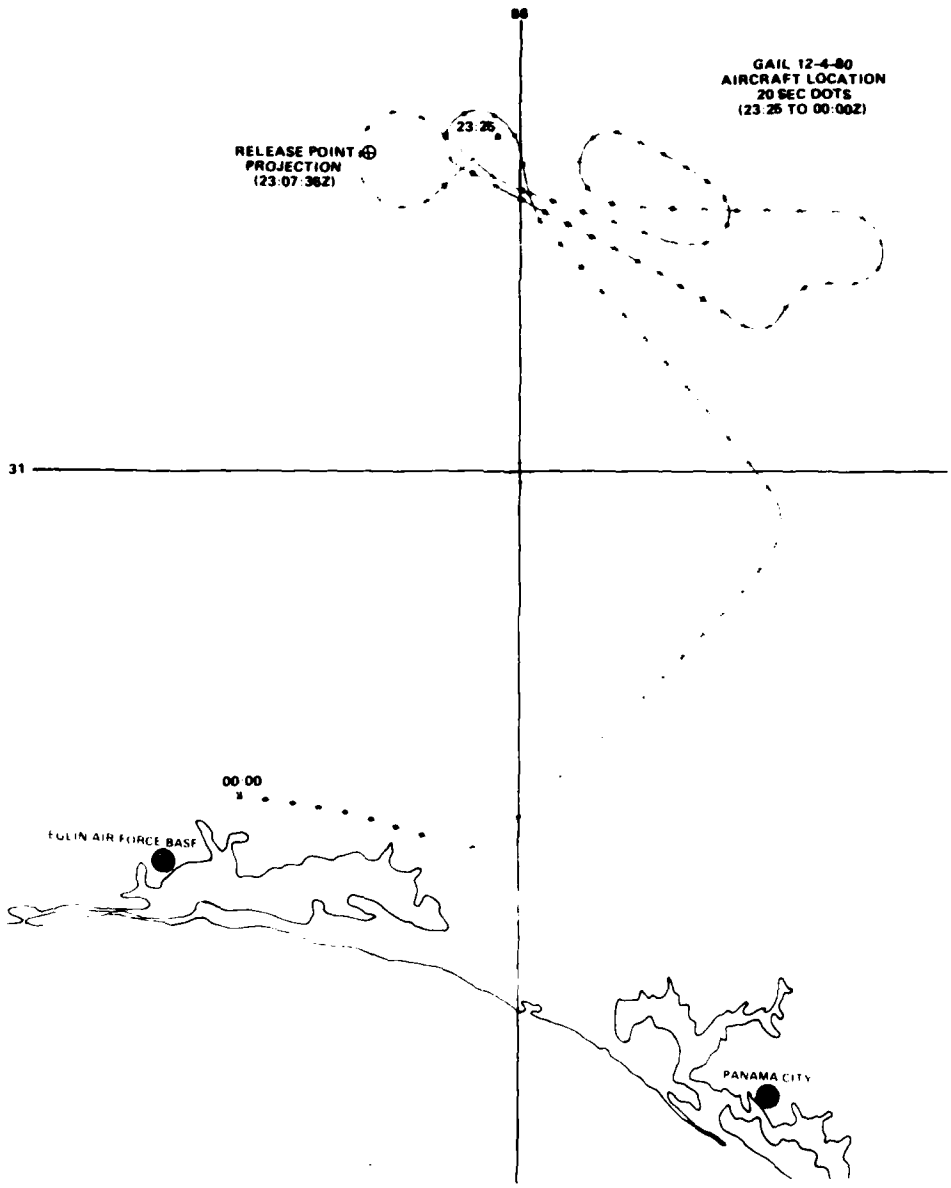

FIGURE 3 AIRCRAFT GROUND TRACK FOR GAIL FROM 23:25 TO 00:00Z

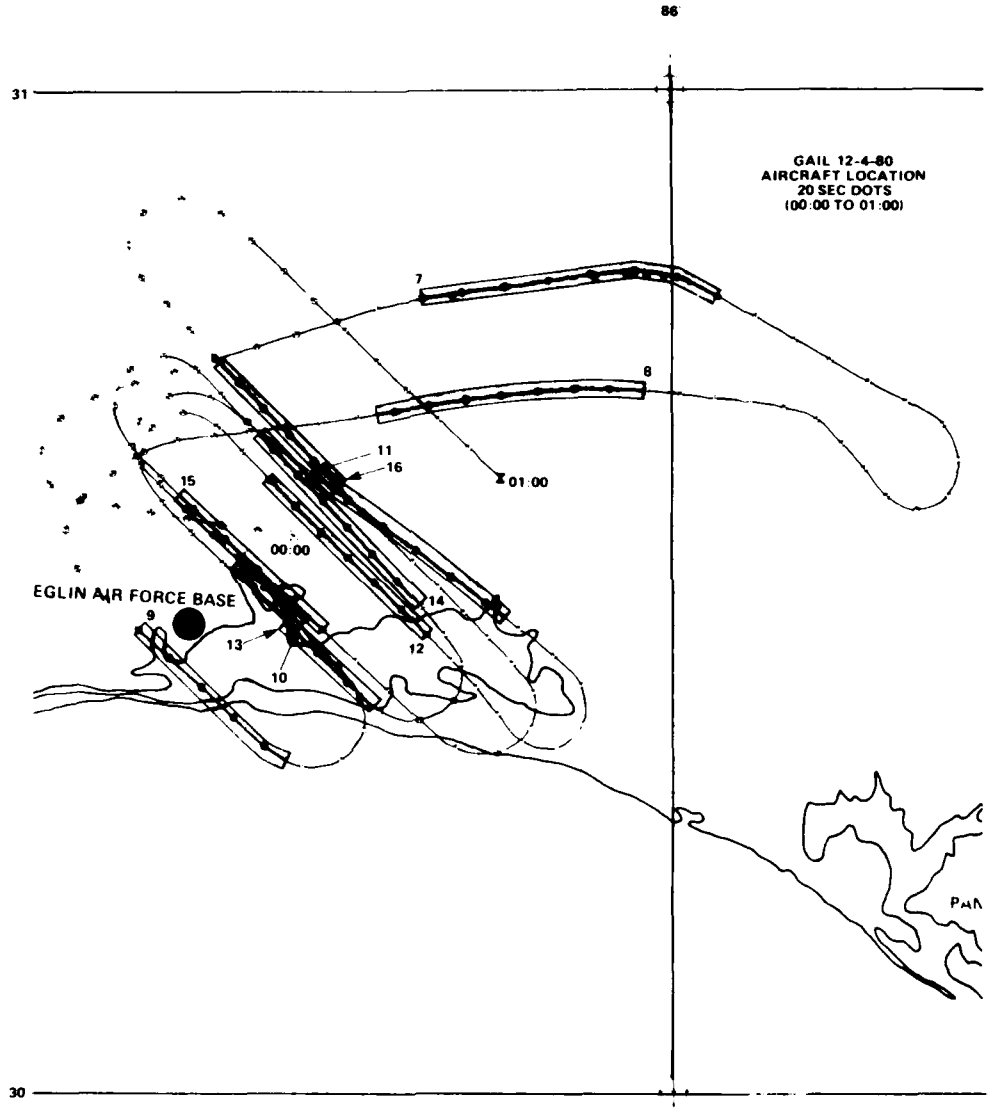

FIGURE 4 AIRCRAFT GROUND TRACK FOR GAIL FROM 00:00 TO 01:00Z. Periods of deep fading are shaded.

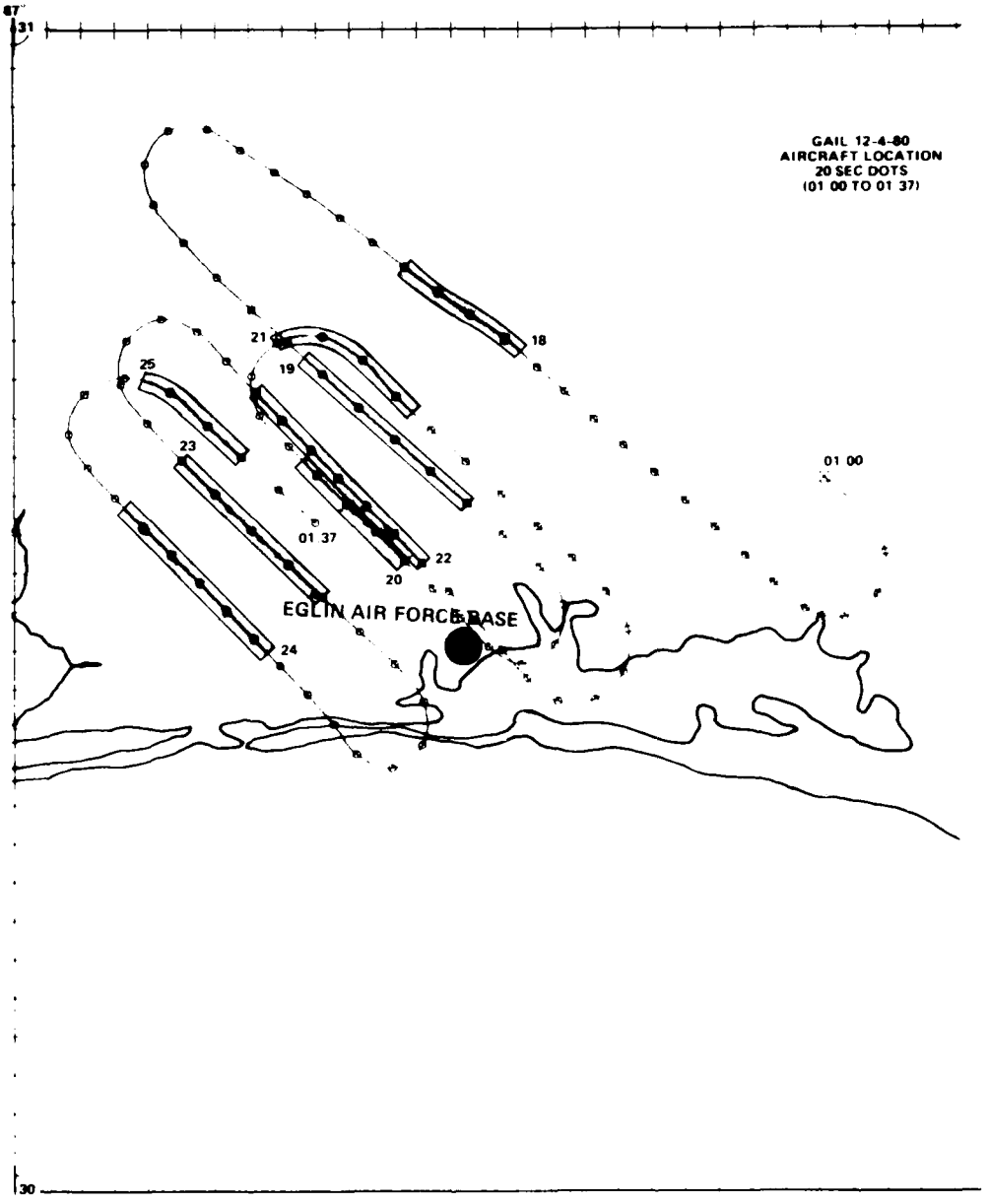

FIGURE 5 AIRCRAFT GROUND TRACK FOR GAIL FROM 01:00 TO 01:37Z. Periods of deep fading are shaded.

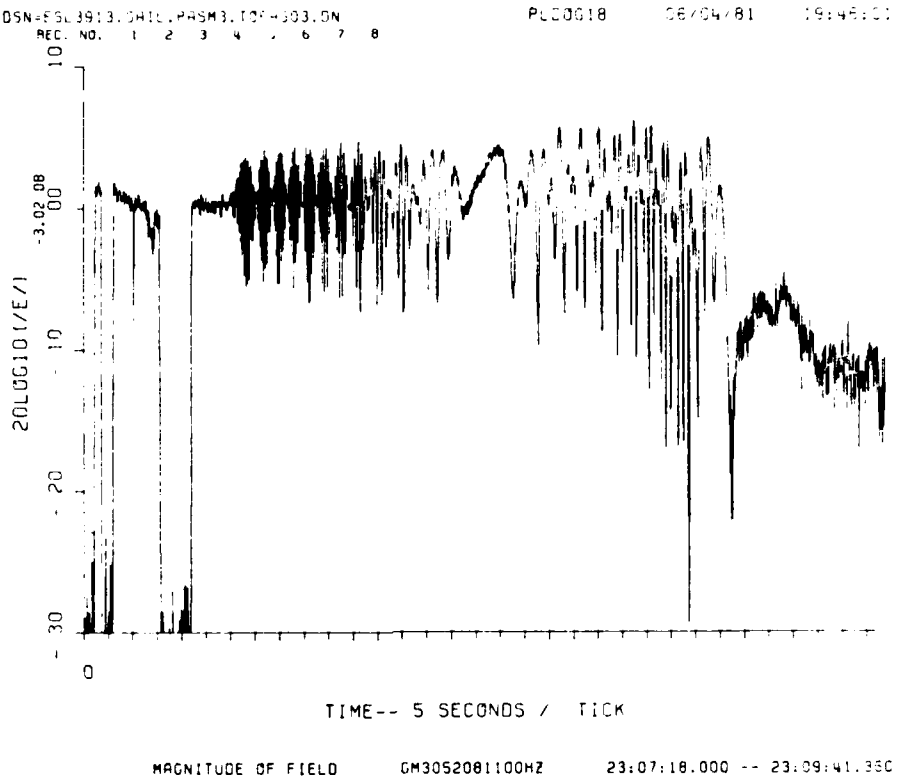

FIGURE 6 DOWNLINK FADING ON GAIL PASS 3, R + 1 MINUTES

IV TEST RESULTS FOR HOPE

The second barium release, called HOPE, occurred on 6 December 1980, at 2307:37.4, at an altitude of 179.4 km and a location of approximately 29.25°N, 87.0°W. This release point was about 5 min southwest of the planned release point. The cloud appears to have moved north-northeast for a few minutes, stopped, then moved south-southwest at a moderate velocity for the rest of the night. The cloud projection was located about 2° south and 1.5° west of release at R + 2 hr 38 min. A plot of the available cloud projection data is shown on Figure 10. The aircraft ground track is shown on Figure 11.

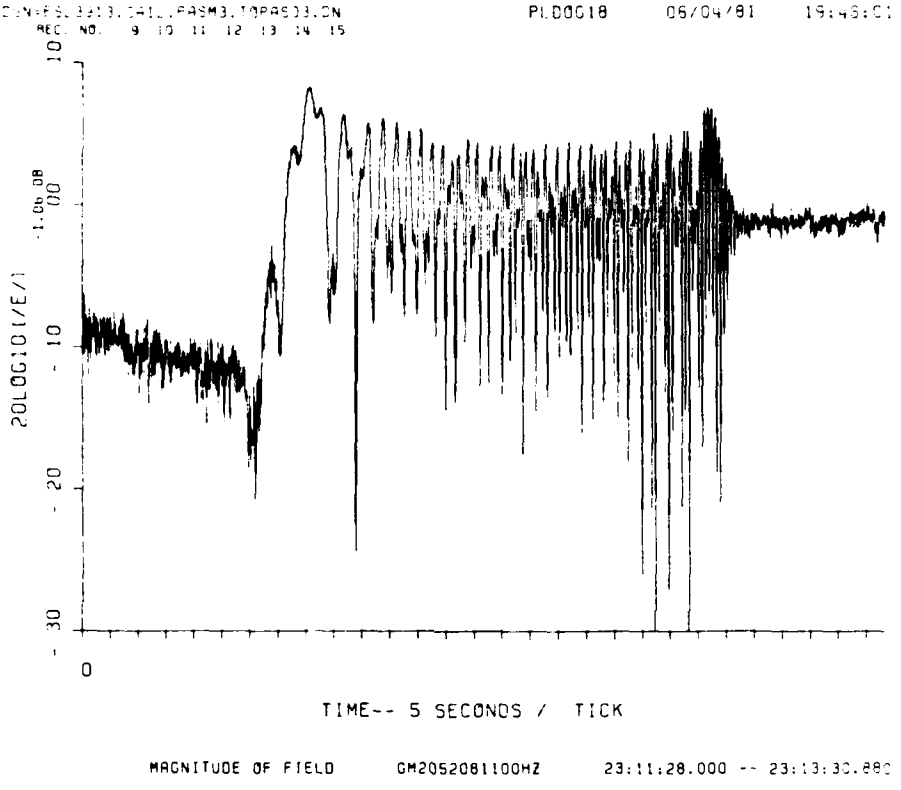

FIGURE 7 DOWNLINK FADING ON GAIL PASS 2, R + 5 MINUTES

Optical track data were used until about R + 55 min, with radar track data being used for the remainder of the experiment. The optics track located the cloud somewhat north of the radar track. The radar track appears to have been more consistent with the observed fading. As shown on Figure 11, the aircraft was vectored nearly 0.5° south of the optics track around 2400Z. Figures 12, 13, and 14 show the aircraft ground track for each hour period. The intervals of strong fading are indicated by the shading.

The ion cloud from HOPE drifted more northerly than during GAIL, and again resulted in an inability to launch a beacon or a probe rocket.

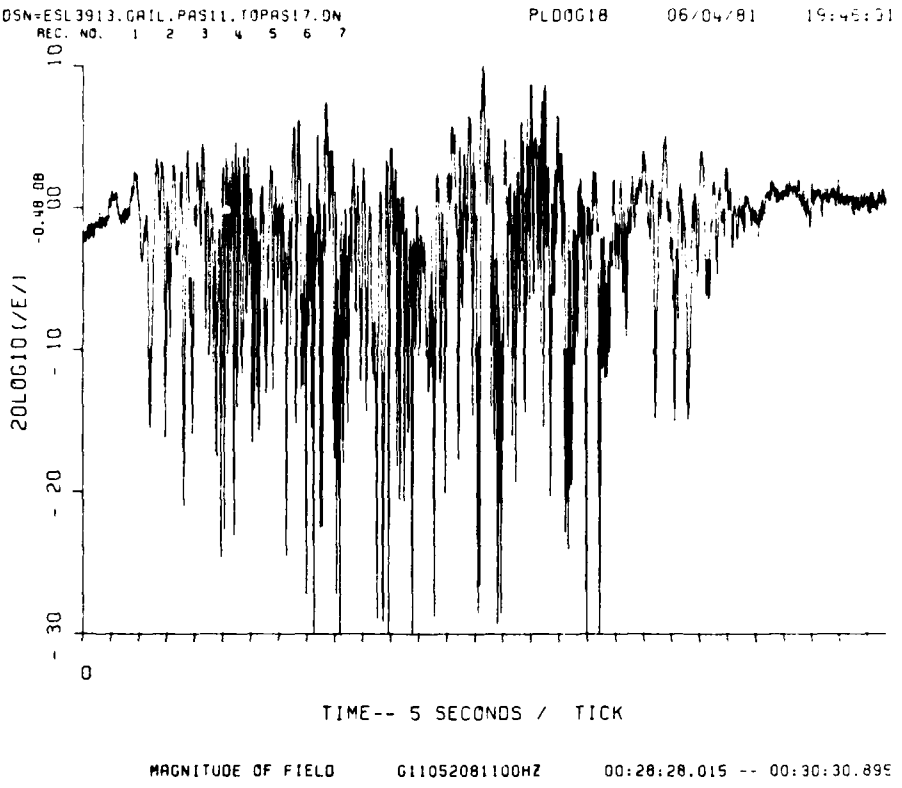

FIGURE 8 DOWNLINK FADING ON GAIL PASS 11, R + 1 HOUR 25 MINUTES

A total of 33 passes were made during this release, with 14 showing moderate to strong fading. The last pass ended at R + 2 hr 57 min, while the last pass with moderate fading observed ended at R + 2 hr 22 min. The first 11 passes, which were between release and R + 55 min, showed strong fading in only two passes and diffraction ringing in one. These passes were made while the aircraft followed the optics cloud track. The time between R + 55 min and R + 1 hr 3 min was spent catching up with the cloud, which was south of the aircraft. Twelve of the next 15 passes showed moderate to strong fading, yielding the total of 14 good passes. Pass 26 is interesting because it shows only one deep fade that may be due to a single object. The last seven passes showed weak fading or no fading.

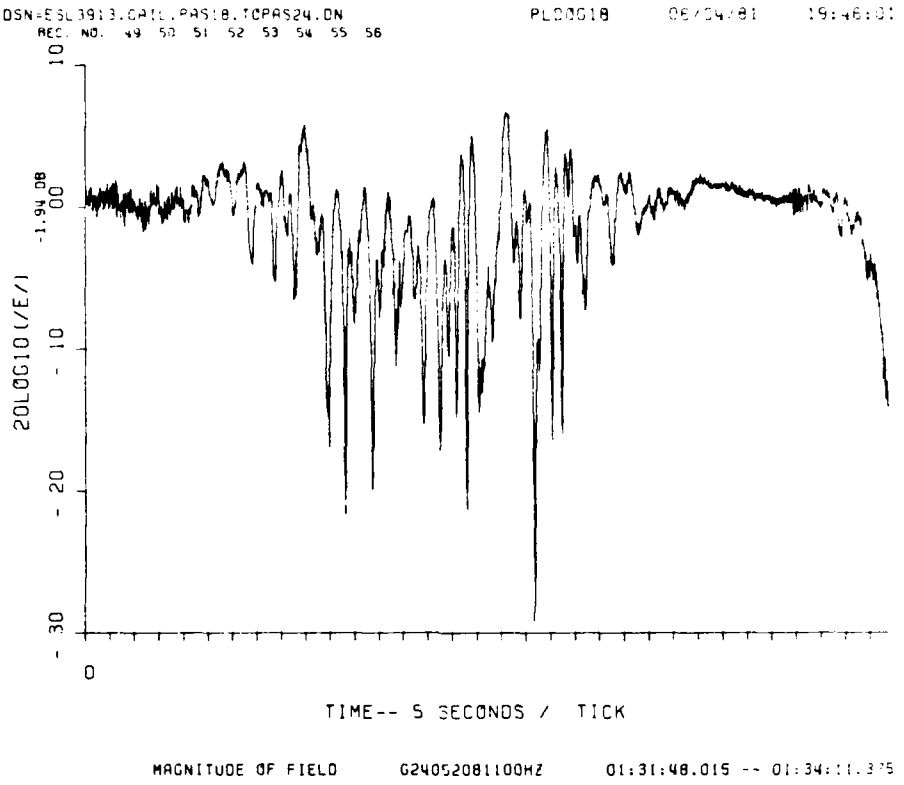

FIGURE 9 DOWNLINK FADING ON GAIL PASS 24, R + 2 HOURS 25 MINUTES

Uplink data are available for 32 of the 33 passes and downlink data are available for all 33 passes. K-band lock was lost during part of one pass, making the uplink data questionable during that pass. Occasionally, as noted, a loss of lock indication was obtained, but the uplink data appeared unperturbed.

A few samples of the data from HOPE are given in Figure 15 through 19. These data have been preliminarily computer processed for this quick-look report. Additional processing is planned. Pass 1, in Figure 15, shows an unusually large defocus of nearly -20 dB, with some diffraction ringing at the edges. The depth and duration of this defocus, lasting approximately 75 s, is remarkable. Defocusing of this magnitude was not

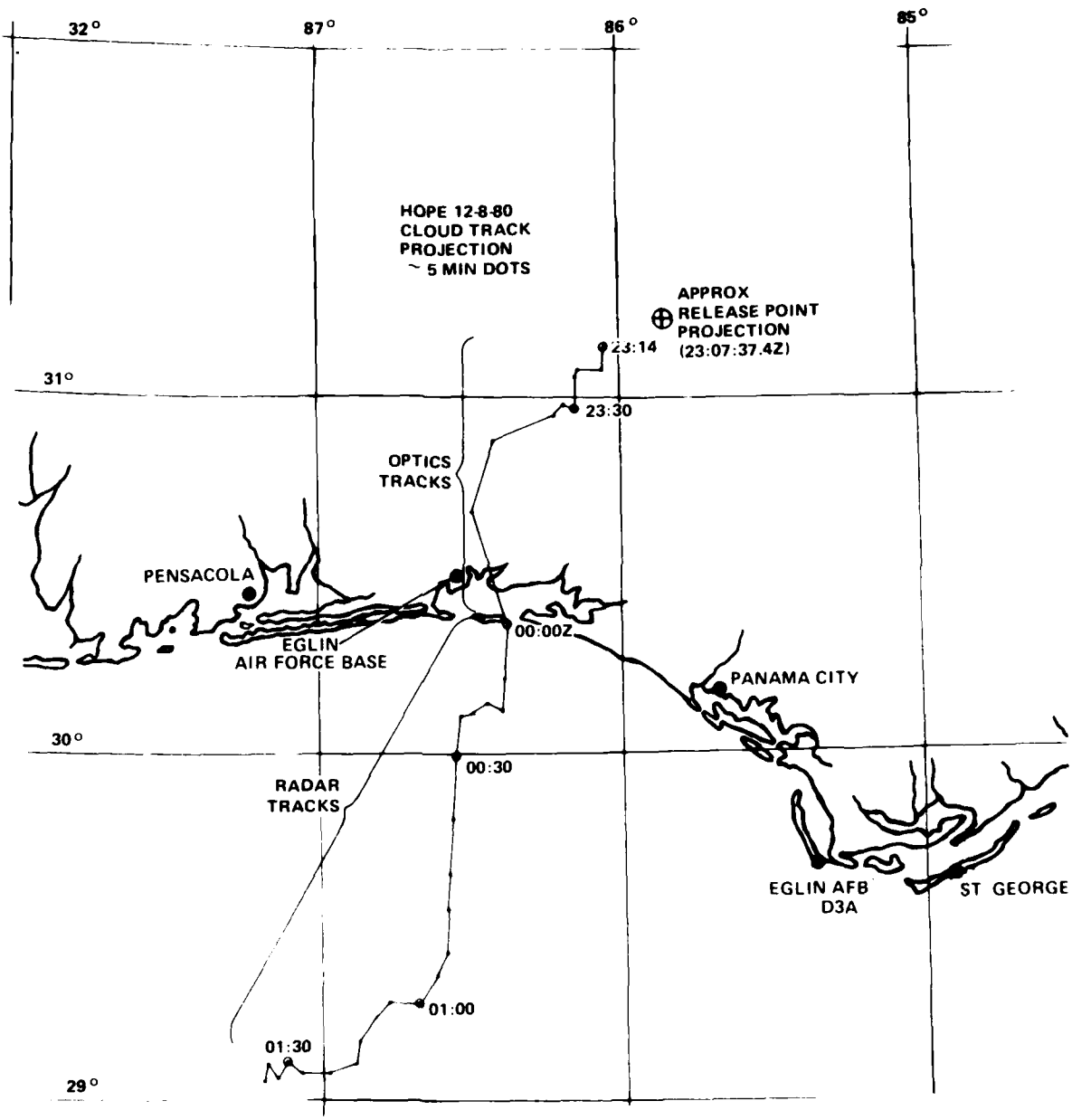

FIGURE 10 ION CLOUD TRACK PROJECTION FOR HOPE

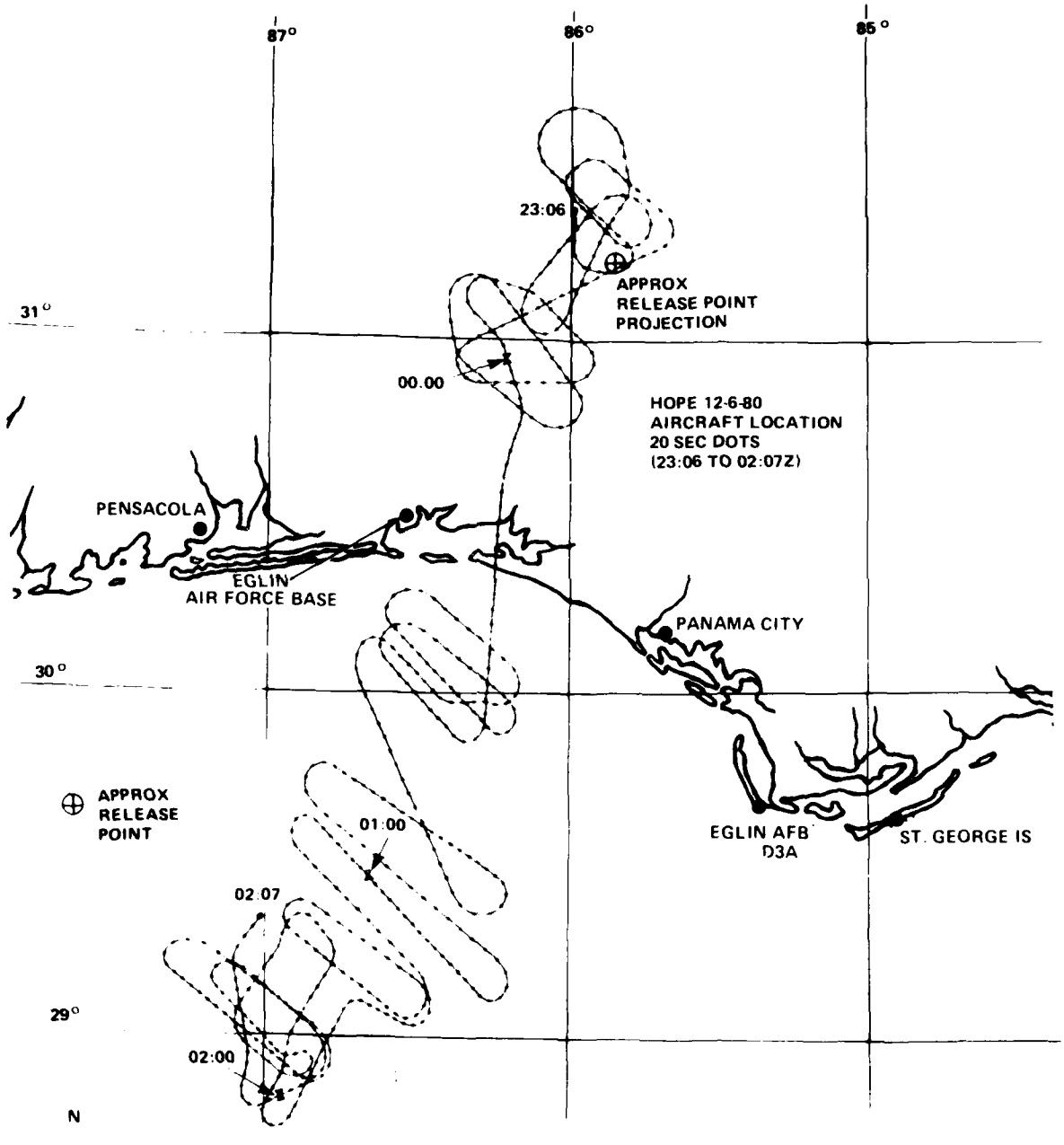

FIGURE 11 AIRCRAFT GROUND TRACK FOR HOPE

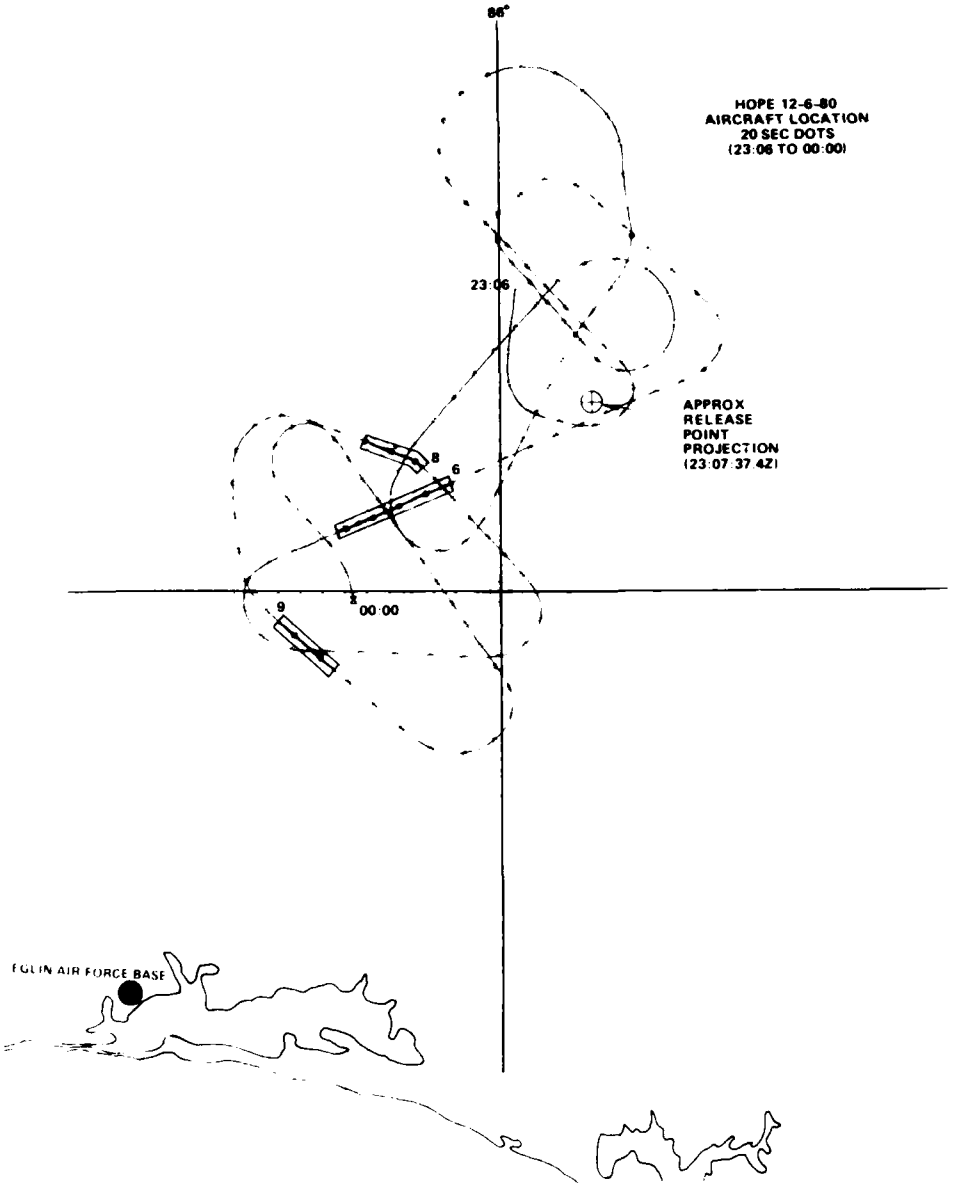

FIGURE 12 AIRCRAFT GROUND TRACK FOR HOPE FROM 23:06 TO 00:00Z. Periods of deep fading are shaded.

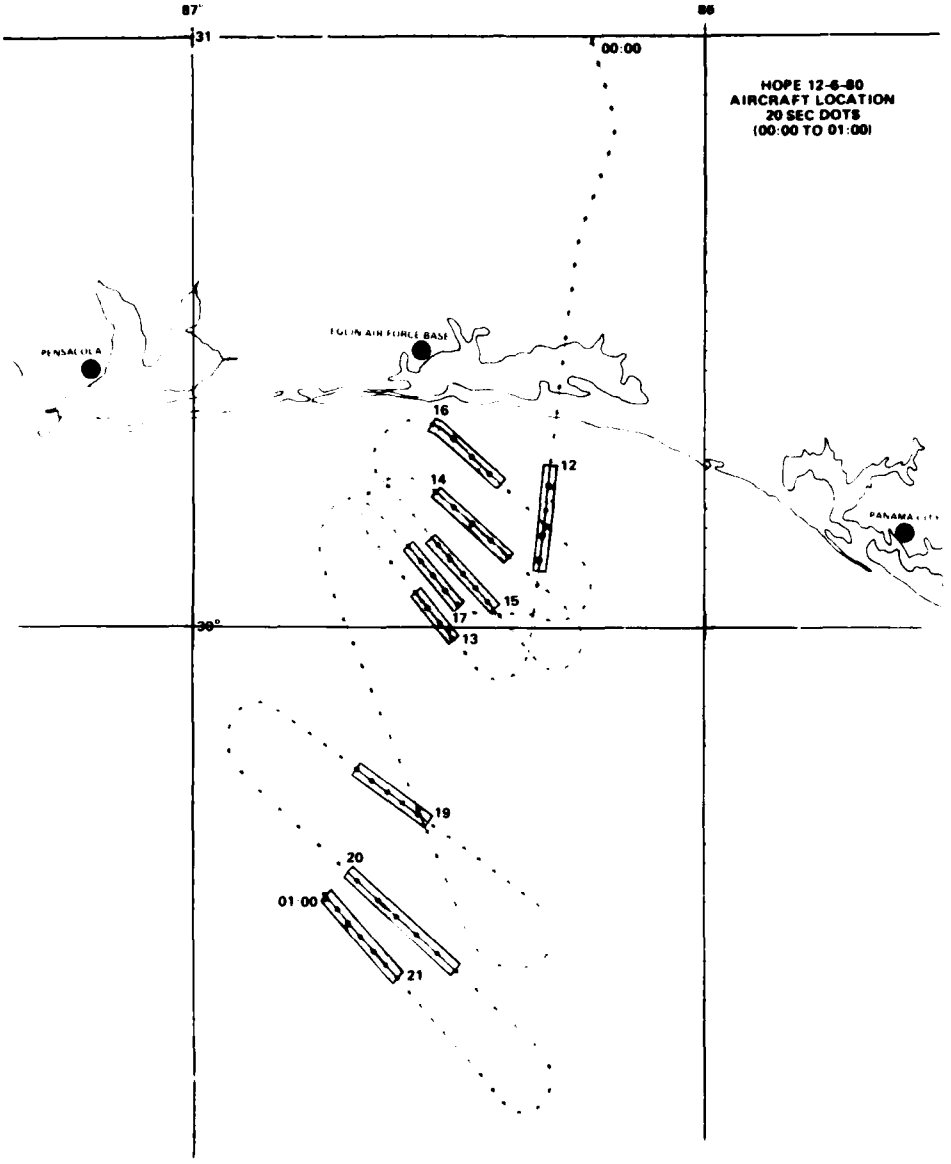

FIGURE 13 AIRCRAFT GROUND TRACK FOR HOPE FROM 00:00 TO 01:00. Periods of deep fading are shaded.

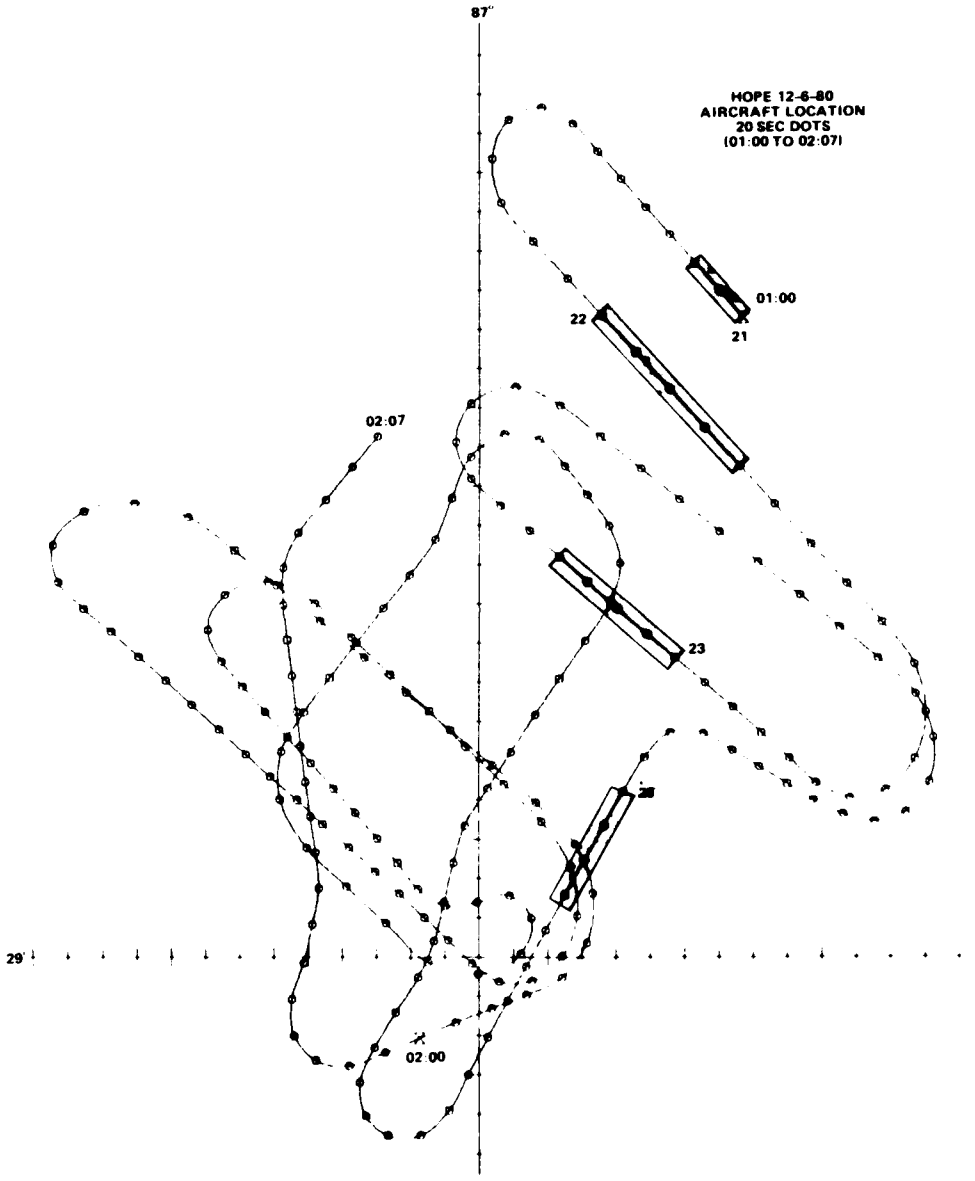

FIGURE 14 AIRCRAFT GROUND TRACK FOR HOPE FROM 01:00 TO 02:07. Periods of deep fading are shaded.

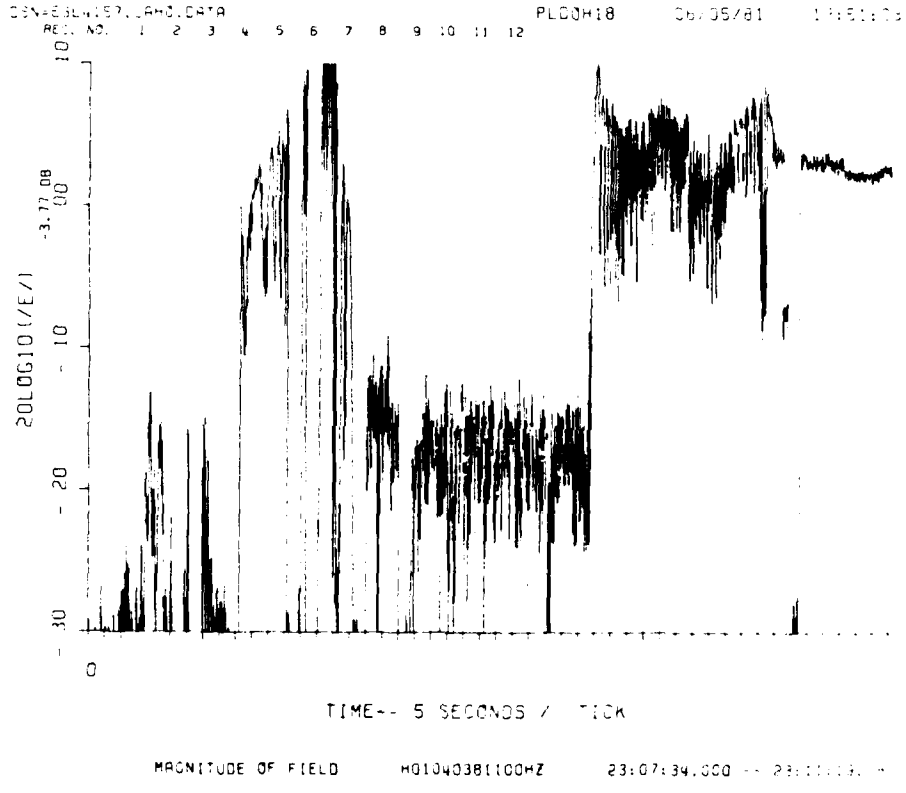

FIGURE 15 DOWNLINK FADING ON HOPE PASS 1, R + 1 MINUTES

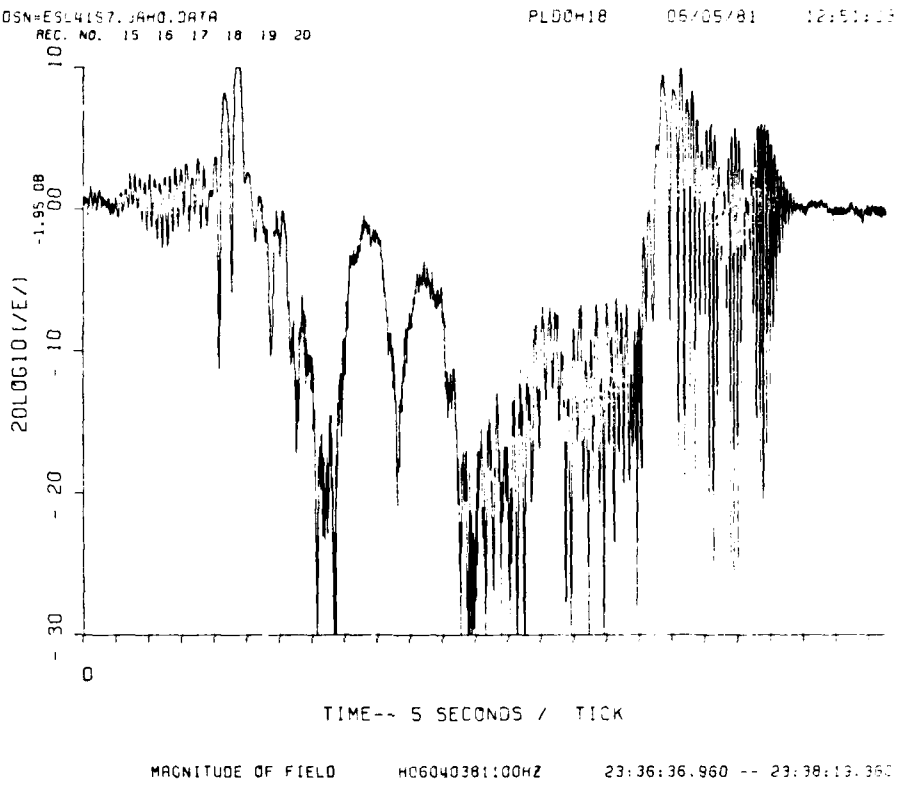

FIGURE 16 DOWNLINK FADING ON HOPE PASS 6, R + 30 MINUTES

observed during the prior STRESS experiment and is believed to be due in part to the alignment of the propagation path and the ion cloud drift (stretching) direction. If the initial stretching direction was along approximately 40° azimuth, and since the azimuth to the satellite at early times was approximately 210°, the raypath would make an angle of about 10° with the stretching direction of the cloud.

As time progresses, Pass 6 at R + 30 min (Figures 16 and 17) shows the development of some structuring superimposed on this still large defocus. This structuring is evident in the amplitude and phase characteristics in the latter half of the pass (cloud). Figures 18 and 19 show Pass 19 at 1 hr and 37 min; again, the slower fading amplitude characteristics

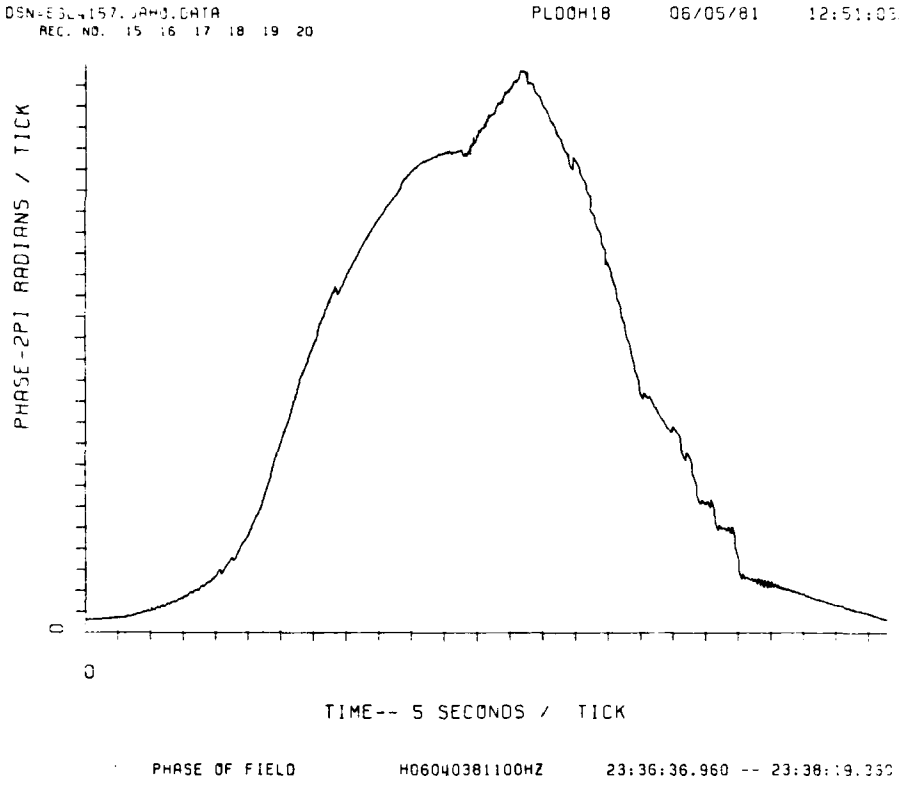

FIGURE 17 DOWNLINK PHASE EFFECTS ON HOPE PASS 6, R + 30 MINUTES

and smaller integrated electron content (less phase wind-up) of the background ion cloud are evident. These figures are indicative of the processed data quality available. The processing bandwidth can be reduced to improve signal quality still further in subsequent planned processing.

V TEST RESULTS FOR IRIS

The third barium release, IRIS, was on 8 December 1980 and occurred at 23:13:06.7. It was released at an altitude of 179.6 km and a location of 28.799°N, 87.166°W. The projection of this release point is 30°40'11"N, and 85°51'24"W. The cloud projection moved in a south-southeast direction

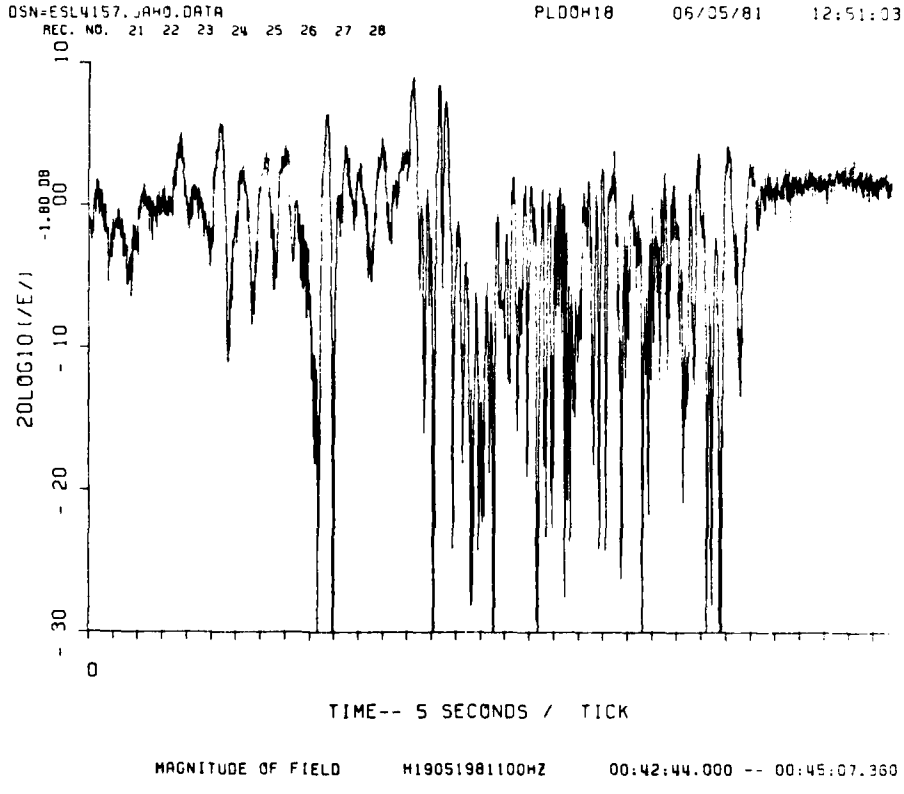

FIGURE 18 DOWNLINK FADING ON HOPE PASS 19, R + 1 HOUR 37 MINUTES

during the entire experiment and was last seen about 3° south and 0.75° east of the release point projection at R + 2 hr 30 min. Plots of the cloud track projection and aircraft ground track are given in Figures 20 and 21. Figures 22, 23, and 24 show the aircraft ground track for each hour, with intervals of strong fading indicated.

No cloud tracking data were available between release and R + 12 min. Optics track data were used from R + 12 min to R + 15 min, and radar track data were used thereafter. The release being low and west of the planned release point resulted in the radar not acquiring the release as planned. The radar track provided a consistent indication of the striation location throughout the night.

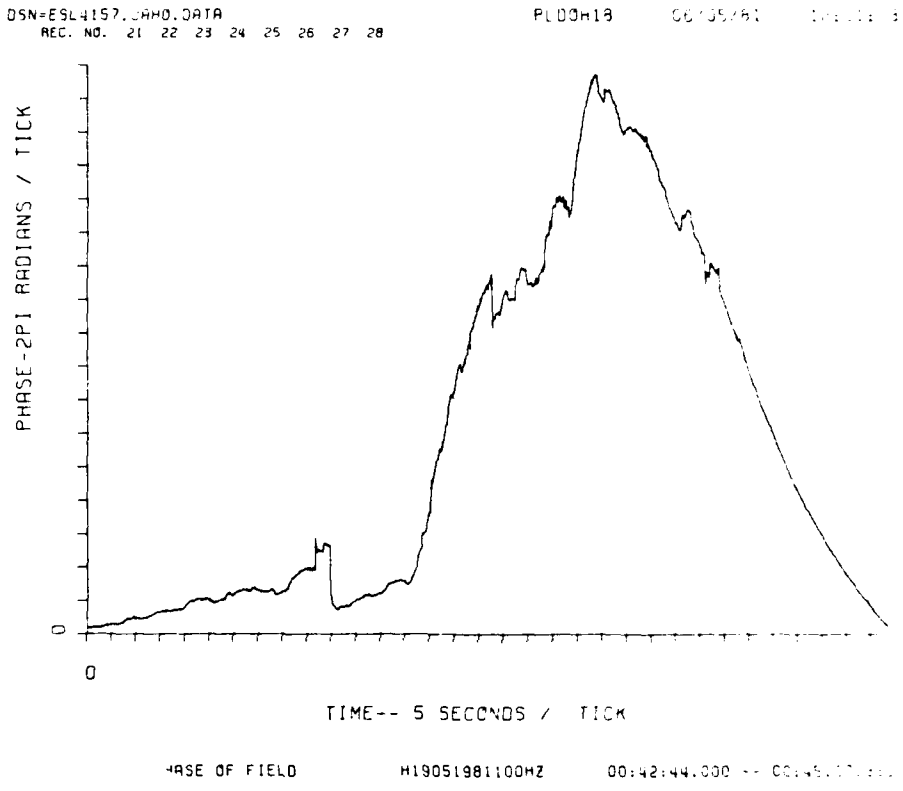

FIGURE 19 DOWNLINK PHASE EFFECTS ON HOPE PASS 19, R + 1 HOUR 37 MINUTES

A total of 31 passes were made, ending at R + 2 hr 48 min. The first strong fading was seen at R + 16 min, the fourth pass. Moderate to strong fading was present during 17 of the next 22 passes, with the last strong fading ending at R + 2 hr 26 min. The last fading seen ended at R + 2 hr 44 min during Pass 29.

Downlink data are available for all 31 passes. K-band lock was never achieved during this experiment, due to an oscillator failure; consequently, no usable uplink data were recorded. Manual Doppler correction was used throughout the night. Prior analyses have shown that the uncompensated Doppler will not corrupt the phase power spectral density data, but will make processing somewhat more difficult.

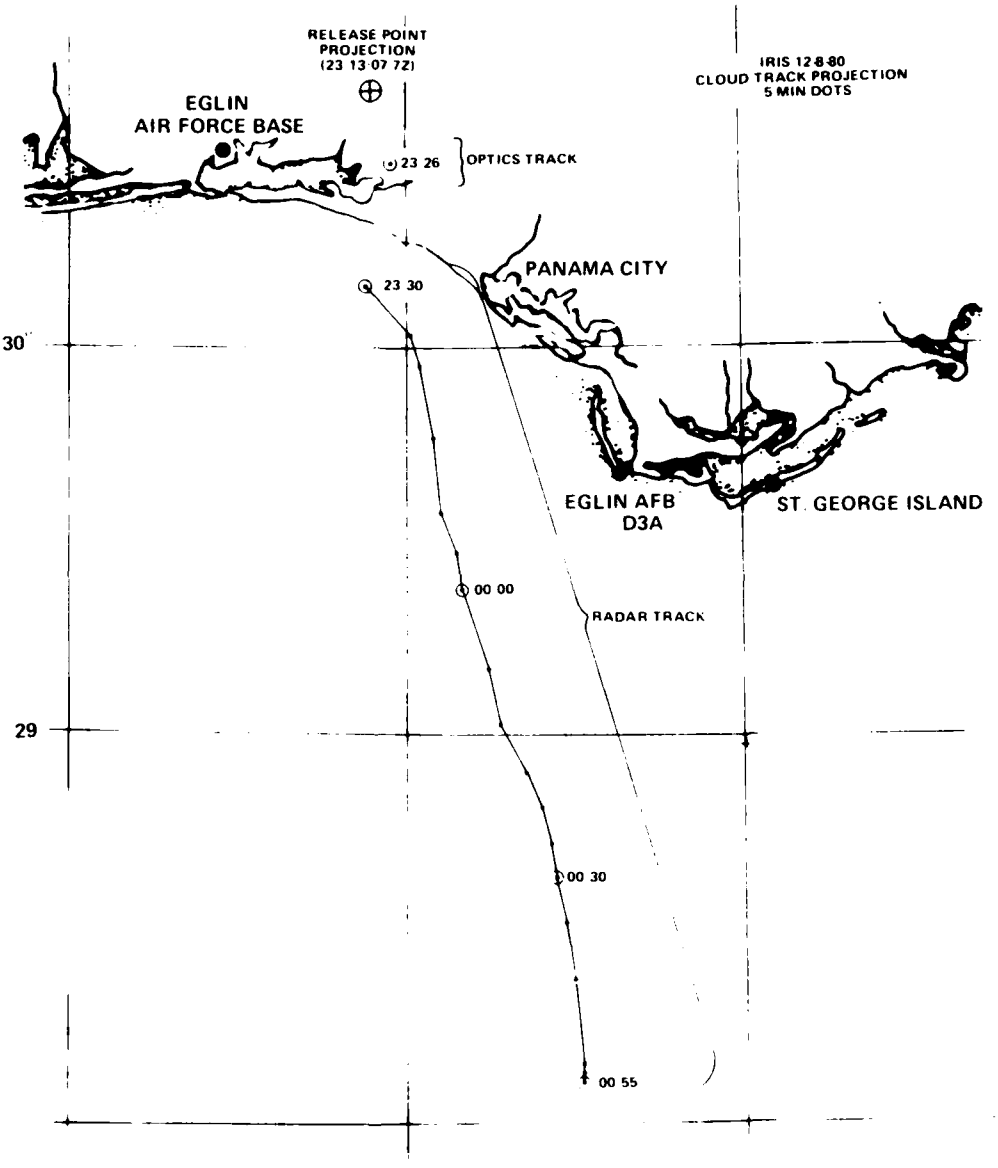

FIGURE 20 ION CLOUD TRACK PROJECTION FOR IRIS

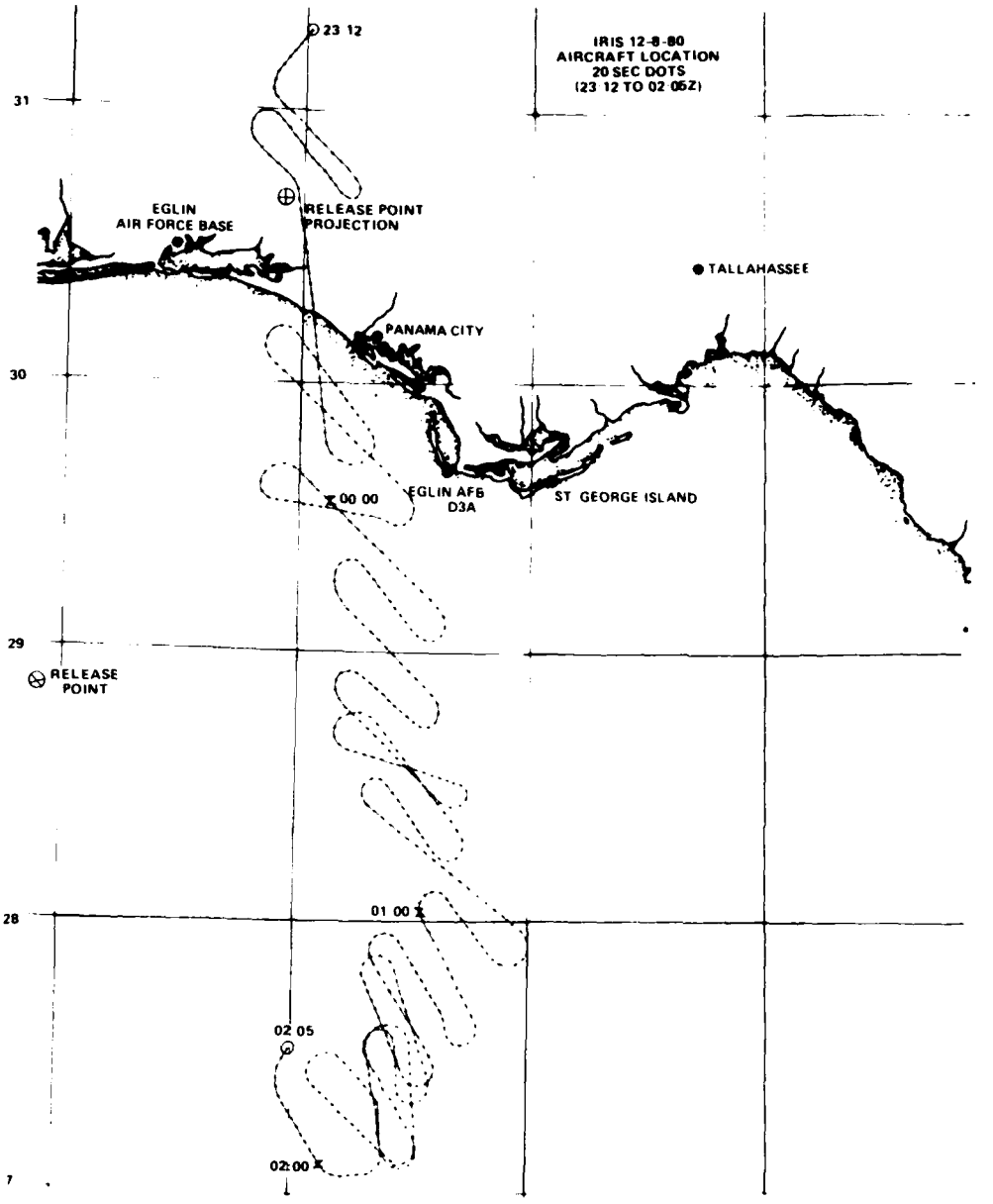

FIGURE 21 AIRCRAFT GROUND TRACK FOR IRIS

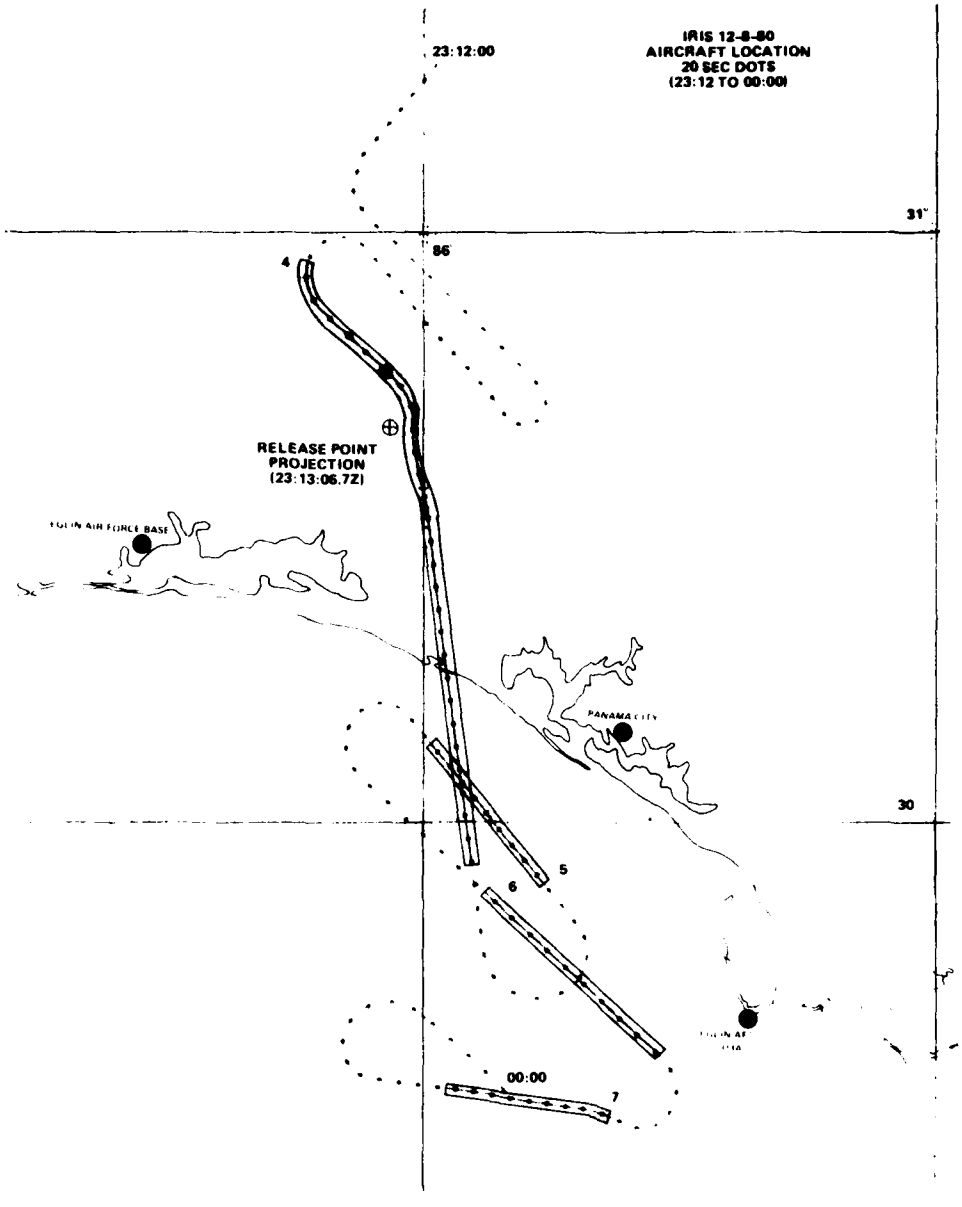

FIGURE 22 AIRCRAFT GROUND TRACK FOR IRIS FROM 23:12 TO 00:00Z. Periods of deep fading are shaded.

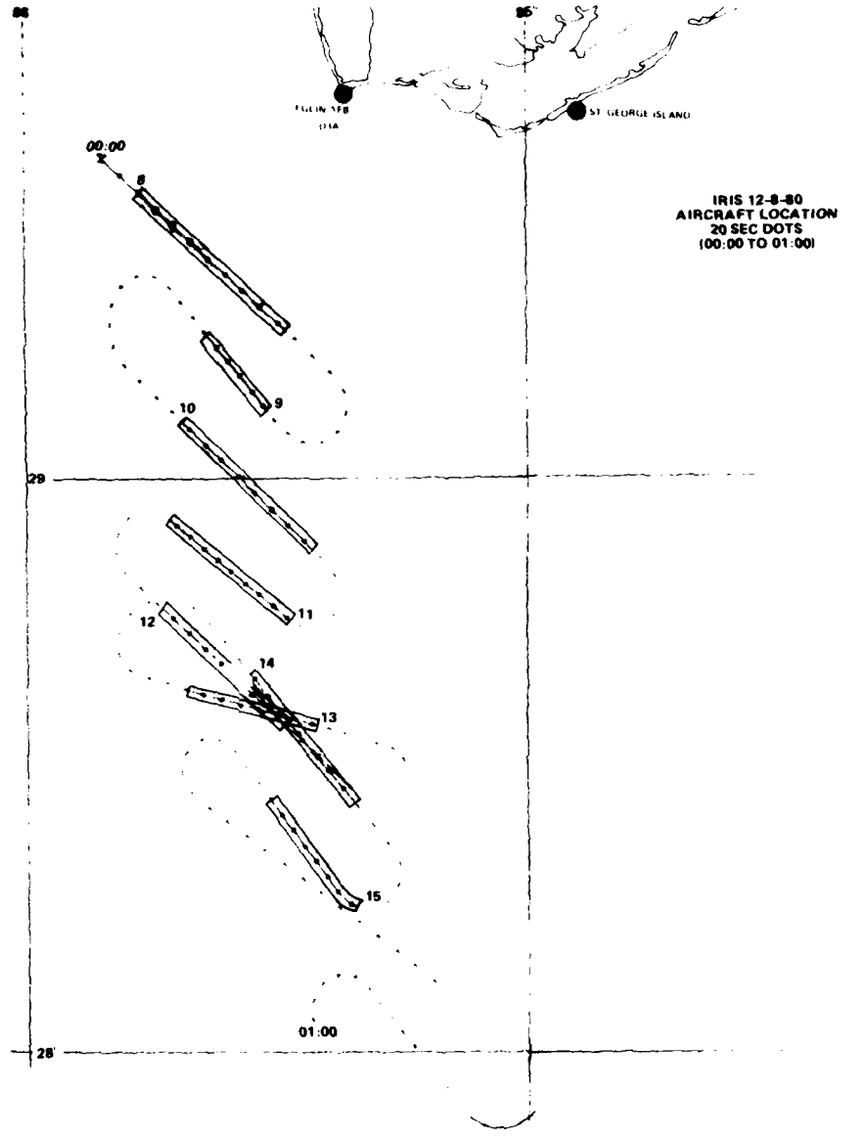

FIGURE 23 AIRCRAFT GROUND TRACK FOR IRIS FROM 00:00 TO 01:00Z. Periods of deep fading are shaded.

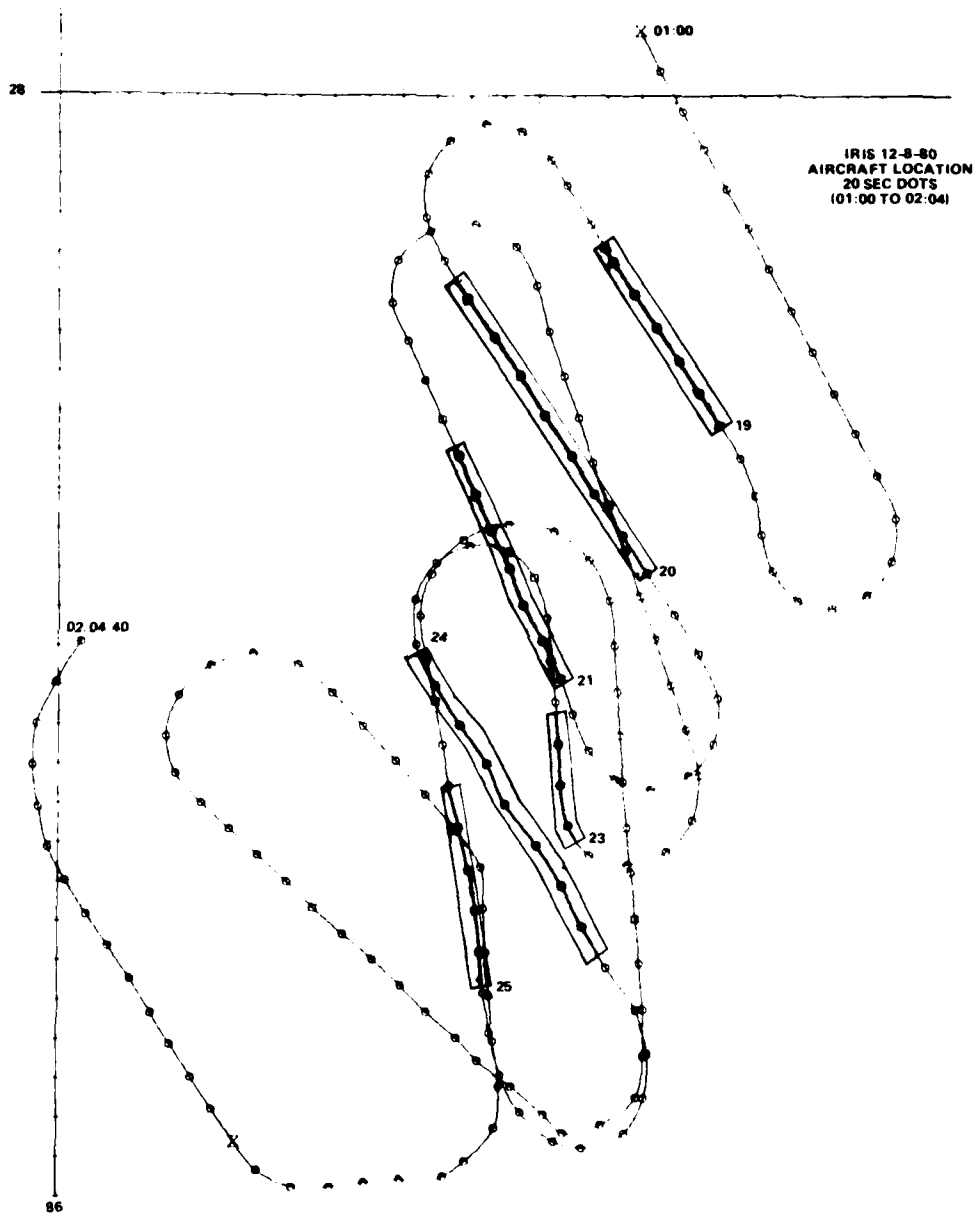

FIGURE 24 AIRCRAFT GROUND TRACK FOR IRIS FROM 01:00 TO 02:04Z. Periods of deep fading are shaded.

Sample plots of the downlink amplitude fading for IRIS are given in Figures 25 through 29. Passes 4 and 5 (R + 18 min and R + 26 min), shown in Figures 25 and 26, show a large -15 dB defocus with rapid, deep fading indicative of structure formation. As the ion cloud was stretched southeast, more perpendicular to the propagation path, this defocus is believed to be indicative of a high ion cloud density and not a geometric artifact. The first beacon rocket occultation occurred approximately 5 min 33 s following Pass 5 (Figure 26). Pass 6 (Figure 27) occurred approximately 2 min 37 s after the first occultation. Pass 7, shown in Figure 28, occurred approximately 5 min before the second occultation and showed strong well developed fading along with a shallow defocus. The next pass occurred approximately 4 min after the second occultation and shows very little fading activity. It is possible the aircraft passed north of the true cloud center and thus traversed the striations low on the field lines. As discussed earlier, a quick look at the radar data indicated a large drop in tracking altitude between the first and second occultations. These data need to be examined further to better establish cause and effect before reaching any conclusion.

VI TEST RESULTS FOR JAN

JAN, the fourth barium release, occurred on 12 December 1980 at 23:13:42. It was released at an altitude of 184.3 km and a location of 29.166°N, 86.993°W. This release drifted on an approximately 40° azimuth and then stopped for a few minutes. It then drifted very slowly west for the remainder of the experiment, with its projection ending up about 1° west of the initial release point projection.

Optics tracking was used until approximately R + 48 min. It gave reasonably consistent information on the cloud location during this time, but the track showed some abrupt changes. Radar tracking was available for the remainder of the experiment, but was inconsistent with the fading observed. The striated portion of the ion cloud was followed using the real-time fading displays and the radar tracking of the aircraft. Plots of the available cloud tracking data and the aircraft ground track are

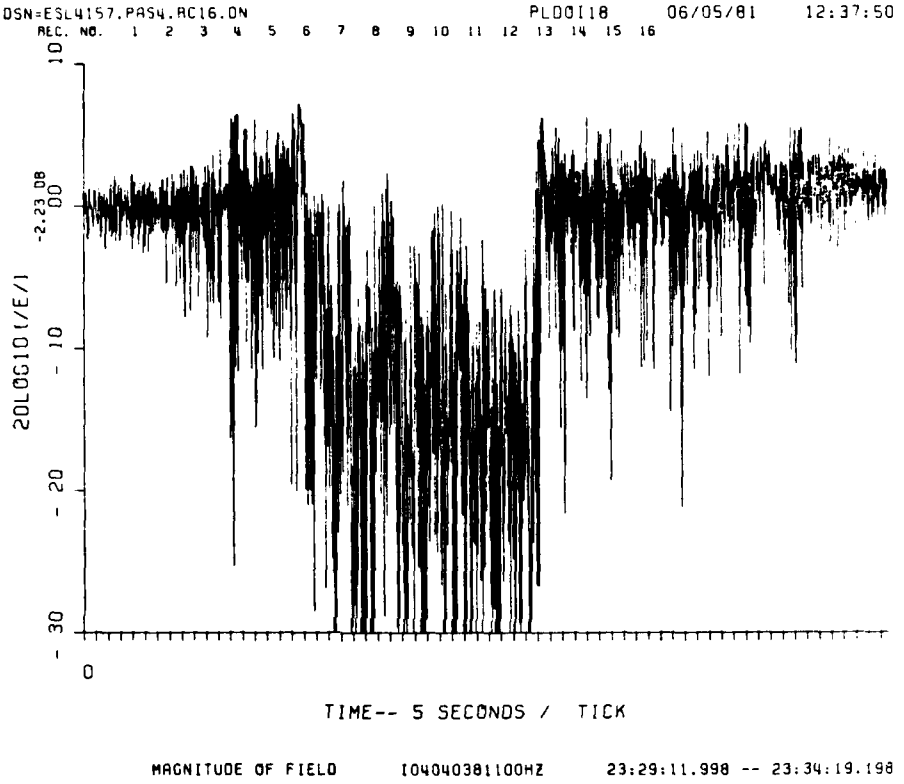

FIGURE 25 DOWNLINK FADING ON IRIS PASS 4, R + 18 MINUTES

given in Figures 30 and 31. Figures 32, 33, and 34 show the aircraft ground track during each hour along with periods of strong fading.

A total of 35 passes were made ending at R + 3 hr 33 min. Diffraction ringing with large ~15 dB defocus was seen during the first three passes. Strong fading was present for all 18 passes between R + 24 min and R + 1 hr 2 min. Very good data were received during this time. Moderate to strong fading was present in four of the next eight passes, ending at R + 2 hr 44 min. Fading was seen as late as R + 2 hr 54 min.

Uplink and downlink data were received for all passes. K-band lock was not lost during this release. Overall, it is believed that the highest quality data were obtained during JAN.

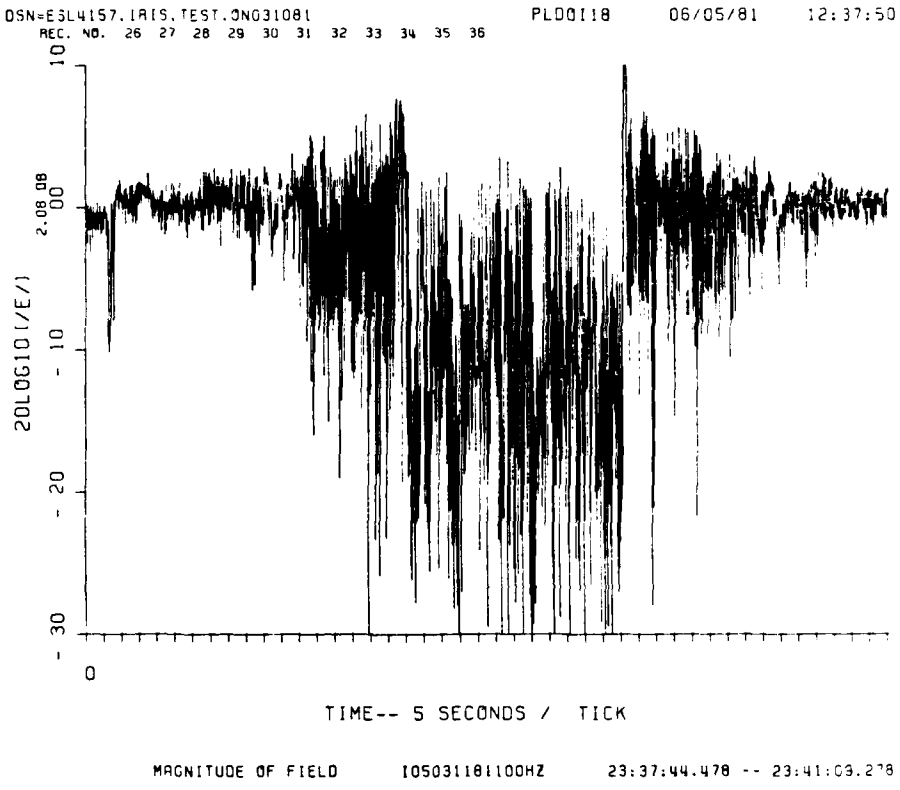

FIGURE 26 DOWNLINK FADING ON IRIS PASS 5, R + 26 MINUTES

Samples of processed amplitude and phase plots for JAN are given in Figures 35 and 39. They show the full progression of cloud development from diffraction ringing to strong deep fading, to the eventual loss of track. These figures have been processed from the uplink tone data.

Figure 35 shows the strong diffraction ringing that was noted about 1 min after release on the first pass. This developed into a large defocus of -10 dB by R + 6 min, as shown in Figures 36 and 37. No structuring is evident during this pass. Again, the alignment of the ion cloud stretch direction with the propagation path may influence the manifestation of the large defocus. Figure 38 shows a large -20 dB defocus with some

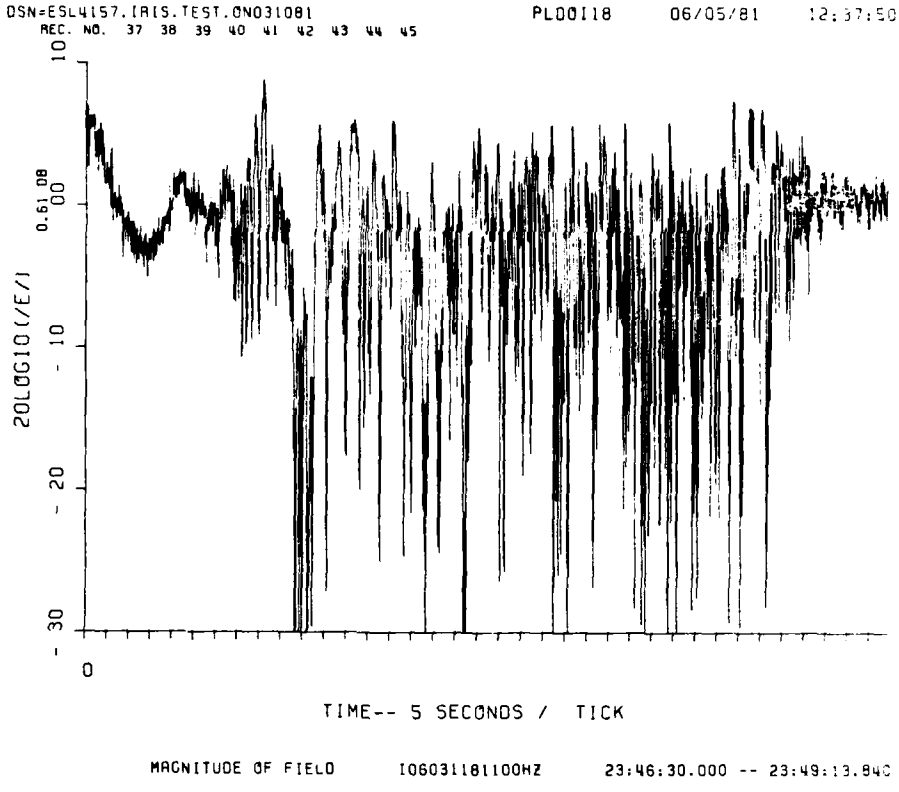

FIGURE 27 DOWNLINK FADING ON IRIS PASS 6, R + 34 MINUTES

developing structure. Figures 39 and 40 show the fading at 1 hr 30 min after release. The last significant fading seen during JAN was R + 2 hr 42 min.

The integrated electron content decreased considerably over the course of the JAN release as one would expect. This is evident in the total phase windup of each subsequent aircraft pass. The phase windup varied from 109π radians in Pass 2 to 5π radians in Pass 29. The integrated electron content is shown plotted for JAN in Figure 41.

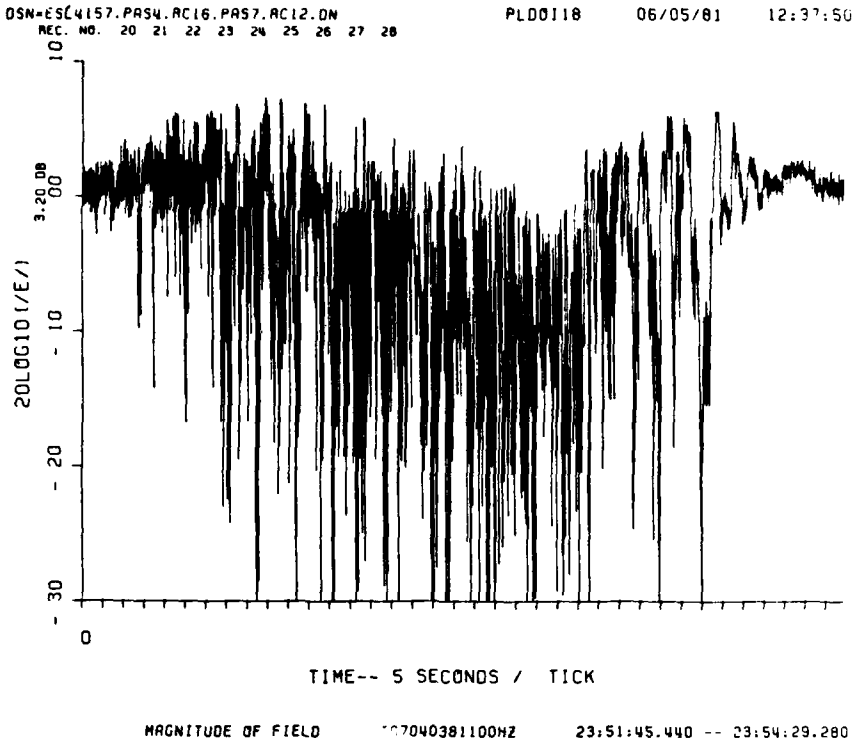

FIGURE 28 DOWNLINK FADING ON IRIS PASS 7, R + 39 MINUTES

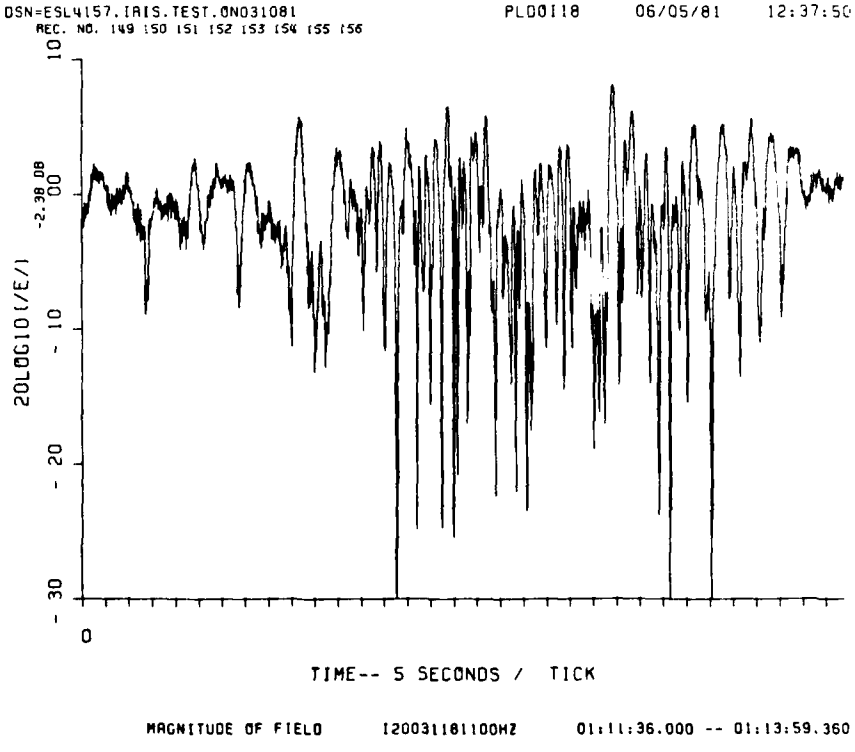

FIGURE 29 DOWNLINK FADING ON IRIS PASS 20, R + 2 HOURS

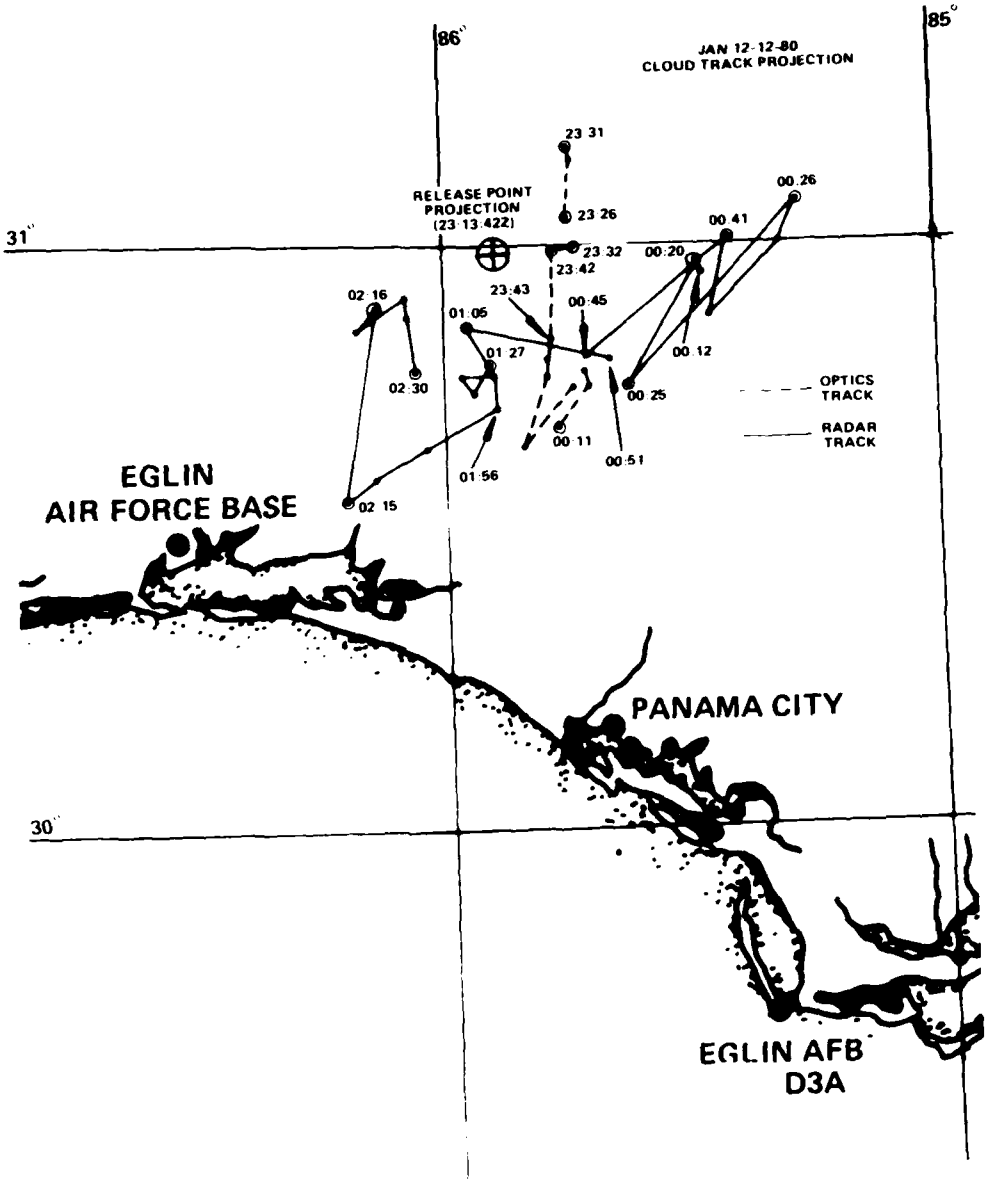

FIGURE 30 ION CLOUD TRACK PROJECTION FOR JAN

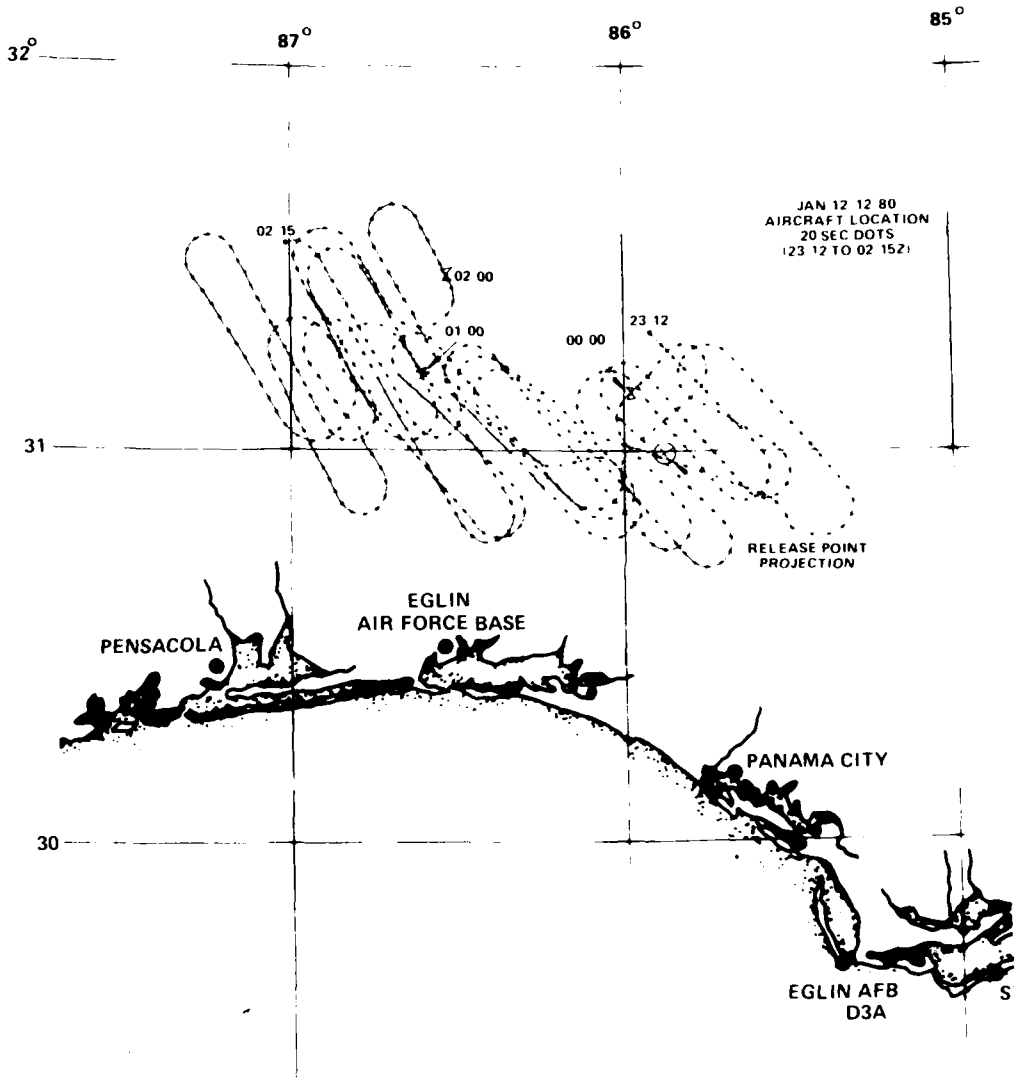

FIGURE 31 AIRCRAFT GROUND TRACK FOR JAN

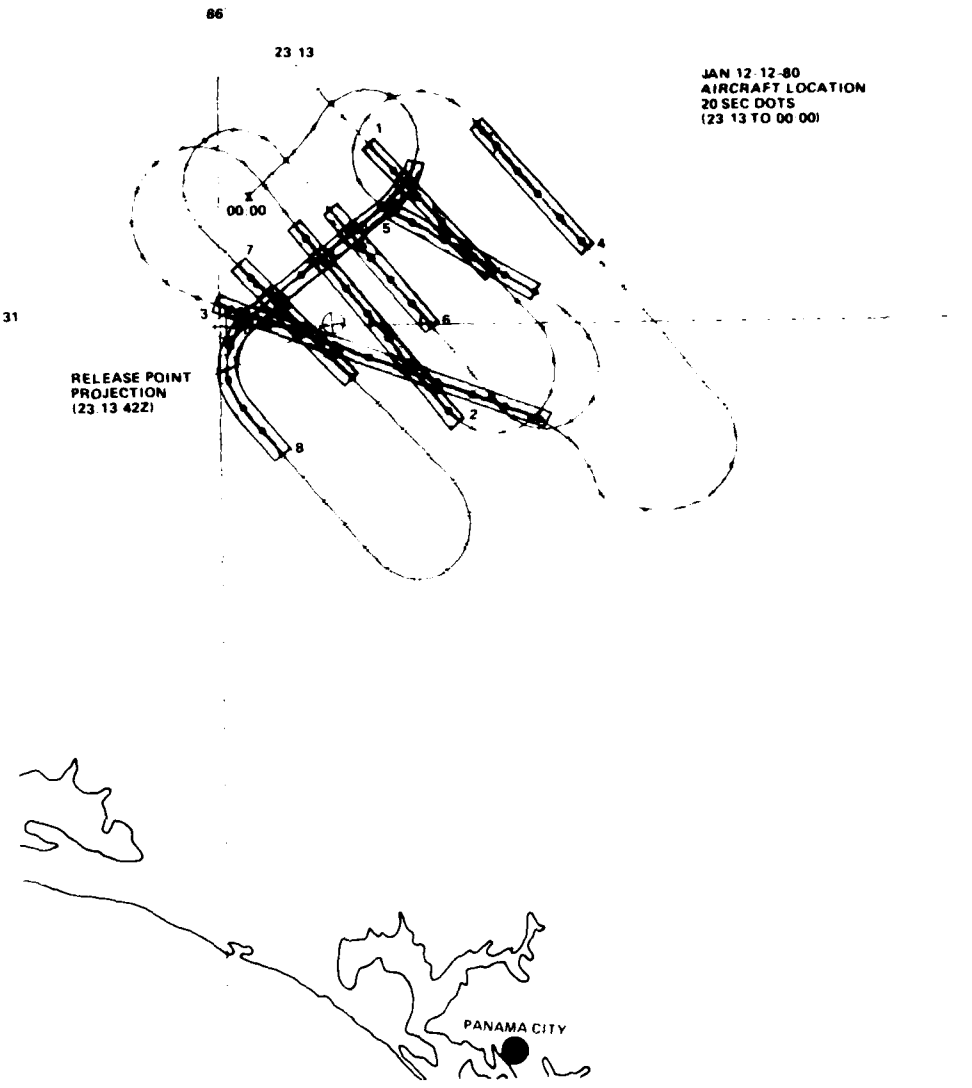

FIGURE 32 AIRCRAFT GROUND TRACK FOR JAN FROM 23:13 TO 00:00Z. Periods of deep fading are shaded.

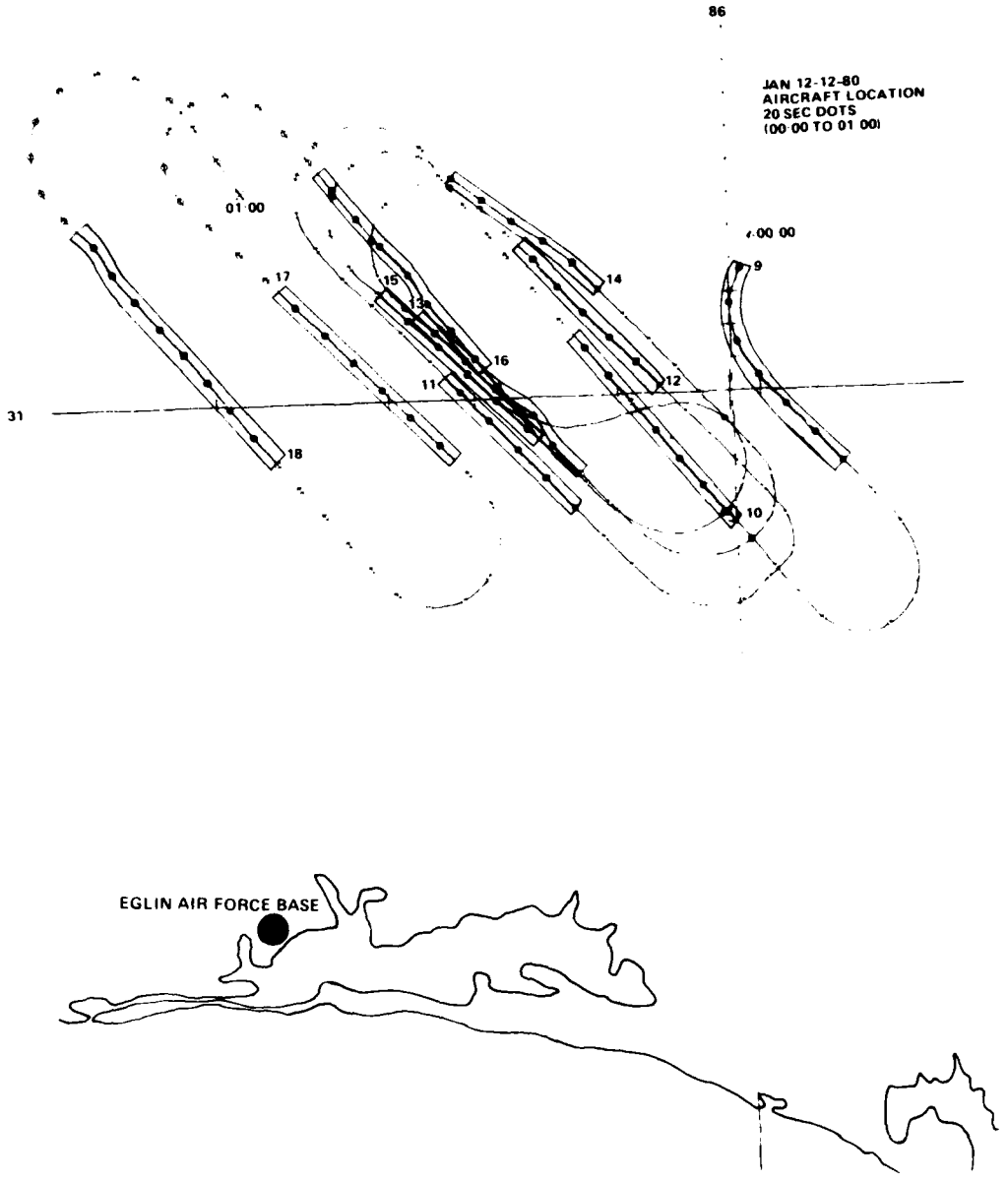

FIGURE 33 AIRCRAFT GROUND TRACK FOR JAN FROM 00:00 TO 01:00Z. Periods of deep fading are shaded.

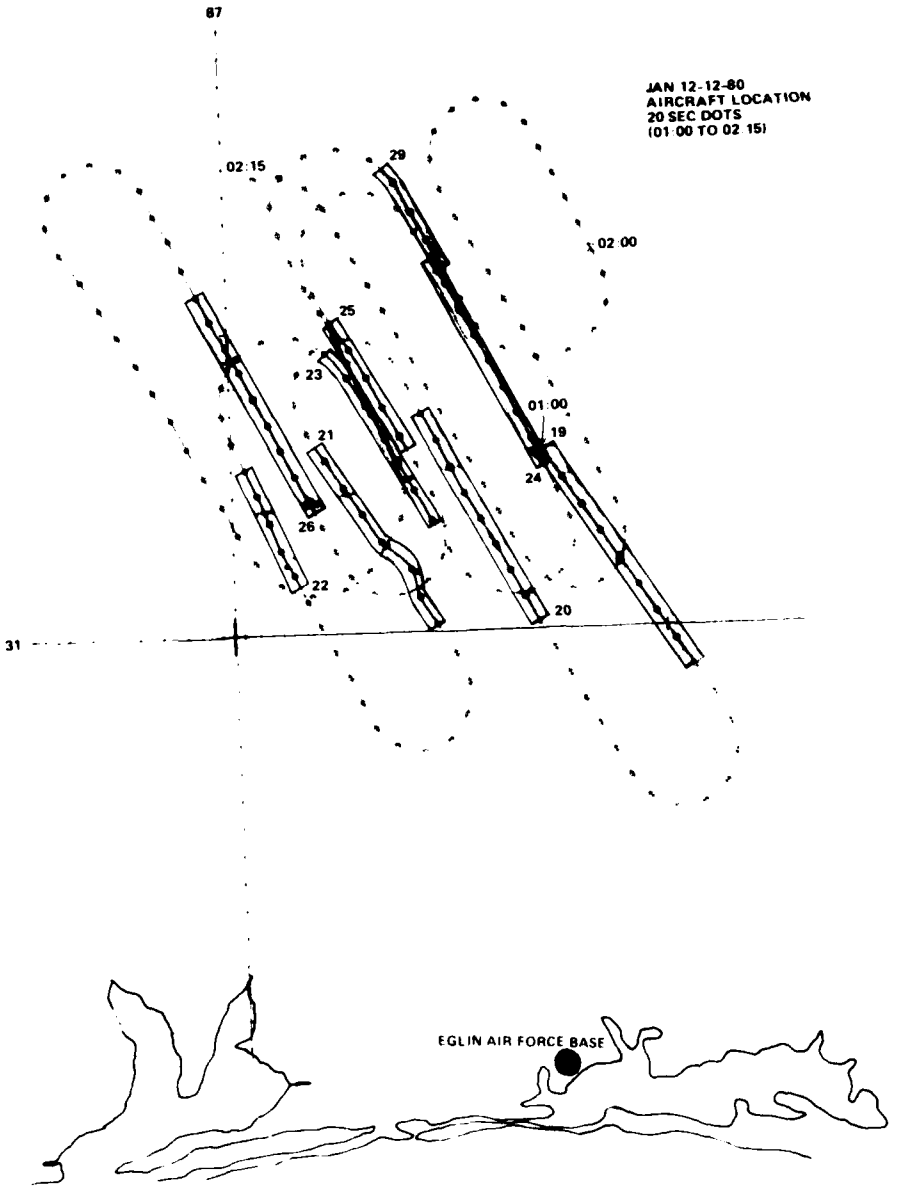

FIGURE 34 AIRCRAFT GROUND TRACK FOR JAN FROM 01:00 TO 02:15Z. Periods of deep fading are shaded.

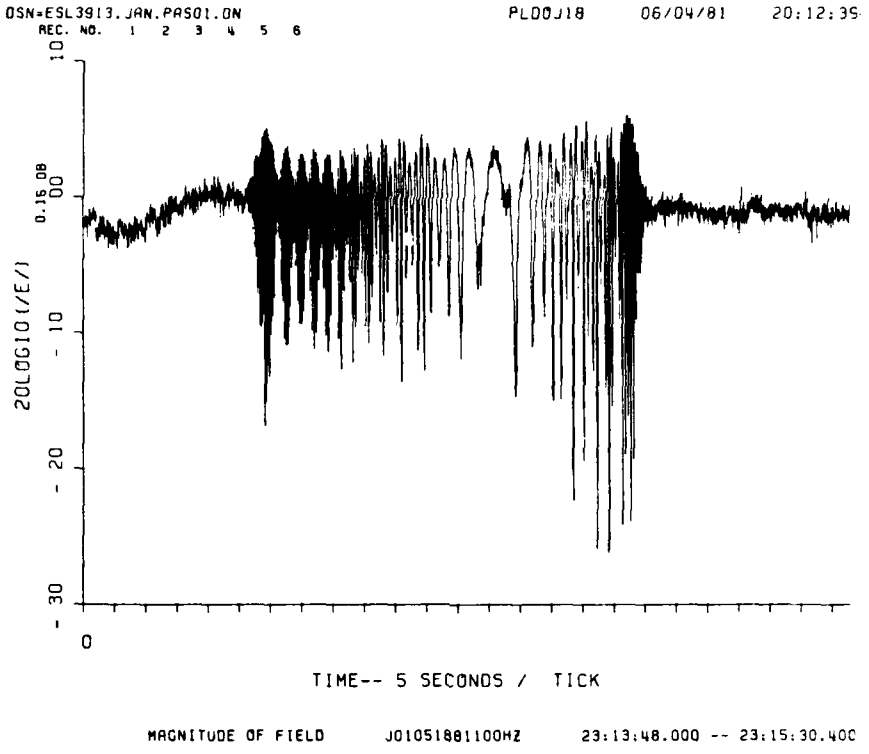

FIGURE 35 DOWNLINK FADING ON JAN PASS 1, R + 36 SECONDS

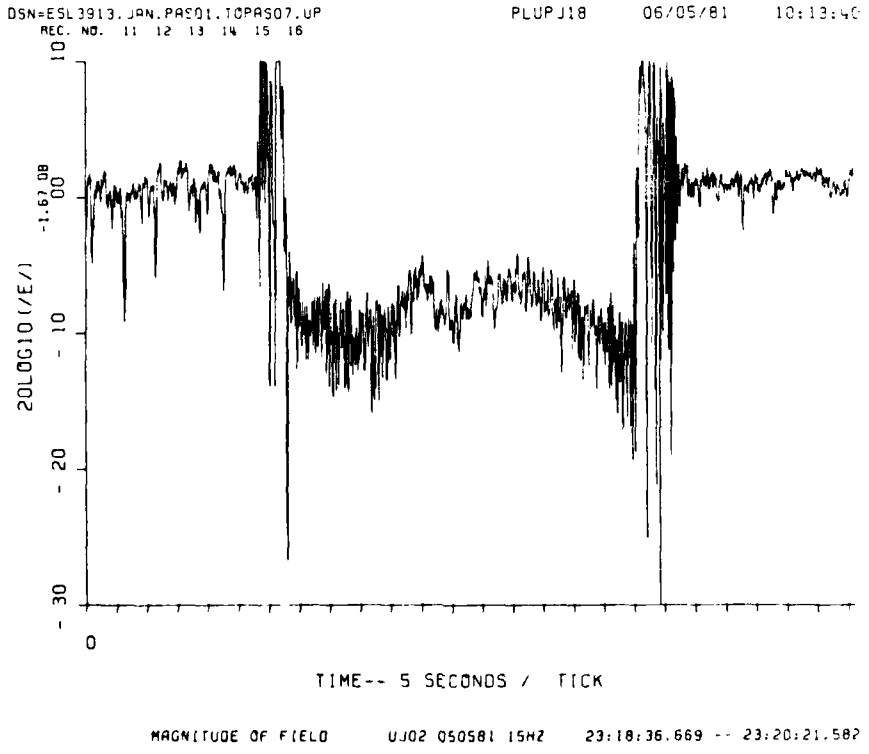

FIGURE 36 UPLINK FADING ON JAN PASS 2, R + 6 MINUTES

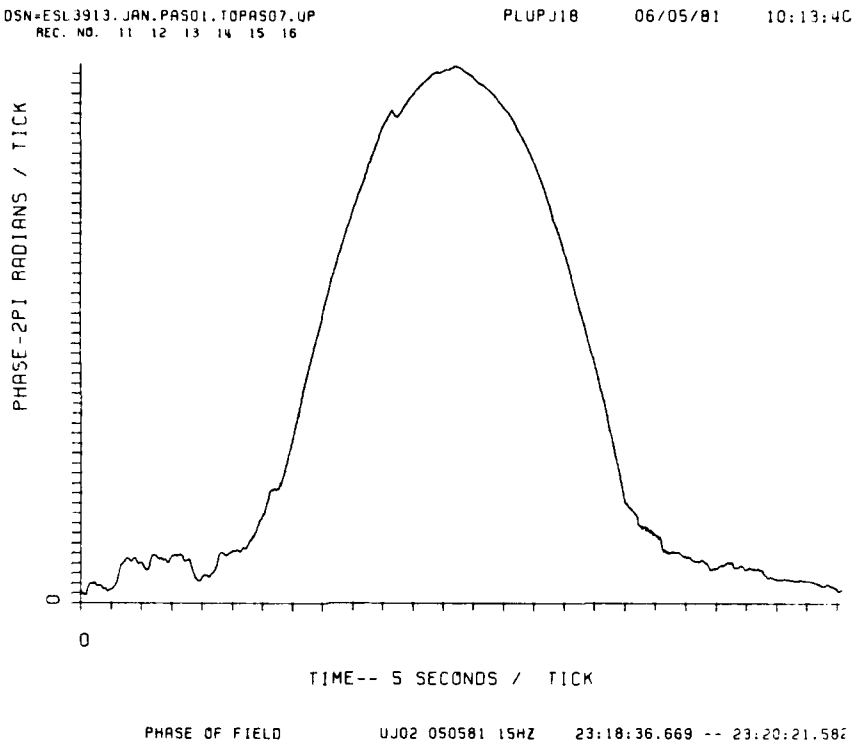

FIGURE 37 UPLINK PHASE EFFECTS ON JAN PASS 2, R + 6 MINUTES

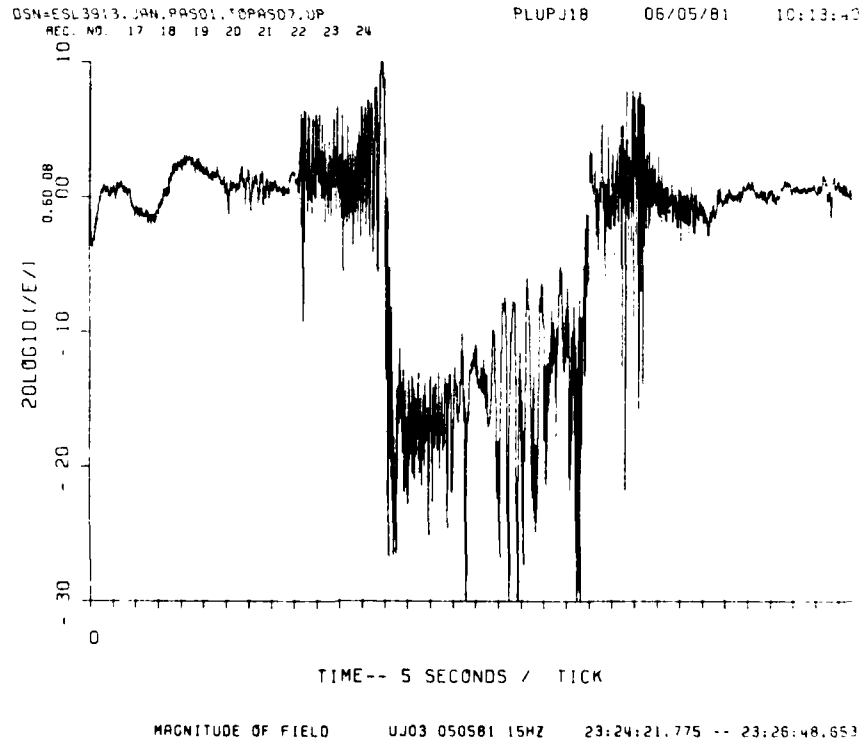

FIGURE 38 UPLINK FADING ON JAN PASS 3, R + 13 MINUTES

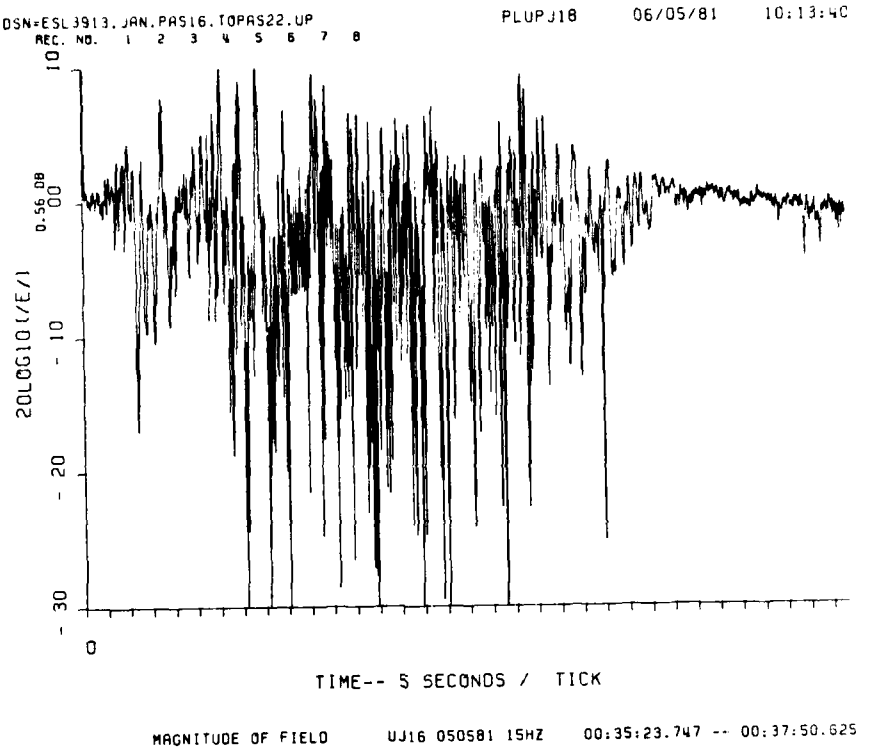

FIGURE 39 UPLINK FADING ON JAN PASS 16, R + 1 HOUR 30 MINUTES

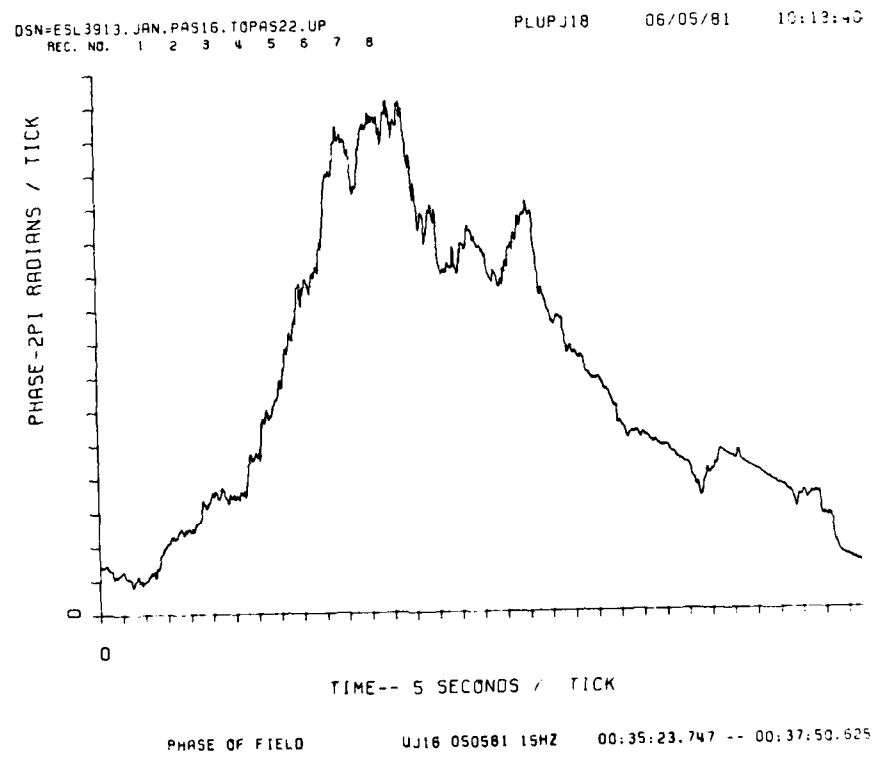

FIGURE 40 UPLINK PHASE EFFECTS ON JAN PASS 16, R + 1 HOUR 30 MINUTES

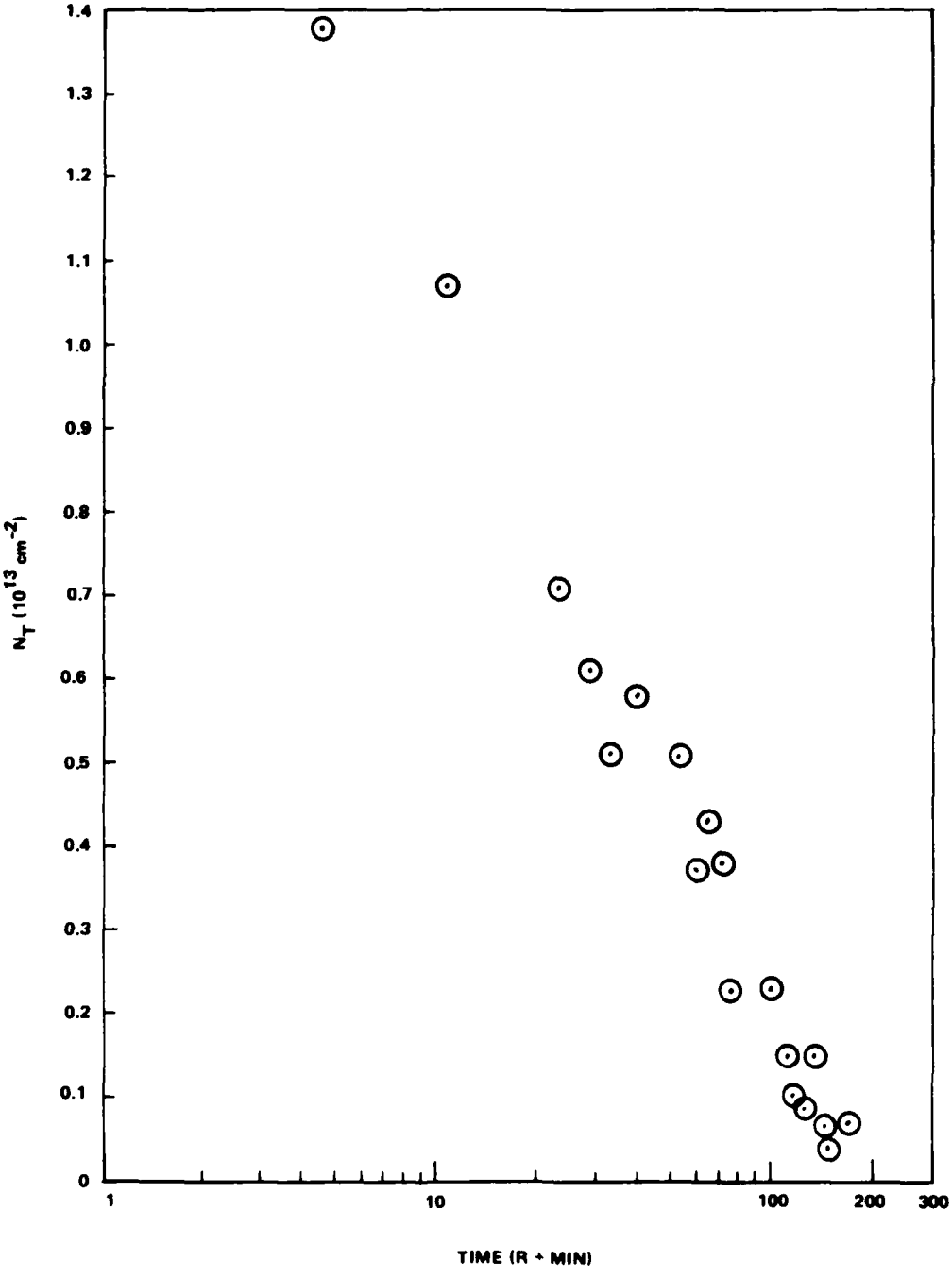

FIGURE 41 INTEGRATED ELECTRON CONTENT vs TIME FOR JAN

VII CONCLUSIONS

The PLACES Aircraft Experiment measured the propagation characteristics of the striated barium ion cloud using the LES-8 satellite in a manner similar to the STRESS experiment. The primary utility of these data is to provide information on striation evolution to late times that can aid theoretical developments. Additionally, the experiment provides an opportunity to work in a "hands on" real world situation with satellite communication systems, striated plasmas, and propagation data that facilitate the physical interpretation of theoretical calculations and predictions. These data have also been helpful in interpreting the beacon experiment results. The downlink tone data obtained during PLACES is of higher quality than that obtained during the STRESS experiment of 1977. Only limited downlink data were available from STRESS due to conflicts with higher priority communication tests. The uplink tone data are believed to be of about the same quality.

The scintillation effects observed are similar to those observed during STRESS, with the exception of the long, deep defocusing seen at early times. During HOPE a -20 dB defocus lasted for approximately 75 s. From this, it should be obvious that even large chunks of high-density plasma ($\sim 10^7$ cm^{-3}) can be important to UHF satellite communication systems.

The IRIS cloud moved rapidly southeast and should therefore have resulted in a morphologically older cloud faster than seen before. Its data are also of interest around the beacon occultation time. JAN, on the other hand, moved more slowly than any event observed before. JAN should yield the highest quality data. Back-propagation processing of these signals to provide estimates of the integrated plasma content through the ion cloud striations is planned during subsequent processing. It is anticipated that these data may be able to provide insight into current issues in striation phenomenology, such as freezing. Freezing is a postulated late-time phenomenon wherein bifurcation stops and the striations move as a unit. The processing software and techniques for reducing the aircraft data were developed during the STRESS data reduction. This same software will be used during the PLACES data reduction.

COMPOSITION AND STRUCTURE MEASUREMENTS IONOSPHERIC BARIUM CLOUD

R. Narcisi, E. Trzcinski, G. Federico, L. Wlodyka, and P. Bench

Air Force Geophysics Laboratory
Hanscom AFB, Massachusetts 01731

ABSTRACT

A 48-kg barium payload was launched from Eglin Air Force Base, Florida, on 12 December 1980 at 2311 UT and detonated at 182.7 km. At 2342:50.8 UT a second rocket, instrumented with an ion mass spectrometer and pulsed plasma probes, penetrated the barium cloud between 147 and 184 km. Composition, ion density, and structure measurements were acquired in both the natural and the disturbed ionosphere. This preliminary report presents the results from the mass spectrometer only. A brief description of the instrumentation and measurement program is also included.

I INTRODUCTION

The only in-situ measurements of atmospheric barium releases are those of the electron density structure performed by Baker and Ulwick[1]* as part of the Defense Nuclear Agency's (DNA) STRESS program. Kelley et al.[2] analyzed the STRESS results and demonstrated that the late-time barium striations agreed with non-linear Rayleigh-Taylor instability development--the same mechanism believed to create equatorial spread F.

This paper describes the first measurements of the ion composition and structure/made in a barium cloud. The effort was part of the DNA PLACES (Position Location And Communication Effects Simulations) program.

---

*References are listed at the end of this paper.

The barium/probe rocket pair and associated measurements were further designated as Event "JAN."

The barium payload was launched from the Eglin Air Force Base, Florida, Test Range on 12 December 1980 at 2311 UT, releasing 48 kg of barium at 182.7 km. At 2342:50.8 UT a Terrier Tomahawk rocket payload was launched containing an ion mass spectrometer and pulsed plasma probes targeted to penetrate the barium cloud. In this preliminary report we present the instrumentation, measurement technique, and data from the ion mass spectrometer only.

II INSTRUMENTATION AND MEASUREMENT PROGRAM

The mass spectrometer was mounted at the forward end of the payload along the vehicle's axis. It was activated following the release of the nose cone, which also removed the vacuum cap. The payload included an attitude control system (ACS) that aligned the payload's axis with the magnetic field to minimize perturbations on the pulsed plasma probes. The ACS maintained the payload to within ±5° of the magnetic field on ascent and on most of descent. Also, the roll rate was held to within $\pm 0.6°\ s^{-1}$. Nevertheless, the angle of attack between the velocity vector and the spectrometer axis was still favorable (less than 25° to about 200 km on upleg) but the angle of attack became large on descent.

Figure 1 shows a schematic of the quadrupole ion mass spectrometer. The two significant data outputs were the total positive ion current collected on the aperture plate for ionospheric structure measurements, and the mass spectra output for species composition. The measurement program for the instrument is presented in Table 1. The spectrometer sampled 64 masses digitally for 10 ms each, yielding a total program period of 0.64 s. The mass number repetitions provided measurements with high spatial resolution. Above 145 km, the aperture plate had a 1 to 1.5 m altitude resolution (varying with vehicle velocity), while the barium and oxygen ion measurements had a resolution of 50 to 65 m. The species identifications for the associated mass numbers in Table 1 are $14(N^+)$, $16(O^+)$, [contaminants from outgassing water vapor of $17(OH^+)$, $18(H_2O^+)$, and $19(H_3O^+)$], $23(Na^+)$,

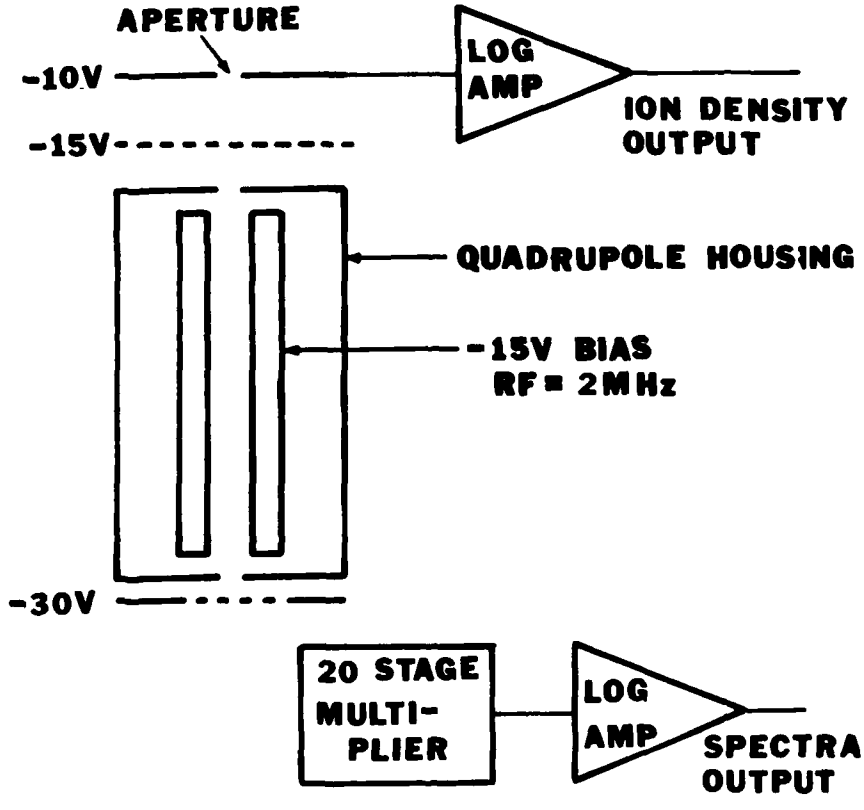

FIGURE 1 SCHEMATIC OF THE QUADRUPOLE ION MASS SPECTROMETER

Table 1

SPECTROMETER PROGRAM FOR THE MEASUREMENT OF
SELECTED ION MASS NUMBERS AT HIGH SPATIAL RESOLUTION

Sequence Number	Mass No.--AMU				
1	16	14	30	136	138
2	16	14	32	136	138
3	16	14	30	136	138
4	16	14	32	136	138
5	16	14	30	136	138
6	16	14	32	136	138
7	16	14	30	136	138
8	16	14	32	136	138
9	16	14	30	136	138
10	13	14	15	16	17
11	18	19	21	23	24
12	27	28	30	32	69
13	136	138	40	56	

Sample rate: 10 ms/AMU
Program time: 0.64 s

24(Mg^+), 27(Al^+), 28(Si^+), 30(NO^+), 32(O_2^+), 40(Ca^+), 56(Fe^+), 69(Ba^{++}), 136-138(Ba^+). The remaining mass numbers were sampled to establish background levels. The barium isotopes of 136 and 138 with relative abundances of 7.81% and 71.66%, respectively, were chosen to provide an added factor of about 9 in sensitivity, in case 138 went off scale (exceeding 10^7 ions cm^{-3}).

III RESULTS AND DISCUSSION

Composition measurements were acquired between 142 and 241.2 km on upleg and on downleg to 180 km, below which the large angle of attack caused signal drop-out. The ion species measured included O^+, NO^+, O_2^+,

Ba^+, Ba^{++}, Ca^+, and H_2O^+; all other species were below the detection limit of 50 ions cm^{-3}.

Figure 2 presents the ascent measurements of O^+, NO^+, O_2^+, and Ba^+. To obtain density values for all species, a single conversion factor of 1.67 (± 50%) x 10^{12} ions cm^{-3} amp^{-1} may be utilized. The accuracy in absolute density values can be improved somewhat by normalizing to the more precise electron density values from the pulsed plasma probes. It is seen that the barium cloud was entered at 147 km and exited at 184 km. The peak barium ion concentration (including all isotopes) was 7 x 10^6 ions cm^{-3} near 161 km. The underside structure of the barium cloud was relatively smooth; the small bite-out at 158 km was due to a nitrogen gas burst from the ACS nozzle. The ACS was deactivated above this altitude and not reactivated until 178 km on descent. In contrast, the top side of the barium cloud had significant density fluctuations (more clearly seen in Figure 3). The NO^+ and O_2^+ ions were, as expected, severely depressed in the barium plasma. It can easily be shown that the increased molecular ion loss rate by electron recombination would deplete the molecular ions to less than 50 ions cm^{-3}, in a matter of a few seconds, at the peak of the barium concentration. On the other hand, the O^+ ions, which are atomic ions with an exceedingly small electron recombination rate, are essentially unaffected by the barium ion plasma, except for some irregularity structure. Interestingly, irregularities or density fluctuations in O^+, NO^+, and O_2^+ persist well above the barium cloud to about 195 km, whereas the ionospheric structure above and throughout descent is strikingly smooth (see aperture plate results shown later in Figure 7).

An expanded plot of the Ba^+ distribution, also showing Ca^+ and Ba^{++}, is presented in Figure 3. Calcium is a typical impurity in barium; the Ca^+/Ba^+ ratio is 2.5 x 10^{-4}. This chemistry and that of Ba^{++} is currently under investigation. Mass 69 (Ba^{++}) was sampled because the second ionization potential of Ba^+ is only 9.95 eV, so that H Lyman α illuminated the release for several minutes before being completely attenuated. The only possible significant chemical loss process for Ba^{++} is $Ba^{++} + NO \rightarrow NO^+ + Ba^+$. This type of reaction has been measured for Ca^{++} and found to

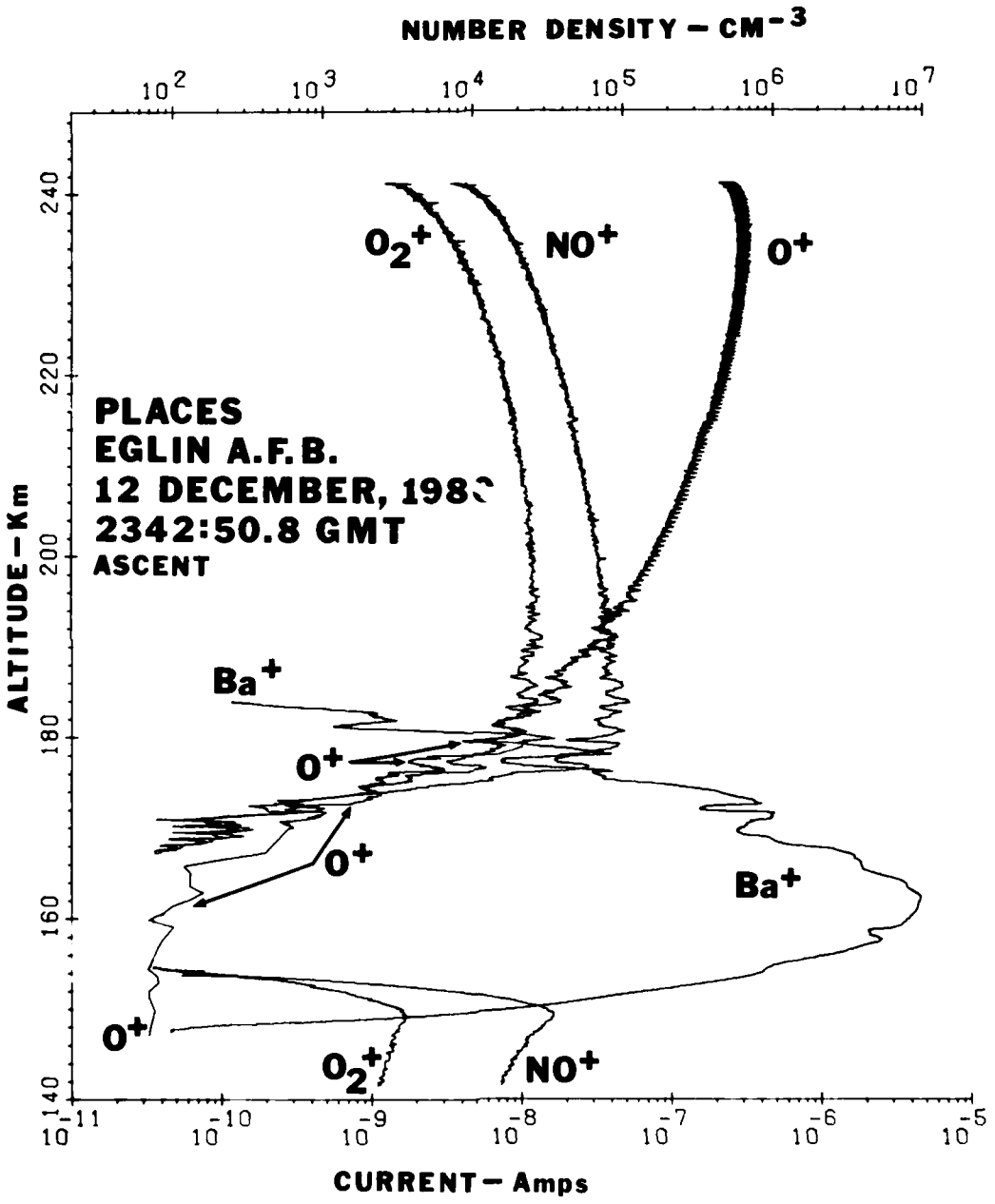

FIGURE 2 ASCENT MEASUREMENTS SHOWING THE PENETRATION OF THE BARIUM CLOUD AND ITS EFFECTS ON THE NORMAL AMBIENT SPECIES NO^+, O_2^+, AND O^+

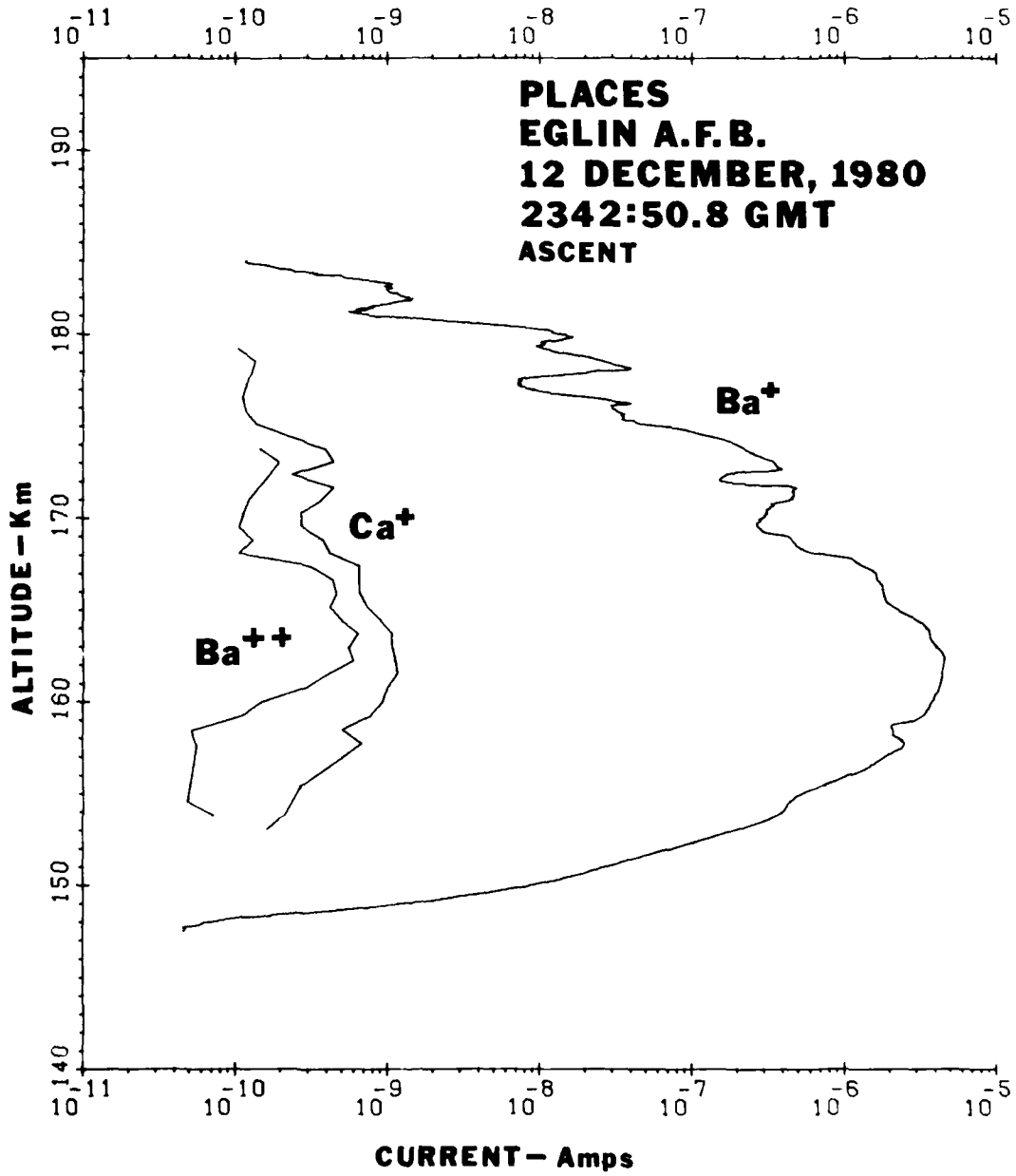

FIGURE 3 DISTRIBUTION OF CONSTITUENTS FROM THE BARIUM RELEASE. Calcium is typically about a 0.6% impurity in barium.

be very fast, but for Ba^{++}, it has not been measured and must be very slow. This would explain the persistence of Ba^{++} about 20 minutes after the ionization is cut off. Neither the photoionization cross section nor the loss processes for Ba^{++} are currently known.

Plotted separately to clearly reveal the structure below 195 km are NO^+ (Figure 4), O_2^+ (Figure 5), and O^+ with H_2O^+ (Figure 7). The H_2O^+ ions are created by the fast charge-transfer reaction, $O^+ + H_2O \rightarrow H_2O^+ + O$. It is seen that even the O^+ density fluctuations are reproduced in the H_2O^+ distribution. The H_2O^+ is produced quite near the vehicle, most likely about 1 m away. We estimate an outgassing water vapor cloud at a pressure of about 5×10^{-7} torr at one meter is sufficient to account for the H_2O^+ signal.

The entire aperture plate current output is given in Figure 7, exhibiting measurements from 98 km to 241.2 km on ascent, and to 80 km on descent. The plate current output is not seriously affected by the large vehicle attack angles. Except for the depression near 178 km on descent (caused by the ACS nitrogen gas burst), the ionosphere is exceedingly smooth outside the barium cloud. An expanded plot of the area of the barium cloud is shown in Figure 8. There is a complete agreement with even the tiniest fluctuations between the aperture plate current and the pulsed probe measurements by Szuszczewicz et al.[3]

The intent of this preliminary report has been to present the ion mass spectrometer measurements; the analyses will be performed in the future.

REFERENCES

1. Baker, K. D., and J. C. Ulwick, "Measurements of Electron Density Structure in Striated Barium Clouds," Geophys. Res. Lett., 5, 723, 1978.

2. Kelley, M. C., K. D. Baker, and J. C. Ulwick, "Late Time Barium Cloud Striations and Their Possible Relationship to Equatorial Spread-F," J. Geophys. Res., 84, 1898, 1979.

3. Szuszczewicz, E. P., J. C. Holmes, M. Swinney, and C. S. Lin, "DNA/PLACES Barium Event JAN: Quick-Look Field Report on In-Situ Probe Measurements," NRL Memorandum Report No. 4476, 26 March 1981.

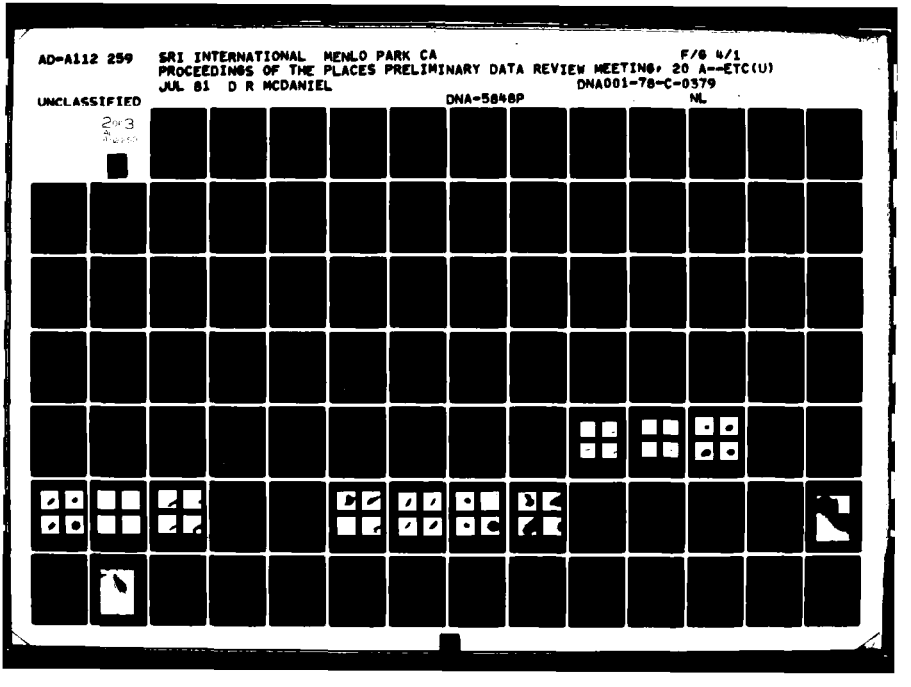
AD-A112 259
SRI INTERNATIONAL MENLO PARK CA
F/G 4/1
PROCEEDINGS OF THE PLACES PRELIMINARY DATA REVIEW MEETING, 20 A--ETC(U)
JUL 81 D R MCDANIEL
DNA001-78-C-0379
UNCLASSIFIED
DNA-5848P
NL
2 of 3

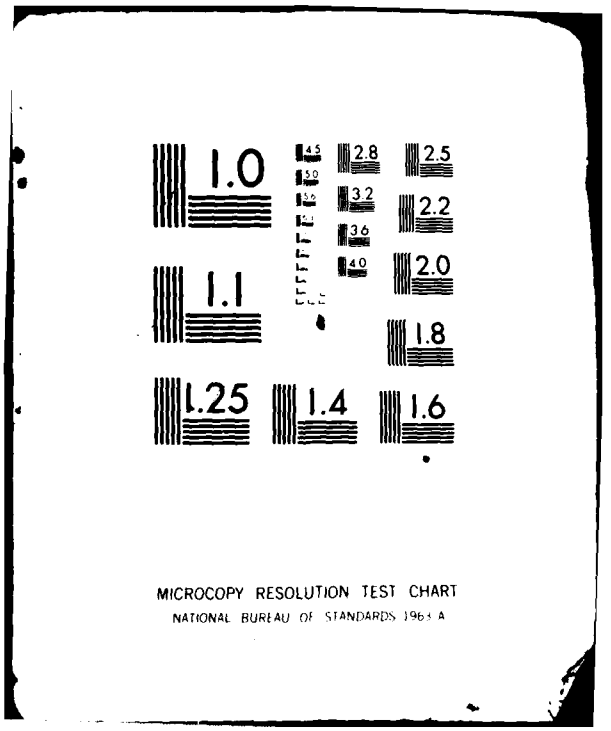
1.0
1.1
1.25
1.4
1.6
1.8
2.0
2.2
2.5
2.8
3.2
3.6
4.0
4.5
5.0
MICROCOPY RESOLUTION TEST CHART
NATIONAL BUREAU OF STANDARDS 1963 A

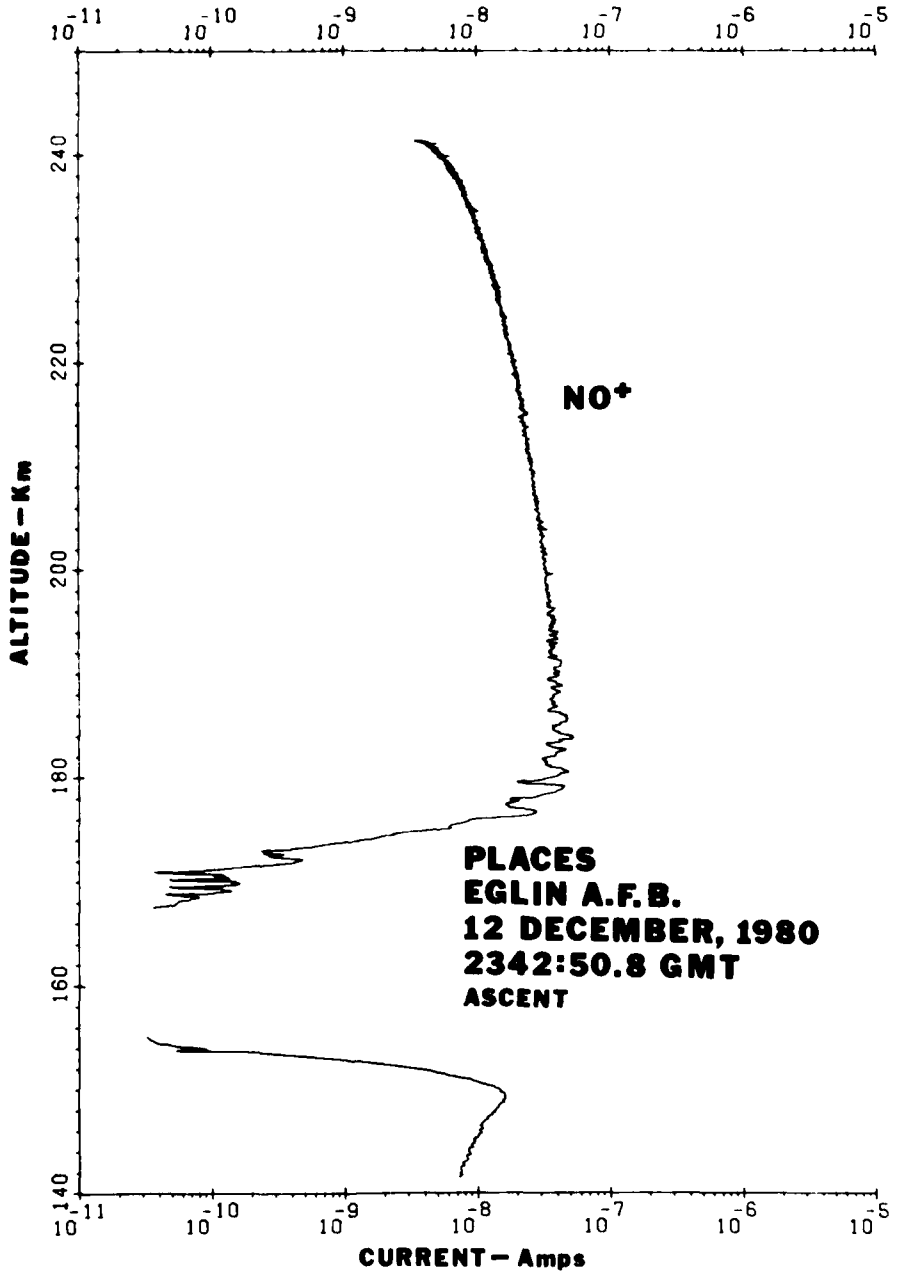

FIGURE 4 THE NO^+ PROFILE MEASURED ON ASCENT

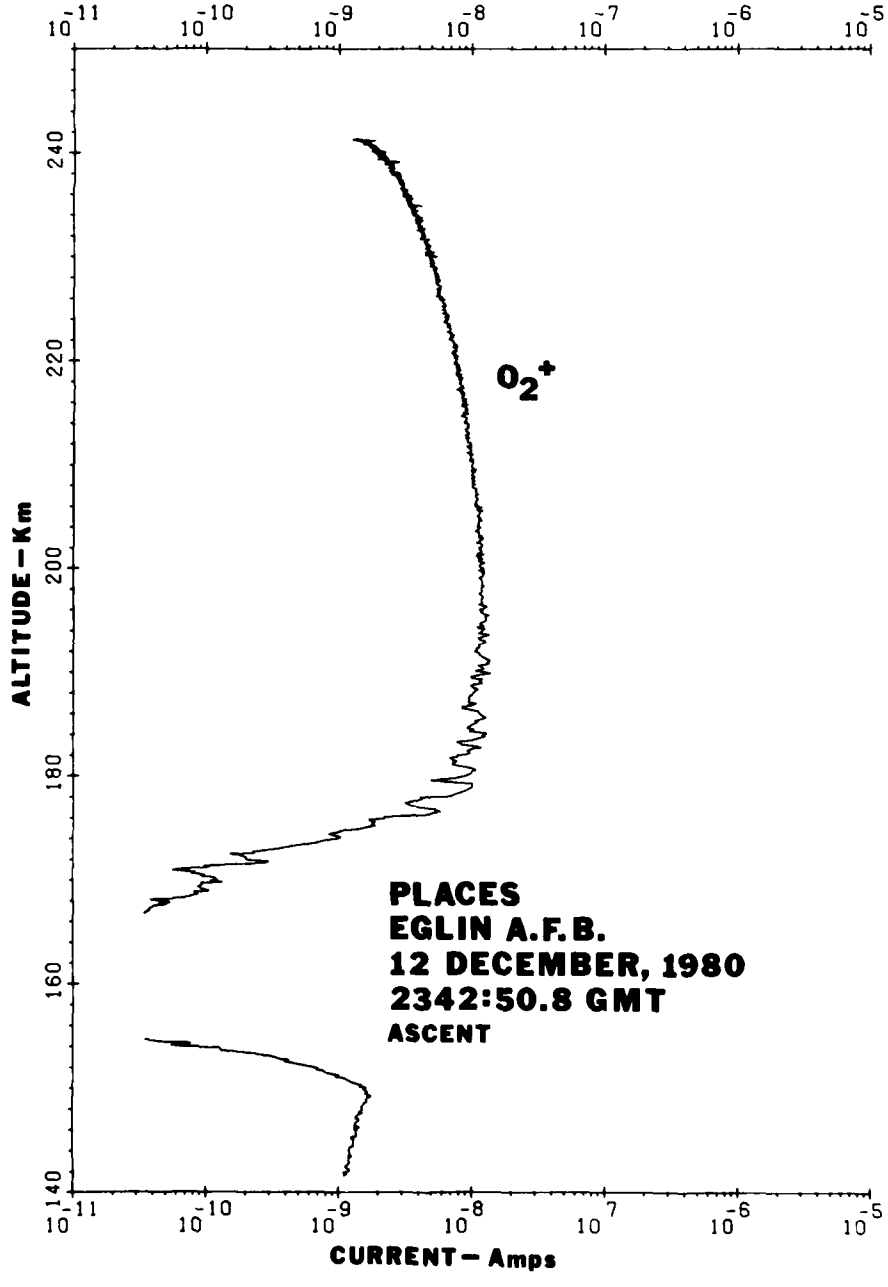

FIGURE 5 THE O_2^+ PROFILE MEASURED ON ASCENT

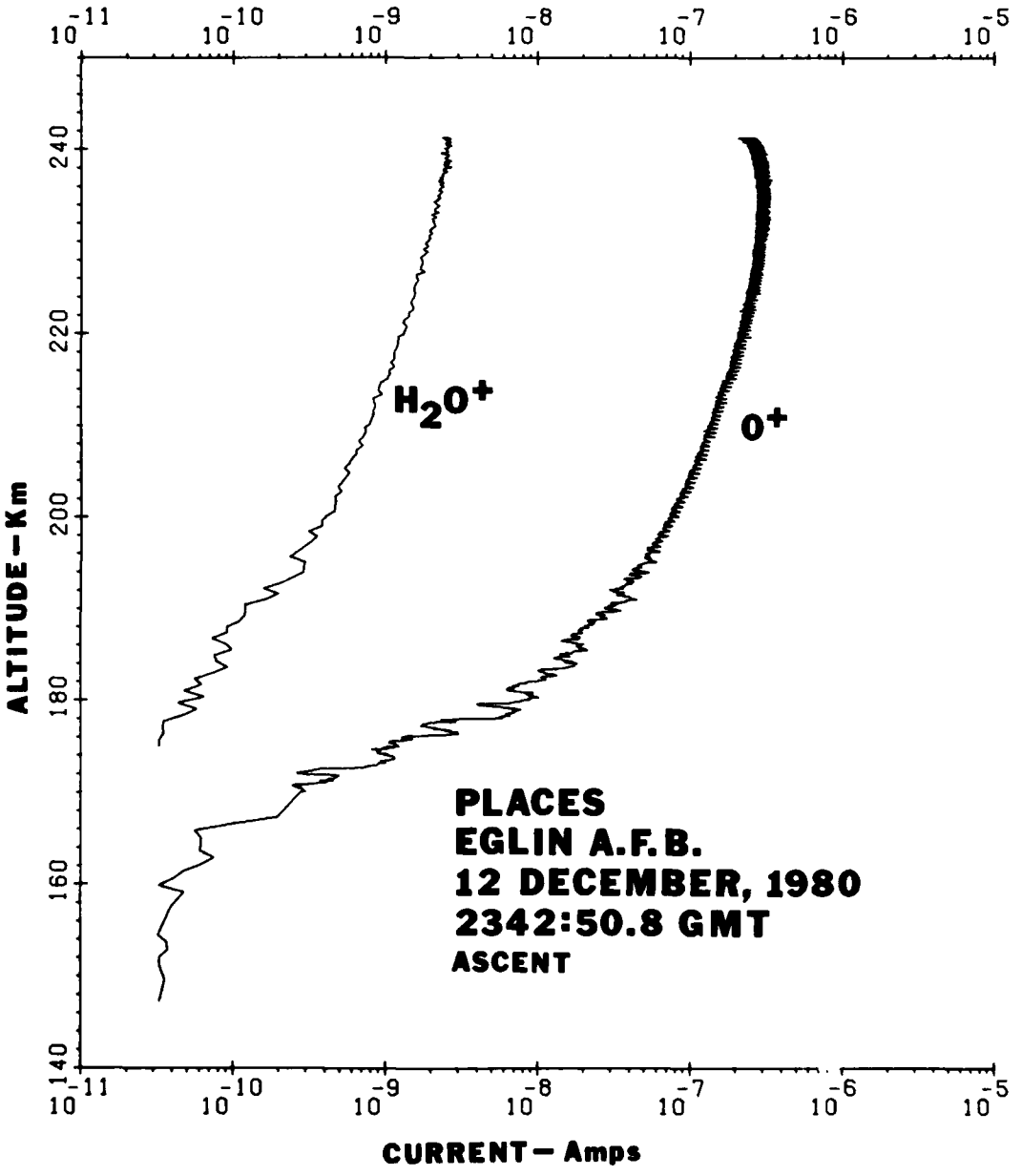

FIGURE 6 ASCENT MEASUREMENTS OF O^+ AND THE CONTAMINANT H_2O^+ (Note the structure similarity and the constant H_2O^+/O^+ RATIO)

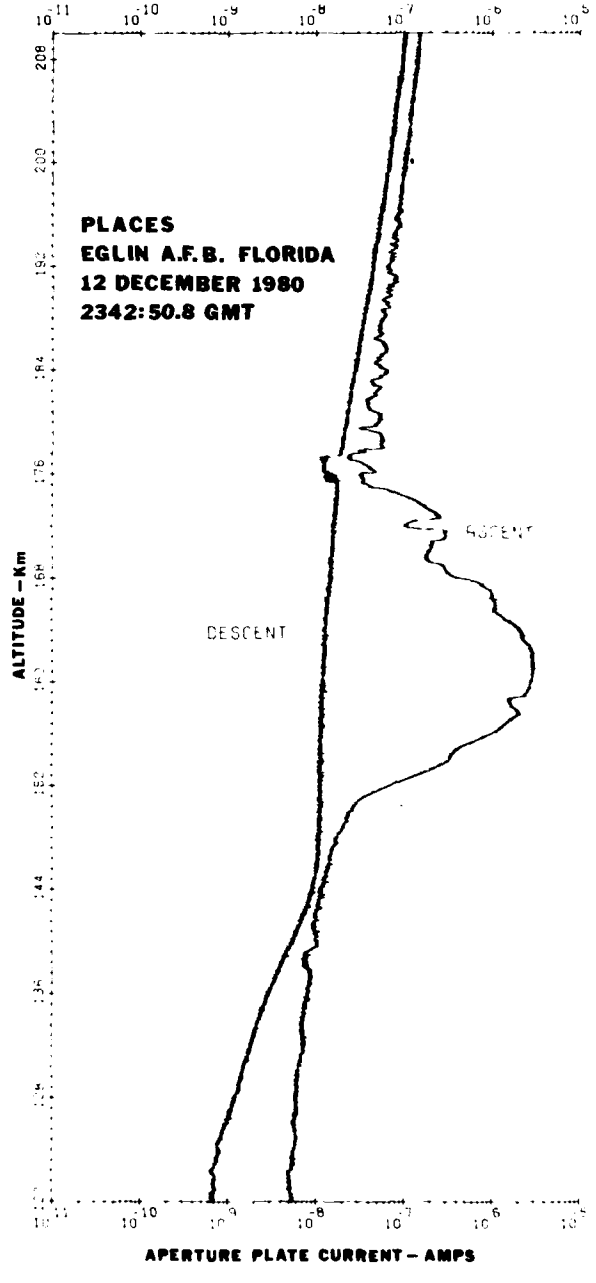

FIGURE 7 A COMPARISON OF THE ASCENT AND DESCENT APERTURE PLATE CURRENT MEASUREMENTS SHOWING THE SMOOTH IONOSPHERE ADJACENT TO THE BARIUM CLOUD

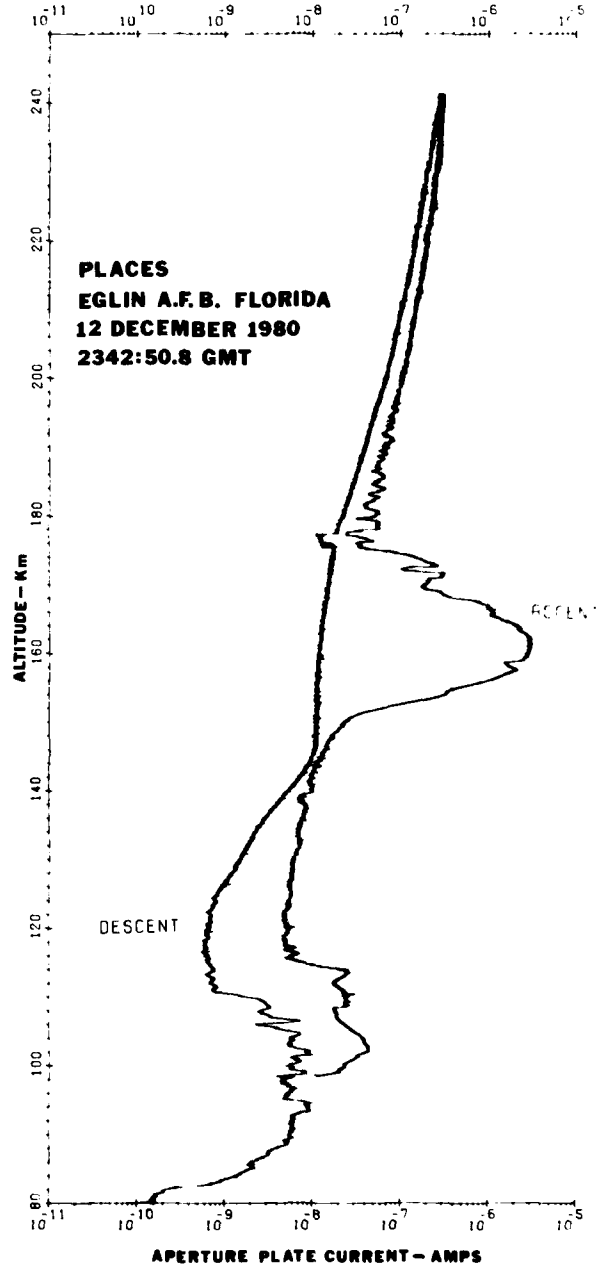

FIGURE 8 AN EXPANDED PLOT OF THE ASCENT AND DESCENT APERTURE PLATE CURRENT MEASUREMENTS IN THE VICINITY OF THE BARIUM CLOUD

BLANK PAGE

FPS-85 RADAR OPERATIONS

Victor H. Gonzalez

SRI International
Menlo Park, CA

I INTRODUCTION

The PLACES communication experiment consisted of a series of high-altitude barium releases that took place at Eglin Air Force Base, Florida. During these experiments, the AN/FPS-85 UHF radar, operating in an incoherent scatter mode, tracked the ionized barium cloud and recorded the measurements that were taken. This mode of measuring electron densities consists of receiving the aggregate reflections from individual electrons that populate the ionized region of interest. The resolution of the radar beam is sufficiently adequate to attain a spatial, as well as temporal, description of the ion cloud. This description can be correlated with optical data that were taken during the short optical window. The spatial and temporal description of the ion cloud will assist the interpretation and analysis of data taken in the course of the main experiment which was the evaluation of communication links during disturbed conditions in the propagating medium.

This report describes the experimental results and a review of the data on a test-by-test basis. The calibration ritual that took place before each experiment will be described in Section II. Sections III, IV, V, and VI will be devoted to the individual tests.

II PRELIMINARY MEASUREMENTS

At the beginning of each test and about 30 min before the launching of the barium payload, a series of measurements designed to calibrate the radar were made. There were two kinds of calibration measurements made: system noise measurements and ionospheric measurements.

Histograms of the system noise and of the system noise plus noise source were made by sampling the ADC output of the radar. Approximately 10^6 samples were obtained for each polarization channel. The ADC output was read directly into the computer through the radar-computer interface (RICE). The numbers obtained from the ADC are those that were translated into electron densities during the cloud tracking exercise.

Figure 1 is an example of the histograms of the system noise and the resulting distribution functions of the horizontal and vertical system noise outputs. These histograms were repeated for every day of the PLACES series, indicating good consistency in the performance of the equipment. The horizontal channel histogram agrees very well with the theoretical curve. The theoretical curve results from assuming that the radar front end noise is a Gaussian-distributed amplitude and an ideal logarithmic amplifier, and it is given by the following formula:

$$f(z) = \ell n(10)\ 10^{x}\ e^{-10^{x}}$$

$$x = z - A$$

$$A = \mathrm{Log}(P_o)$$

where P_o = the average power of Gaussian process.

The vertical channel histogram, on the other hand, shows anomalous spikes at certain equally spaced levels. This is definitely produced by a malfunction in the ADC that persisted throughout the PLACES series. Fortunately, the effect of this malfunction was not very serious and was compensated for by the calibration and the averaging during the tests.

The calibration procedure itself is shown in Figure 2. A correspondence is formed between the ADC output numbers and a scale of power normalized to the average front end noise. The basis for the correspondence is equal distribution function values for the measured curves (of Figure 1) and for the theoretical power distribution curve given by:

$$F(p) = 1 - \exp(-p/P_o) \quad .$$

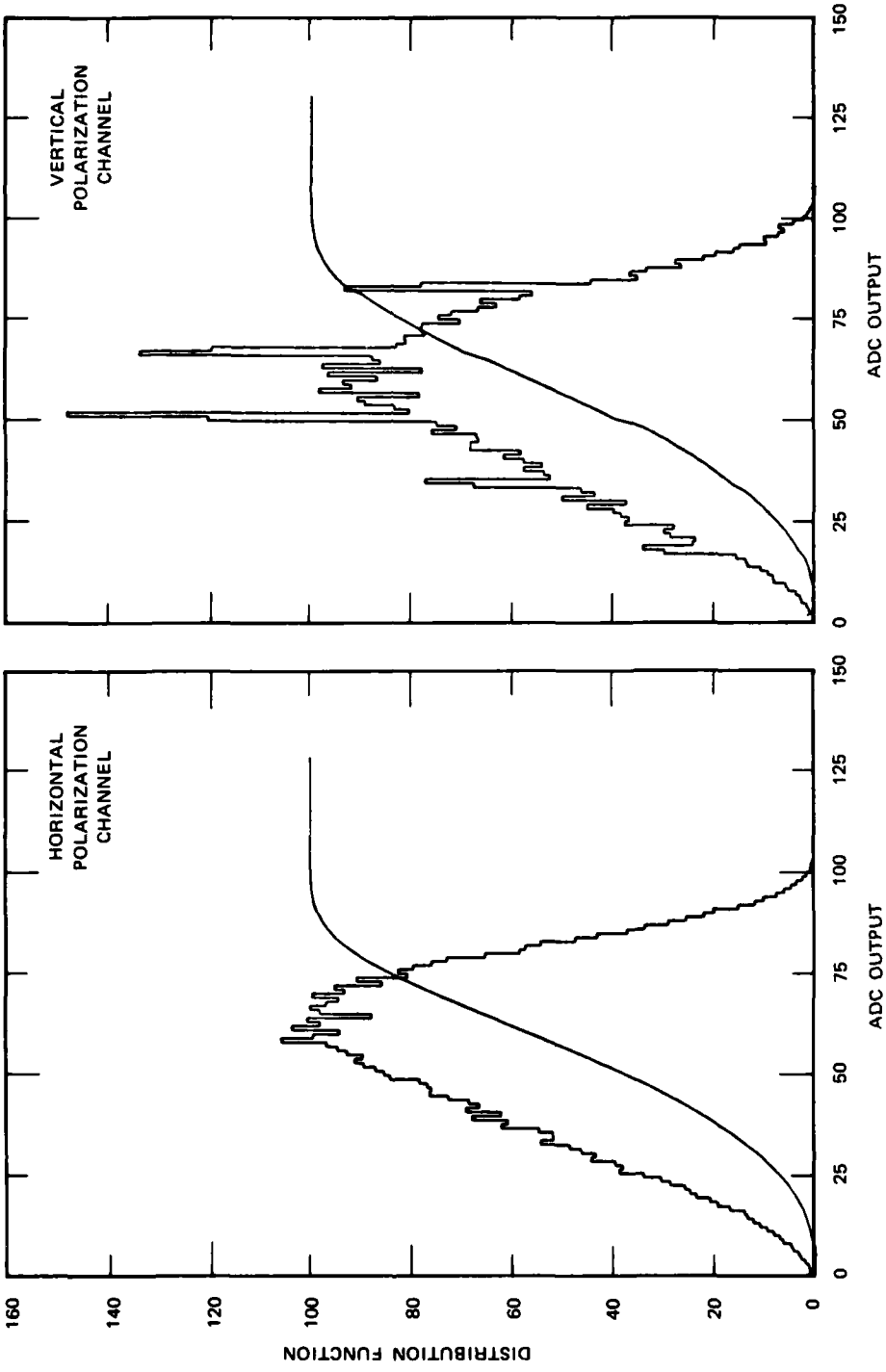

FIGURE 1 SYSTEM NOISE HISTOGRAMS AND DISTRIBUTION FUNCTIONS — EVENT GAIL

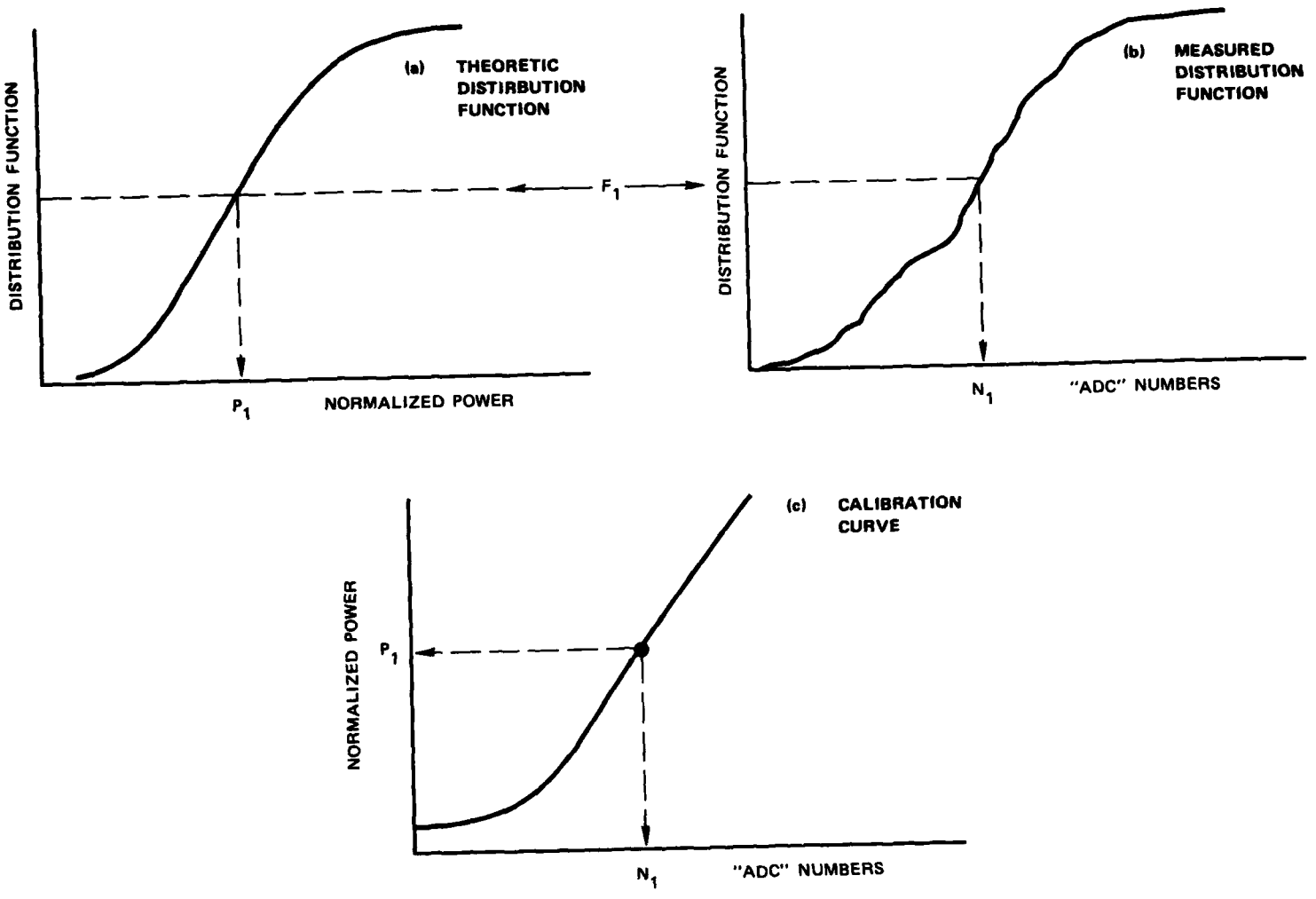

FIGURE 2 USE OF THE NOISE HISTOGRAM TO CALCULATE THE RECEIVER CALIBRATION CURVE

To clarify the procedures, let us assume that N_1 is the ADC number corresponding to a measured distribution function level, F_1. Solving the formula above, we determine the normalized power level p_1/P_o:

$$p_1/P_o = -\mathrm{Ln}(1 - F_1)$$

In this manner the calibration curve (C) of Figure 2 is formed. Actually, the computer computes and stores the power levels for each ADC level as a look-up calibration table.

This type of calibration is advantageous because it can calibrate output readings below the average noise level. In an incoherent-scatter-type measurement, this calibration is necessary because a large percentage of the samples result in measurements below the average noise power level.

The second type of measurement taken before each test is of the ambient ionosphere. Ionospheric profiles, such as shown in Figure 3, are taken by integrating returns from the ionosphere for periods of 2 to 10 min, according to the available time. A comparison with the maximum value of f_oF_2 values obtained with an ionosonde provides a point of reference in the conversion of normalized power to absolute electron densities. Ionosondes are able to measure the critical frequency of the ionosphere with a high degree of accuracy so that the measured constant relating the returned power to the electron density is very reliable.

Figure 4 summarizes the f_oF_2 values measured during the hour preceding each event, and verbally transmitted over the experimental network.

III EVENT GAIL

Event GAIL was tracked for approximately two hours after release. Figure 5 shows the small motion followed by the tracked point of the ion cloud, except for the first few minutes after release when the track was still not well established. The drift was eastward up to about T + 45 min and westward until the track was interrupted. The northbound motion on the cloud could be caused by a descent of the ion cloud along the magnetic field line or it may be caused by the change of the position of the point with the largest electron density within the cloud itself.

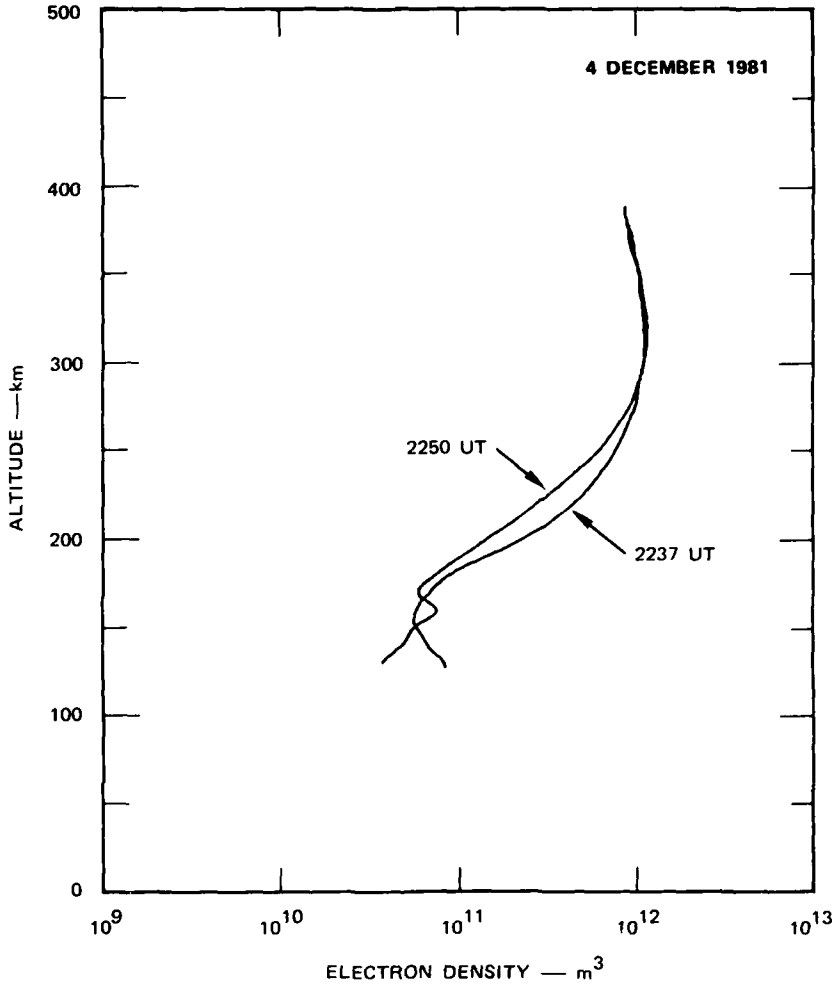

FIGURE 3 IONOSPHERIC PROFILES OBTAINED BEFORE LAUNCHING THE PAYLOAD FOR EVENT GAIL

The chance of altitude of the ion cloud is shown in Figure 6. The cloud has dropped rapidly, and in two hours descended to an altitude of 125 km. The average vertical rate of descent was 7.8 m/s, and the initial downward velocity was 23 m/s.

Figure 6 also shows, by the spread of the data points in altitude, the times at which the tracking of the ion cloud was good and the times at which it was not. From T + 20 min until T + 130 min, the vertical spread of altitude data was very narrow, indicating that a good track was

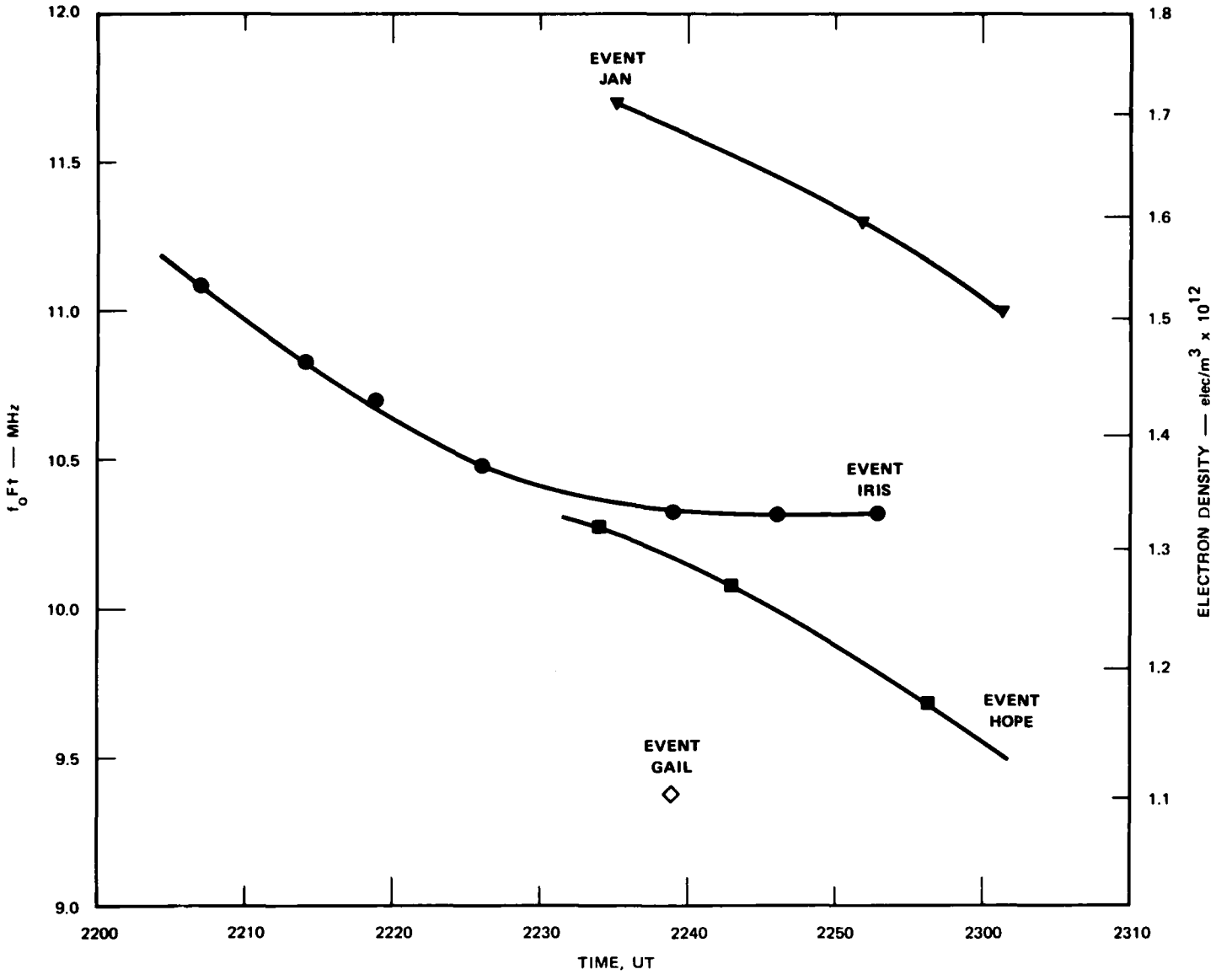

FIGURE 4 f_oF_2 VALUES READ FROM THE IONOSONDE IN REAL TIME

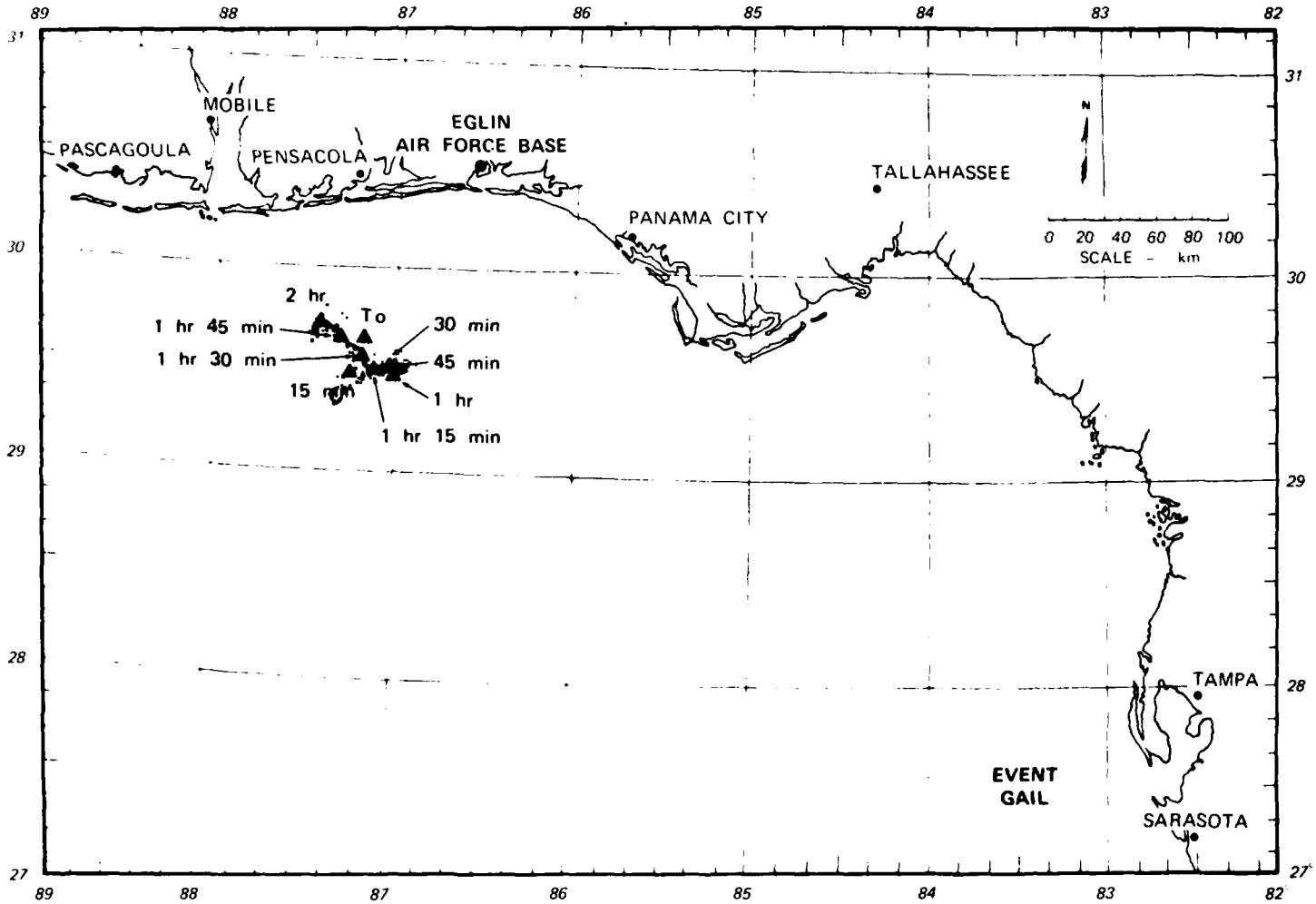

FIGURE 5 HORIZONTAL TRACK OF EVENT GAIL

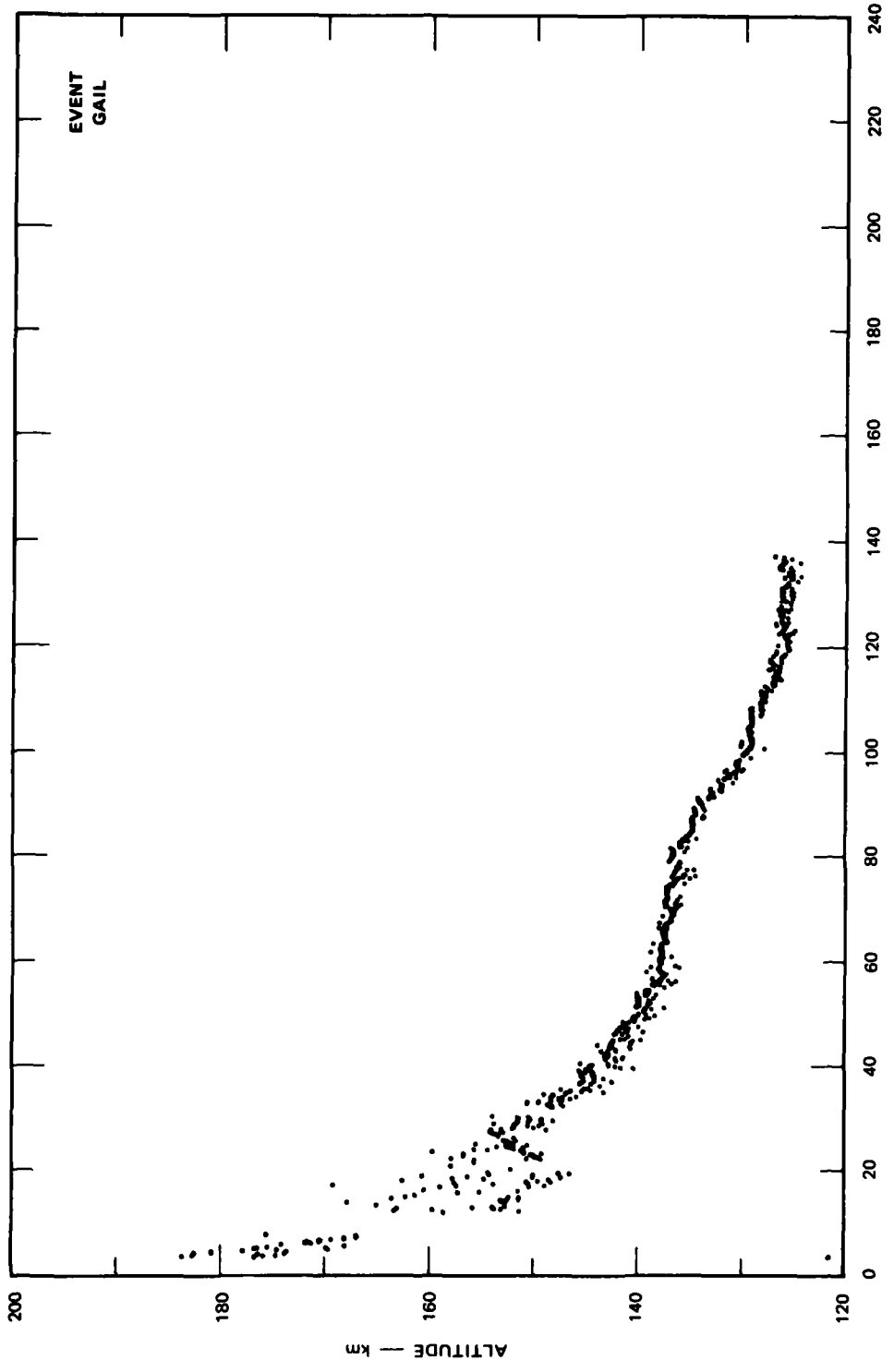

FIGURE 6 ATTITUDE DATA FROM EVENT GAIL

established during this period. Before the T + 20 min mark, a very wide spread in the data points indicates problems in the tracking process. A cable in the radar controlling the sampling of data broke at about the time of release. Data and track were lost during the time necessary to diagnose and solve the problem. When the radar finally began following the proper sequence of measurements to track the cloud, it took some time before zeroing in on the point of greatest electron density.

The time history of the maximum electron density is shown in Figure 7. The small spread of data after T + 20 min is also evident on this graph. The spread in electron density measurements is caused by random errors and by pointing errors. The statistical errors occurred because a limited number of pulses was used for integration at each antenna beam position and these statistical errors were the limit of the accuracy for the electron density measurements. The pointing errors on the other hand reflect a limitation in the tracking algorithm which did not always point the antenna beam to the point of maximum electron density. The pointing errors depend on a complicated set of geometric considerations and are difficult to describe; however, they appear to be larger than the random errors in some circumstances. The total spread of points in Figure 7 has a sigma of about 4 to 5%. The main limitation in the electron density measurement is the accuracy of the absolute calibration of the radar.

IV EVENT HOPE

Event HOPE was the smoothest running test from the point of view of radar tracking. The ion cloud was tracked for over 4 hours after release, and good quality data were obtained. The ground track of Event HOPE is shown in Figure 8. There is a monotonic westward motion throughout the life of the ion cloud. There are some reversals of motion in the North-South direction, however, that should be reviewed with care. The southward motion is unquestionably a drift involving ionization that crosses magnetic field lines. The motion to the north may be caused by the vertical fall of the ion cloud with a tendency to slide northward along the magnetic field lines. As has happened in other experiments, the radar sometimes changes the tracked point from one region of the cloud to

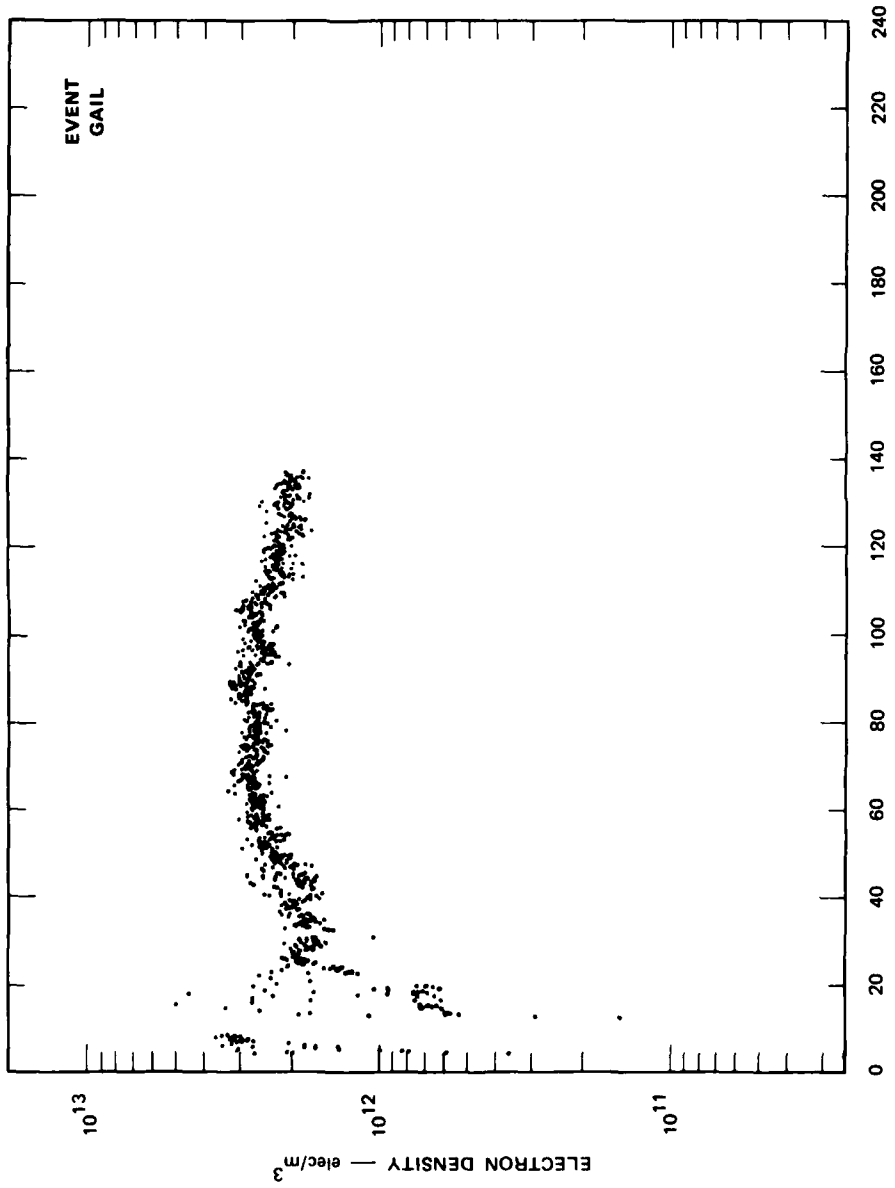

FIGURE 7 MAXIMUM ELECTRON DENSITY AS A FUNCTION OF TIME FOR EVENT GAIL

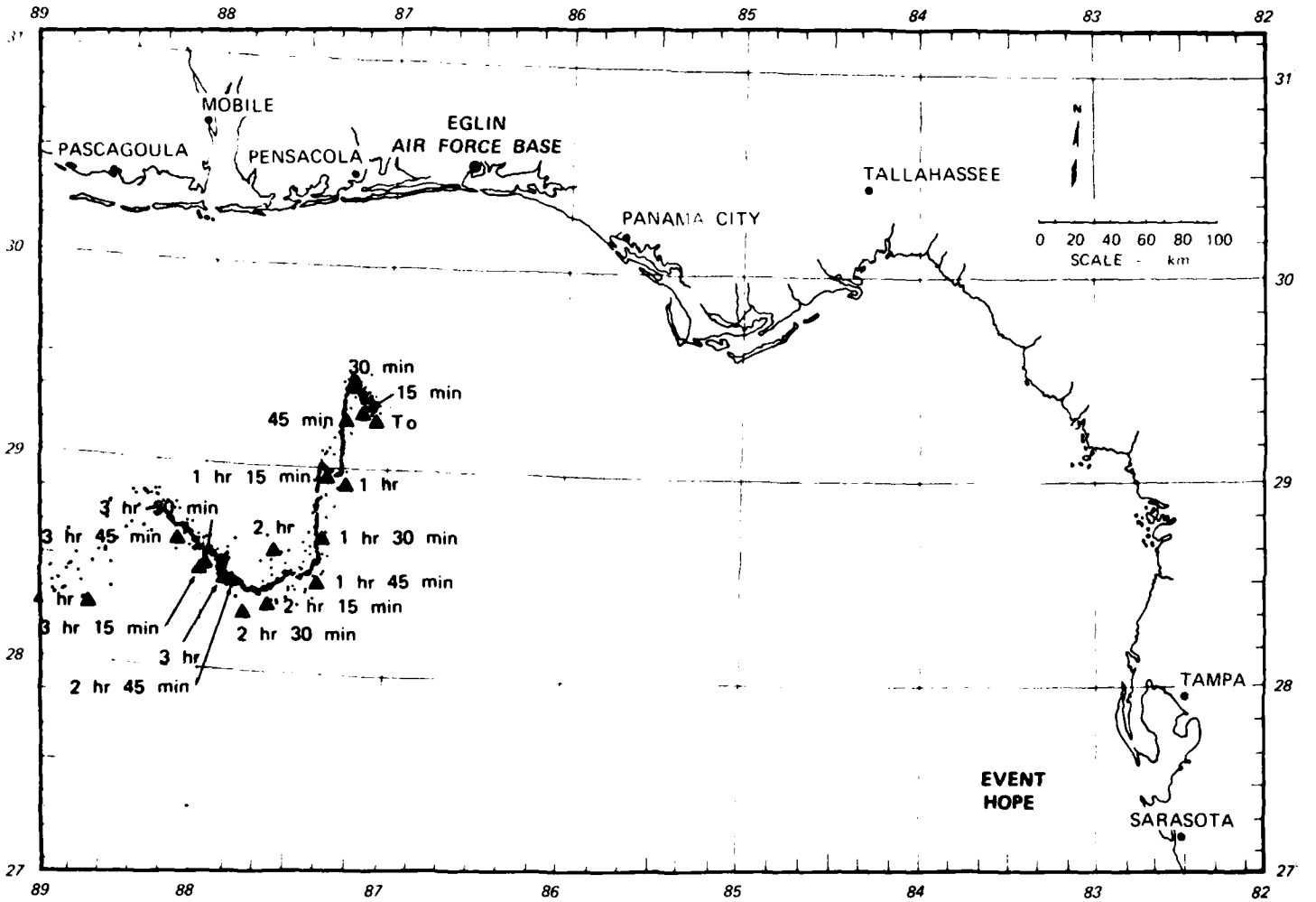

FIGURE 8 HORIZONTAL TRACK OF EVENT HOPE

another, and this tendency could be responsible for the apparent reversal between T + 60 min and T + 75 min.

The vertical descent of the ion cloud shown in Figure 9 indicates a rate of descent of 11 m/s during the first 50 min. The vertical velocity then slowed to only 2.5 m/s and the ion cloud dropped to an altitude of 120 km at four hours after release. Understanding the evolution of an ion cloud and following its changes when it reaches such a low altitude are interesting to researchers on this field.

The maximum electron density shown in Figure 10 shows a remarkably constant value after the first 20 min. This near constant value occurs as the ion cloud changes its altitude by several kilometers. To have confidence in the altitude history of the ion cloud, we have closely examined the quality of the data acquired at times separated by three hours. Figure 11 shows the received power data acquired with 2-s or 80-pulse integration and plotted as a function of altitude. We see that even though the returns from the ion cloud at 0227:27 UT are five times smaller than at 2311:51 UT, the returns from the ion cloud are still clearly well defined and definitely above the noise level. Figure 12 shows the same data after the system noise, normalized to 2, has been subtracted, the range correction has been made, and the conversion to electron density has been completed. The ionosphere background above 200 km is evident. The vertical profile of the ion cloud a 0227:27 UT seems narrower than at 2311:51 UT. This may not be the case, however, because the radar beam traversed the ion cloud at a very low-elevation angle and the apparent narrow vertical extent of the ion cloud may be caused by the radar beam entering through one side of the cloud and leaving through the other side of the ion cloud. In other words, the cloud may extend above and below 120 km and remain outside the radar beam. This problem should be studied in greater detail, in case another barium release program is contemplated.

Vertical profiles of the ion cloud were formed by choosing the maximum electron density at a given height from a set of approximately 40 to 50 antenna-beam positions. We can reasonably assume that these profiles

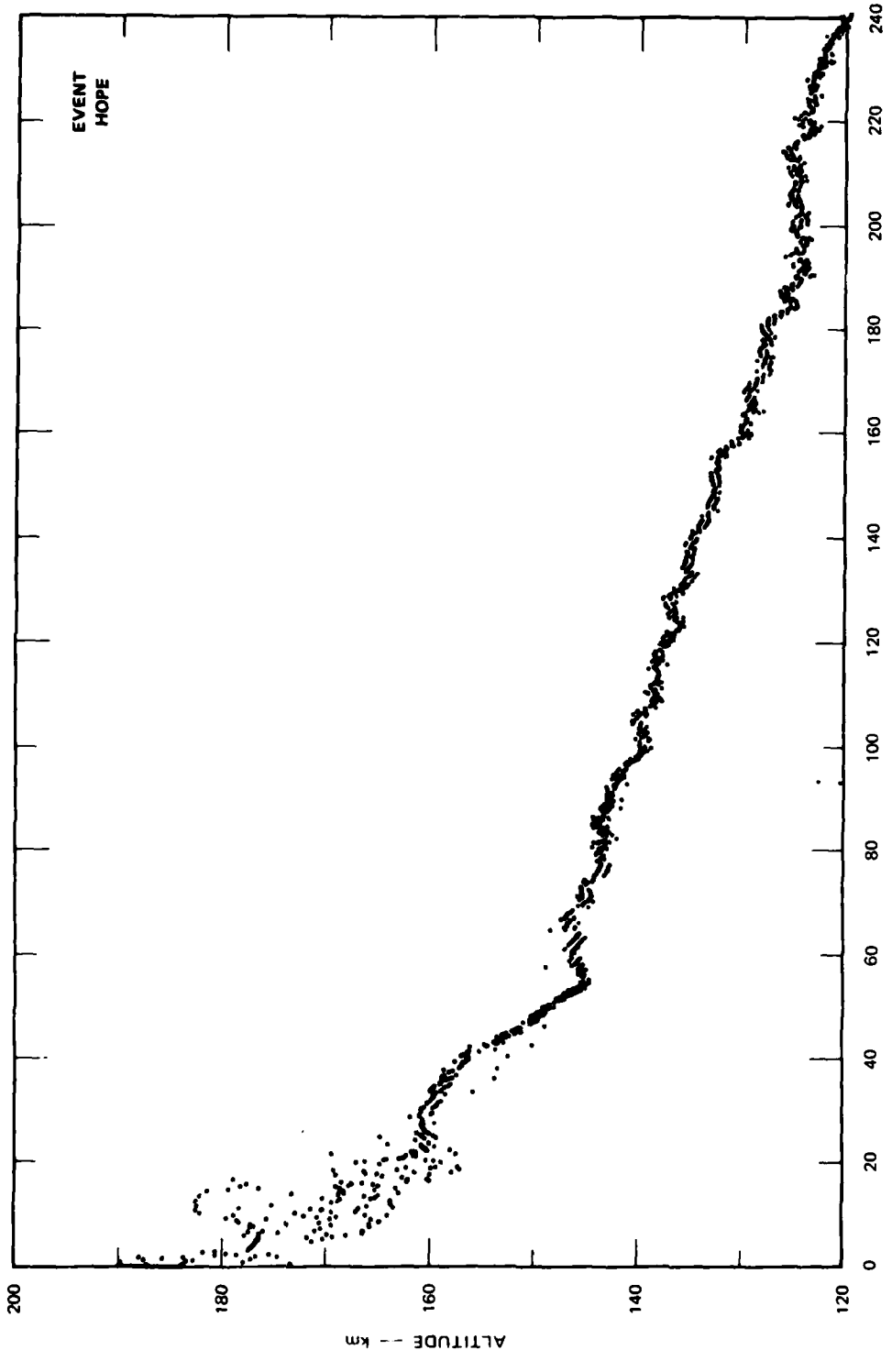

FIGURE 9 ALTITUDE DATA AS A FUNCTION OF TIME OF EVENT HOPE

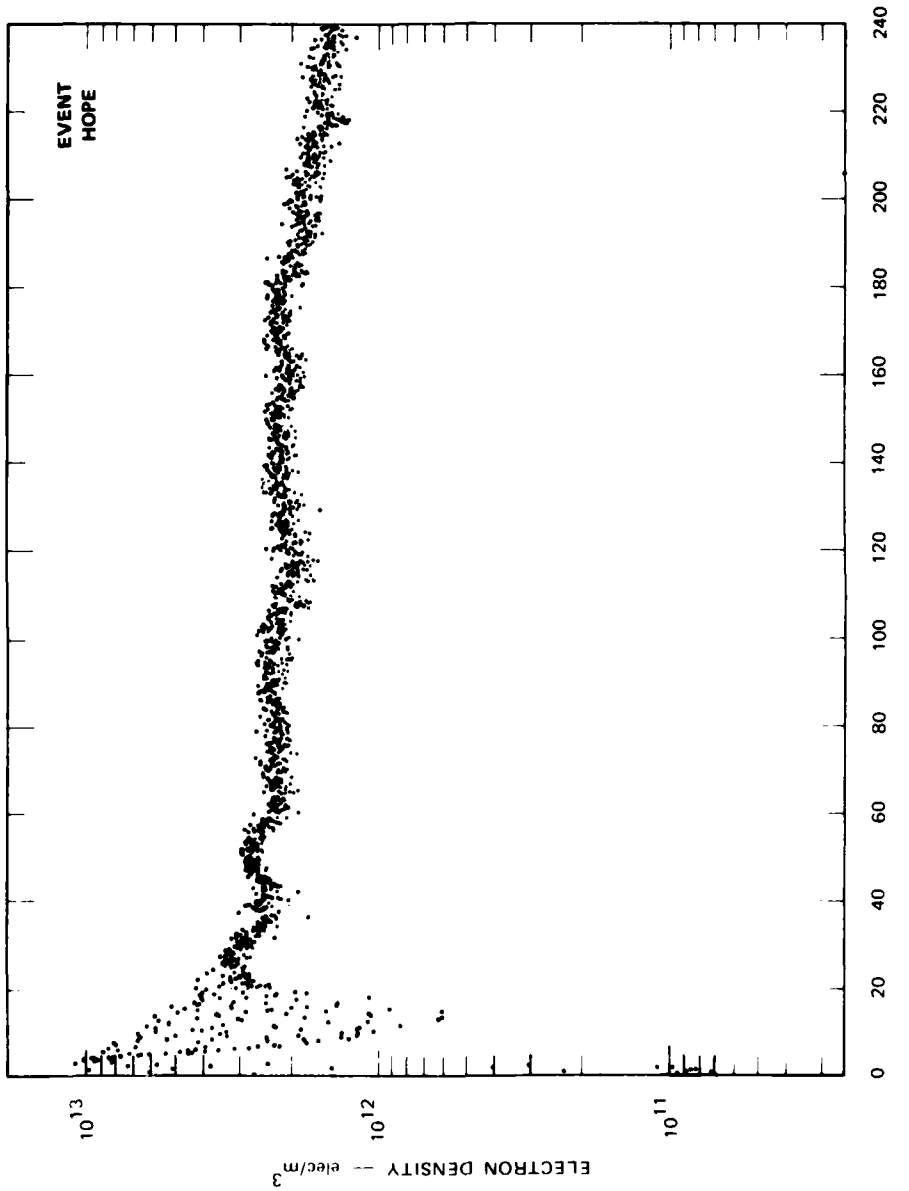

FIGURE 10 MAXIMUM ELECTRON DENSITY AS A FUNCTION OF TIME FOR EVENT HOPE

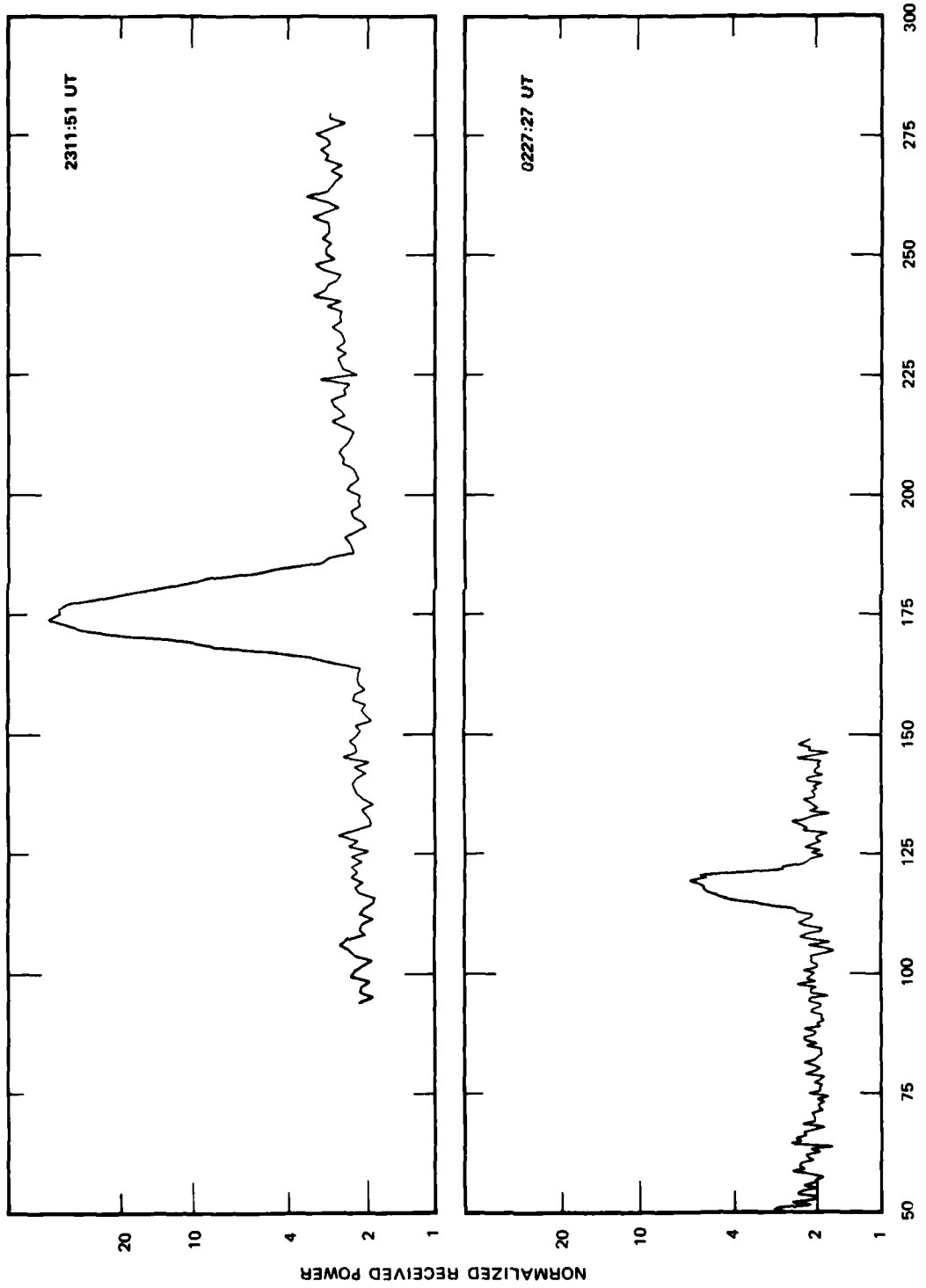

FIGURE 11 ROUGH DATA ACQUIRED FOR TWO ANTENNA-BEAM POSITIONS WITH TWO-SECOND INTEGRATION TIME OF EVENT HOPE

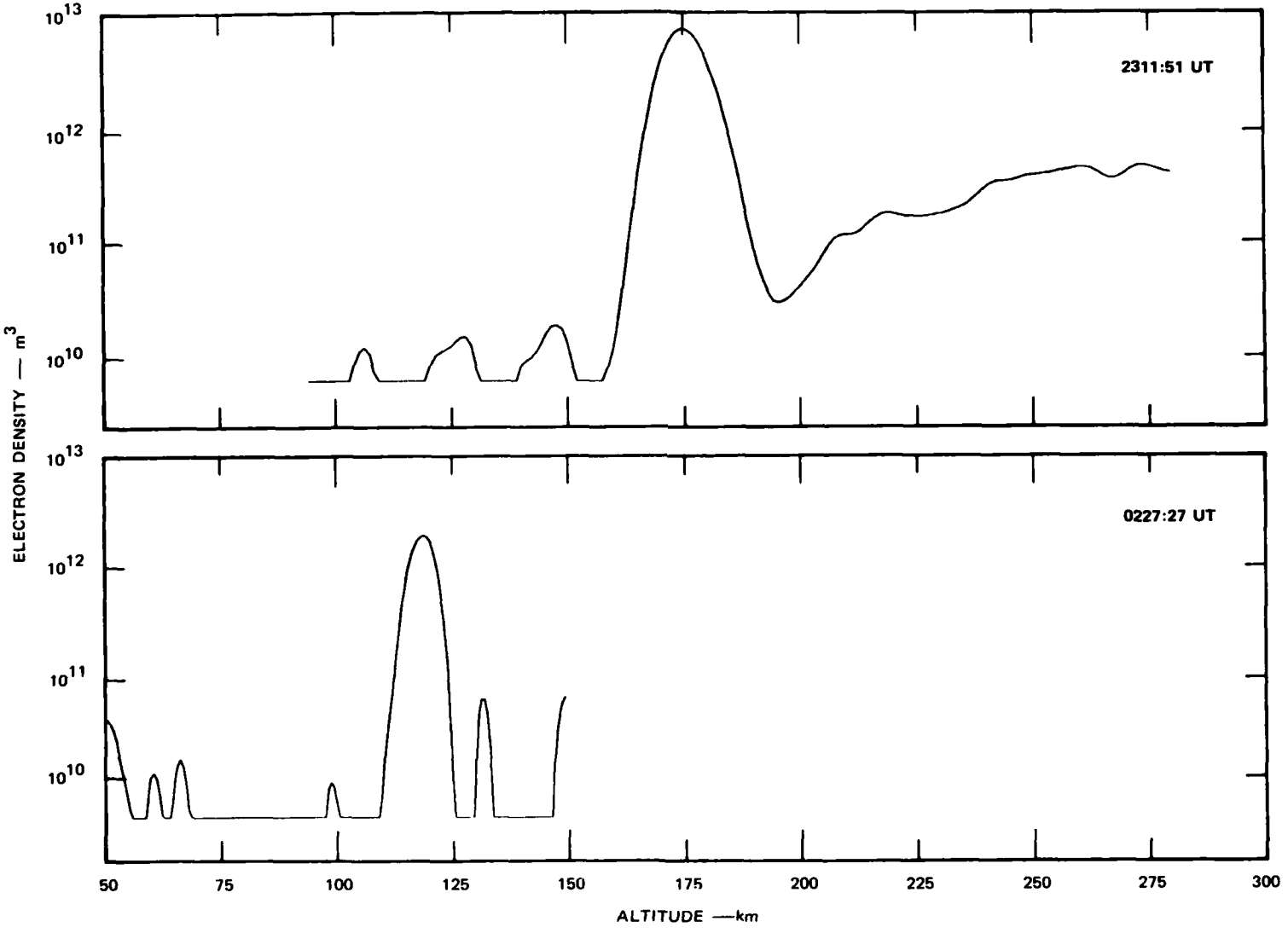

FIGURE 12 ELECTRON DENSITIES DERIVED FROM DATA IN FIGURE 11 FOR EVENT HOPE

show the electron density along the magnetic field line with the maximum electron content. Some words of caution should be added because the discrete number of antenna beam positions used during tracking do not assure that all the points along the magnetic field line of interest have been observed and measured. The resulting vertical profiles are shown in Figures 13, 14, 15, and 16 for various times.

The first vertical profile at 2325 UT is about 18 min after release and the 3-dB width is 20 km. As the ion cloud grows older and drops to lower altitudes, the 3-dB width narrows to 12 km at 2404 UT to 10 km at 2417 UT, and to about 7 km after 0220 UT. This decrease of the ionization in the vertical direction should be investigated further to verify whether it is caused by the geometric configurations of the observations since the horizontal range combined with the low altitude require very low-elevation pointing of the radar beam. A somewhat different view of this vertical extent of the ion cloud is seen in the next section, devoted to Event IRIS.

V EVENT IRIS

The ground track of Event IRIS is shown in Figure 17. The ion cloud location was well established about 10 or 15 min after release. The motion of the ion cloud was very steady throughout the period of observation, and the average velocity was 26 m/s southward and 18 m/s eastward. This drift velocity carried the ion cloud out of the preset sampling range of the radar about 90 min after release.

The maximum electron density as a function of time is shown in Figure 18. The low electron densities during the first few minutes after release show that the radar was not pointing to the center of the ion cloud. When the ion cloud was found and the radar zerod in on the densest part of the ion cloud, the electron density climbed up to 8×10^{12} el/m^3. The drop in electron density after T + 80 min and after T + 100 min were caused by pointing problems when the cloud drifted out of range and when the operator tried to change the preset range limits for the electron density measurements. The drop in electron density between T + 20 min and T + 30 min, however, seems to be an actual change in the ion cloud itself since the track was well established at this time.

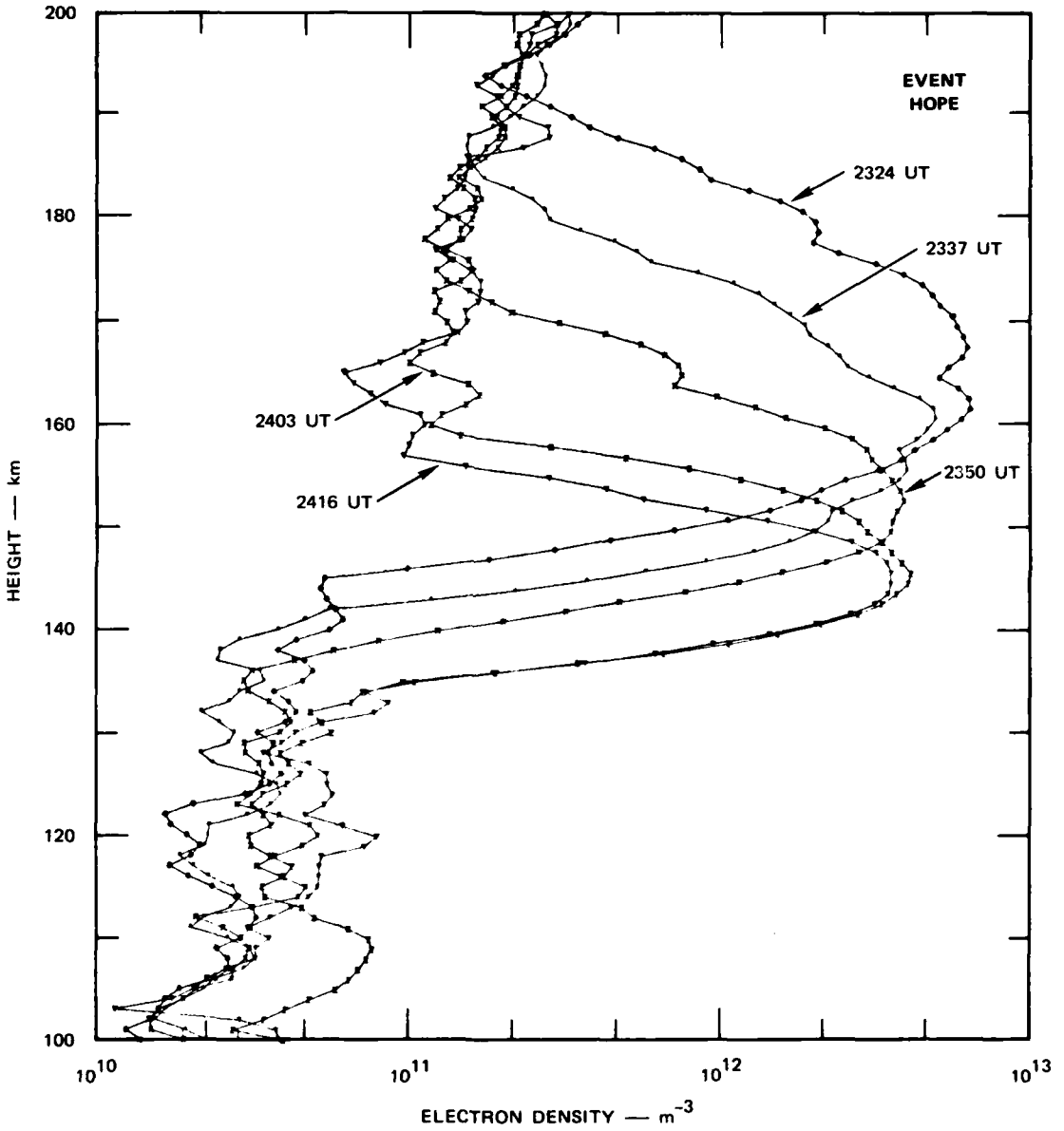

FIGURE 13 VERTICAL ELECTRON DENSITY PROFILES OF EVENT HOPE AT VARIOUS TIMES

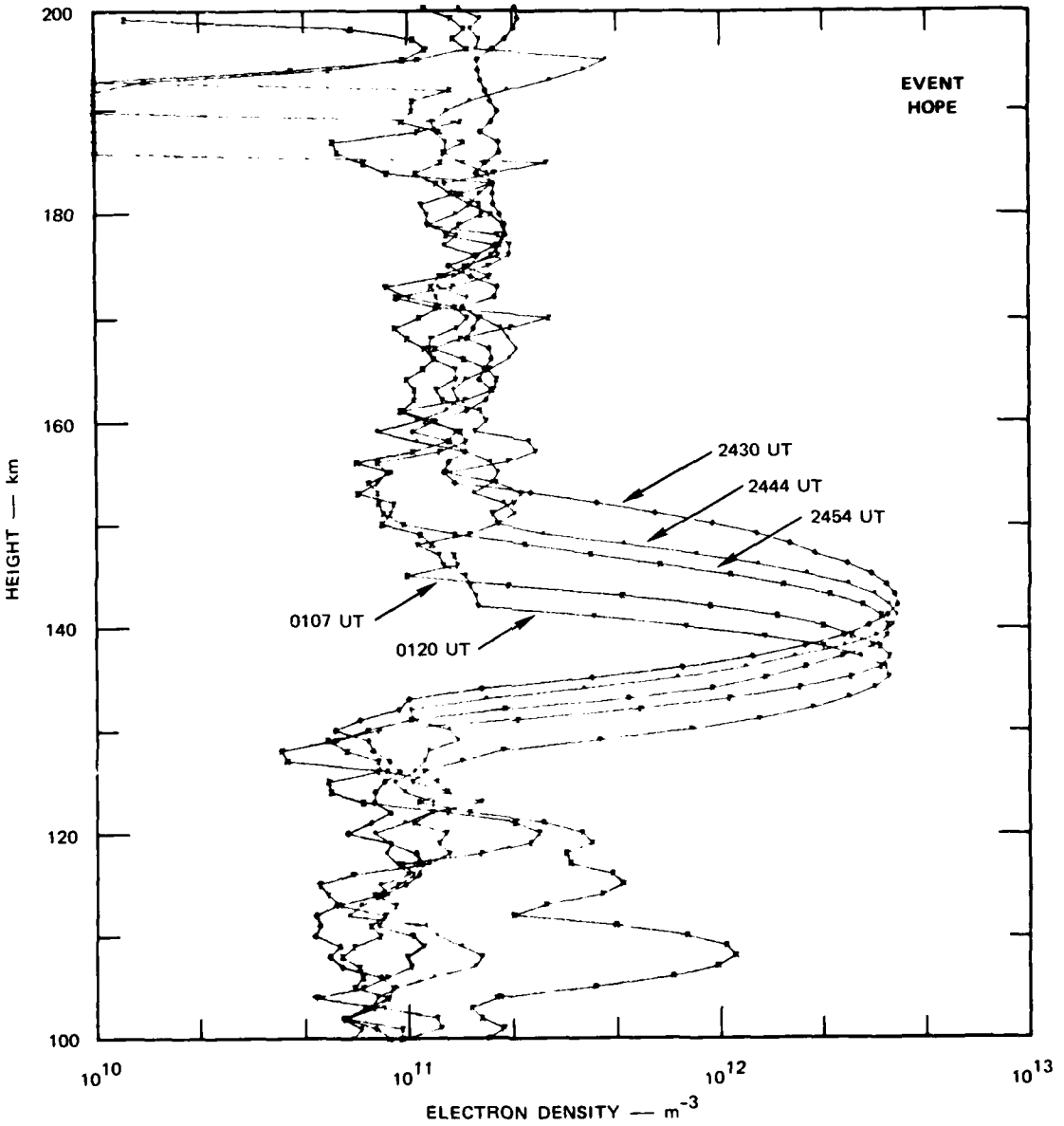

FIGURE 14 VERTICAL ELECTRON DENSITY PROFILES OF EVENT HOPE AT VARIOUS TIMES

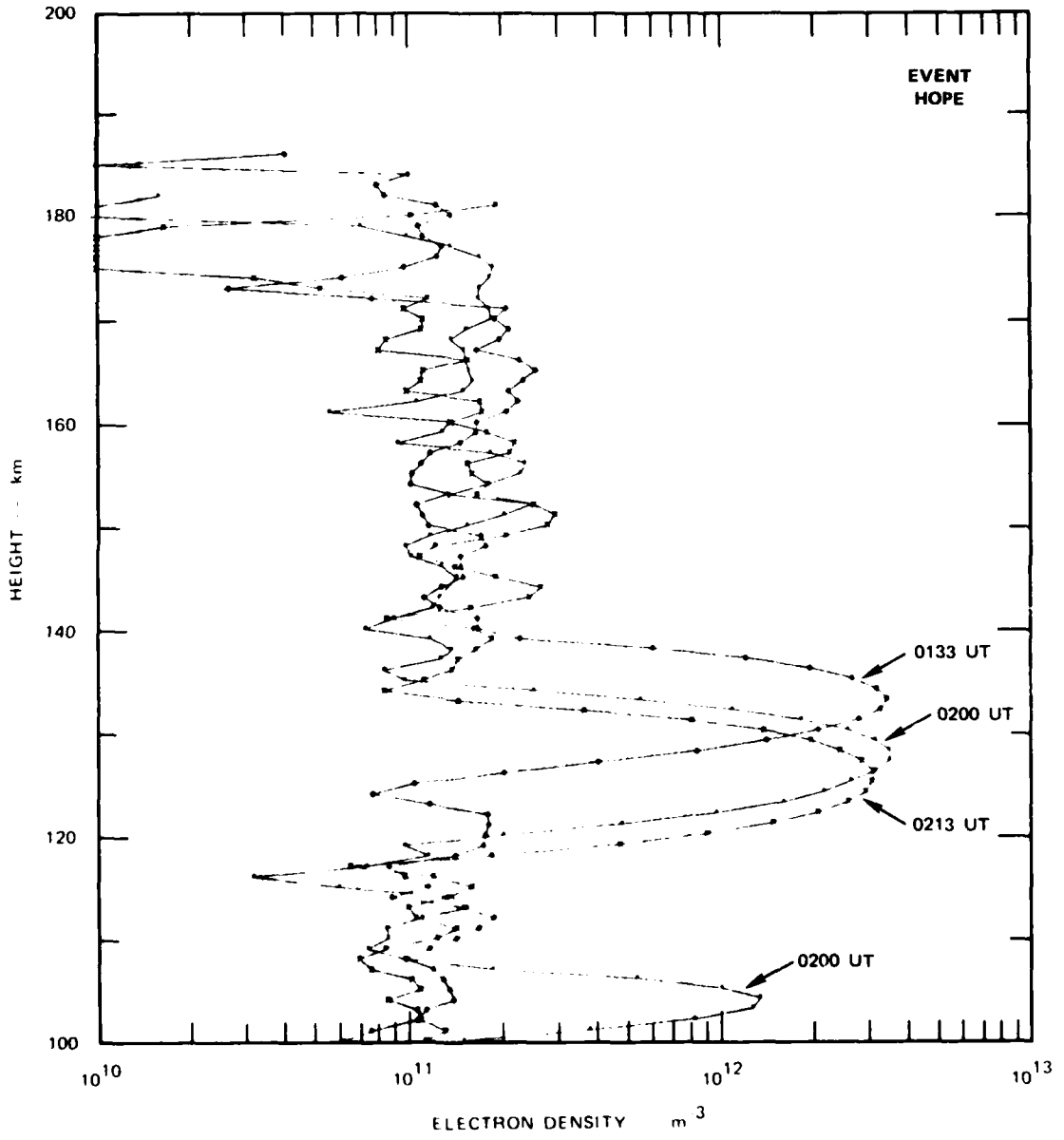

FIGURE 15 VERTICAL ELECTRON DENSITY PROFILES OF EVENT HOPE AT VARIOUS TIMES

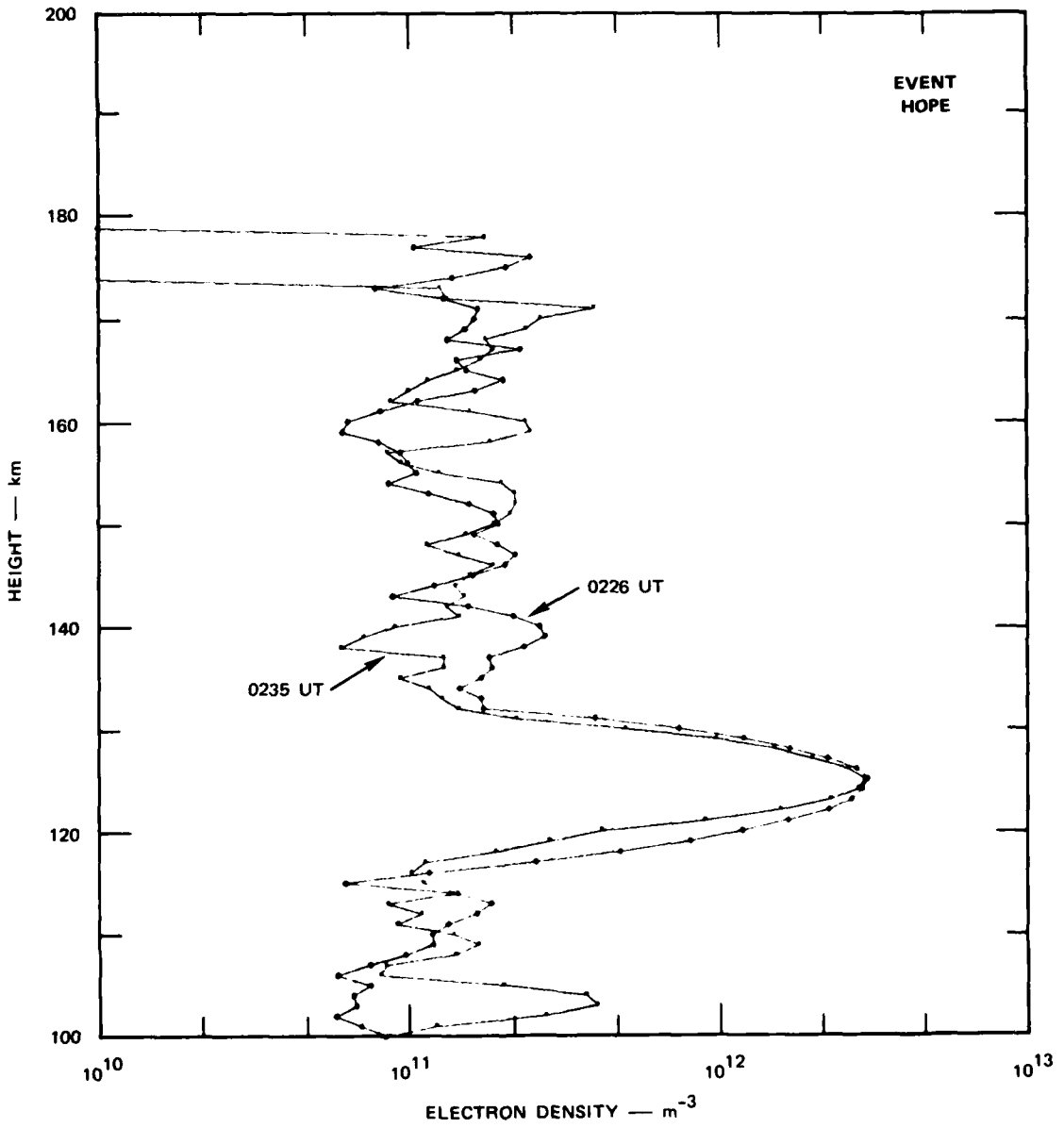

FIGURE 16 VERTICAL ELECTRON DENSITY PROFILES OF EVENT HOPE AT LATE TIMES

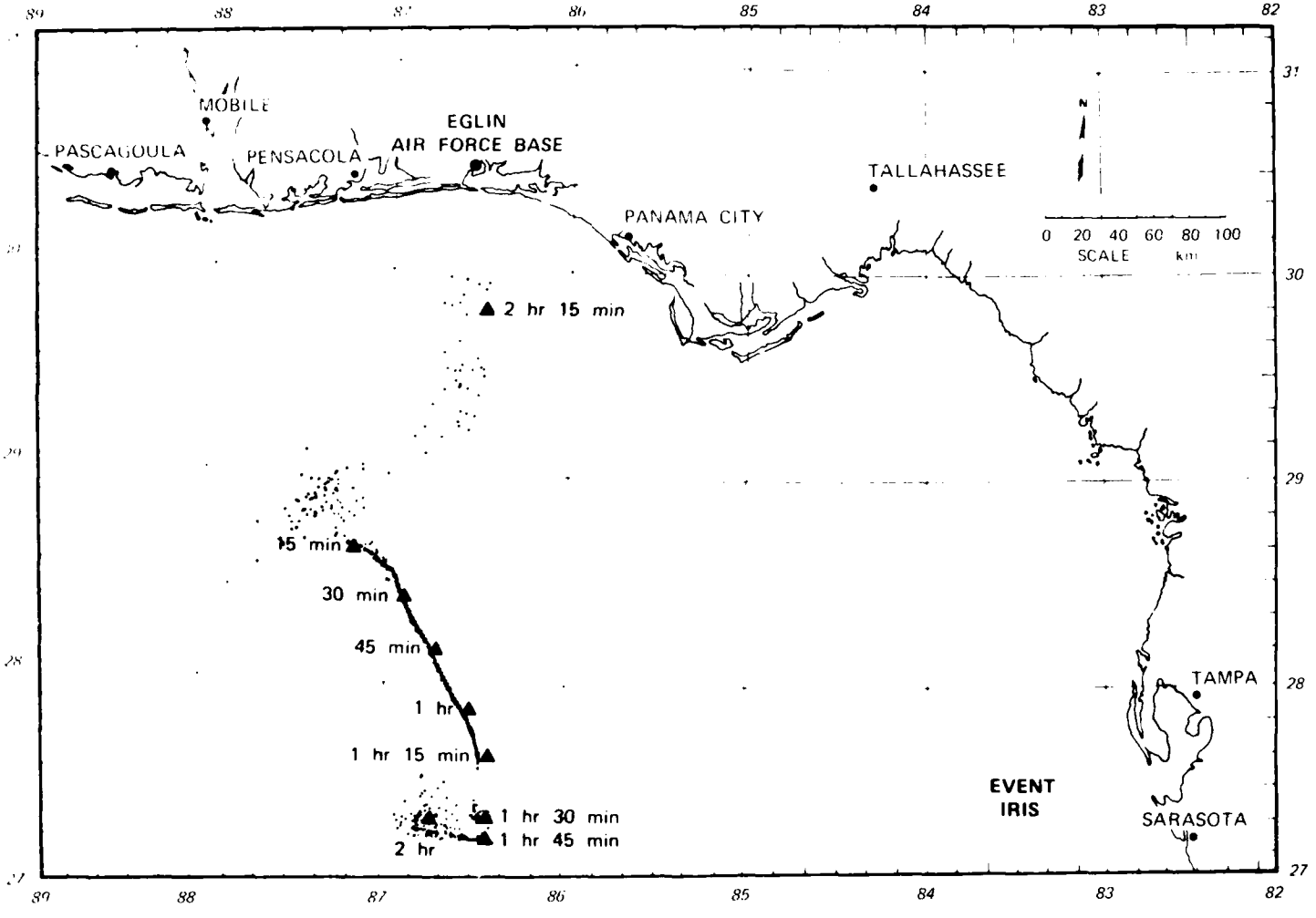

FIGURE 17 HORIZONTAL TRACK OF EVENT IRIS

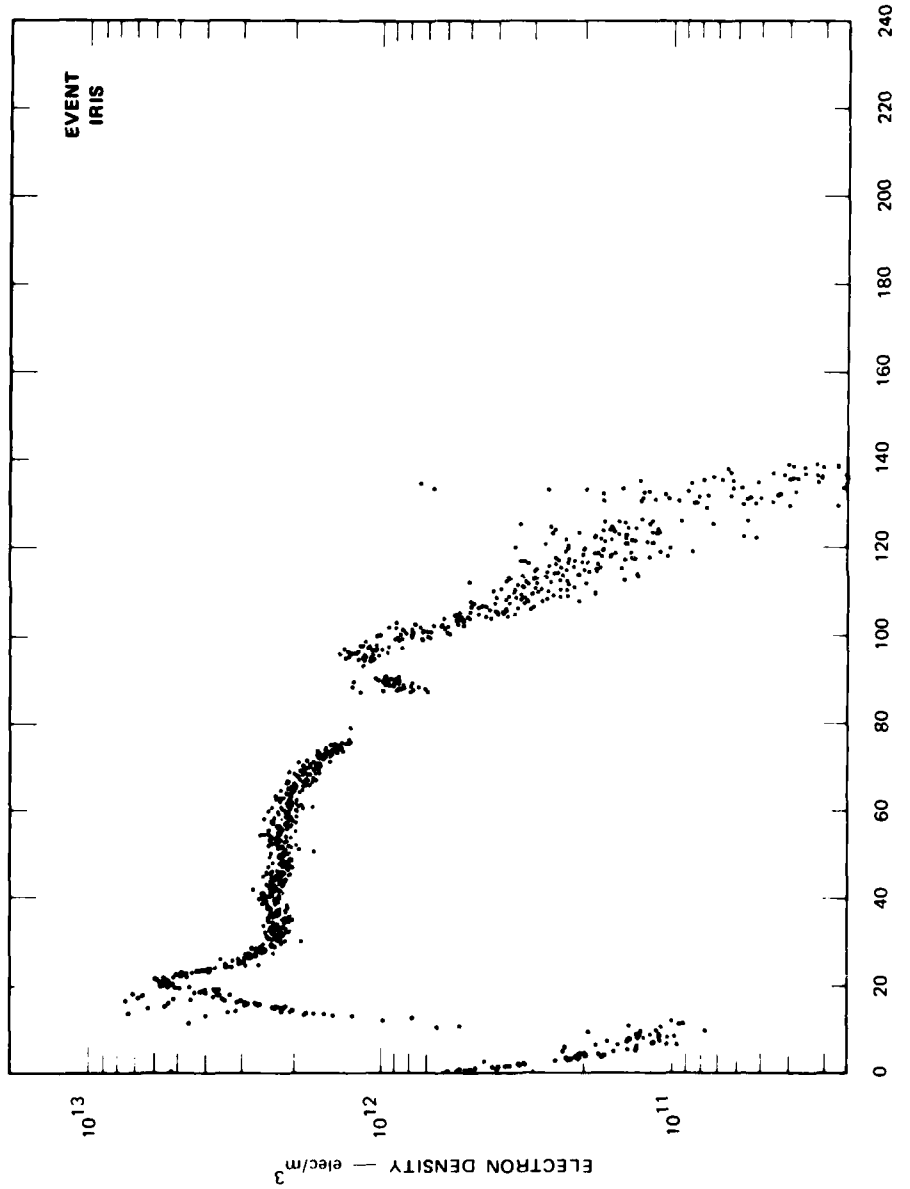

FIGURE 18 MAXIMUM MEASURED ELECTRON DENSITY OF EVENT IRIS AS A FUNCTION OF TIME

The altitude of the ion cloud is shown in Figure 19. The anomalies in these data define the times at which problems were encountered during the tracking of the ion cloud. The data before T + 10 min and after T + 75 min are very erratic with very wide scatter in the points. The narrow spread of data between T + 10 min and T + 75 min indicates that during this period good quality data were obtained.

Vertical profiles of the ion cloud at various times are shown in Figure 20 and the narrowing of the ion cloud in the vertical direction as the ion cloud reaches lower altitudes is not as obvious for Event IRIS as it was for Event HOPE. However, the measurements of Event IRIS do not span as large a period or as large a difference in height. The vertical narrowing of the ion cloud seems to be present in Figure 20, but on a smaller scale.

The horizontal shape or cut of the ion cloud has been obtained three different times, separated by about 20 min. These horizontal contours are shown in Figures 21, 22, and 23. The direction of elongation of the ion cloud is nearly perpendicular to the direction of motion of the ion cloud. The contours shown in Figure 21 show an ion cloud with a well-defined center and strong gradients. The contours of Figure 22 show a more elongated ion cloud that maintans strong gradients on its side. The third display of contours of Figure 23 shows a larger, but considerably less dense cloud with smaller gradients and a not-so-well defined shape.

We chose this later time to explore the vertical extent and shape of the ion cloud. Figure 24 shows the vertical profile of the ion cloud in the North-South vertical plane. According to Figure 22, the North-South dimension is close to the smallest dimension of the ion cloud, and certainly is considerably smaller than the East-West dimension. Figure 24 also shows, for reference, the size of the radar beam and the area within which measurements were acquired. This area is within the limits marked as boundary for acquisition of data. The approximate direction of the Earth's magnetic field is also shown in this figure.

A few observations can be made at this point. The short vertical width of the ion cloud seems to be a real feature of this cloud: 9 km

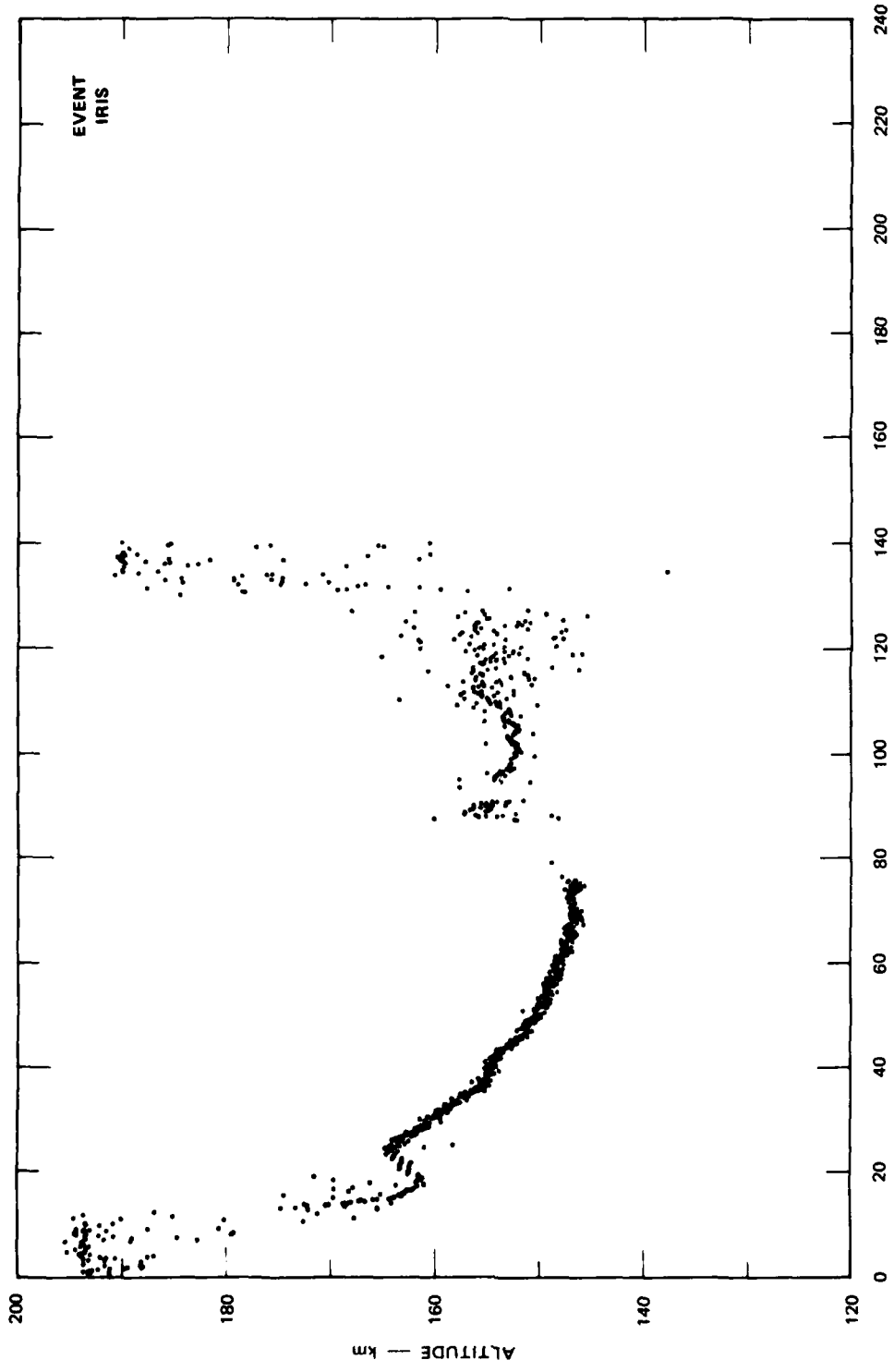

FIGURE 19 ALTITUDE DATA OF EVENT IRIS AS A FUNCTION OF TIME

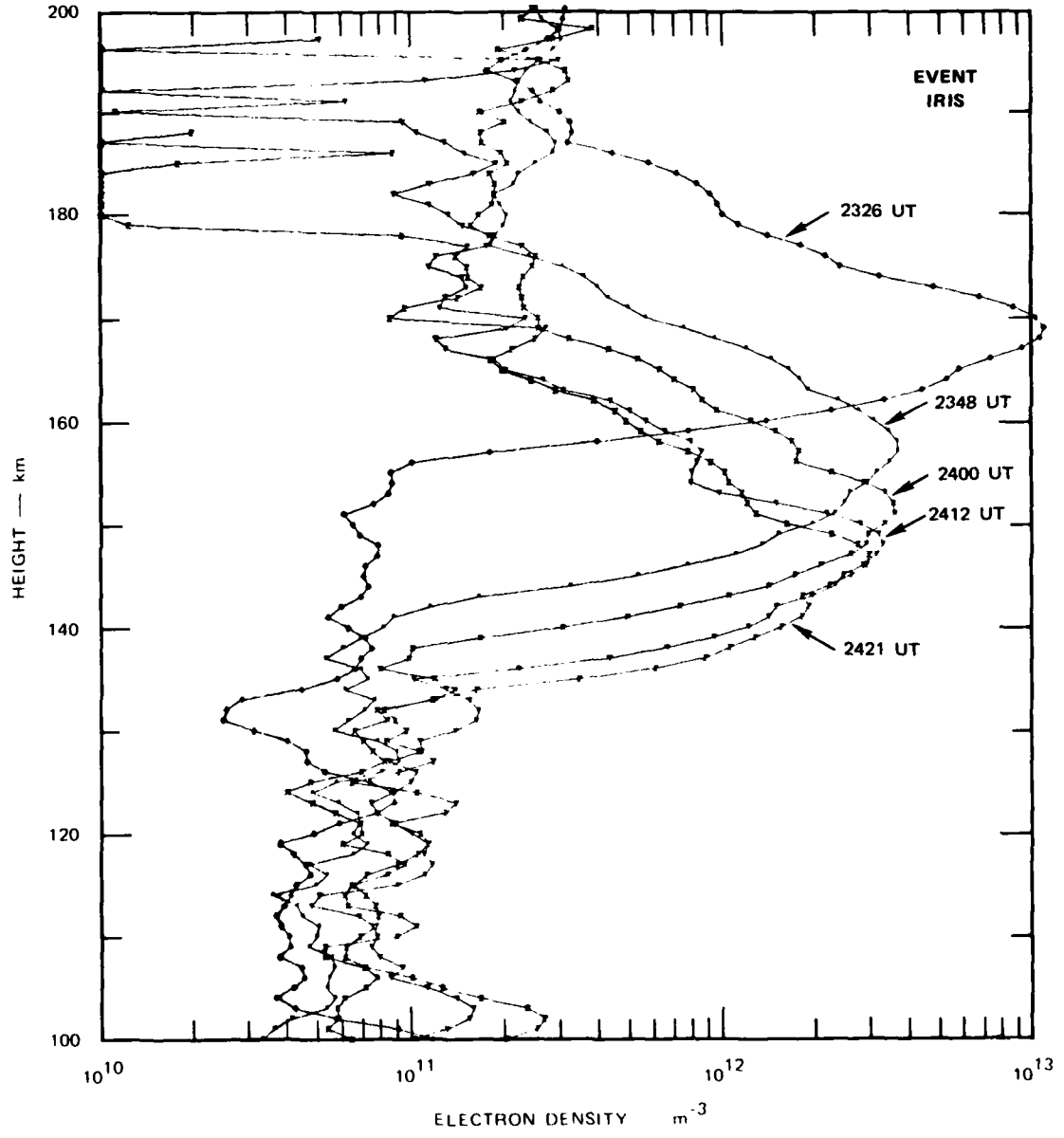

FIGURE 20 VERTICAL ELECTRON DENSITY PROFILES OF EVENT IRIS AT VARIOUS TIMES

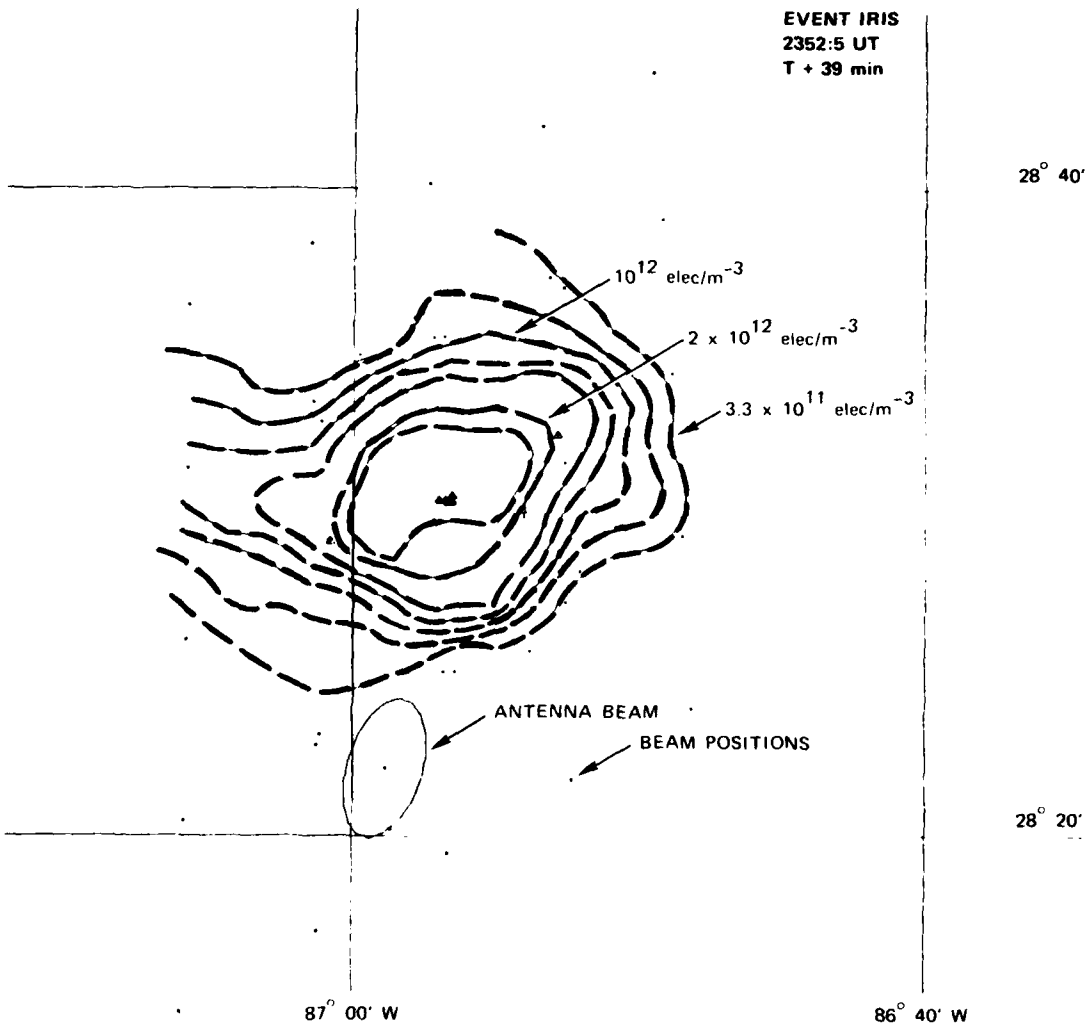

FIGURE 21 HORIZONTAL CONSTANT ELECTRON DENSITY CONTOURS AT T + 21 min

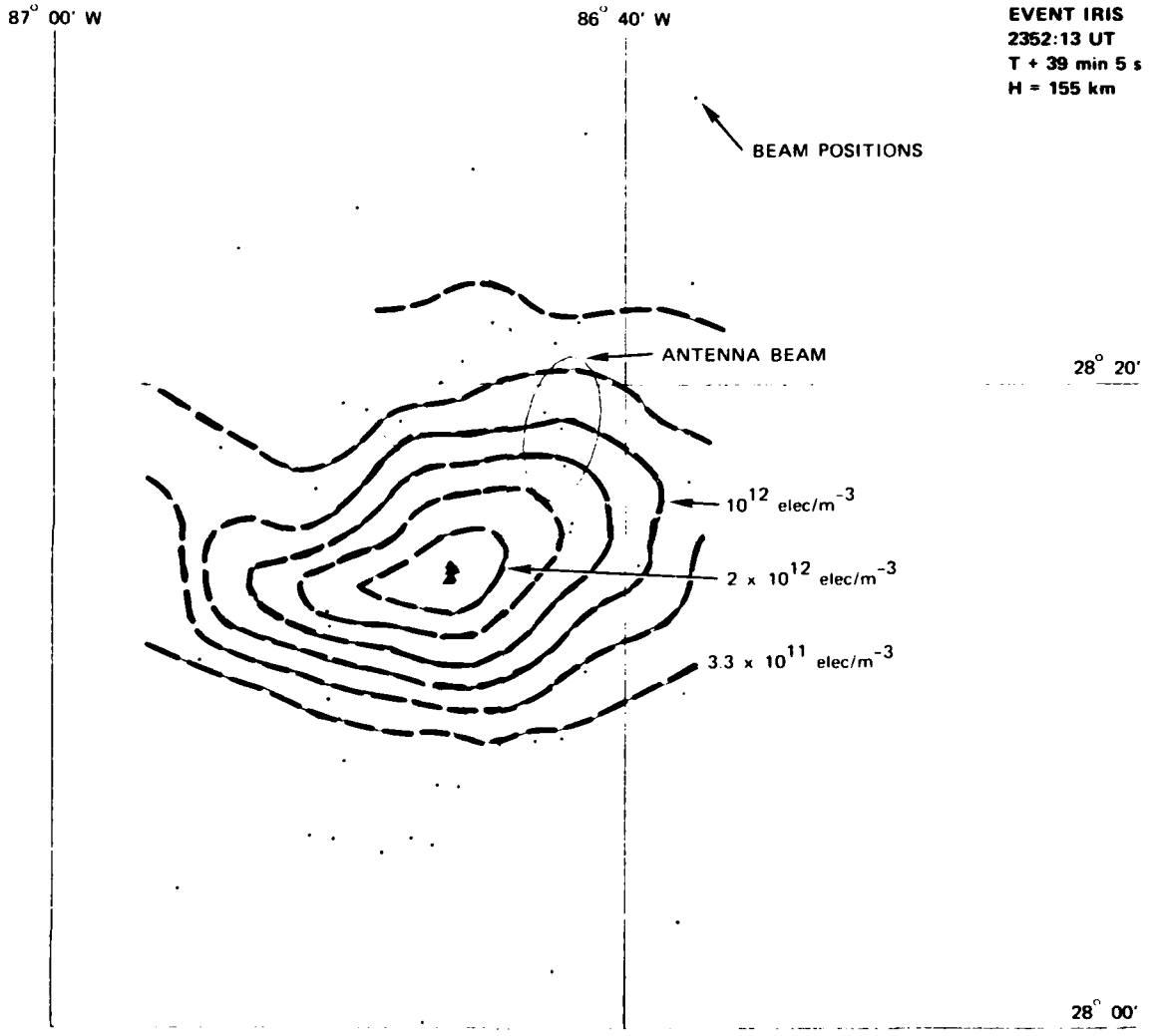

FIGURE 22 HORIZONTAL CONSTANT ELECTRON DENSITY CONTOURS OF EVENT IRIS AT T + 39 min

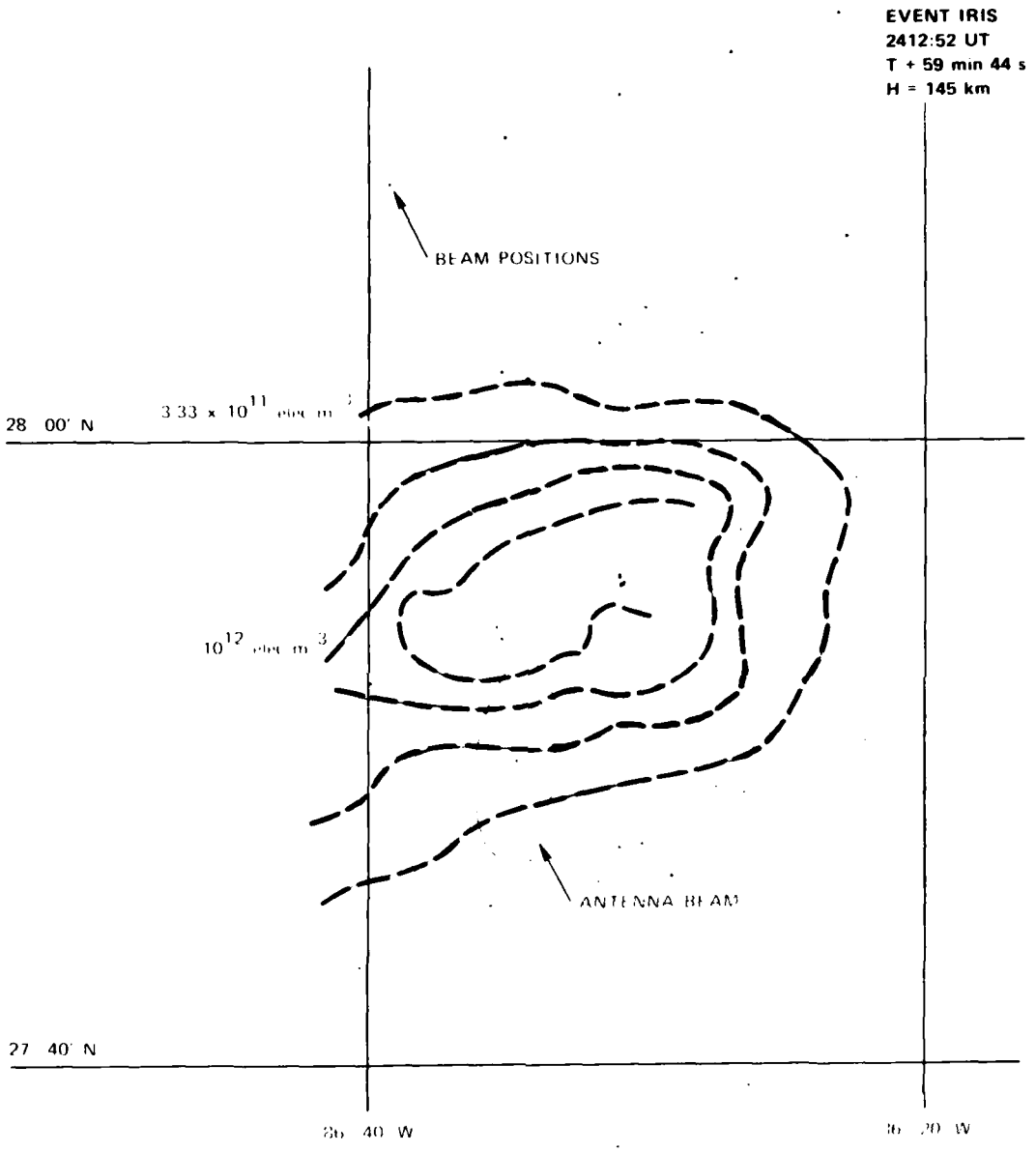

FIGURE 23 HORIZONTAL CONSTANT ELECTRON DENSITY CONTOURS OF EVENT IRIS AT T + 60 min

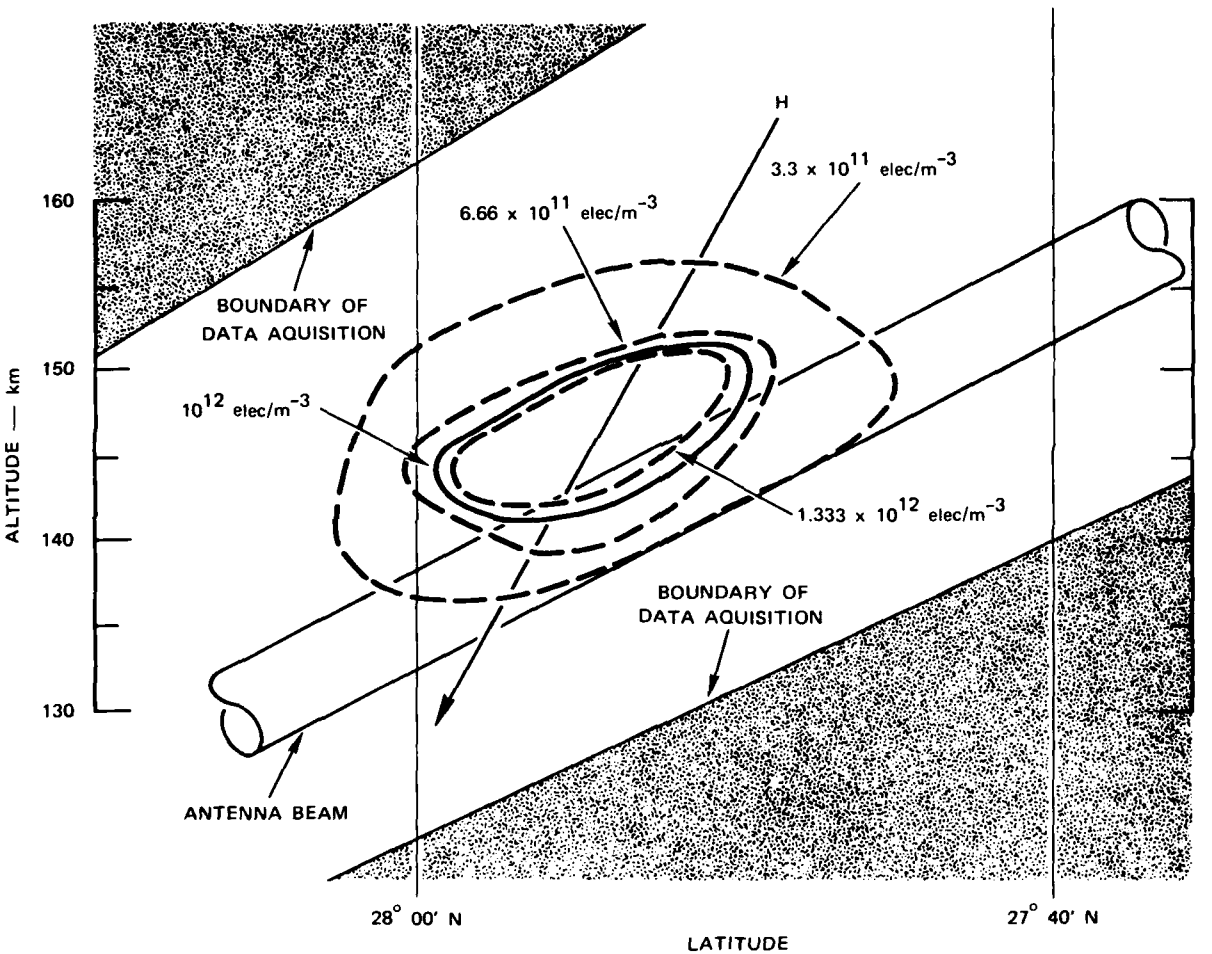

FIGURE 24 VERTICAL SLOPE OF EVENT IRIS AT 2413 UT (T + 60 min)

for 3-dB width. The overall shape of the ion cloud does not seem to align with the Earth's magnetic field. This last feature could be understood by saying that different regions of the ion cloud have descended to different altitudes. That is, if the northern part of the ion cloud which also happens to be the east part is 5 km lower than the southern part, then we can understand better the relation of the contours of Figure 24 to the magnetic field line. Again, these observations should be made with caution because of the limitations on the data acquired by the radar. The radar antenna beam uses a discrete number of positions to acquire data, and Figure 24 may be incomplete because not enough points were observed.

VI EVENT JAN

Event JAN was affected by two failures in the computer system. After a partial recovery between T + 8 min and T + 25 min, the second breakdown occurred and all efforts to reacquire the ion cloud were unsuccessful. The ground track, the altitude data, and the maximum electron density data obtained are presented in Figures 25, 26, and 27 for the sake of completeness. The very wide spread in the data points indicates the "no-track" situation that was present for most of the time.

The period of time between T + 8 min and T + 25 min may yield useful information for correlation with the probe rocket if the time for a careful data analysis is invested.

VII SUMMARY

During the PLACES series of experiments, Event GAIL was tracked for 2 hours. Event HOPE for 4 hours, Event IRIS for 1-1/2 hours; some data were obtained for Event JAN for about 15 min. The four-hr track of Event HOPE is the longest time a barium ion cloud has ever been tracked and the time could have been longer if we had not been constrained by the availability of the radar. Event JAN is singled out by the different extreme. It is the worst event in terms of tracking results. Thus, the PLACES series exceeded the STRESS series in one aspect and falls short of it in another.

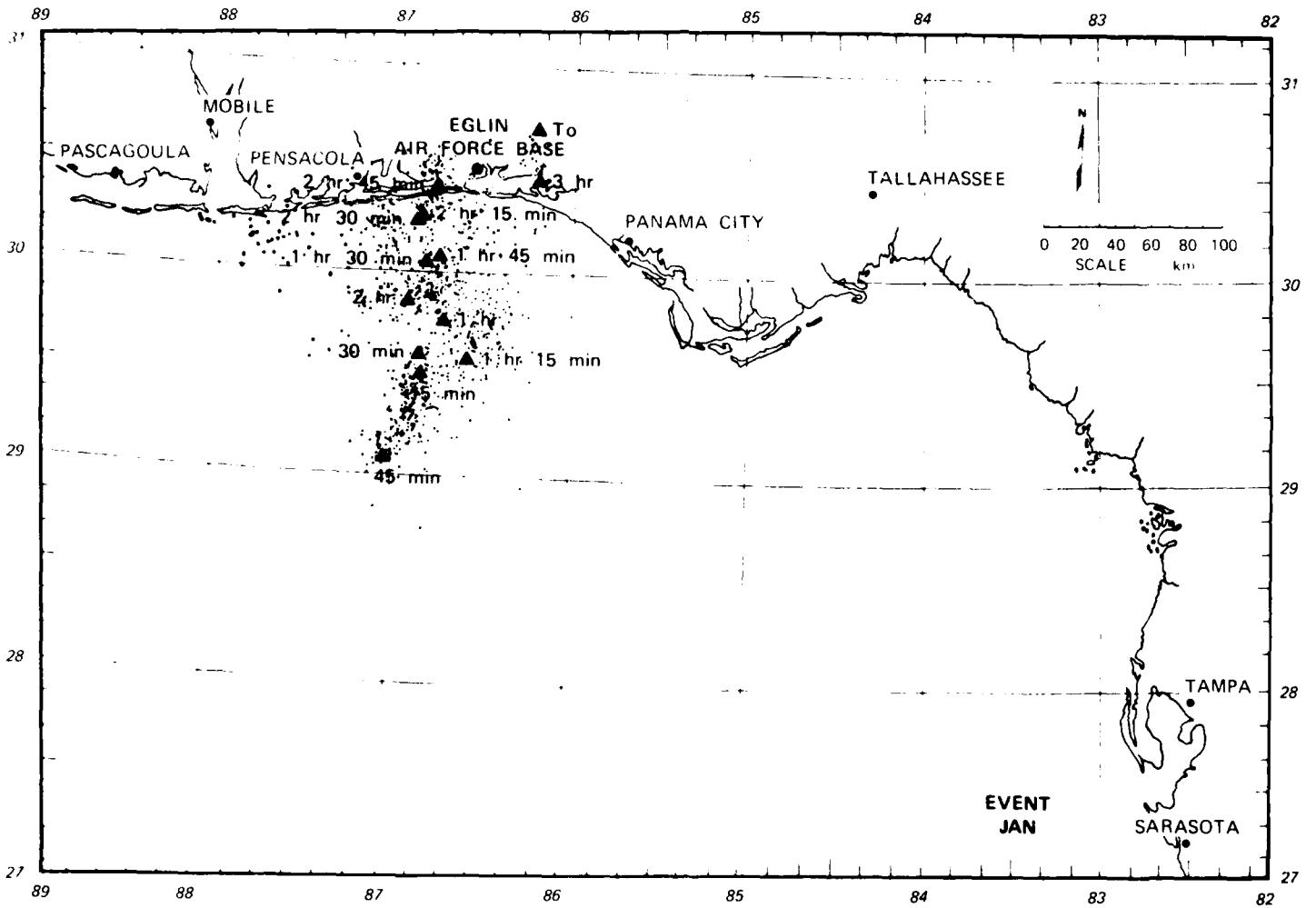

FIGURE 25 HORIZONTAL TRACK DATA OF EVENT JAN

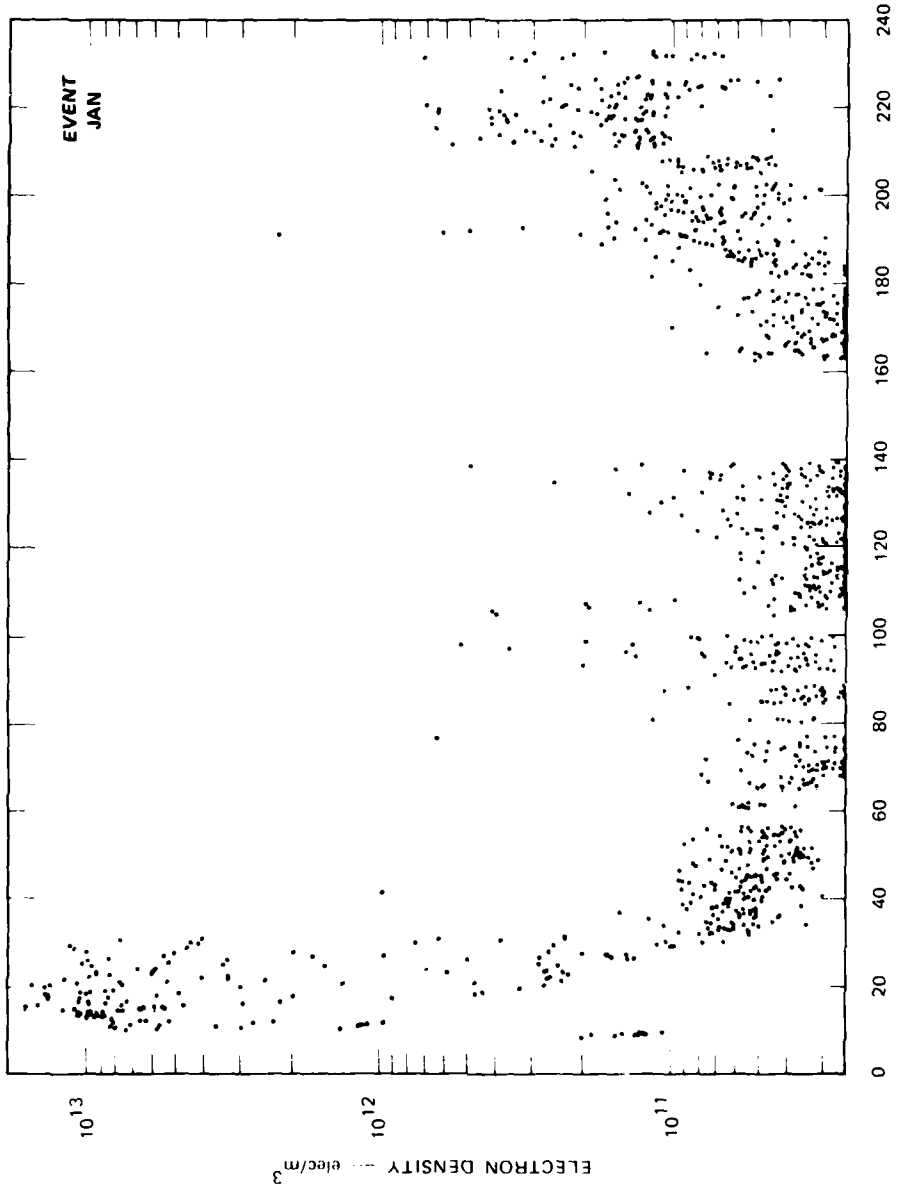

FIGURE 26 ELECTRON DENSITY DATA OF EVENT JAN AS A FUNCTION OF TIME

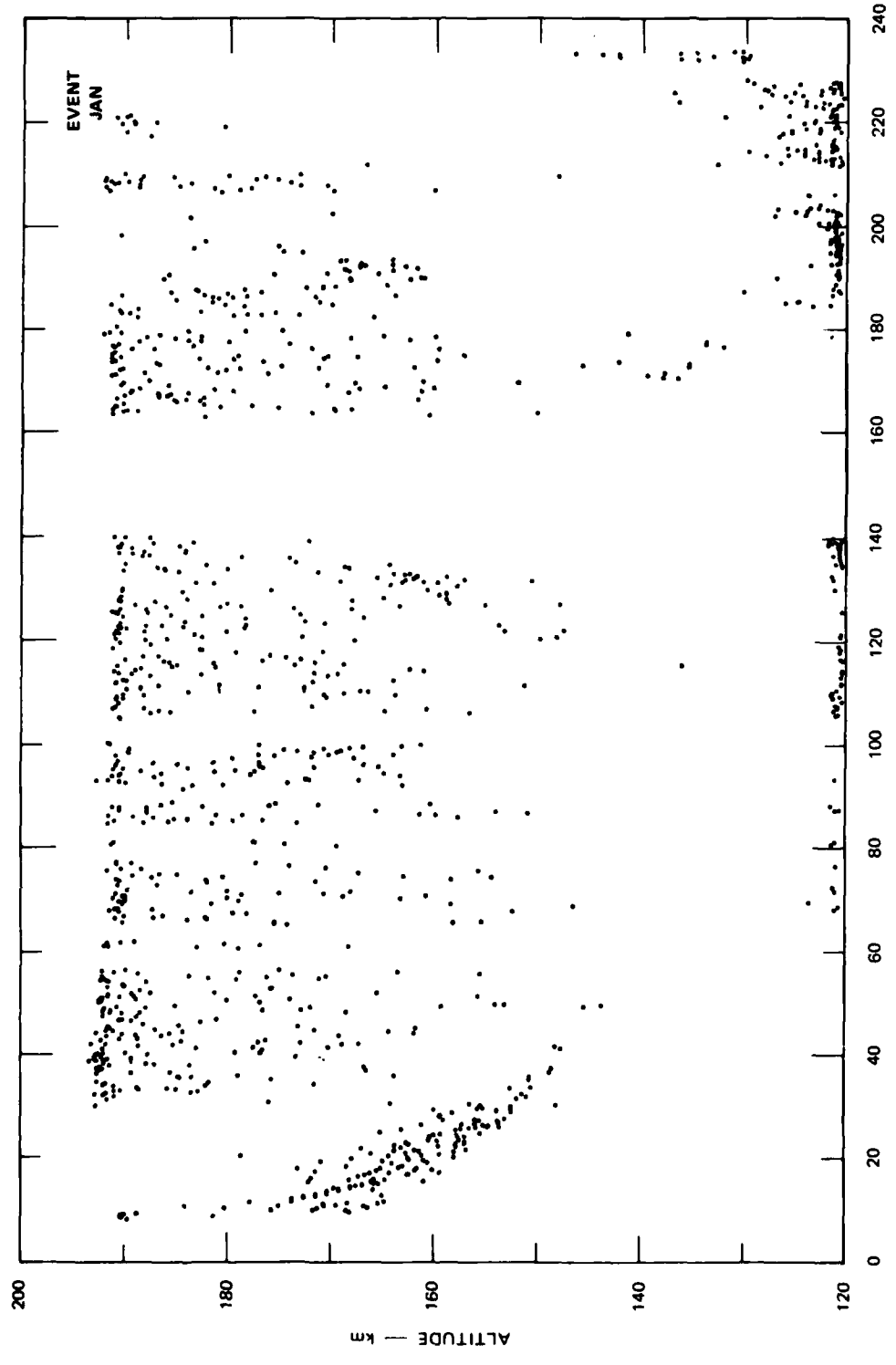

FIGURE 27 ALTITUDE DATA OF EVENT JAN AS A FUNCTION OF TIME

Part of our shortcomings were caused by the aging and cumbersome computer system in the radar. The results of the programming are small compared with the effort applied. The new tracking algorithm, coupled with our new sampling hardware, did not start to work in time to be effective.

Were a new series of releases to take place in the future, several aspects of the work done could be picked up where we left off. The continuous change in the operating system of the FPS-85 will require some reprogramming. Event JAN has demonstrated the need for a more flexible tracking algorithm.

GROUND OPTICS PHOTOGRAPHIC MEASUREMENTS

W. P. Boquist
Technology International Corporation
Bedford, MA

I INTRODUCTION

Technology International Corporation (TIC) provided the ground optics support measurements for the DNA PLACES program at the Eglin Gulf Test Range, Florida during November and December 1980. The optical measurements were intended to, and did, obtain data for use in support of the operational aspects of the experimental field program as well as for use in subsequent phenomenological studies related to both the PLACES program and more general applications.

The PLACES program consisted of four high-altitude barium release events. The thermite type barium payloads were of the 48-kg yield category and were timed to release at a nominal 185 km altitude on rocket ascent. Table 1 presents the operational parameters of each of the four events, including the time at which the solar depression angle (SDA) is at 6°, and the temporal extent of optical coverage for each event. Also included is the approximate time of aircraft-satellite transmission fading coverage and the times of occultation for the beacon and probe rocket experiments which occurred on the last two events only, as indicated.

In order to support both the operational and phenomenological aspects of the barium release program, the ground optics stations were instrumented to provide five major categories of coverage, from site locations described in Section II, which are as follows:

(1) Triangulation of barium neutral and ion cloud motion
(2) Morphological development of ion cloud structure

Table 1

PLACES EVENT MATRIX

Event	Date (LT)	Time, GMT	Time at Which SDA = 6°, GMT	HOB (km)	Remarks
GAIL	4 Dec	2307:35	2313	181.3 (radar = 180)	Optics to R + 39 min A/C to R + 2 hr 29 min
HOPE	6 Dec	2307:37	2313	182.6	Optics to R + 41 min A/C to R + 2 hr 6 min
IRIS	8 Dec	2313:08	2313	182.2	Beacon 1, 2345:19 GMT Beacon 2, 2358:20 GMT Optics to R + 36 min A/C to R + 2 hr 37 min
JAN	12 Dec	2313:42	2314	183.7 (radar = 184.3)	Probe 1, 2344:41 GMT Optics to R + 35 min A/C to R + 2 hr 43 min

(3) High-resolution measurements of striation geometry

(4) Ion cloud radiometric brightness history

(5) Probe type rocket trajectory determination.

Certain additional coverage was also provided by TIC to augment this primary coverage, as discussed in the following section.

II OPERATIONAL PROCEDURE

The ground optics instrumentation was located almost in its entirety at three primary optical triangulation stations. The station locations were chosen to optimize the relative cloud perspective for morphological study, and the optical triangulation base leg between the sites, and so as to most efficiently utilize the siting and communication facilities available at the Eglin and Tyndall Air Force bases. Figure 1 shows the location of the three TIC triangulation sites, at Eglin A-105, Eglin C-6, and Tyndall 9702, with respect to the launch site at Eglin A-15, and the subsequently triangulated burst point projections for the four events. Also shown are the locations of two secondary sites for which TIC supplied camera instrumentation at Eglin D-3A and at St. George Is. Additional camera equipment was also provided for use on the AFAL KC-135 aircraft operating out of Eglin AFB for the period of the operation.

The results of the ground optics coverage for the four PLACES events were generally extremely good throughout. In two of the events (GAIL and JAN) a triangulation station was viewing the barium ion cloud up (or very nearly so) the field lines and obtained excellent data on the structural formation and development of the ion cloud. Except for Event IRIS, all three sites observed the release history for the order of one-half hour or more; dense clouds unfortunately obscured the A-105 site for the IRIS Event.

Photographic tracking of the probe rocket in the JAN event was also very successful. The Sandia coded strobe flash sequence was observed and recorded from at least two sites, and triangulation of the in-situ probe is expected to present no significant problem. The IRIS beacon rocket

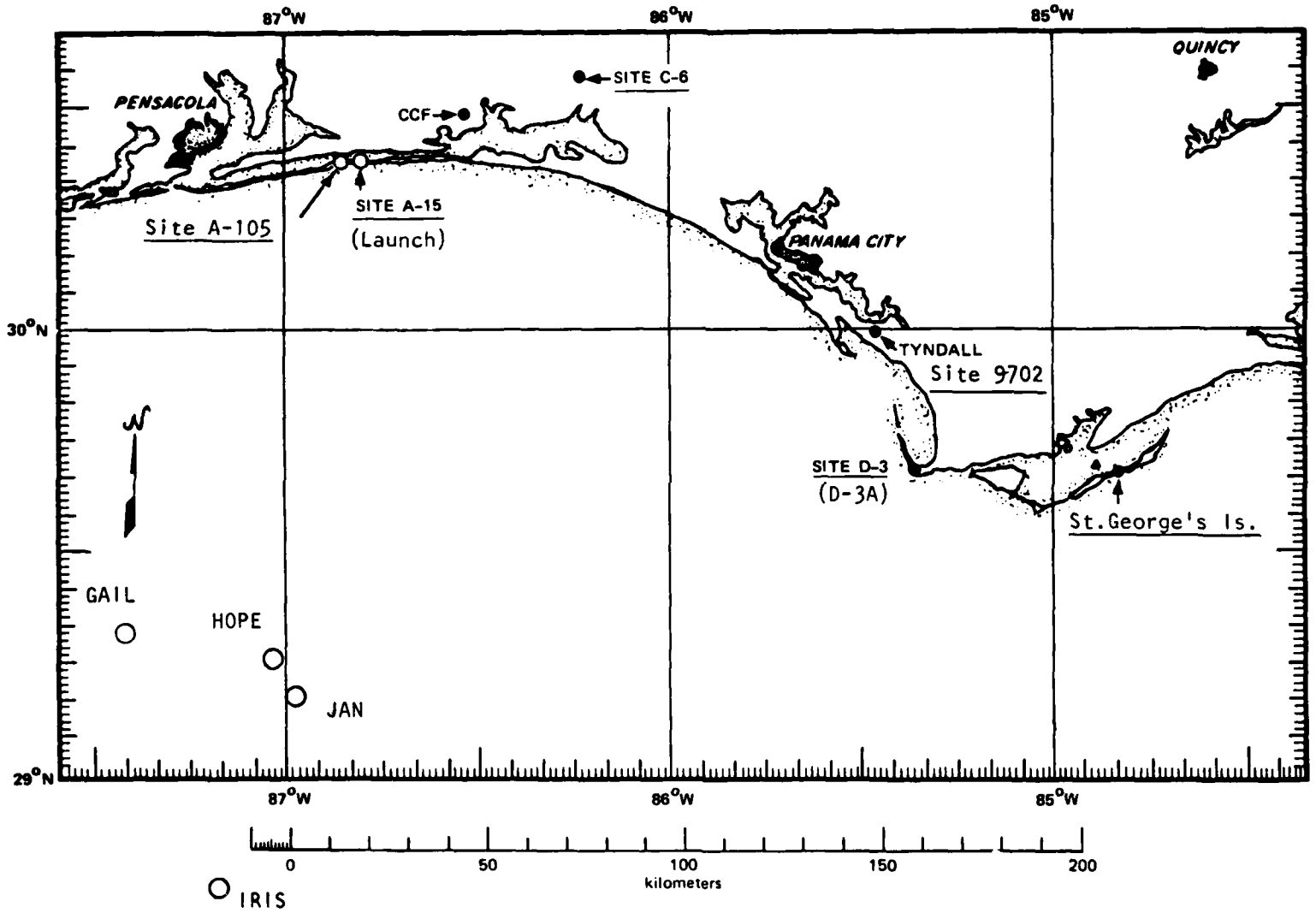

FIGURE 1 PLACES GROUND OPTICS SITE LOCATIONS

experiments, however, were launched during periods of intermittent partial cloud obscuration, and those strobe flashes have not as yet been observed.

III DATA REDUCTION MEASUREMENTS

A significant fraction of the scheduled data reduction of the PLACES ground optics photographic records has been achieved as of the time of this report. This section is a summary of some of the preliminary data, excluding the color pictorial history data which will be included as black and white photographs in the TIC final report and of course the time lapse films produced as an analysis aid for phenomenological studies.

The calculated event burst point locations for the PLACES events are presented in Table 2. The measured burst height is given in kilometers above mean sea level, together with the geographic coordinates for each event. The burst point calculation is based on an image of the neutral cloud obtained in the first one to two seconds after release, and therefore may be slightly different from the altitude at which the initiation of the thermite reaction occurs.

Having defined the time of ion cloud striation onset as being the time at which a complete first (apparent) striation has been formed with respect to the ion cloud as a whole, the color morphology records were examined from each triangulation site for each event, and the time after release noted. The results of this determination are presented in Table 3. In general, because of a combination of effective sky background and perspective advantage, one site out of the three will see the striation onset before the other two in this particular experiment geometry. Aside from the intrinsic value of the onset time data for operational considerations, the data will have application to theoretical models used for predicting ion cloud structural development in the midlatitude environment.

In addition to the burst point triangulation calculations described above, the ground tracks of the neutral and ion clouds for the IRIS and JAN events were determined for this preliminary report. The cloud position data were obtained from release to plus 20 min for each of the events,

Table 2

PLACES BURST POINT LOCATIONS

Event	HOB (km)	Geographic Coordinates
GAIL	181.3	29°19'02"N 87°25'11"W
HOPE	182.6	29°15'48"N 87°02'29"W
IRIS	182.2	28°45'48"N 87°11'07"W
JAN	183.7	29°10'34"N 86°58'40"W

Table 3

PLACES STRIATION ONSET TIMES*

Event	A-105 Site	C-6 Site	Tyndall Site
GAIL	R + 10 min 14 s	R + 10 min 14 s	R + 9 min 30 s
HOPE	R + 15 min 20 s	R + 17 min 10 s	R + 17 min 13 s
IRIS	(clouds)	R + 10 min	R + 9 min 44 s
JAN	R + 11 min 11 s	R + 12 min 36 s	R + 13 min 07 s

*Time for first observable separated structure.

together with an altitude determination at each time of triangulation. The neutral cloud was measured at the geometrical center of the apparent cloud outline, initially a circle and often an elliptical shape at late times due to upper atmospheric wind shear. The ion cloud data, on the other hand, were determined from the measured position of an estimated center of the striated region of the ion cloud after striations had occurred in a given cloud.

Figure 2 is a plot of the IRIS neutral and ion cloud height history; the circles are the neutral cloud data and the triangles are the structured ion cloud data. The IRIS ground track data are shown in Figure 3 in 5-min increments. From these preliminary data it appears that the neutral cloud, after heading southeast for about 10 min at a relatively constant altitude, began to fall slowly and adopt a more easterly course. The IRIS ion cloud structured region appeared to undergo a slight direction change at about 10 min and a somewhat more radical change to the south after about 16 to 17 min while falling more rapidly than the neutral cloud during the 10-to-20-min period.

The corresponding JAN triangulation data are shown in Figures 4 and 5 for the cloud height and ground track data, respectively. The height history of the neutral cloud shows (after an initial small ballistic rise) a gradual descent over a 20-min period. The ion cloud structured region, after appearing to fall a few kilometers between 9 and 12 min, maintained a relatively constant altitude until about 20 min, at which point it appeared to begin to fall further.

The JAN ground tracks shown in Figure 5 exhibit a smooth, consistent motion to the north-northeast. The consistency of cloud motion permitted a predictable continuing cloud trajectory such that a probe rocket could be programmed and fired successfully into the ionized barium at R + 31 min.

Table 4 summarizes the neutral and ion cloud motion velocities averaged over the ground track of the respective clouds from release to plus 20 min. The two events triangulated thus far, while not differing significantly in velocity, did however exhibit conformity with the predicted net easterly motion and were within the velocity range of 20 to 100 m/s observed at these latitudes in prior DNA experiments.

IV CONCLUSIONS

The PLACES optical coverage obtained on each of the four barium events was of high quality and very extensive. Except for very late times, data records averaged a temporal resolution of about 10 s for a

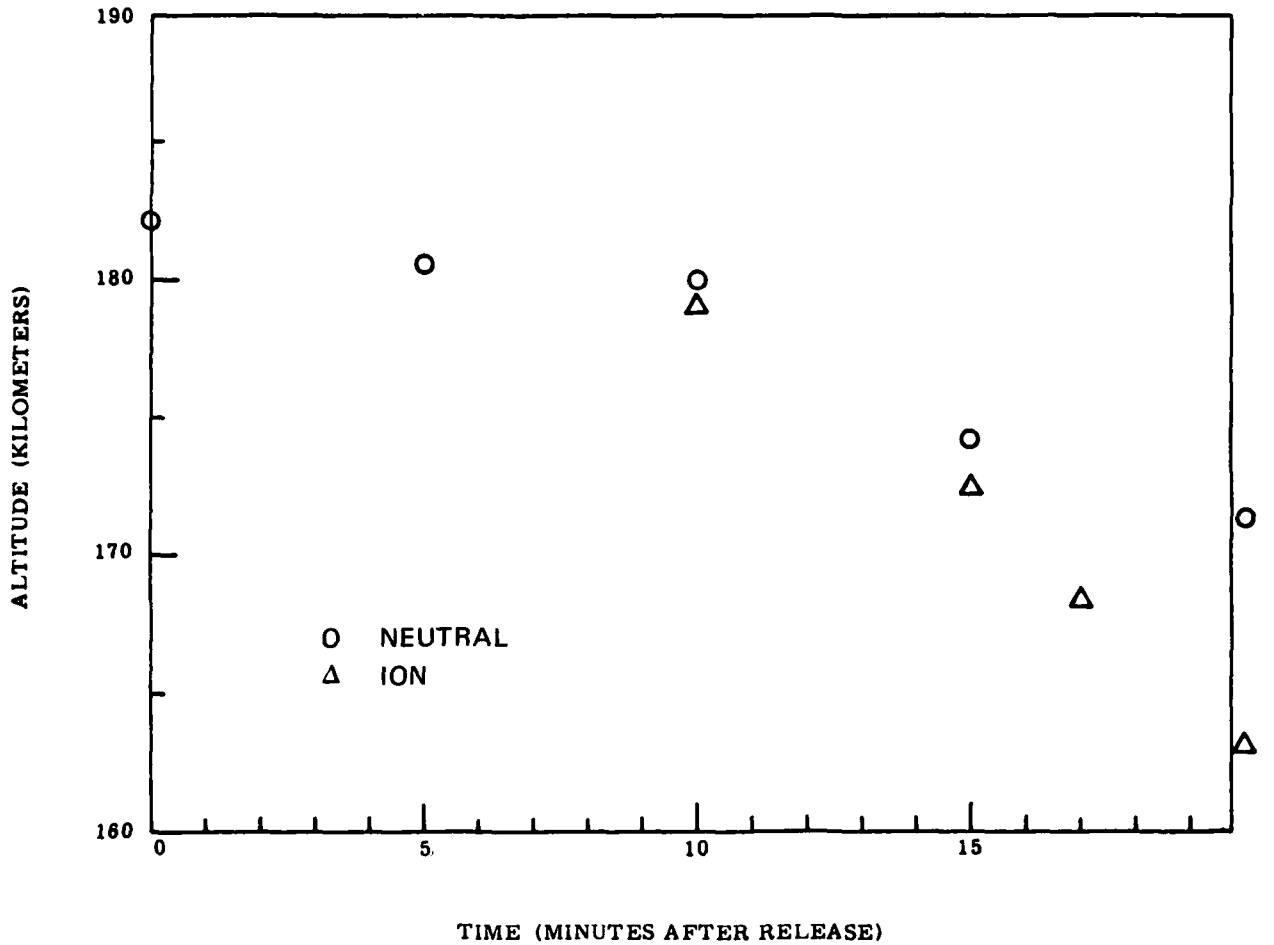

FIGURE 2 IRIS NEUTRAL AND ION CLOUD CENTER HEIGHT

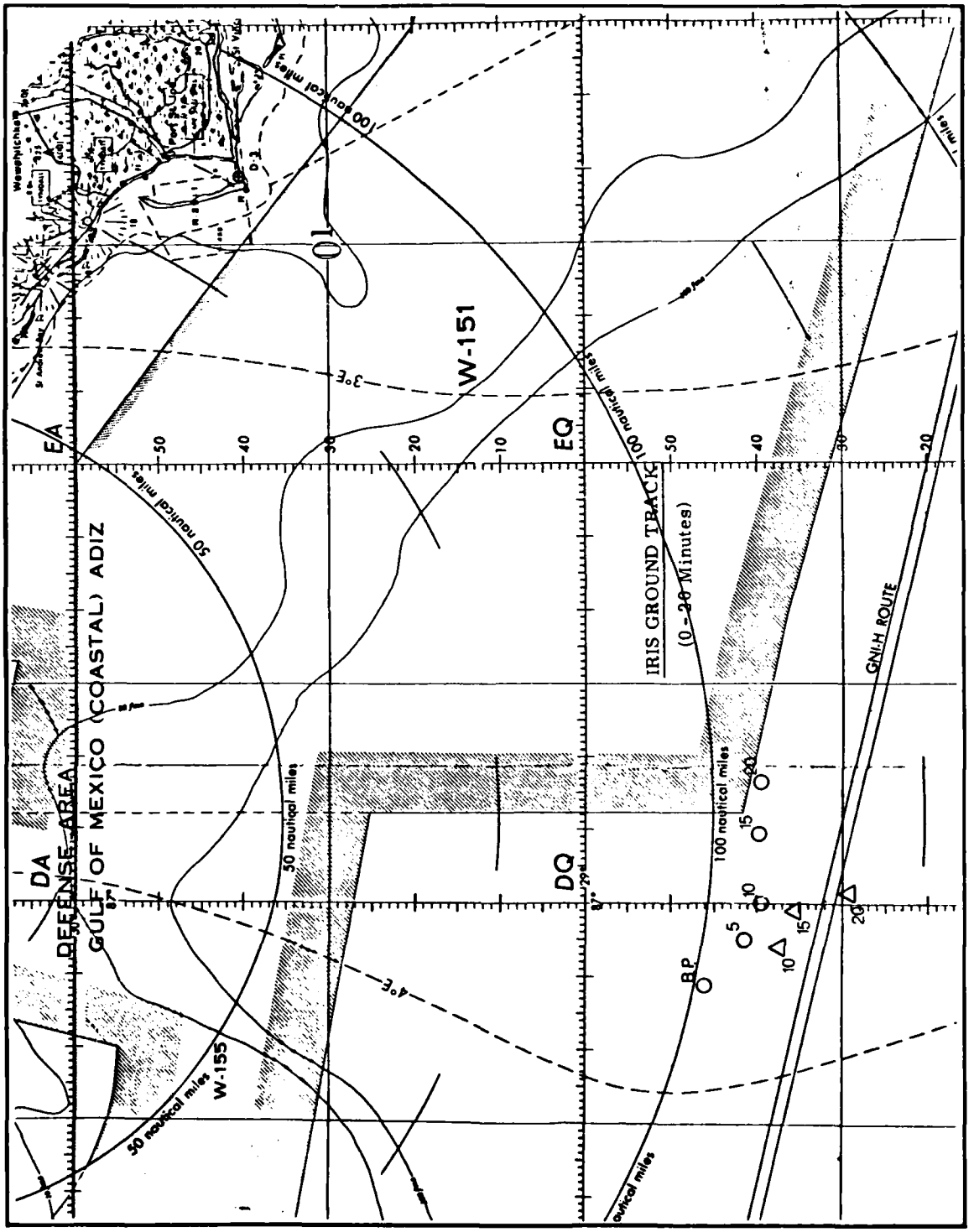

FIGURE 3 IRIS GROUND TRACK (0 TO 20 min)

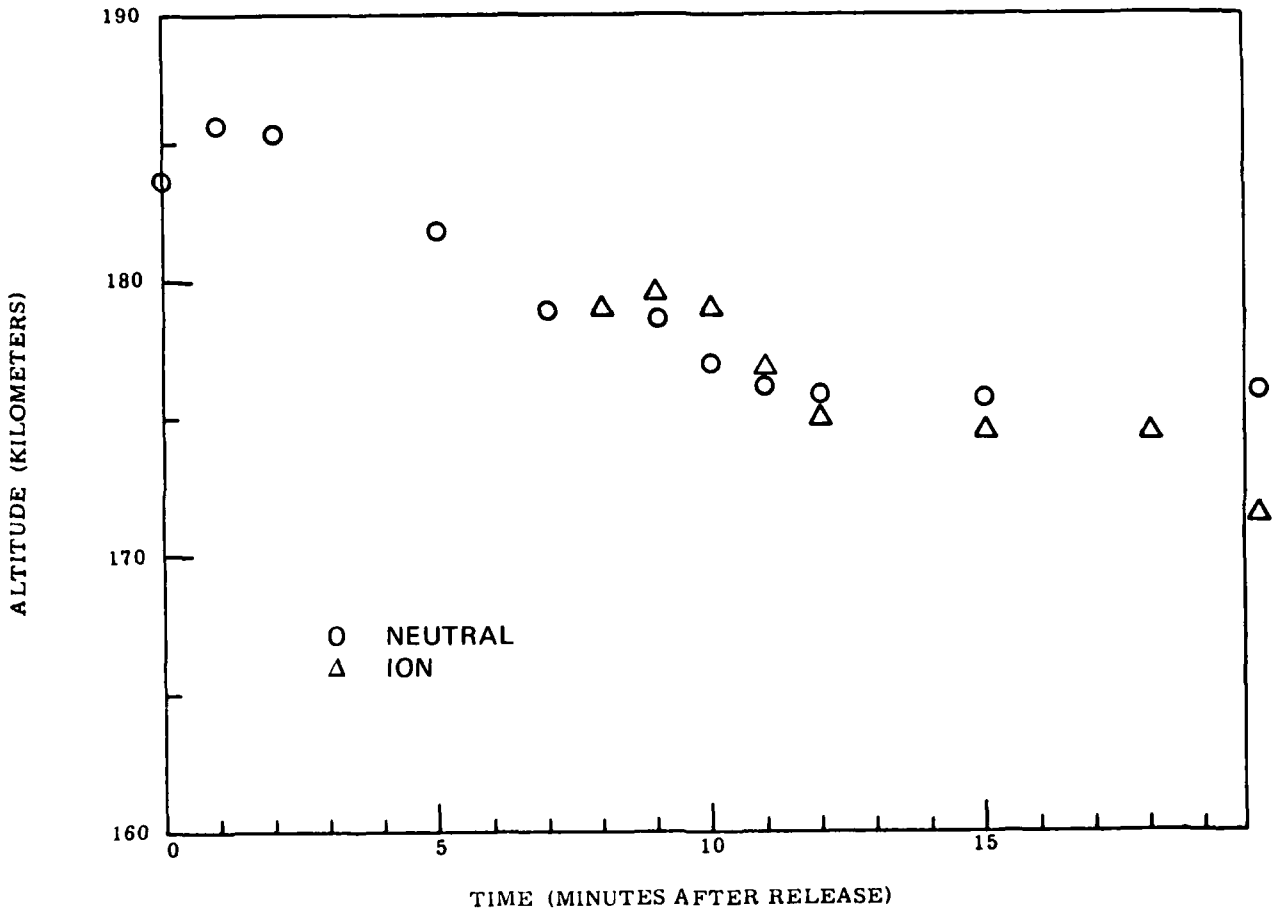

FIGURE 4 JAN NEUTRAL AND ION CLOUD CENTER HEIGHT

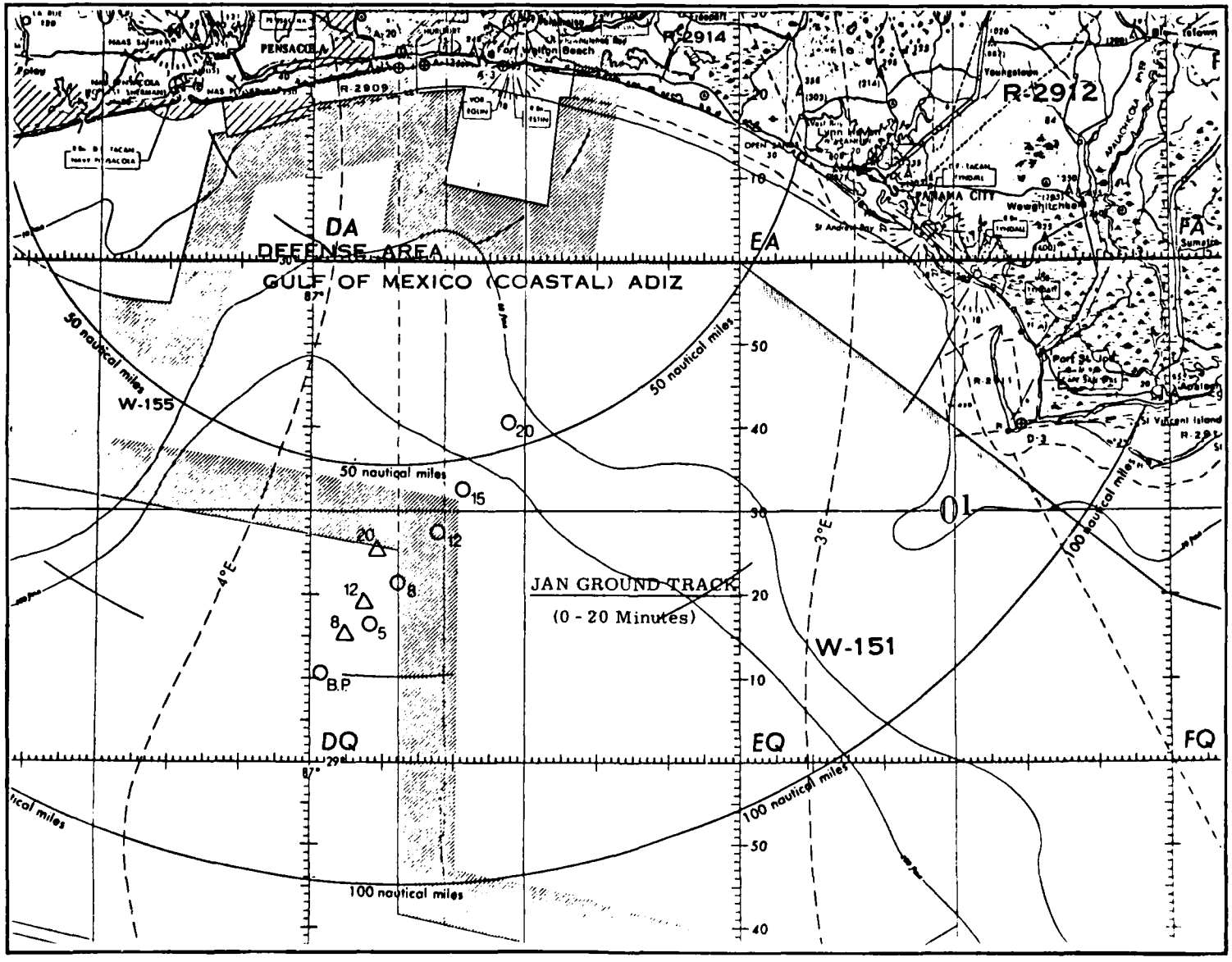

FIGURE 5 JAN GROUND TRACK (0 TO 20 min)

Table 4

PLACES BARIUM CLOUD
VELOCITY MEASUREMENTS

Event	Average Ion Cloud Velocity, 0 to 20 min (m/s)	Average Neutral Cloud Velocity, 0 to 20 min (m/s)
IRIS	35	47
JAN	24	58

period of approximately one-half hour, providing good coverage of morphological changes in the cloud structure and general development.

Continuing data reduction of the PLACES film records will provide triangulation for the GAIL and HOPE events, and a detailed measurement of the east-west component of the neutral and ion cloud velocities. It is also planned to provide brightness time history data for the IRIS and JAN ion clouds, for which either a beacon or probe rocket was deployed during the period of optical coverage.

INTENSIFIED OPTICS

D. J. Simons, M. B. Pongratz, G. Smith
Los Alamos National Laboratory
Los Alamos, New Mexico

I INTRODUCTION

The PLACES experiments were a Defense Nuclear Agency sponsored series of ionospheric barium releases to investigate the effect of structured ionospheric plasma on satellite communication systems. The experiments took place during December 1980, at Eglin Air Force Base, Florida. The Space Sciences Office (formerly Group P-4) at the Los Alamos National Laboratory provided and manned two optical stations during these experiments for the acquisition of data, using intensified optical systems.

The Space Sciences Office at Los Alamos has been taking intensified pictures of the weaker of the five Ba II emission lines in an attempt to determine ion column density when barium clouds are optically thick in the two primary lines (455.5 nm and 443.4 nm). These two primary lines are resonantly pumped by the incident solar radiation. At barium column densities in excess of 10^{11} ions/cm^2 these two lines become optically thick so that photons undergo multiple scattering before exiting the cloud. The PLACES barium clouds were predicted to yield ion column densities in the range of 10^{12} to 10^{13} ions/cm^2. These column densities precluded the possibility of using the ion cloud brightness in the principal lines as a direct measure of column density. Since the weaker ion lines require much greater column densities before multiple scattering becomes significant, it seemed possible that they might provide the appropriate diagnostic. One-dimensional numerical radiation transport does support this conclusion.

Los Alamos identified three objectives for its experimental participation in PLACES. These objectives were:

(1) To measure the spatial frequency power spectral density of the barium cloud striations.

(2) To confirm the principles of the measurement technique--i.e., that images of the barium ion cloud accurately reflect the integrated column density.

(3) To make ancillary measurements of ion and neutral cloud morphology.

II SITE LOCATION

We felt that proper site selection was critical to satisfying the experimental objectives. We studied the effects of background sky brightness, magnetic field geometry, cloud cover, and azimuth and elevation to possible cloud positions. The results of this study were reported by M. B. Pongratz[2] previously. We chose two sites: the primary site was located at Tarpon Springs, Florida, within a facility of Eglin AFB, Site D-4 at the Anclote Power Station (28.185°N, 85.44°W). The primary site was selected to optimize all of the diagnostic requirements, while the secondary site was selected to provide photographs of column density and morphology at a beacon receiver location. The secondary site also provided data for cloud triangulation in addition to some site diversity for purposes of reducing the impact of local weather. The site locations are indicated on the maps in Figures 1 and 2.

III INSTRUMENTATION

The primary intensified optical systems are mounted on trackers that are steerable in azimuth and elevation. The azimuth and elevation are encoded and displayed in real time for the individual controlling the mount pointing. The real-time pointing selection and tracking capabilities are facilitated by including an intensified video system filtered at the primary barium ion line, 455.4 nm, on each tracker, with a monitor display site. Table 1 shows the photo plan for this site.

In addition to our primary objectives, we generally include several instruments for the purpose of documentation of such things as general

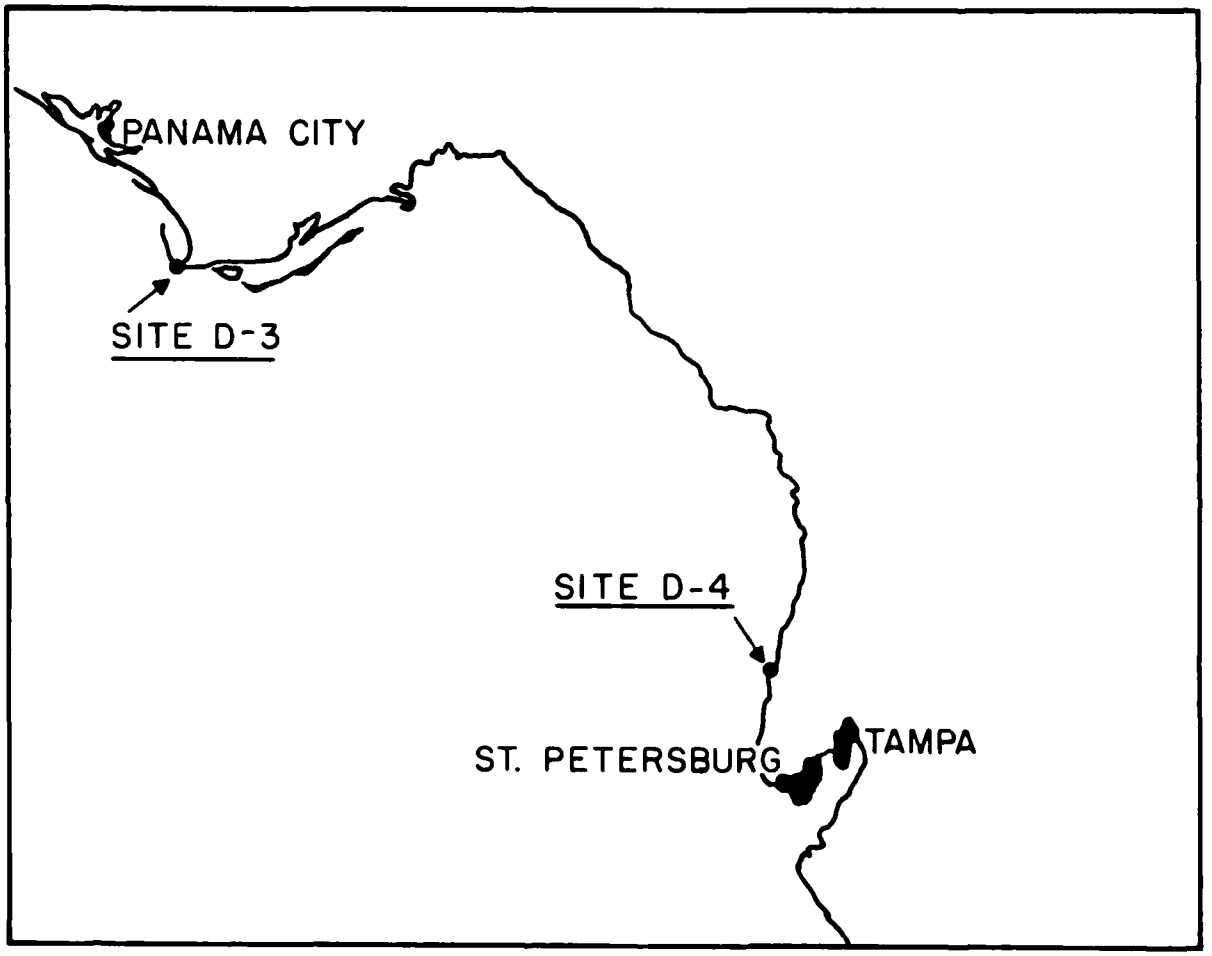

FIGURE 1 LOCATION OF THE PRIMARY STATION AT SITE D-4

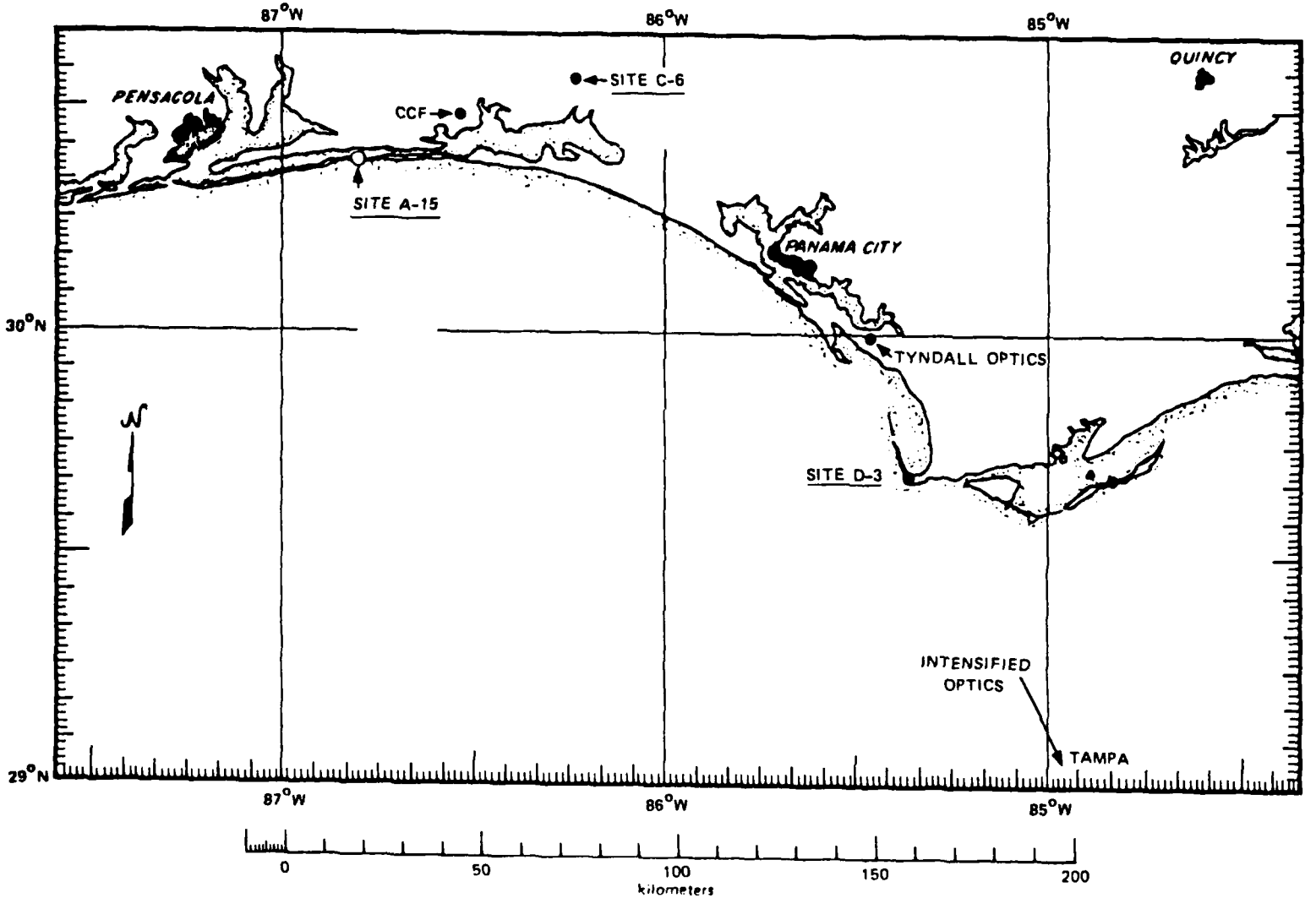

FIGURE 2 LOCATION OF THE SECONDARY STATION AT SITE D-3

Table 1

PHOTO PLAN

EVENT PLACES — PREPARED BY Gordon Smith — DATE 25 Sept. 1980

STATION NO. D-4 ANCLOTE — EVENT DATE December, 1980

STATION TYPE GROUND

CAMERA								LENS			FILTER		AIMING		TIME		MARKER	FILM					
			NOM.		EXPOSURE			F.L.		FIELD													
NO.	TYPE	S/N	SPD.	POS.	SHUT	SHUT	APER	MM	S/N	H/V	TYPE	NO.	H	V	ON	OFF	RATE	SIZE	LENGTH	EMUL. NO.	TYPE	PERF. H
				T																		
1174	ICA-78		16 F/M	R	(3)		1.8	400	-062	5°/3.5°	6142						WT	35mm	100'		TRI-X	
Y26 1211	ICA-78		16 F/M	A	(3)		1.8	400	-065	5°/3.5°	5854						WT	35mm	100'		TRI-X	
	1-SIT	1		C			1.3	15-120	730225	VAR	4554						WT	VIDEO				
	CANON	1	(4)	K			2.5	135	32087	15°/10°	NONE						WT	35mm	36 exp		K-400	
				E																		
				R																		
				T																		
1185	AC BIRD	1	16 F/M	R	(3)		5.6	360	6247128	25°/20°	(1)						WT	35mm	100'		TRI-X	
	CANON	2	(4)	A				105-200	30020	12°/9°	NONE						WT	35mm	36 exp		K-400	
Z-Stage Mag.	ICA-78		16 F/M	C II	(3)		14	2500	-6CVQZ	0.8°/0.6°	6142						WT	35mm	100'		TRI-X	
	ICA-78		16 F/M	K	(3)		1.5	203	2141	10°/7°	(2)						WT	35mm	100'		TRI-X	
	1-SIT	2		E			1.3	15-120	730338	VAR	4554						WT	VIDEO				
				R																		
	PRITCHARD PHOTOMETER	1		TRIPOD			3.5	175	-	VAR								VISICORDER				
(5)	ICA-75		16 F/M	TRIPOD	(3)		1.8	150		12°/9°	6142						WT	35mm	100'		TRI-X	

DATE FILM LOADED

DATE CAMERA LOADED

DATE EXPOSED

DATE PROCESSED

NOTES (1) 3900 - 8000 Å Grating, Slit ~ 300 μ (Horizontal)

(2) 5535 Å Change to 5854 Å @ + 2 min.

(3) Exposure Sequence: ½, 2, 8, ½, ½ Off

(4) Manual Exposure

(5) Location - D-3

cloud morphology and background sky brightness. The 35-mm Canon cameras, on both trackers at Site D-4, were for recording general impressions of cloud size and color characteristics. Several pictures from these cameras are included in this report. Some instruments, of course, serve multiple purposes. The two 400-mm f/1.8 systems on Tracker I were designed to be as nearly identical as possible except for their interference filters, which are 614.2 and 585.4 nm. This arrangement will permit a quantitative comparison of brightness as well as such deduced quantities as power spectral density between these two weaker barium lines. Most of the power spectral density evolution will be determined with the 614-nm, 400-mm system because 614.2 nm is considerably brighter than 585.4 nm, and these 400-mm systems cover more of the ion cloud than the longer-focal-length higher-resolution 2500-mm systems. The AG-Bird (called Silverbird) is a spectrometer that measures relative intensities of the five barium ion lines. This will permit us to compare the theoretical calculations of Horak and Whitaker[1] with the actual brightness in the various PLACES clouds.

Briefly, the remaining instruments on the photo plan are: the Pritchard photometer, which was used to measure sky brightness in the region of the release; a 203-mm, intensified 35-mm format camera filtered initially at 553.5 nm to observe the barium neutral cloud and then switched to 585.4 nm to observe the ion cloud; a 150-mm, intensified 35-mm format camera filtered at 614.2 nm to document the size and shape of the entire ion cloud; and a 2500-mm, 35-mm format camera with a two-stage magnetic intensifier filter at 614.2 nm to record fine structure in the ion cloud.

The intensified cameras are all operated on the same exposure sequence. This exposure sequence is selected to provide for the possibility that the cloud is not as bright as predicted. On the other hand, the shortest possible exposures reduce image motion and allow for the highest spatial resolution. In general, the short exposures were quite adequate for early times in these experiments, but, as the cloud diffused, the longer exposures became necessary. The intensified camera exposure sequence was 1/2, 2, 8, 1/2 (in seconds), with 1/2 s between exposures. Each camera was radiometrically calibrated so that film density could be

converted to spectral radiance. The calibrations also permit us to plan sequences of neutral-density filters if the ion cloud is sufficiently bright to cause overexposures. Figure 3 shows a typical plot of diffuse density versus spectral radiance (H and D curve) for our intensified systems. In this case it is for the 400-mm, f/1.8, 614.2-nm system mentioned above.

IV WEATHER

The intensified optics were not treated as a No-Go in the launch criteria for the individual PLACES experiments. It was for this reason that we felt it was relatively important to plan for site diversity. As it turned out, we were relatively fortunate to have generally cloud-free lines of sight to each of the four PLACES events. For Events HOPE, IRIS, and JAN we had a cloud-free line from the primary station at Site D-4 to the events. There was very dense cloud cover at Site D-4 during most of Event GAIL, but we obtained excellent data from Site D-3 using a 150-mm intensified system filtered at 614.2 nm. We also obtained data from Site D-3 during Events IRIS and JAN, using this same system.

V DATA REVIEW AND SUMMARY

The initial release was clearly visible from both stations on all experiments so that the trackers had no difficulty in acquiring the clouds and following them through all stages of striation development. Typically, a more-or-less diffuse ion cloud existed out to about 10 or 15 min on each event, at which time a steep edge became evident. This edge produced a well-defined striation and then rather rapidly was followed by the formation of many striations. This was not so evident with Event HOPE, for which we obtained data only from Site D-4. As it appeared from Site D-4, HOPE formed only a few well pronounced striations and evolved very slowly. On all four events there is about 30 min of usable data before the solar terminator has passed the altitude of the ion cloud.

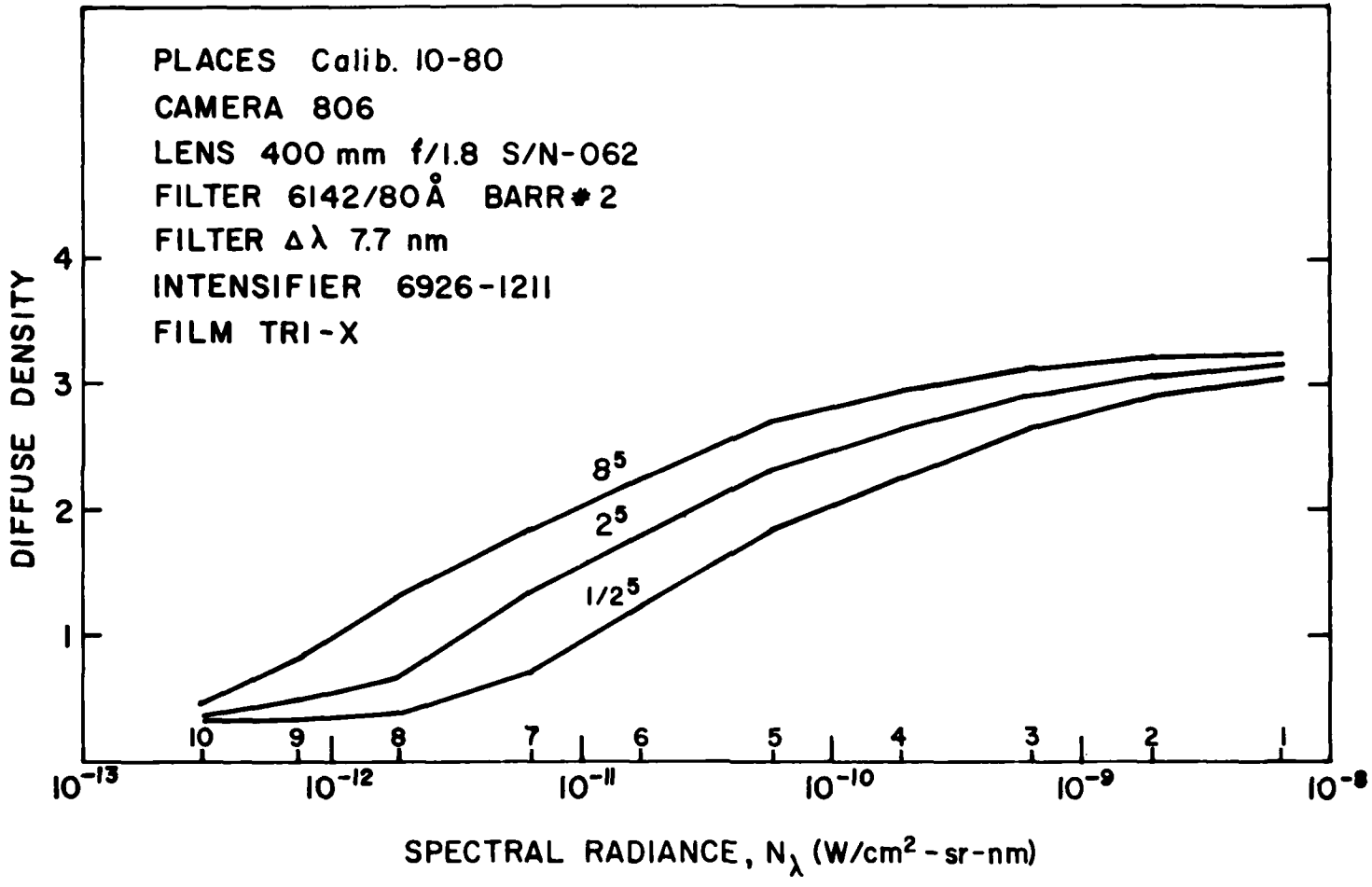

FIGURE 3 TYPICAL INTENSIFIED CAMERA CALIBRATION

In Figure 4 we show a color picture taken from the Anclote Station (Site D-4) for each of the four events. The pictures were all taken at about 20 min into each event. These photographs emphasize the markedly different appearance of the events as viewed from our primary station. Event GAIL is shown only for completeness and to serve as a reminder that Anclote had severe cloud cover during this event.

Figure 5 is a set of color photographs taken by the same camera as those shown in Figure 4. In this set of pictures one can see the initial injection of the neutral barium. HOPE seems relatively spherical, while IRIS and JAN have pronounced asymmetry. It does seem unlikely that, at the highly collisional altitude of these injections, this difference is very significant in terms of the eventual evolution of striations. The pictures of IRIS and JAN show another rather interesting feature which appears to be a shock-like structure propagating out in one direction. In Figure 6 we show a more detailed time development of this feature as it was recorded by the 400-mm, 614.2-nm system. Its appearance on this camera indicates that it was most likely a phenomenon that was seen in white light. This agrees with the impression from the color film as well.

As is evident from Figure 5, the sky background was relatively low for all of the events as viewed from Anclote. This was one of the advantages of our choosing a site as far east of the events as D-4. Table 2 lists each event time as determined from the video tapes from D-4.

Table 2

PLACES EVENT TIMES

Event	Release Time
GAIL	23:07:37 UT
HOPE	23:07:39 UT
IRIS	23:13:08 UT
JAN	23:13:42 UT

GAIL

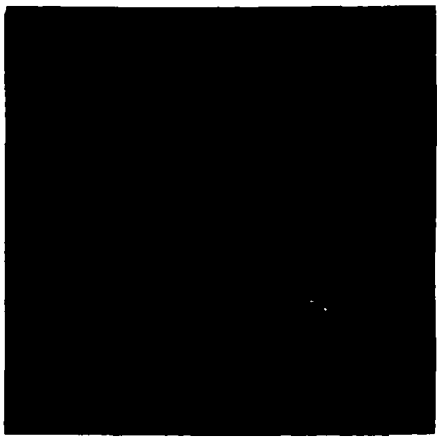

HOPE

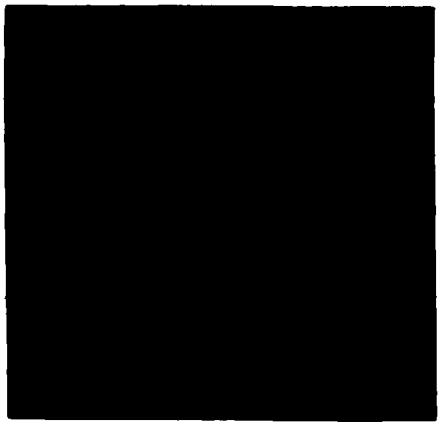

IRIS

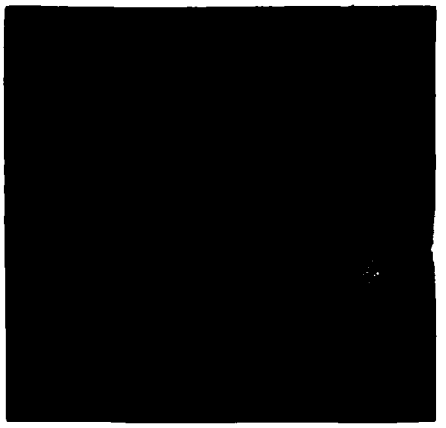

JAN

FIGURE 4 THE FOUR EVENTS SEEN FROM SITE D-4 AT ABOUT T + 20 MINUTES

PLACES

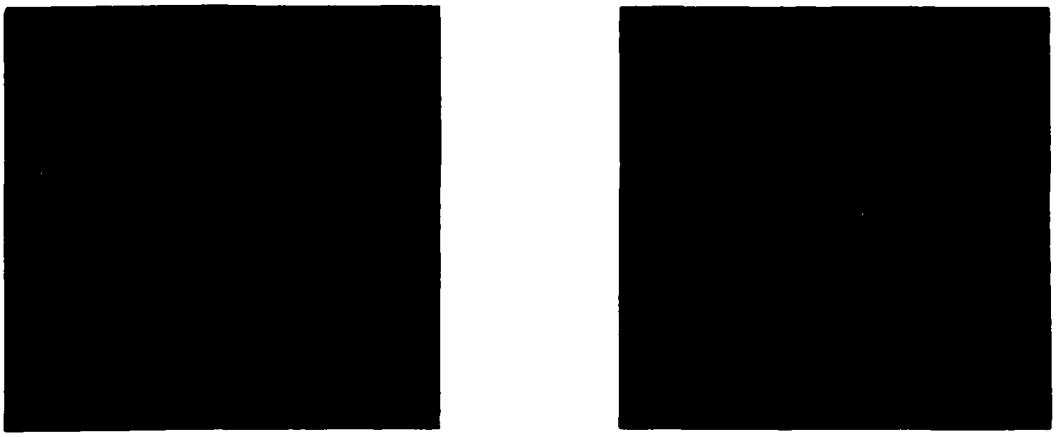

GAIL HOPE

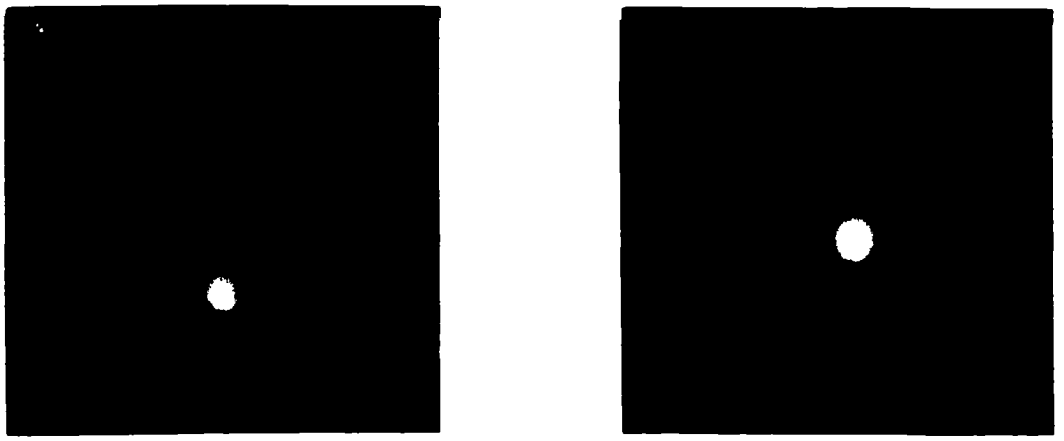

IRIS JAN

FIGURE 5 THE FOUR RELEASES AS SEEN FROM SITE D-4

PLACES

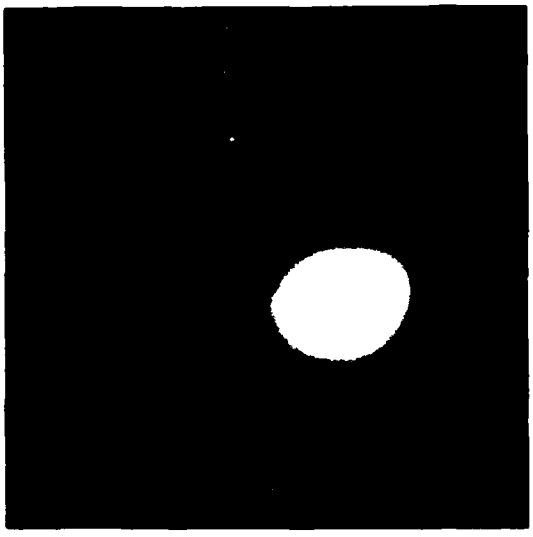

t = 0min

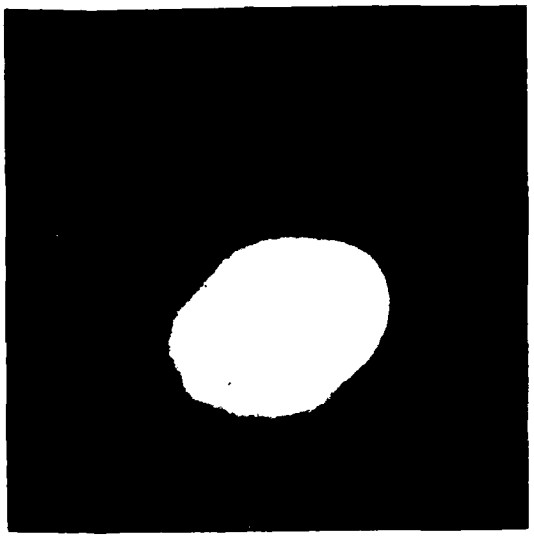

t = .09min

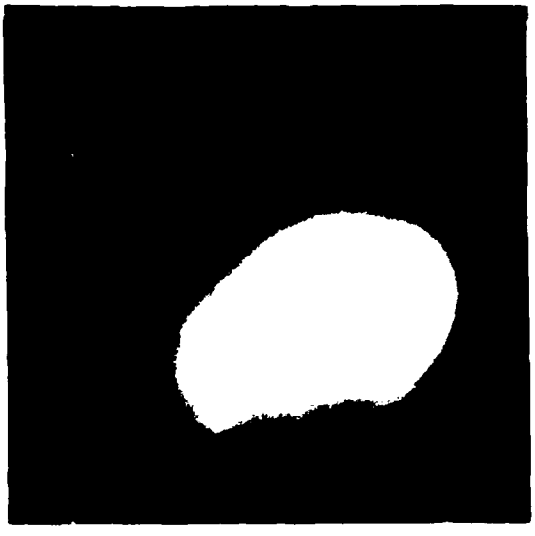

t = .10min

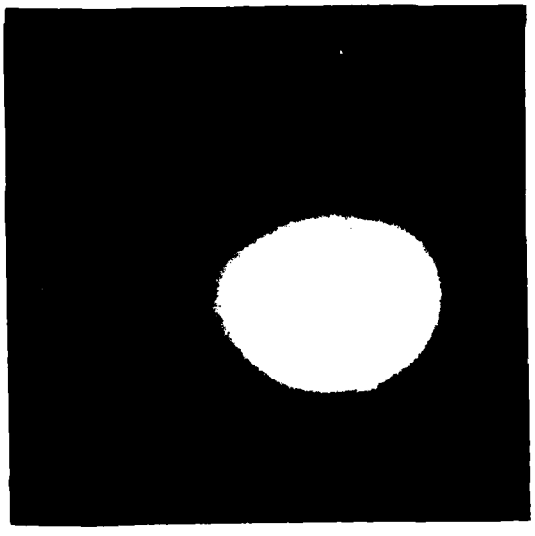

t = .12min

FIGURE 6 DETAILED DEVELOPMENT OF THE INITIAL PARTICULATE RING EXPANDED OUT OF THE THERMITE. Event JAN, ICA-78-806, 400 mm F.L., 585.4 nmi.

Figure 7 is a plot of solar depression angle and moonrise-moonset at Anclote for late November and early December 1980. The event times are also indicated on this figure. The first two events occurred at very near a solar depression angle of 7°, while the moon was on the eastern horizon. The excess cloud brightness in the first picture of Figure 5 is probably reflected moonlight. The moon added an insignificant background enhancement for early time in Event HOPE. This is particularly true because the event was in the northwest sky and essentially opposite to the moon direction. The moon had already set for Events IRIS and JAN, both of which occurred very near to 12° solar depression angle.

A. Event GAIL

The data for GAIL are basically restricted to the camera system from Site D-3 because the primary station was covered with heavy clouds to about 20 min into the experiment. The 150-mm f/1.8 system filtered at 614.2 nm obtained beautiful and exceedingly well focused pictures of the ion cloud. Due more to the serendipitous nature of high-altitude winds than to forethought, the ion cloud geometry as seen from this site seems very conducive to power spectral analysis of field-aligned structure. Figure 8 shows a sequence of photographs from 10.94 min, when a hard edge developed out to 24.64 min, where the cloud appears fully structured. There are some data from Anclote after 20 min. An example is shown in Figure 9.

B. Event HOPE

HOPE appeared to be a most unusual barium thermite release as viewed from Anclote. Because of a temporary personnel difficulty, we did not have a camera station at Site D-3 during Event HOPE, so we have only the one perspective from which to judge. The evolution of the cloud was very slow, with the first striations appearing after 15 min. This is most likely due to the existence of very weak ionospheric winds in the altitude region of the release. Figure 10 shows a sequence of photographs taken with the 400-mm f/1.8 system filtered at 614.2 nm. As late as 26 min after release only a very few striations were visible from Anclote.

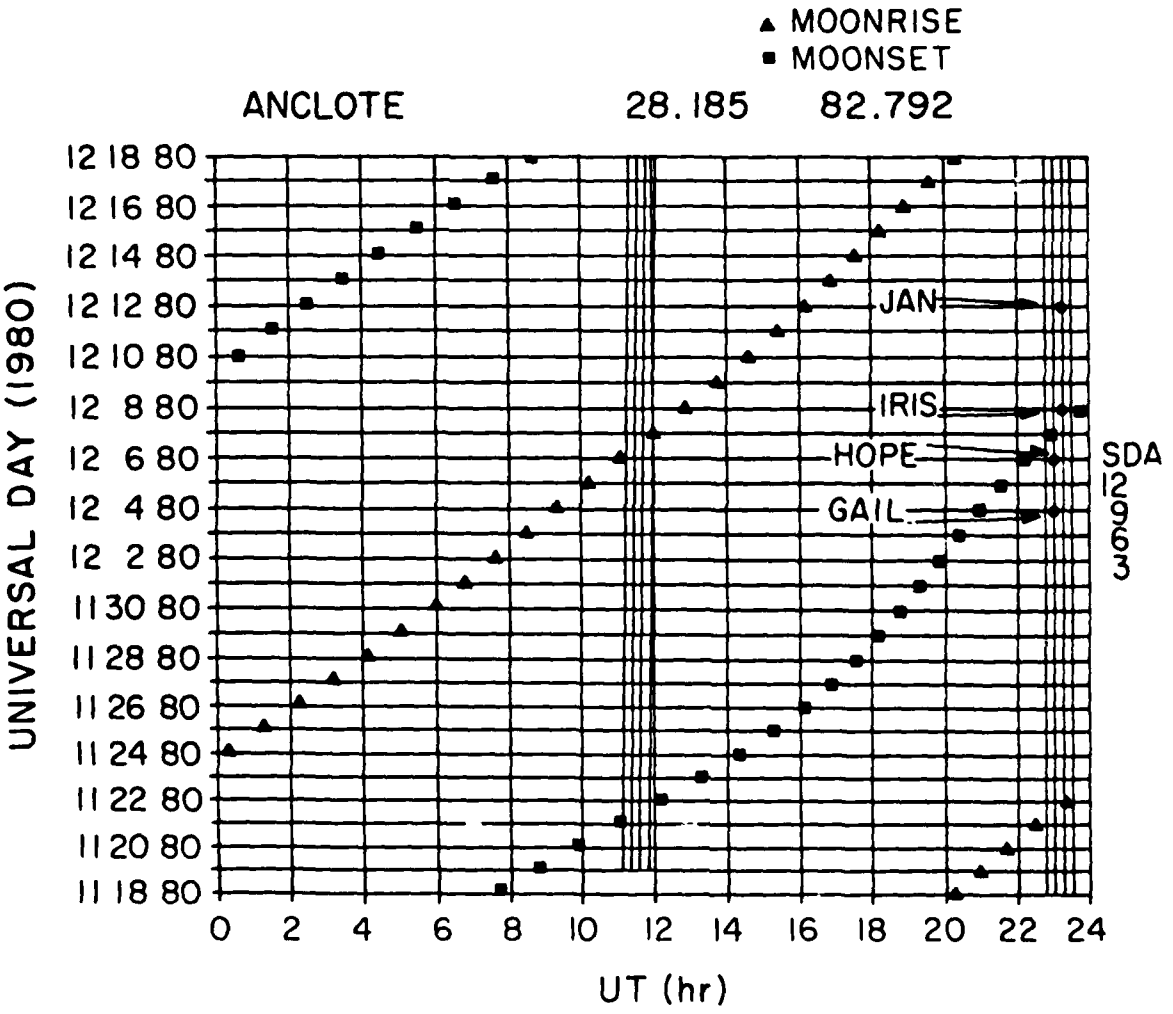

FIGURE 7 SOLAR DEPRESSION ANGLE AT SITE D-4 vs DAYTIME, FOR NOVEMBER AND DECEMBER 1981

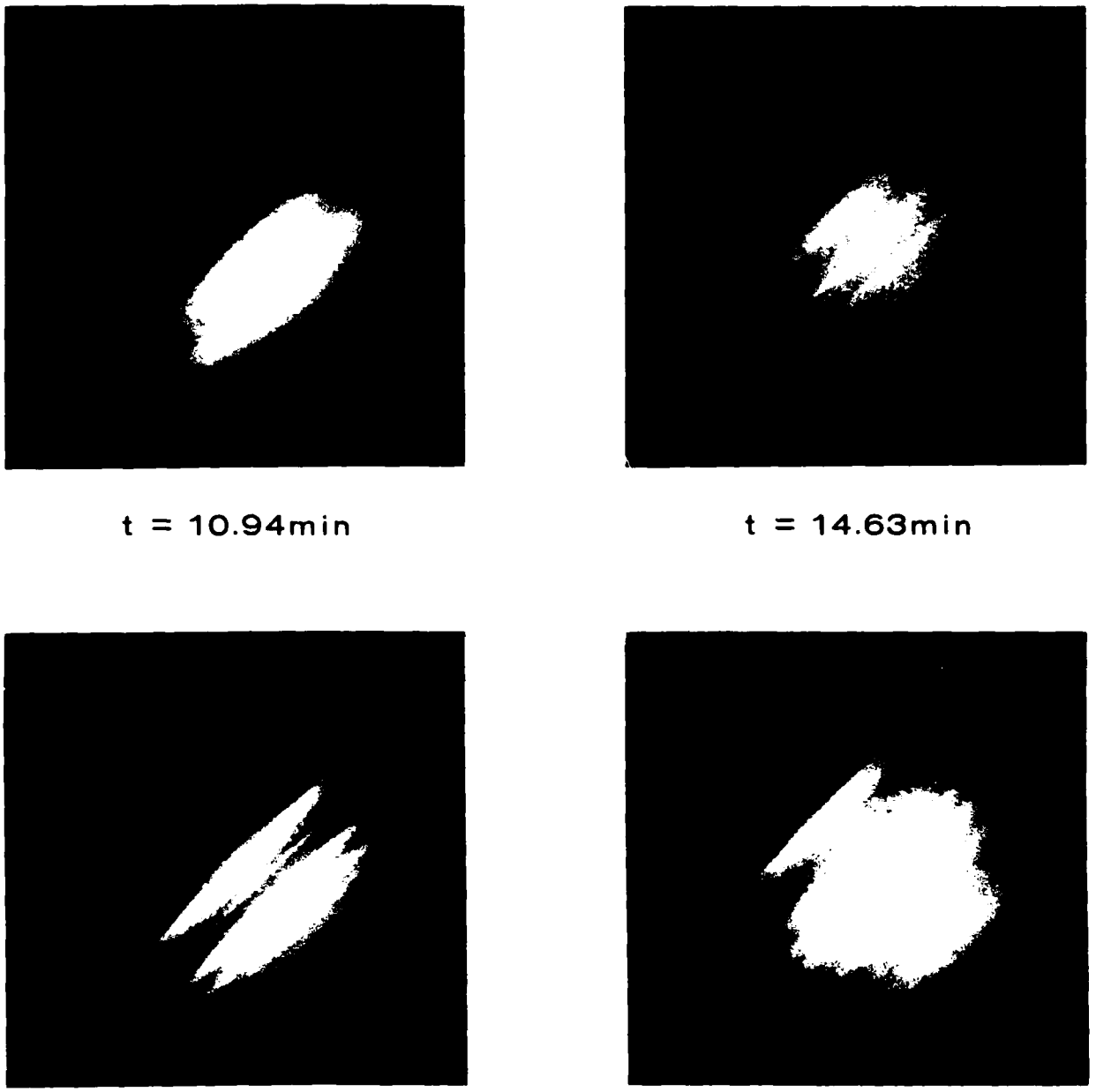

FIGURE 8 EVENT GAIL FROM SITE D-3, ICA-75-503, 150 mm F.L., 614.2 nm

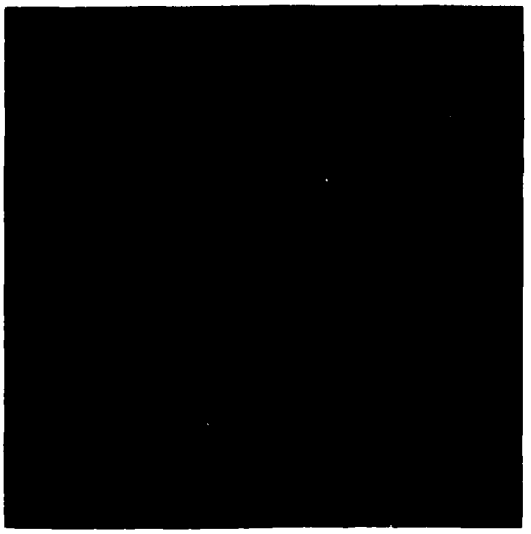

t = 22.88min

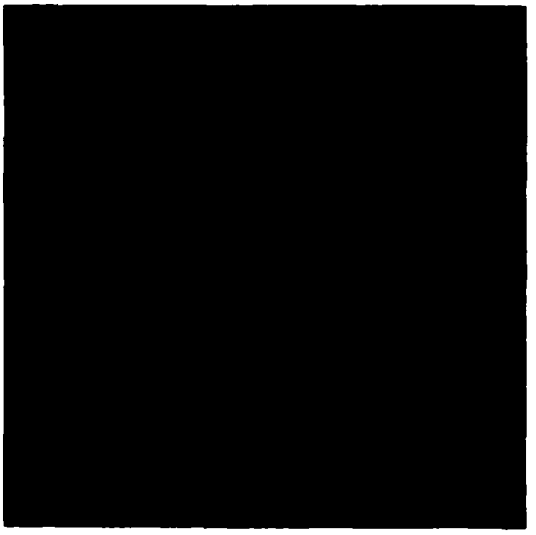

t = 23.91min

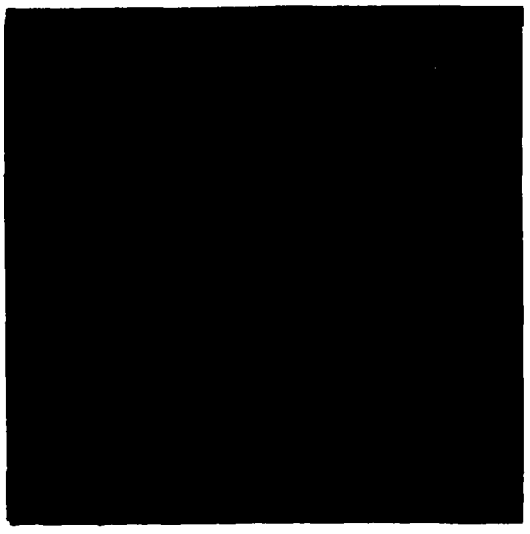

t = 25.20min

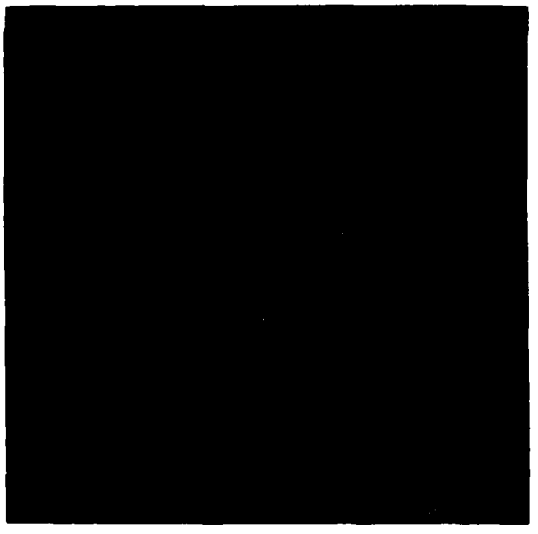

t = 25.85min

FIGURE 9 EVENT GAIL FROM SITE D-4, ICA-78-806, 400 mm F.L., 585.4 nm

t = 15.81min

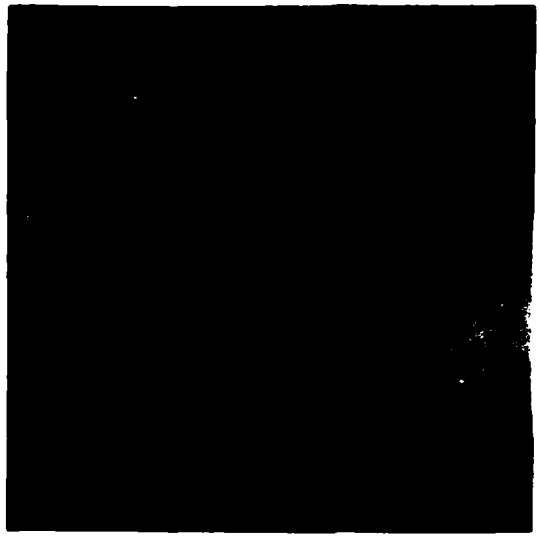

t = 18.09min

t = 22.62min

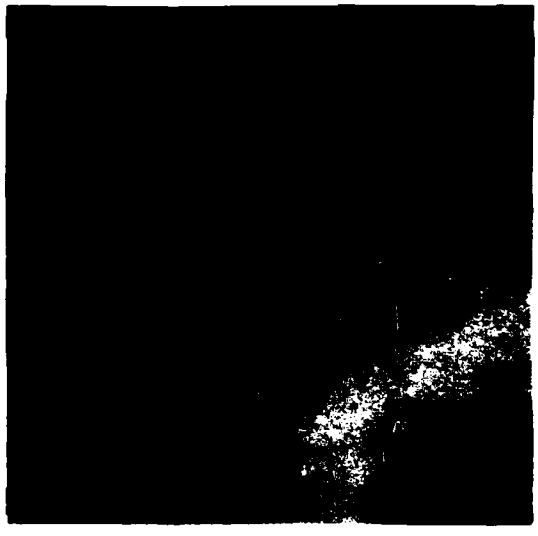

t = 25.96min

FIGURE 10 EVENT HOPE FROM SITE D-4, ICA-78-806, 400 mm F.L., 585.4 nm

Using the video tape pictures of the ion cloud for this event, we have tracked the cloud location in azimuth and elevation from 2309 to 2339 UT. This provides only a very rough estimate of the cloud location but gives a reasonable qualitative feeling for it. Assuming that the center of the cloud remained at an altitude of 185 km, we have produced the cloud track shown in Figure 11. One can see from this track that the cloud hardly moved for the first 30 min following release.

C. Event IRIS

This event was followed from both camera stations. The compact appearance of the ion cloud as seen from Anclote suggests that the cloud may have gone southeast initially toward this location. This interpretation seems consistent with the view from D-3, although we have as yet performed no triangulations. Figure 12 shows the cloud development from Anclote, while Figure 13 shows it from Site D-3.

D. Event JAN

This event was clear from both camera stations. A hard edge was developed by 13 min and the cloud was well striated at the leading edge by 17 min. As seen from Site D-3, the development of JAN was a classic example of the gradient drift development of structure. The leading edge steepened by 13 min. The striations pulled out of the leading edge, leaving an unstructured ion cloud in the back of the cloud. The structures appeared to penetrate back into the cloud as the striations were pulled further forward. Eventually, by 25 min, the structures had penetrated completely through the cloud, giving a fully striated barium cloud. This sequence of events is very clearly seen in the set of pictures shown in Figure 14, which are from the 150-mm f/1.8 system at Site D-3. A corresponding sequence of pictures from the 400-mm, 614.2 nm system at Anclote is shown in Figure 15.

E. Camera Motion

For the purposes of spatial frequency analysis of photographic data, it is critical that the camera be motionless during exposure. We normally

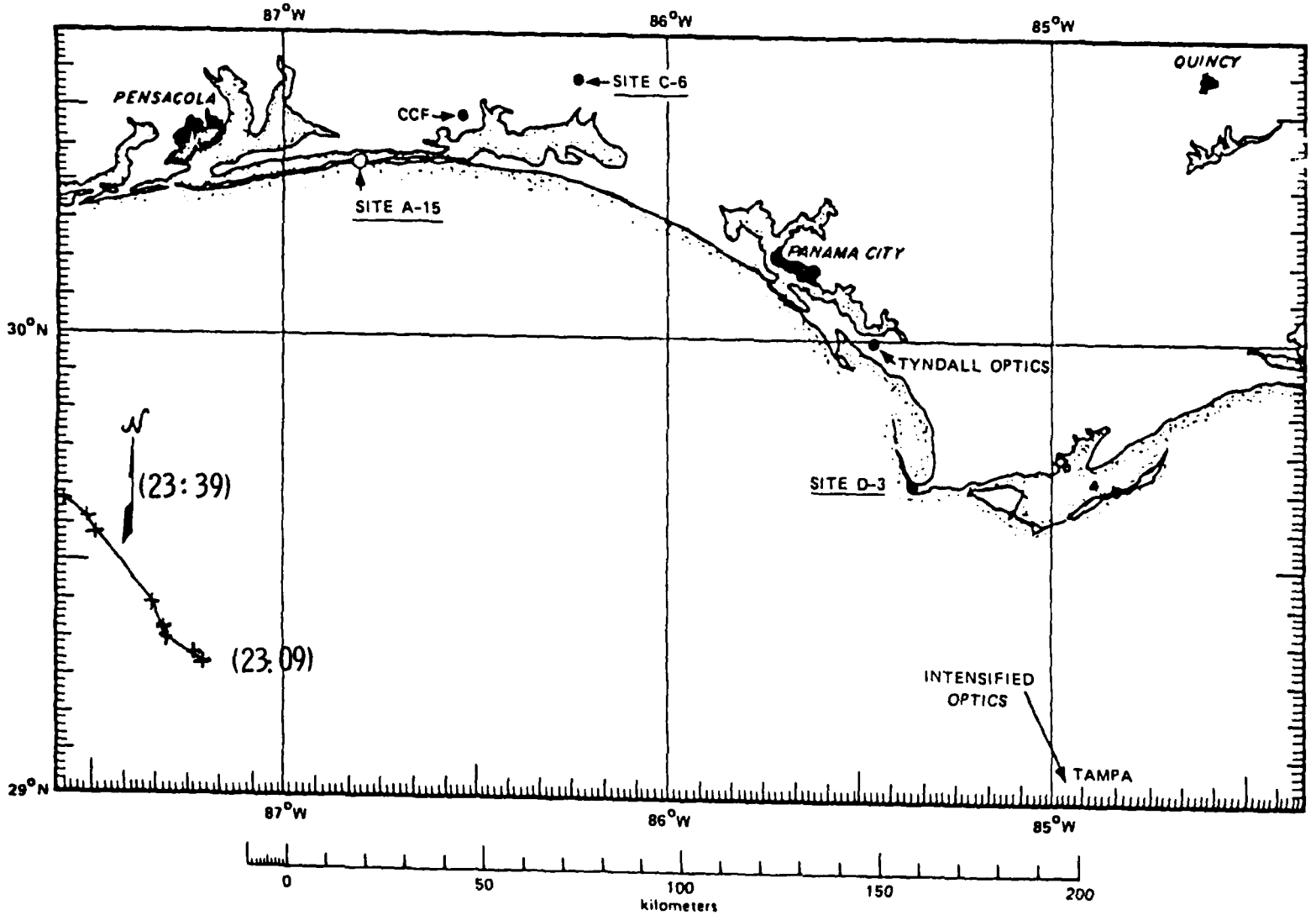

FIGURE 11 ONE-STATION ESTIMATE OF THE GROUND TRACK OF HOPE
(Altitude assumed to be 185 km)

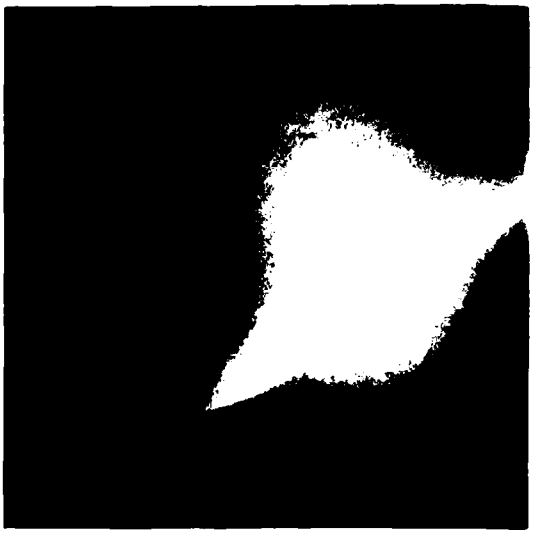

t = 9.34min

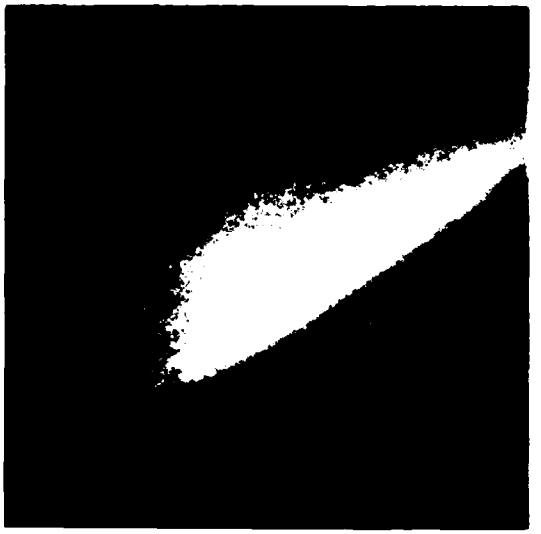

t = 19.19min

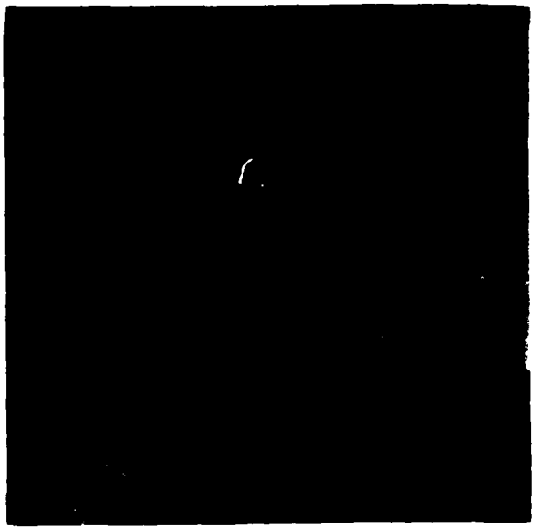

t = 32.17min

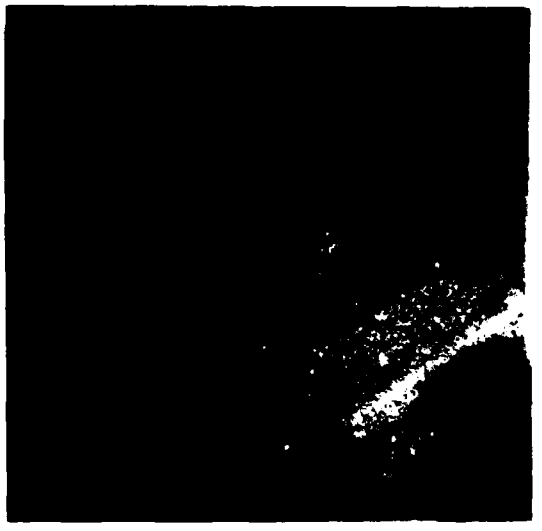

t = 34.47min

FIGURE 12 EVENT IRIS FROM SITE D-4, ICA-78-806, 400 mm F.L., 585.4 nm

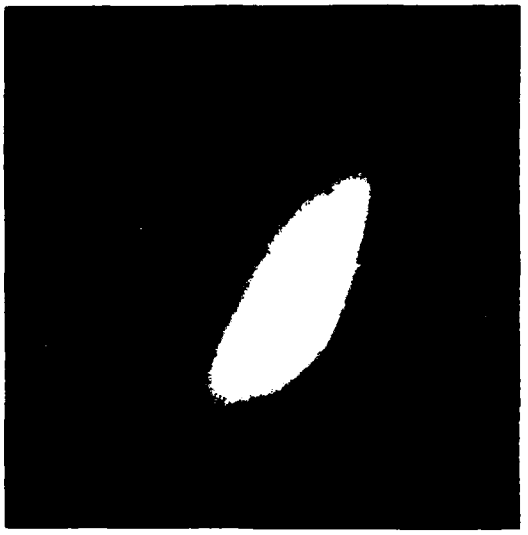

t = 9.28min

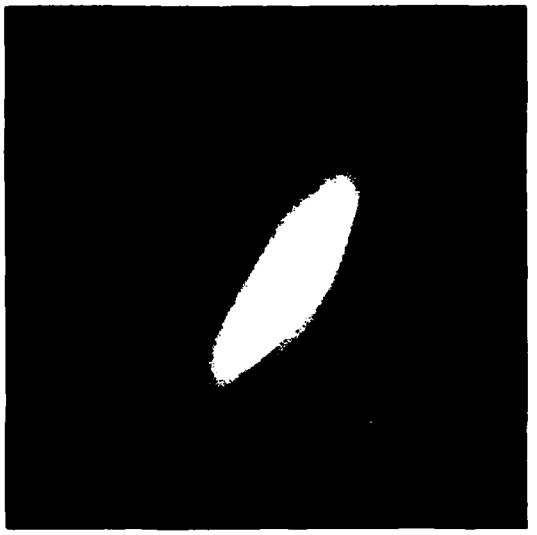

t = 12.11min

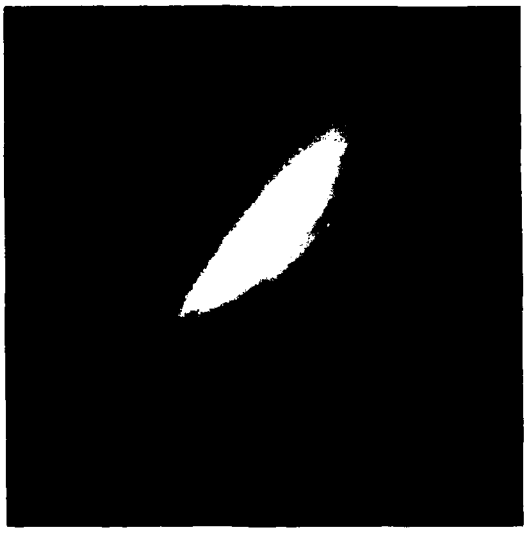

t = 18.92min

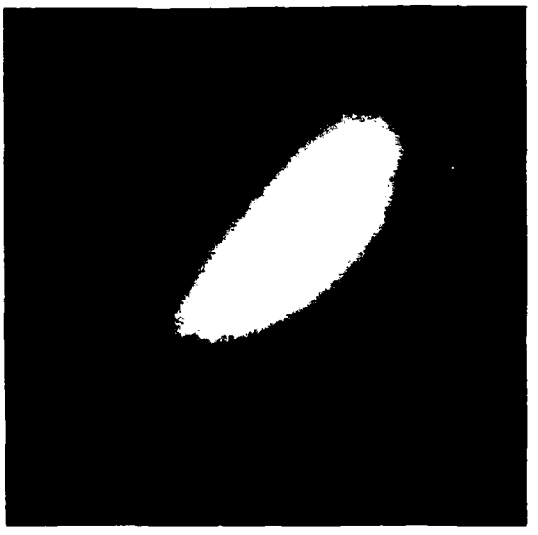

t = 27.92min

FIGURE 13 EVENT IRIS FROM SITE D-3, ICA-75-503, 150 mm F.L., 614.2 nm

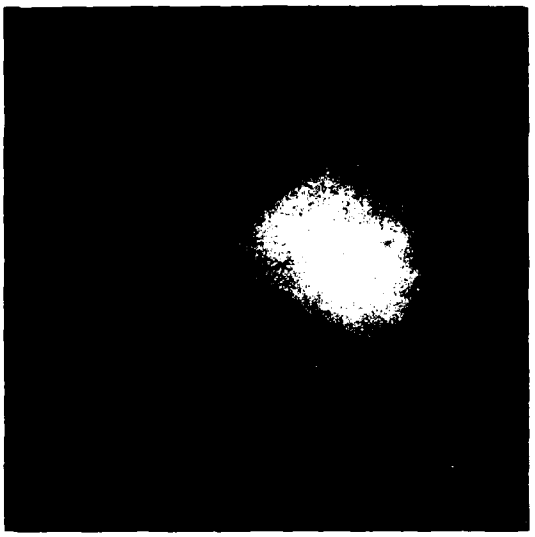

t = 13.12min

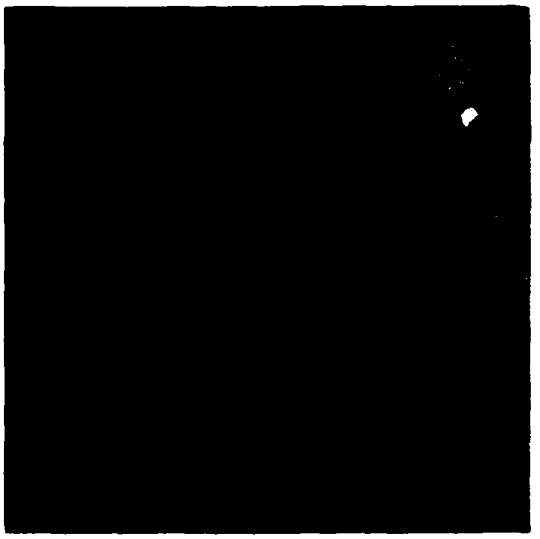

t = 17.12min

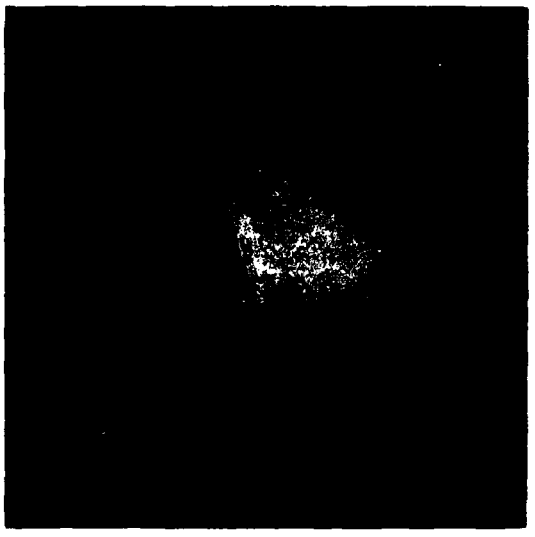

t = 20.12min

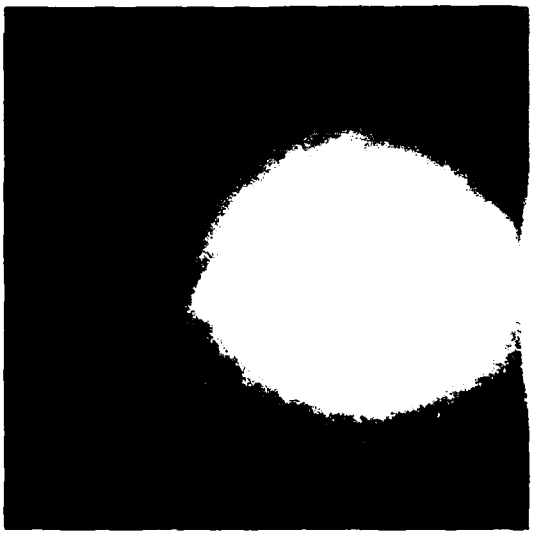

t = 25.09min

FIGURE 14 EVENT JAN FROM SITE D-3, ICA-75-503, 150 mm F.L., 614.2 nm

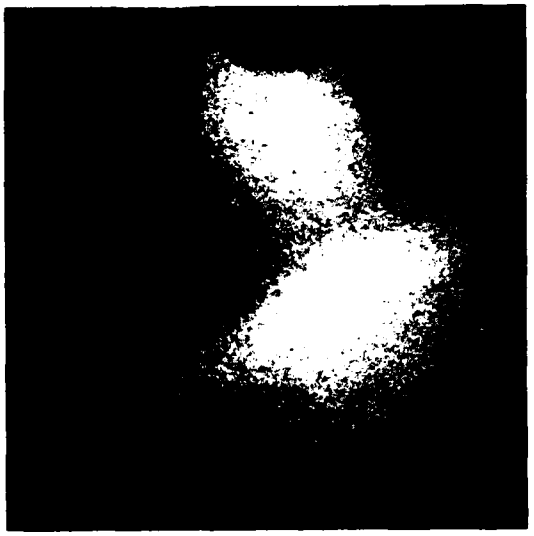

t = 13.18min

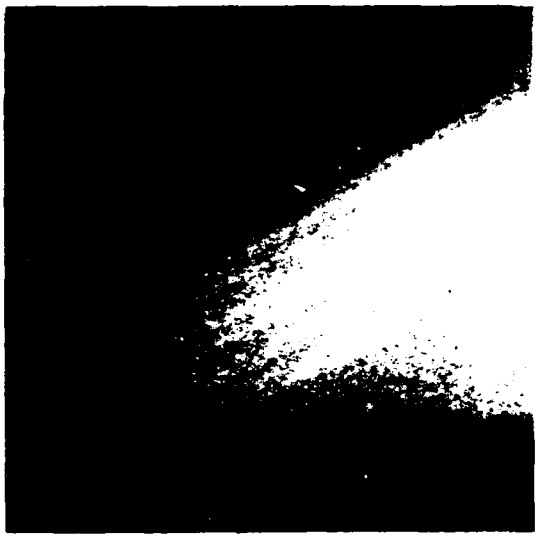

t = 17.82min

t = 20.80min

t = 24.89min

FIGURE 15 EVENT JAN FROM SITE D-4, ICA-78-806, 400 mm F.L., 585.4 nm

search the video record from each tracker and record the periods when they are not moving, indicating azimuth and elevation. Table 3 lists this information for each of the events.

F. Ion Column Density and Optical Depth

The question of the relationship between cloud brightness and ion column density is a crucial one for the determination of power spectral density from photographs of barium clouds that are optically thick in 455.4 nm. Although we cannot hope to present a thorough analysis of the data at this early time, we felt that this would be an appropriate place to discuss the scope of our proposed research and present some very preliminary results.

The motivation for attempting to determine the ion column density from 614.2 nm and 585.4 nm intensified photography emerges from a study performed at Los Alamos by H. Horak and R. Whitaker. The results of that study have been submitted for publication.[1] Quite simply put, they have demonstrated that, at least in a one-dimensional radiation transport calculation, the brightness of 614.2 and 585.4 nm continues to increase in a linear fashion with ion column depth, even after 455.4 nm has become fully saturated. This is explained by the rise of the diffuse radiation field in 455.4 nm to replace the incident solar radiation field deep within the ion cloud. Figure 16 is a typical calculational result. In this case, the calculation has been performed for conditions typical of the PLACES clouds.

Our program of research will consist of comparing this calculational result with many frames of 614.2-nm and 585.4-nm data from the various events. Since we have two identical systems looking at the same place in barium clouds, we can perform a large series of point-by-point comparisons. By adding the spectrometer data to this, we will have the necessary data to quantify the behavior of all five Ba II lines. As an additional feature of the analysis, we will determine spatial frequency power spectra from the two different spectral lines (585.4 and 614.2) as a measure of consistency.

Table 3

TRACKER AZIMUTH AND ELEVATION

OPERATION = PLACES DATE = 12/04/80
STATION = GAIL TAPE# = J10V-1679

EVENT = 1 TRACKER = 1
EVENT TIME = 23:07:37

AZ.	EL.	FIXED TIME FROM	--- TO:
287.9	019.4	23:06:39	23:07:41
287.5	017.8	23:07:45	23:10:02
288.2	017.8	23:10:04	23:12:46
289.0	017.8	23:12:48	23:15:01
290.1	017.8	23:15:32	23:17:30
291.1	017.8	23:17:32	23:19:06
291.1	018.9	23:19:07	23:20:25
292.3	020.4	23:21:09	23:21:50
292.9	019.1	23:21:53	23:22:20
292.9	018.5	23:22:22	23:23:10
292.9	019.6	23:23:13	23:24:04
292.9	018.3	23:24:05	23:24:35
293.9	018.3	23:24:37	23:24:54
293.5	017.4	23:24:56	23:25:45
295.1	021.3	23:25:50	23:27:03
295.1	020.5	23:27:05	23:30:05
291.3	020.5	23:30:15	23:30:35
290.9	022.1	23:30:37	23:30:50
292.0	020.4	23:30:52	23:31:15
292.5	019.4	23:31:17	23:31:46
293.7	017.7	23:31:49	23:32:09
294.3	016.1	23:32:13	23:33:43
295.0	015.0	23:33:45	23:33:58
292.0	021.6	23:34:06	23:34:26
291.3	023.5	23:34:28	23:34:51
290.5	024.3	23:34:53	23:35:35
289.2	022.3	23:35:37	23:35:58
292.1	018.5	23:36:02	23:36:18
293.5	020.8	23:36:20	23:36:44
292.6	022.3	23:36:45	23:37:15
292.0	023.4	23:37:17	23:37:58
293.5	021.3	23:38:02	23:38:30
294.4	018.1	23:38:34	23:39:09
295.5	019.2	23:39:11	23:39:34
295.2	020.0	23:39:39	23:40:07
291.4	022.8	23:40:13	23:40:47
290.5	019.5	23:40:51	23:41:08
292.9	016.6	23:41:12	23:41:44
290.3	020.4	23:41:49	23:42:15
289.3	022.0	23:42:17	23:43:02
291.4	019.5	23:43:07	23:43:29
290.3	021.2	23:43:42	23:44:33
291.7	019.3	23:44:37	23:45:57
290.6	021.4	23:46:17	23:46:29
289.8	022.6		23:47:17
290.7	021.4	23:47:20	
290.4	022.0	23:50:	
301.2	032.5	23:53:55	23:57:02

OPERATION = PLACES DATE = 12/04/80
STATION = GAIL TAPE# = J10V-1692

EVENT = 1 TRACKER = 2
EVENT TIME = 23:08:44

AZ.	EL.	FIXED TIME FROM	--- TO:
288.4	019.3	23:07:02	23:07:55
291.4	014.2	23:08:01	23:08:23
289.2	017.9	23:08:39	23:08:56
286.5	017.9	23:09:00	23:09:10
286.5	018.6	23:09:12	23:09:50
286.4	018.6	23:09:52	23:10:06
286.4	019.1	23:10:07	23:10:21
287.0	017.9	23:10:22	23:12:49
287.6	017.9	23:12:51	23:13:10
287.6	017.3	23:13:12	23:13:50
288.6	018.6	23:13:52	23:15:39
289.2	017.5	23:15:40	23:17:05
289.2	018.8	23:17:06	23:17:49
290.3	017.2	23:17:42	23:18:31
290.3	016.1	23:18:32	23:18:57
289.2	020.0	23:19:01	23:21:20
290.0	022.1	23:21:22	23:21:53
290.8	019.8	23:21:55	23:24:10
290.8	018.8	23:24:11	23:27:07
293.5	021.8	23:27:10	23:29:23
290.1	021.8	23:29:28	23:30:29
289.6	022.7	23:30:30	23:31:01
291.3	020.4	23:31:05	23:31:50
292.4	018.1	23:31:52	23:32:19
293.6	016.7	23:32:20	23:32:32
293.5	016.7	23:32:32	23:33:02
293.6	016.7	23:33:02	23:33:49
292.4	020.8	23:33:53	23:34:13
292.4	022.0	23:34:14	23:34:35
290.6	024.3	23:34:39	23:35:26
287.6	021.4	23:35:30	23:35:49
291.0	018.5	23:35:52	23:36:07
290.9	018.5	23:36:11	23:36:24
291.0	018.5	23:36:25	23:36:35
292.2	022.4	23:36:37	23:37:02
290.7	024.9	23:37:06	23:37:38
291.2	022.1	23:37:40	23:38:06
291.9	019.1	23:38:09	23:38:51
293.6	016.9	23:38:53	23:39:23
294.8	019.5	23:39:25	23:39:46
293.1	022.4	23:39:49	23:40:28
287.7	021.1	23:40:44	23:41:14
290.9	017.5	23:41:24	23:41:53
289.1	021.7	23:41:56	23:42:33
288.1	023.2	23:42:35	23:43:18
288.7	020.9	23:43:21	23:43:54
288.1	022.6	23:43:55	23:44:42
291.2	019.4	23:44:53	23:46:16
289.9	021.3	23:46:23	23:46:44
289.1	022.7	23:46:45	
290.3	022.3		23:54:47

OPERATION = PLACES DATE = 12/06/80
STATION = HOPE TAPE# = J10V-1682

EVENT = 2 TRACKER = 1
EVENT TIME = 23:07:39

AZ.	EL.	FIXED TIME FROM	--- TO:
283.4	020.8	23:06:36	23:06:58
283.4	020.8	23:07:00	23:07:41
287.0	020.8	23:07:49	23:08:04
287.1	020.1	23:08:05	23:08:26
287.2	020.1	23:08:27	23:08:52
287.3	019.8	23:08:53	23:10:04
287.5	019.8	23:10:05	23:10:28
287.6	019.4	23:10:29	23:11:07
287.6	020.2	23:11:08	23:12:08
288.3	020.2	23:12:12	23:13:08
287.9	019.0	23:13:10	23:13:32
287.6	020.6	23:13:36	23:14:33
287.6	020.6	23:14:36	23:14:53
287.3	020.6	23:15:05	23:15:55
286.9	022.4	23:15:59	23:16:15
287.4	020.8	23:16:17	23:16:33
287.9	019.3	23:16:35	23:16:50
288.9	017.3	23:16:55	23:17:32
288.2	019.9	23:17:36	23:18:17
287.8	021.0	23:18:18	23:19:31
287.3	021.6	23:19:33	23:20:21
287.8	019.8	23:20:24	23:20:52
288.5	018.0	23:20:55	23:21:39
289.1	016.8	23:21:41	23:23:38
288.7	019.1	23:23:46	23:24:36
287.9	020.4	23:24:38	23:24:56
288.1	019.5	23:24:57	23:25:35
288.0	020.3	23:25:39	23:26:01
287.6	021.2	23:26:02	23:26:15
287.3	021.2	23:26:16	23:26:37
288.2	019.7	23:26:39	23:27:34
288.4	018.9	23:27:35	23:27:58
289.0	018.7	23:28:02	23:28:33
289.4	017.2	23:28:38	23:28:54
289.9	016.9	23:29:01	23:29:17
289.4	017.7	23:29:19	23:29:53
289.1	018.8	23:29:54	23:30:14
288.3	020.1	23:30:24	23:30:55
287.7	021.2	23:30:57	23:31:23
288.9	019.5	23:31:28	23:31:59
289.7	017.3	23:32:03	23:32:48
290.7	016.0	23:32:50	23:33:30
289.4	018.5	23:33:33	23:34:15
288.5	020.1	23:34:17	23:35:21
289.7	017.6	23:35:25	23:36:12
291.0	015.8	23:36:14	23:36:46
289.9	018.2	23:36:52	23:37:39
288.8	020.4	23:37:42	23:38:12
290.2	017.7	23:38:15	23:39:41
291.5	015.9	23:39:43	23:41:01
290.7	018.5	23:41:04	23:41:29
289.5	019.6	23:41:30	23:42:25
291.2	017.1	23:42:28	23:43:22
289.6	019.6	23:43:25	23:43:56
290.2	018.3	23:43:58	23:44:19
292.5	016.1	23:44:22	23:45:26
290.5	019.3	23:45:31	23:46:45
291.7	016.8	23:46:50	23:47:44
291.5	019.1	23:47:44	23:48:00
291.5	019.1	23:48:04	23:48:38
290.8	021.5	23:53:28	23:53:38
291.4	021.5	23:53:40	23:55:03

Table 3 (concluded)

OPERATION = PLACES DATE = 12/06/80
STATION = HOPE TAPE# = J10V-1683

EVENT = 2 TRACKER = 2
EVENT TIME = 23:07:39

AZ.	EL.	FIXED TIME FROM	--- TO:
282.8	021.5	23:07:05	23:07:53
286.5	020.2	23:07:57	23:08:19
286.5	020.5	23:08:13	23:10:10
286.9	020.5	23:10:10	23:10:32
286.9	019.5	23:10:33	23:13:12
286.7	019.5	23:13:20	23:15:23
286.7	021.7	23:15:32	23:15:42
285.8	020.6	23:15:46	23:16:21
288.0	017.4	23:16:27	23:17:21
286.7	020.9	23:17:26	23:18:23
286.2	021.5	23:18:24	23:19:14
285.6	022.5	23:19:15	23:20:26
286.2	020.3	23:20:29	23:21:07
287.5	019.0	23:21:08	23:21:50
288.8	017.5	23:21:52	23:23:49
287.3	020.2	23:23:50	23:24:27
286.2	022.1	23:24:29	23:25:42
285.5	023.7	23:25:45	23:26:45
287.2	020.2	23:26:49	23:27:31
287.9	019.1	23:27:32	23:28:28
288.8	018.1	23:28:29	23:29:29
288.0	019.9	23:29:30	23:30:00
287.1	021.0	23:30:01	23:30:28
286.0	022.9	23:30:33	23:30:46
287.2	020.2	23:30:50	23:31:32
288.4	018.6	23:31:34	23:32:22
289.0	017.4	23:32:23	23:33:04
290.2	015.8	23:33:06	23:33:42
288.8	019.0	23:33:45	23:34:21
287.6	020.7	23:34:23	23:35:31
289.1	017.8	23:35:35	23:36:20
290.5	015.3	23:36:22	23:36:56
289.0	018.9	23:37:00	23:37:34
287.9	020.5	23:37:36	23:38:19
289.5	017.4	23:38:22	23:39:48
291.2	015.5	23:39:50	23:40:55
289.6	018.7	23:40:58	23:41:33
288.9	020.3	23:41:36	23:42:19
290.1	017.4	23:42:22	23:43:29
289.2	019.9	23:43:31	23:44:27
290.5	017.4	23:44:29	23:45:35
289.7	019.4	23:45:37	23:47:03
290.8	017.1	23:47:05	23:47:31
289.9	019.7	23:47:34	23:49:00
290.3	019.1	23:49:05	23:52:22
290.3	020.5	23:52:25	23:54:16
291.8	021.2	23:54:17	23:56:12

OPERATION = PLACES DATE = 12/08/80
STATION = IRIS TAPE# = J10V-1686

EVENT = 3 TRACKER = 1
EVENT TIME = 23:13:08

AZ.	EL.	FIXED TIME FROM	--- TO:
282.5	021.2	23:12:32	23:13:17
279.9	019.4	23:13:19	23:14:43
279.6	020.0	23:14:47	23:15:32
279.1	020.0	23:15:33	23:16:27
278.9	019.7	23:16:28	23:17:33
278.2	020.1	23:17:39	23:23:25
277.4	021.2	23:23:28	23:24:04
276.9	021.2	23:24:06	23:25:15
276.7	021.2	23:25:16	23:26:14
275.7	022.5	23:26:15	23:27:23
276.5	020.5	23:27:25	23:30:18
275.5	021.5	23:30:22	23:32:02
275.7	019.7	23:32:04	23:32:47
277.1	018.2	23:32:49	23:33:19
278.0	016.4	23:33:21	23:33:51
277.2	018.7	23:33:54	23:34:19
275.1	020.2	23:34:23	23:35:28
274.0	021.5	23:35:30	23:36:21
273.9	022.1	23:36:22	23:37:25
274.9	021.8	23:37:28	23:39:22
274.0	022.2	23:39:25	23:39:59
275.8	020.7	23:40:03	23:42:50
274.8	019.5	23:42:52	23:43:56
273.8	021.8	23:43:58	23:45:09
272.5	023.3	23:45:12	23:45:55
272.5	021.9	23:45:57	23:46:09
272.5	021.4	23:46:10	23:47:57
271.9	022.4	23:47:58	23:48:32
271.0	020.7	23:48:34	23:51:21
270.6	020.7	23:51:23	23:51:35
270.3	020.7	23:51:35	23:55:21

OPERATION = PLACES DATE = 12/08/80
STATION = IRIS TAPE# = J10V-1687

EVENT = 3 TRACKER = 2
EVENT TIME = 23:13:08

AZ.	EL.	FIXED TIME FROM	--- TO:
278.9	019.9	23:13:15	23:15:36
277.7	019.9	23:15:37	23:21:30
277.6	019.2	23:21:31	23:23:44
275.7	021.8	23:23:48	23:26:40
275.2	021.8	23:26:41	23:27:36
277.2	018.6	23:27:41	23:29:03
275.8	020.7	23:29:09	23:30:40
277.3	017.6	23:30:44	23:31:54
275.0	021.2	23:31:59	23:34:02
273.9	021.2	23:34:07	23:37:31
272.5	022.1	23:37:33	23:40:20
273.7	018.7	23:40:25	23:41:05
274.4	017.5	23:41:07	23:42:07
272.5	020.7	23:42:10	23:45:32
271.3	023.4	23:45:40	23:46:30
271.3	021.9	23:46:33	23:48:43
269.9	021.9	23:48:45	23:52:38

OPERATION = PLACES DATE = 12/12/80
STATION = JAN TAPE# = J10V-1690

EVENT = 4 TRACKER = 1
EVENT TIME = 23:13:42

AZ.	EL.	FIXED TIME FROM	--- TO:
286.3	022.2	23:12:18	23:13:51
286.2	020.5	23:13:56	23:15:23
286.6	020.5	23:15:24	23:16:53
287.6	020.5	23:16:55	23:19:38
287.2	021.8	23:19:40	23:20:03
287.2	021.8	23:20:06	23:25:01
287.2	022.5	23:25:03	23:25:30
288.4	019.4	23:25:34	23:26:30
289.2	019.4	23:26:33	23:27:00
290.1	017.5	23:27:02	23:27:15
290.1	017.4	23:27:15	23:27:47
289.8	018.8	23:27:51	23:28:32
288.9	020.7	23:28:34	23:29:39
288.5	022.0	23:29:41	23:30:14
289.2	020.7	23:30:16	23:31:20
290.0	020.0	23:31:27	23:31:54
291.0	016.8	23:31:59	23:32:19
289.2	021.1	23:32:26	23:33:17
288.6	022.7	23:33:19	23:33:52
290.1	020.7	23:33:55	23:34:27
290.9	018.9	23:34:29	23:35:02
291.7	017.1	23:35:04	23:35:36
290.3	021.8	23:35:42	23:36:56
291.7	018.4	23:37:00	23:37:42
292.3	015.8	23:37:47	23:38:17
291.1	020.7	23:38:23	23:39:01
290.6	022.3	23:39:03	23:39:51
292.6	020.0	23:39:55	23:40:39
293.3	018.4	23:40:40	23:41:06
293.0	021.6	23:41:10	23:42:20
293.9	020.5	23:42:25	23:44:26
293.2	018.6	23:44:28	23:45:13
292.0	019.3	23:45:19	23:52:06

OPERATION = PLACES DATE = 12/12/80
STATION = JAN TAPE# = J10V-1691

EVENT = 4 TRACKER = 2
EVENT TIME = 23:13:42

AZ.	EL.	FIXED TIME FROM	--- TO:
286.4	022.2	23:13:00	23:13:47
285.6	020.5	23:13:59	23:14:25
285.2	020.7	23:14:26	23:15:10
285.6	021.0	23:15:15	23:18:14
286.7	021.0	23:18:16	23:21:16
286.3	022.2	23:21:19	23:22:21
285.2	021.2	23:22:23	23:23:24
287.0	020.3	23:23:29	23:24:14
286.2	022.5	23:24:17	23:24:43
285.6	023.6	23:24:44	23:25:46
287.5	019.5	23:25:53	23:26:53
289.6	018.0	23:26:56	23:27:56
288.9	019.5	23:28:00	23:28:39
287.6	021.9	23:28:43	23:29:43
287.1	023.1	23:29:45	23:30:37
288.3	020.9	23:30:44	23:31:10
289.0	019.5	23:31:12	23:31:45
290.3	017.5	23:31:51	23:32:30
289.0	020.3	23:32:37	23:33:04
288.0	022.5	23:33:07	23:34:08
290.3	019.5	23:34:35	23:35:24
289.0	021.6	23:35:29	23:37:03
290.6	018.6	23:37:08	23:38:09
288.9	021.6	23:38:13	23:38:40
290.3	023.2	23:38:42	23:39:42
290.8	020.8	23:39:46	23:40:30
291.9	018.2	23:40:35	23:41:14
292.5	021.2	23:41:19	23:41:36
292.1	022.8	23:41:38	23:42:04
291.3	024.1	23:42:05	23:42:29
290.8	020.8	23:42:40	
291.6	019.4		23:43:51
292.6	021.0	23:43:54	23:45:58
290.3	022.3	23:45:59	23:53:10
302.2	026.7	23:53:22	23:53:42
302.1	026.5	23:53:49	23:55:04
301.7	024.5	23:55:14	23:56:59

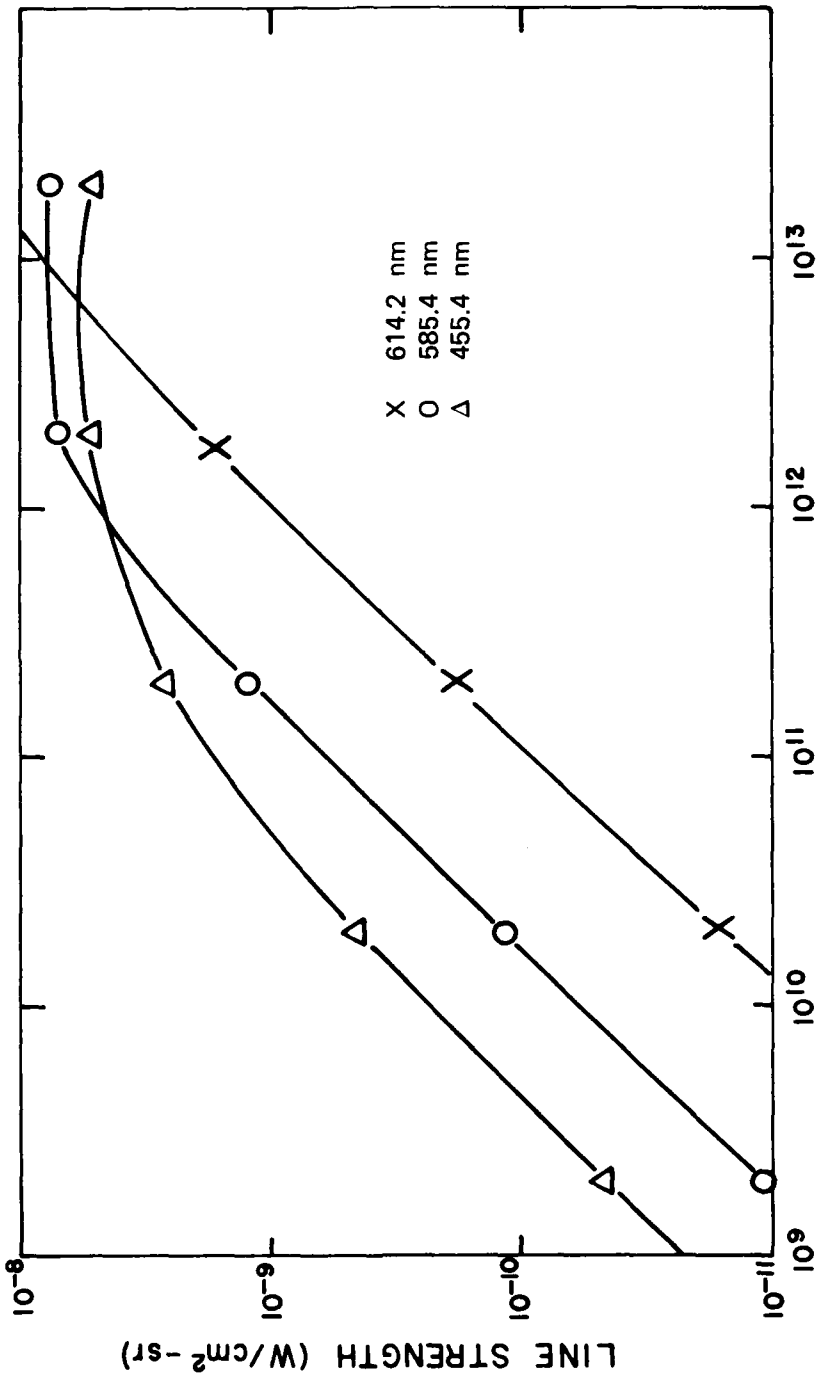

FIGURE 16 CALCULATED LINE STRENGTH IN 614.2 nm, 585.4 nm, AND 455.4 nm vs COLUMN DENSITY

FIGURE 17 SELECTED FRAME OF 614.2 nm DATA FROM HOPE

As an initial example, we have chosen to analyze a set of photographs from Event HOPE. The two frames were selected for no special reason other than that they appeared interesting. The frames are from the 614.2-nm and 585.4-nm, 400-mm intensified systems and are shown in Figures 17 and 18. The time of the frames is the same--2333:36.8 UT. These two frames have been digitized and radiometrically reduced to produce radiance versus position on the film. It is evident from the photographs that the pictures are very much the same in gross features. Note that the stars are more easily discernible through the cloud in the 585.4-nm line. Film grain and photon counting statistics add significant noise in fine scale of the photographs. Using the stars as the common feature in both pictures, we have synthesized a series of scan lines perpendicular to the magnetic-field-aligned structures. These scan lines for each picture have been averaged together (20 lines in each case) to reduce the effect of noise. The averaged scan lines are shown in Figure 19.

The scans start at essentially a background brightness level, enter the edge of the cloud, and then follow into an essentially unstructured portion of the cloud. We thought that it would be informative to make a comparison point-by-point of the brightness from the two scans and then produce a similar result from the theoretical determination shown in Figure 16.

First, we determined that the indicated background brightness was consistent. From Figure 7, solar depression angle versus time, we can see that on 6 December at 2333:36 UT, the solar depression angle was 12°. From Table 3, we can read off the azimuth and elevation of the tracker, which were 289.40° and 18.5°, respectively. From standard tables of sky brightness, which we have computerized, we find that the background at 614.2 nm is 3.5×10^{-11} W cm^{-2} sr^{-1} nm^{-1} and, at 585.4 nm, it is 1.5×10^{-11} W cm^{-2} sr^{-1} nm^{-1}. The filters had an effective width of 80 Å. The corrections for air transmission and filter transmissions are already in the data. The effective background levels should then be 2.8×10^{-10} W cm^{-2} sr^{-2} at 614.2 nm and 1.2×10^{-10} W cm^{-2} sr^{-1} at 585.4 nm. These values are quite consistent with the data shown in Figure 19.

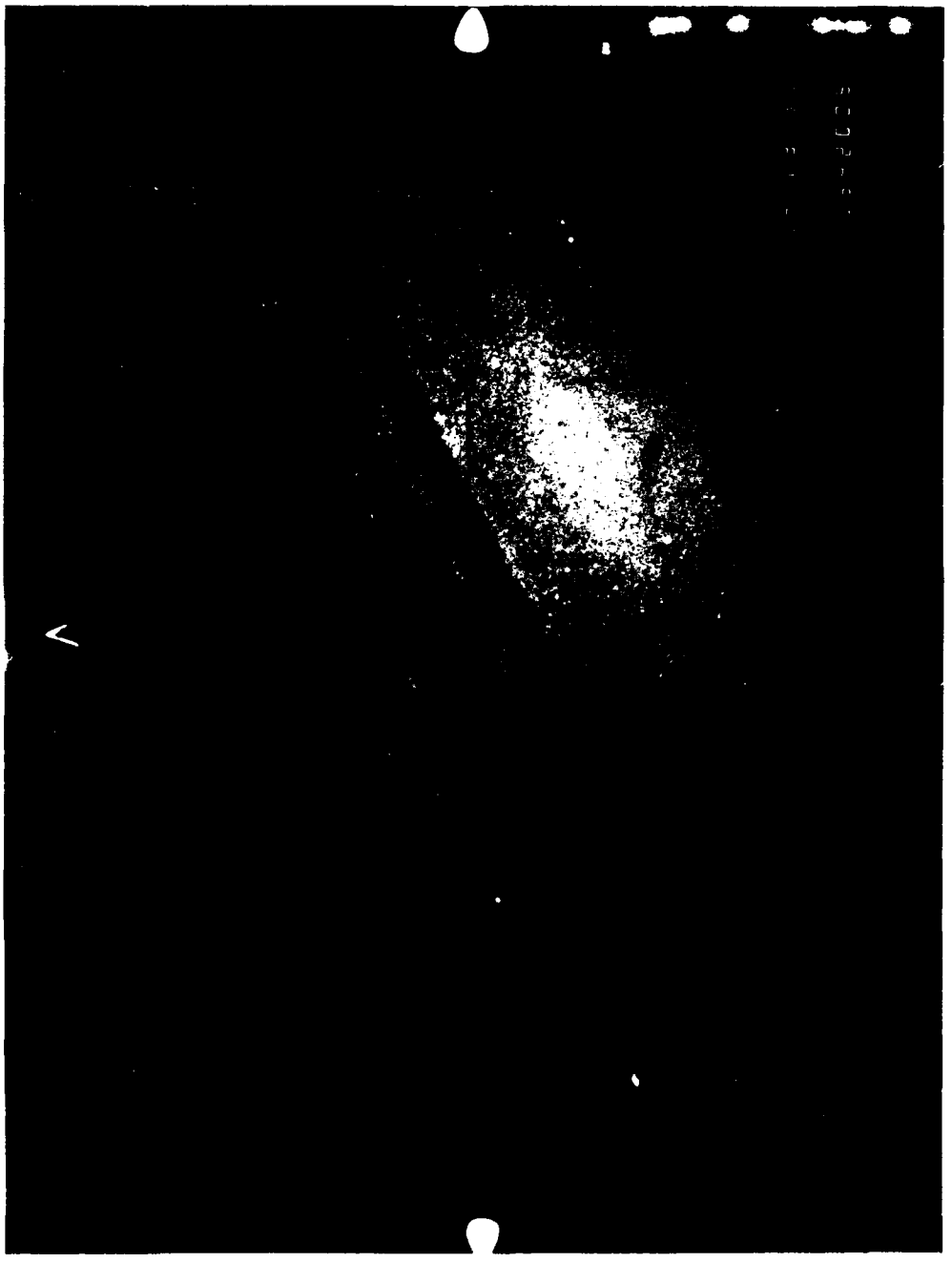

FIGURE 18 SELECTED FRAME OF 585.4-nm DATA FROM HOPE

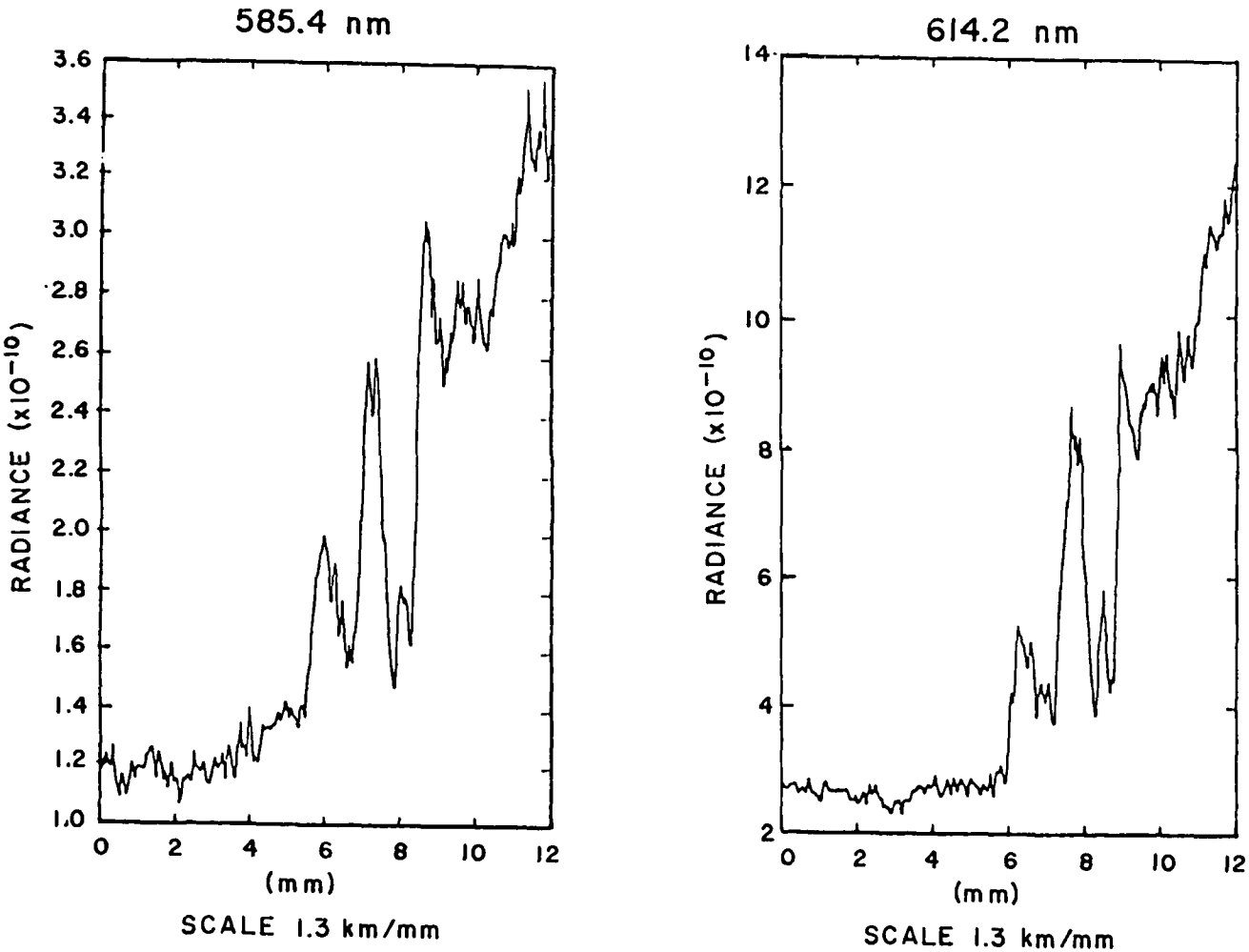

FIGURE 19 AVERAGE SCAN LINES FROM HOPE

In Figure 20 we have plotted the corresponding values, 614.2 nm and 585.4 nm, in a scatter plot, with the value from the theoretical calculations being shown for comparison. The brightness level indicates that the region of the cloud that we scanned was not optically thick, having a highest column density on the order of 2×10^{11} ions/cm^2. The theoretical calculation just gives a straight line in this region of ion densities. This particular set of data is reassuring for consistency, but inconclusive in that it does not address the problem of optical depth.

As a final example of possible data analysis, Figures 21, 22, 23, and 24 show the power spectral density determined from the line profiles in Figure 19. In Figures 21 and 22 we show the power spectra calculated without detrending the data but only applying a Kaiser-Bessel (Jo) window. Figures 23 and 24 show the power spectra after the data have been detrended. The difference in the two techniques only influences the low-frequency part of the spectrum, leaving the high-frequency portion unchanged. The 585.4-nm and the 614.2-nm results are nearly identical.

REFERENCES

1. H. G. Horak and R. W. Whitaker, "Resonance-Fluoresence in Artificial Barium Ion Clouds," submitted to Planetary and Space Science, 1980.

2. M. B. Pongratz, P-4 2nd Quarter 1980 Input to the DNA Quarterly, Los Alamos National Laboratory, Los Alamos, NM (1980).

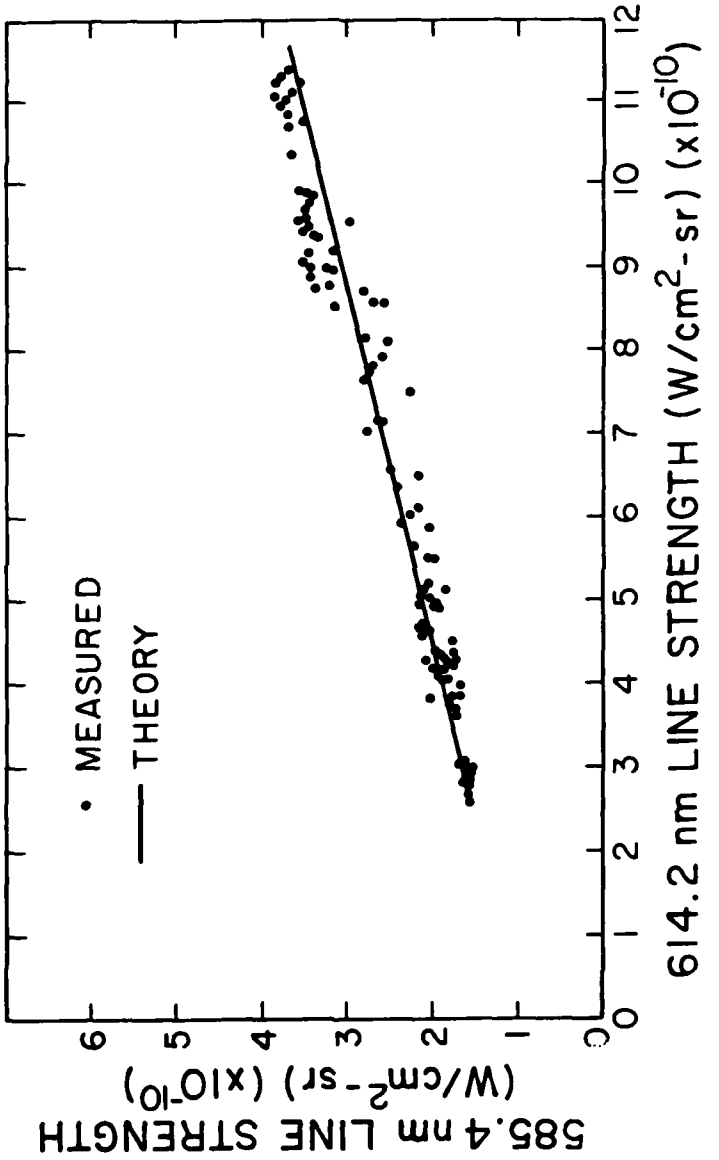

FIGURE 20 SCATTER PLOT OF 614.2-nm BRIGHTNESS vs 585.4-nm BRIGHTNESS COMPARED TO THEORETICAL RATIO

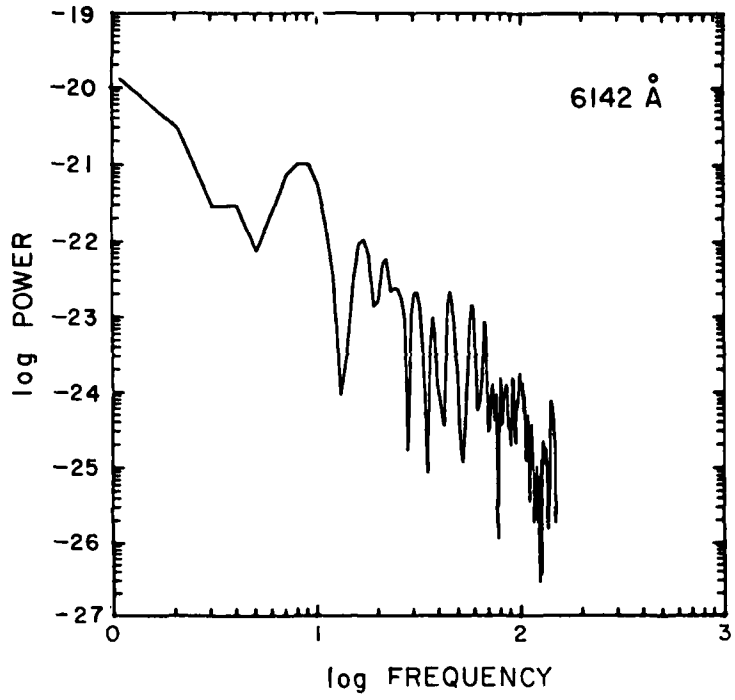

FIGURE 21 POWER SPECTRA FROM PROFILE SHOWN IN FIGURE 19 WITH ONLY A WINDOW APPLIED (614.2 nm)

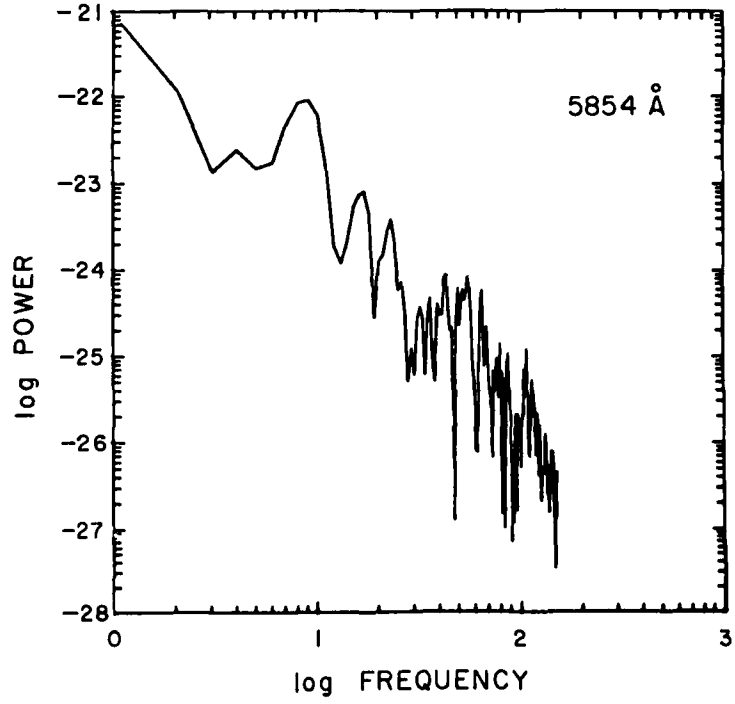

FIGURE 22 POWER SPECTRA FROM PROFILE SHOWN IN FIGURE 19 WITH ONLY A WINDOW APPLIED (585.4 nm)

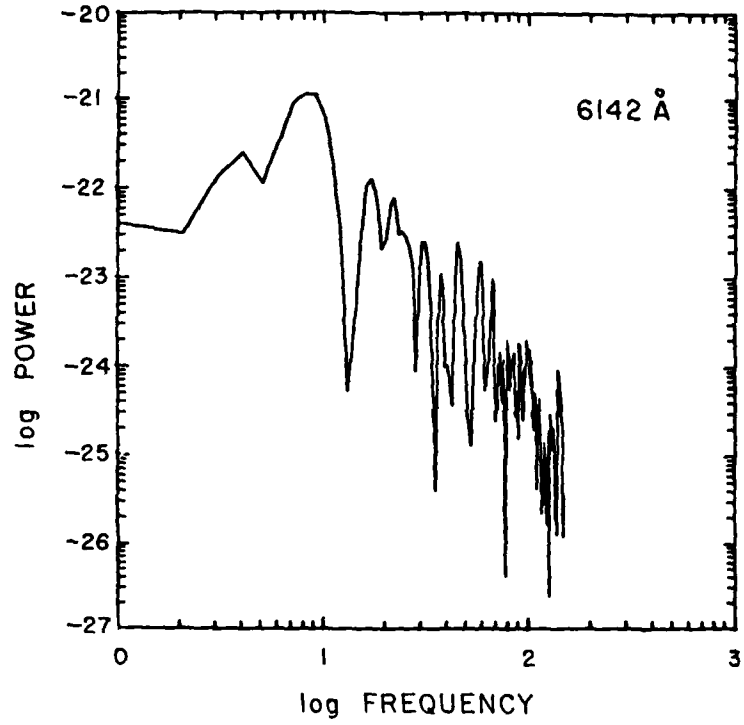

FIGURE 23 POWER SPECTRA CORRESPONDING TO FIGURE 21 WITH DETREND APPLIED TO DATA (614.2 nm)

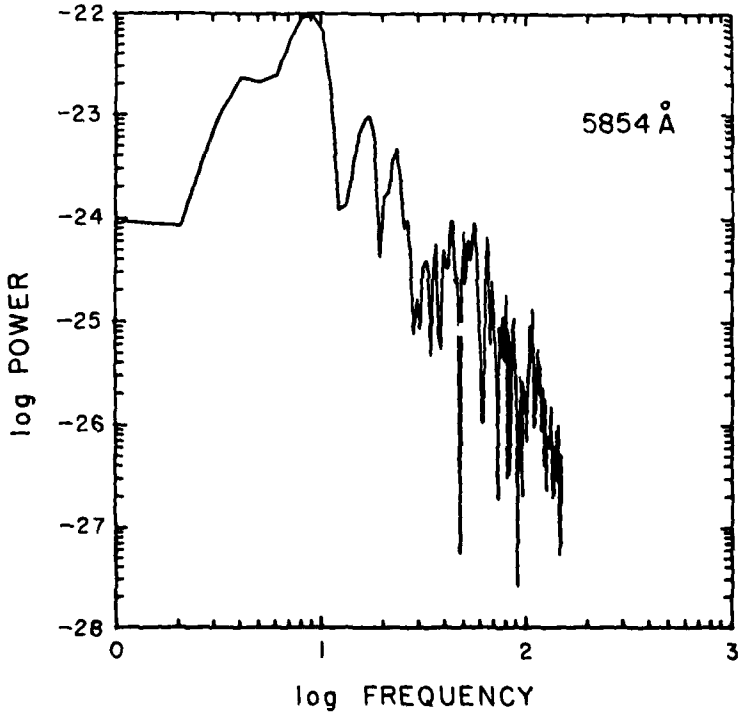

FIGURE 24 POWER SPECTRA CORRESPONDING TO FIGURE 22 WITH DETREND APPLIED TO DATA (585.4 nm)

BLANK PAGE

TV-TRACK, IONOSONDE, AND MAGNETOMETER OPERATIONS

Norman J.F. Chang

SRI International
Menlo Park, CA

ABSTRACT

This report describes the TV tracking system, the slow-scan TV system, the KEL ionosonde, and the magnetometer that were operated in support of the PLACES experiment conducted at Eglin AFB, Florida in December 1980. A procedure for determining the proper launch time and aim point for both the beacon rockets and the probe rocket was developed after post-mission analysis of the first two releases. This procedure contributed to a successful beacon occultation for Event IRIS, and a successful probe penetration for Event JAN.

I INTRODUCTION

The PLACES experiment, conducted at Eglin AFB, Florida in December 1980 was designed to test the effects on radio signals that are propagated through field-aligned electron-density enhancements (striations). Specifically, the test was designed to validate the prediction of serious degradation caused to phase-coherent systems by striation-induced phase effects. It was intended that these effects be demonstrated on signals from the LES 8/9 satellites. The striations were produced by 48-kg barium payloads released at approximately 185 km in the F-region of the ionosphere on four separate days. In addition to the satellite measurements made by an aircraft vectored to the proper location by a ground controller, there was a rocket-borne beacon transmission experiment, an in-situ probe experiment, and ground support instrumentation.

The primary data for aiming both the beacon rockets and the probe rocket and for aircraft vectoring were obtained from TV tracking of the barium cloud from two stations (A-15 and D-3). To coordinate TV aiming points and to aid in determining launch times for both beacon and probe rockets, a slow-scan TV system was constructed and operated with TV displays at CCF and at A-15. These displays provided images of the barium cloud seen by both TV tracking cameras. This report addresses operation of the TV tracking system, the slow-scan TV system, the KEL ionosonde, and the magnetometer.

II EQUIPMENT SETUP IN FLORIDA

SRI International personnel and equipment from Menlo Park, California arrived at Eglin, Florida by 10 November 1980 as scheduled. Setup of the TV tracking and the slow-scan TV systems commenced shortly after. Considerable difficulties were encountered with the data lines connecting A-15 with CCF, C-6, and D-3. Most of the problems, however, were resolved by 2 December 1980, the first scheduled launch day.

The TV tracking system was completely operational by the first launch day, although for Event GAIL a noisy data line between D-3 and A-15 caused bad pointing angles to be passed occasionally to the Sandia computer. This problem was corrected for subsequent launches by lowering the baud rate for data transmission between D-3 and A-15 from 1200 baud to 300 baud. On the second event, HOPE, the graphic board at D-3, which was used to provide the electronic boresight, failed shortly before launch. A boresight was manually located on the TV monitor and calibrated against the sun and a few known reference points. At the conclusion of the event the boresight was checked against the stars and both elevation and azimuth at the D-3 site were found to be in error by approximately two degrees. Drift in the TV monitor was believed to be the primary cause of this error.

The TV tracking systems at D-3 and A-15 were completely recalibrated following HOPE, and no other problems were encountered for Event IRIS and

JAN. Calibration checks for the last two events indicate that the TV-track pointing angles at both D-3 and A-15 were accurate to within a few tenths of a degree.

The slow-scan TV system was also fully operational on 2 December, but because of data line problems, slow-scan displays were provided only to A-15 and CCF. When the data line problems between A-15 and C-6 were corrected toward the end of the PLACES experiment the slow-scan system was not installed at C-6 as planned. The reasons for this were that the slow-scan displays were not required for the particular operating mode used for the FPS-85, and that the system intended for C-6 was being used at A-15 to provide D-3 cloud images needed for cloud tracking and launch decisions.

The KEL ionosonde was shipped directly to Florida from Australia without the receiver. The receiver was hand carried to Florida by Mr. Terry Kelly and Mr. Derrick Horton of KEL Aerospace, who arrived on 29 November 1980. The ionosonde was checked out and the antenna was installed by the two KEL engineers. The ionosonde was fully operational by 1 December 1980.

The magnetometer was operational by 1 December 1981 and was continuously operated to monitor magnetic field variations. Magnetic activity was visually monitored by means of the meters on the magnetometer and periodic strip chart recordings. Continuous recording of the magnetic field variations was not done, due to the excessive speed of the chart recorder. From meter readings and occasional recordings we estimate that the magnetic activity was quiet during the entire PLACES experiment.

III RESULTS

A. TV Tracking

Tracking data from D-3 and A-15 were provided to the Sandia computer and recorded at approximately 3-Hz rate. Digital tapes for each of the four events contain time of day and pointing angles from the two sites. These data were recorded for documentation and possible post-mission

analysis. In particular, the tracking data would be useful for designing and testing barium cloud tracking algorithms.

Video information from each site was also recorded for each of the releases. These video tapes were extremely useful for post-mission critique. The quality of the video was sufficient to show the development of the barium cloud, and for Event JAN the flashing beacon aboard the probe rocket can be seen on the A-15 video tape.

With the experience gained from GAIL and HOPE, the following procedure evolved to provide good tracking data:

(1) After tracking has stabilized (about 10 to 15 s after release), a two-station solution is used to determine the release height.

(2) After calculating the release height, the station providing the "best" track is used for cloud location (single station solution).

(3) After the initial release, the TV track operator should estimate the location of the ion cloud and move slowly to its projected position. When the cloud is sufficiently developed to permit an assessment of the point tracked, a correction should be made if necessary. If a significant change is required, the tracking filter should be reinitialized.

B. Slow-Scan TV

The slow-scan TV system consisted of four separate units for each of four sites--CCF, C-6, A-15, and D-3. The units at CCF and C-6 were two-channel, receive only, while the unit at D-3 was provided with a single-channel transmit capability. The A-15 unit had a single-channel receive and a single-channel transmit capability, but a timing problem prevented the A-15 slow-scan unit from operating in both transmit and receive modes. Hence, it was necessary to use the C-6 unit to receive slow-scan transmissions from D-3.

Each channel of the slow-scan TV system consisted of a CROMENCO SCC (single-card computer) system. The SCC is a Z-80, S-100 bus microprocessor. Each was interfaced with a Digital Video Systems CAT-100/C (computer assisted television system). With this configuration a television frame could be

digitized at a 21-MHz rate. The resolution of each frame was 240 X 256 pixels (4-bits per pixel), but only 240 X 128 pixels were transmitted, in order to maintain a reasonable update time for each frame. With the 1200-baud telephone line used, a complete television frame was transmitted in approximately 70 s.

The four-bit quantization of each pixel provides a 16-level gray scale. To enhance the digitized image, the digitization range was adjusted to provide the best picture. This feature was added after Event GAIL and produced a significant improvement in picture quality.

C. Ionogram

Verbal readings of the F-layer critical frequency were provided on request to Dr. Victor Gonzalez at the FPS-85. Ionograms were also recorded every 20 s for Event GAIL. These ionograms showed returns from the barium ion cloud starting at approximately 2305 UT and ending at approximately 0150 UT. Because of interference to another experiment operating at A-15, the ionosonde was not operated during Event HOPE except when necessary to provide a reading of f_oF_2. The ionosonde was operated on a 15-minute schedule for Events IRIS and JAN, but because of a film jam, ionograms are not available for these events.

D. Magnetometer

Permanent records were not kept of the magnetometer output since it was used only as a real-time indicator of magnetic conditions.

IV CONCLUSIONS AND RECOMMENDATIONS

Considerable difficulties were encountered in tracking the barium ion cloud and in determining the proper launch time and aim point for both beacon and probe rockets. Most of the difficulties stemmed from the requirement that the beacon occult, or that the probe penetrate, the highest-density and most structured part of the barium ion cloud. To accomplish this in the limited optical window available, both the time

and location of the properly developed ion cloud must be predicted in real time based on optical information. The slow-scan images were valuable for providing two near simultaneous views of the barium cloud at one site to enable decisions on launch time and TV tracking points to be made.

The following recommendations are made for future PLACES-type experiments:

(1) The single-station solution (adopted partly because of the experience gained from the STRESS experiment) proved to be a viable procedure and is recommended for any future PLACES-type beacon or probe launches.

(2) The tracking algorithm used during PLACES was unduly restrictive in that it required a long period of "good" tracking data. Other types of tracking algorithms should be investigated based on the experience gained during PLACES. Candidate algorithms could be assessed by use of the actual PLACES digital tracking data.

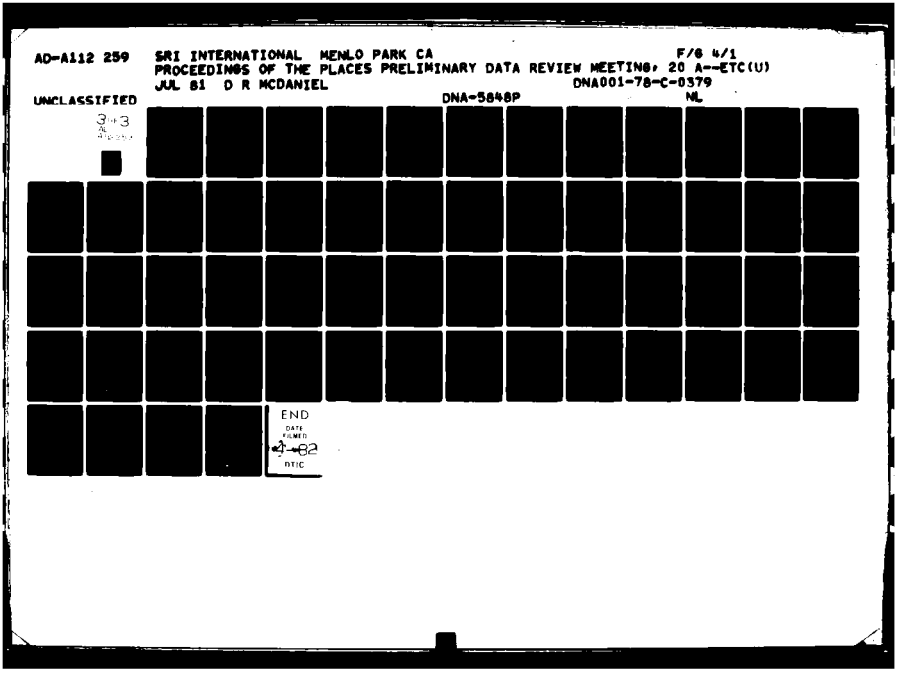
AD-A112 259
SRI INTERNATIONAL MENLO PARK CA
F/G 4/1
PROCEEDINGS OF THE PLACES PRELIMINARY DATA REVIEW MEETING, 20 A--ETC(U)
JUL 81 D R MCDANIEL
DNA001-78-C-0379
UNCLASSIFIED
DNA-5848P
NL
END
DATE FILMED
DTIC

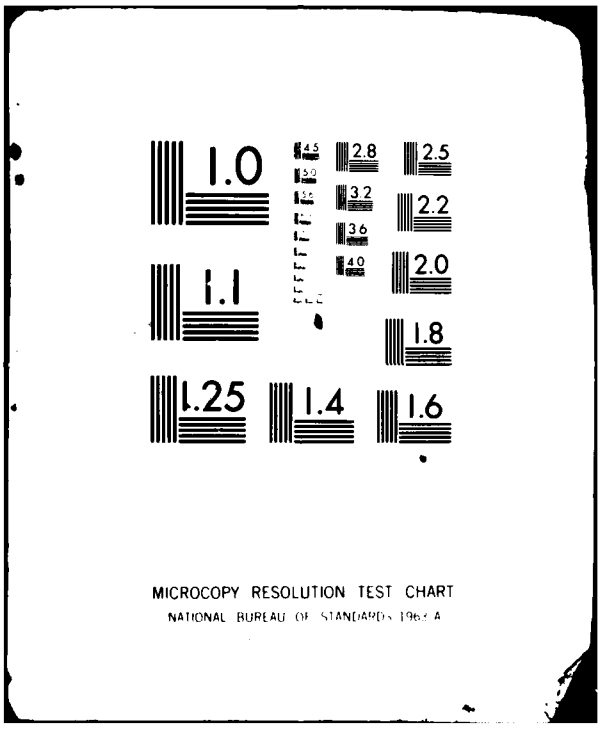
1.0
1.1
1.25
1.4
1.6
1.8
2.0
2.2
2.5
2.8
3.2
3.6
4.0
4.5
MICROCOPY RESOLUTION TEST CHART
NATIONAL BUREAU OF STANDARDS 1963 A

ROCKET OPERATIONS

L. R. Rollstin

Sandia National Laboratories
Albuquerque, NM

I INTRODUCTION

Sandia's responsibility in the PLACES project included the following tasks:

(1) Aeroballistics and computing

- Experiment geometry calculations
- Selection of rocket systems
- Trajectory determinations
- Computer system design
- Wind radar system
- Cloud location and rocket targeting programming
- Wind-weighting, launcher set, and rocket impact programming
- Range safety interface with range
- Aeroballistic/computer operations.

(2) Rocket vehicles

- Procurement of motors and hardware
- Aeroheating studies and thermal coating of motors
- Preparation of safe operating procedures
- Ground (explosive) safety interface with range
- Assembly and launch preparation of vehicles.

(3) Payloads

- Definition of flight environment and loads criteria
- Thermal (aeroheating) analysis of all payloads
- Design and fabrication of barium payload telemetry and firing set section

- Design and fabrication of probe payload less plasma probe and mass spectrometer instruments
- Design and fabrication of beacon payload telemetry, firing set, and flashing light section
- Payload integration and functional testing
- Environmental tests and dynamic balancing
- Prelaunch checkout and preparation
- Payload launch operations
- Telemetry receiving and recording.

(4) Launch facilities

- Liaison with range on storage, preparation, and launch facilities
- Refurbishment, modification, and checkout of launchers and launcher cabling
- Checkout of booster firing system
- Operation of launch facility.

II SUMMARY OF ROCKET OPERATIONS

During the period 6 October to 15 October 1980, the two existing launchers at Eglin Site A-15A were modified for PLACES by Sandia personnel. Extensions were added to the twin booms of the 4-K3 launcher on Pad 2 and new rails were adapted to both the 4K3 and to the 7.5 K launchers on Pad 3. The purpose of these modifications was to enhance the accuracy of the PLACES rockets. The launchers were checked out to ensure that they were in good operating condition. The rocket motors and igniters and the barium canisters were shipped by truck from Albuquerque and Ogden, respectively, to arrive during this period and be received by the Sandia personnel. The rockets were stored at Site A-15A and the barium at Site A-11.

Integration of the RF beacon and probe payloads was accomplished at Sandia during the period of 20 October to 7 November 1980. During this period, these payloads as well as the Sandia (nonexplosive) portion of the barium payloads were subjected to system, functional, and environmental tests, and were dynamically balanced. The silicone rubber thermal protective coating was applied to the RF beacon payloads.

The Sandia computer trailer, wind radar trailer, and some Sandia personnel arrived at Eglin on 3 November. Rocket vehicle assembly and setup and checkout of the computer trailer and radar were started during that week.

On 10 November, the remaining Sandia personnel and all of the rocket payloads (except barium canisters) and payload checkout equipment were flown to Eglin in a DOE F-227 aircraft. Field checkout of payloads, including final system tests, took place during the weeks of 10 November and 17 November. During this period, checkouts of the wind radar and computer system continued, using actual balloon tracks and simulated barium cloud tracks to check the targeting and rocket aiming capability of the system. Figure 1 is a diagram of the computer system.

Each of the three launch rails was loaded with a payload/rocket system (one a barium, one a beacon, and one a probe payload--the planned GAIL configuration), and the first mock countdown was held on 25 November. After a break for the Thanksgiving holiday, additional mock countdowns were held on 2 and 3 December. Live launch attempts were scheduled on even-numbered days from 4 December through 20 December, weather permitting.

The four live PLACES events took place on 4, 6, 8, and 12 December. The scheduled attempt for 10 December was cancelled early because of cloud cover in the Eglin area. Table 1 gives the launch dates and times of the PLACES events as well as barium release times. Table 2 compares the PLACES event configurations as planned before the operation, as revised during the operation, and as they actually occurred. On GAIL and HOPE, only barium payloads were flown, because the ionized clouds drifted outside the predicted drift envelope, yielding target points for the beacon and probe payloads that would have resulted in impacts outside of range safety limits. Since, after HOPE, only two barium payloads remained, and the beacon experiment carried a higher priority than the probe experiment, IRIS was configured for a barium and two beacon payloads, to enhance the probability of getting one or more occultations with a beacon payload. Since IRIS resulted in occultation by both beacon payloads, JAN was con-

figured for barium, beacon, and probe payloads in the hope of getting simultaneous penetration of the cloud by a probe and occultation by a beacon. Again, the cloud drift precluded the launch of a beacon rocket for range safety reasons, but the probe was launched and did penetrate the ionized cloud.

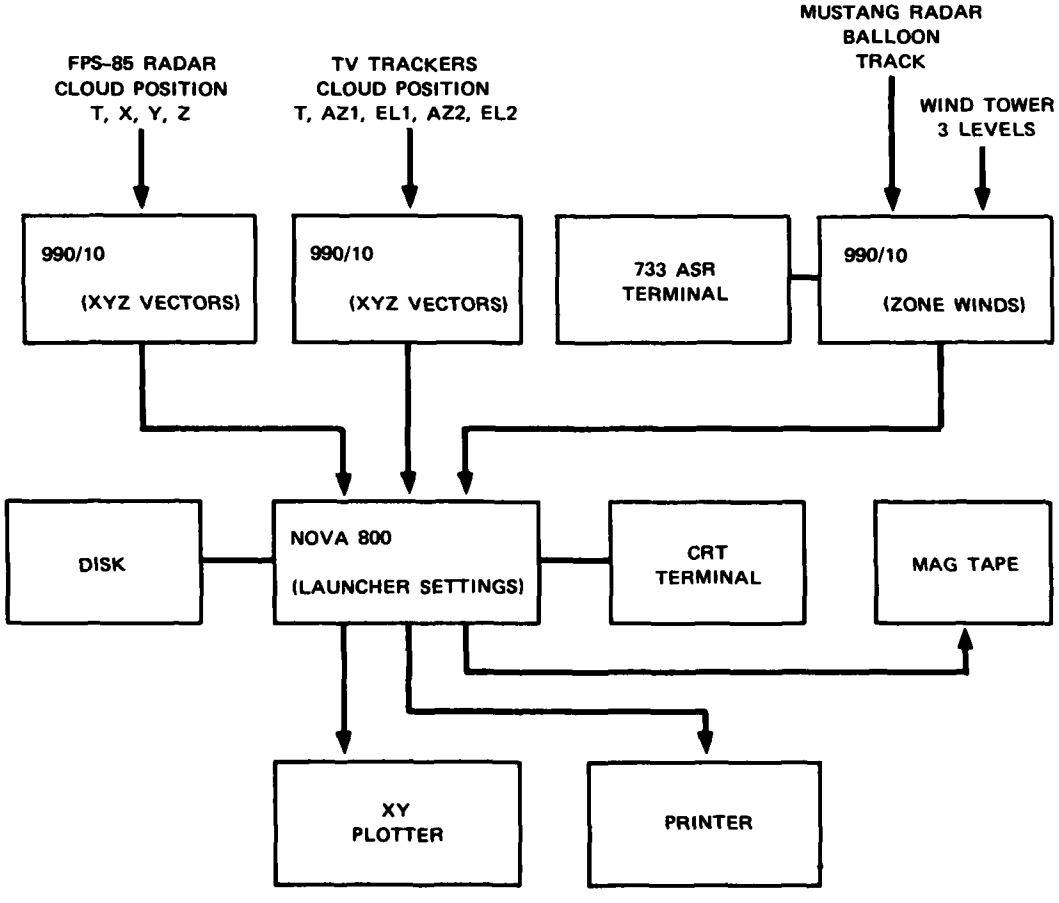

FIGURE 1 PLACES COMPUTER SYSTEM

Table 1

PLACES EVENT TIMES

Event	Date	Flight Number	Payload Type	Launch Time (Z)	Barium Release Time (Z)	Barium Release Time After Launch (s)
GAIL	12/4/80	152-225	Barium	23:04:59.87	23:07:35.8	155.9
HOPE	12/6/80	152-226	Barium	23:05:00.25	23:07:37.9	157.6
IRIS	12/8/80	152-227	Barium	23:09:59.91	23:13:07.3	187.4
		152-233	Beacon	23:38:36.8		
		152-232	Beacon	23:51:36.26		
JAN	12/12/80	152-228	Barium	23:11:00.03	23:13:41.6	161.6
		152-229	Probe	23:42:50		

Table 2

PLACES EVENT CONFIGURATION CHANGES

Event	Original Plan	Field Revision	Actual Launches
GAIL	Ba, Be, Pr	None	Ba
HOPE	Ba, Be, Be	Ba, Be, Pr	Ba
IRIS	Ba, Be, Pr	Ba, Be, Be	Ba, Be, Be
JAN	Ba	Ba, Be, Pr	Ba, Pr

Ba = Barium Payload

Be = RF Beacon Payload

Pr = Plasma Probe Payload

All rocket systems performed within predicted limits (see Table 3). All Sandia-furnished payload systems--sequencing and firing, telemetry, radar transponders, external flashing lights, and attitude control--performed as desired. Table 4 gives some probe payload attitude angles of interest. Cloud tracking, vehicle targeting, and ballistic performance are discussed in detail in the following section.

III ION CLOUD TRACKING AND VEHICLE TARGETING

A. Event GAIL

The barium for Event GAIL was released on 4 December 1980 at an altitude of 178.8 km. The time of release was 2307:35.8Z. The beacon vehicle targeting was based on data received from the two TV trackers (beacon TV tracker located at D-3 and the probe TV tracker located at A-15A). The real-time cloud location track was determined using the beacon TV tracker look-line or pointing vector to the cloud. This look-line was intersected by the local vertical plane, which contained the probe TV tracker and its corresponding look-line or pointing vector, to determine the real-time location of the ion cloud.

Table 3

PLACES ROCKET PERFORMANCE

Vehicle		Dispersion, σ
GAIL	Barium	0.1
HOPE	Barium	1.4
IRIS	Barium	0.1
JAN	Barium	1.0
IRIS	Beacon 1	0.3
IRIS	Beacon 2	1.2
JAN	Probe	*

*Data not yet reduced; quick-look indicates $\ll 3\ \sigma$.

During the operation, this real-time cloud track appeared to be moving on an azimuth of 25° to 30°T (see Figure 2). This track direction was taking the ion cloud outside the area of allowed cloud positions for targeting the beacon vehicle within range safety constraints. The "allowed" area was defined by azimuthal lines of 70°T and 146°T and radial distances from 40 km to 100 km from the nominal release point of Event GAIL.

The cloud was tracked for 6-1/2 minutes prior to computing the first predicted location for beacon vehicle targeting. An eleven-minute offset or future time was used to comput this future cloud location to allow for computation time (included vehicle targeting and nominal launch angle corrections because of atmosphere winds), for obtaining a "green-range" condition from range safety, for setting the launcher and conducting a terminal countdown, and for the vehicle flight time to the target (usually in excess of 7 min).

The first three predicted cloud locations (determined in the period of R + 6-1/2 min to R + 18 min) were all well outside the allowed cloud

Table 4

PROBE PAYLOAD ATTITUDE ANGLES

Time After Launch (s)	Angle Between Flight Path and Magnetic Field (deg)	Angle Between Payload Axis and Flight Path (deg)	Event
64	2.3	0	Exit Atmosphere
76	4.0	1.7	ACS Activate
97	7.1	7.1	ACS Pointed
108	9.2	9.2	ACS Deactivate

track area with beacon vehicle impacts well inside a range-safety hazard area. Subsequent beacon vehicle target points were erratic and provided no confidence in the tracking data received (see Figures 3, 4, and 5). Thus, no companion vehicles (beacon or probe) were launched with the developed GAIL barium ion cloud.

A data analysis after the operation revealed some inaccuracy in the beacon TV track. This track may have been oriented on the neutral cloud. A combination of the probe TV tracker data and a constant height of 178 km over the time period of R + 7 min to R + 10 min, generated after the operation, showed that the ion cloud drift azimuth was probably closer to 60°T (see Figure 2). It should be noted that even this drift direction was north of the extreme north azimuth expected for the PLACES ion clouds (70°T). Thus, even if the ion cloud track had been accurately received, the beacon vehicle impacts may still have been within the range safety hazard area. No provision had been made for the launch of a probe vehicle with no beacon vehicle launch, since the targeting of the probes was to be such that simultaneous beacon vehicle occultation and probe vehicle penetration would occur. If an accurate cloud track had been received, a probe vehicle launch would not have been prevented by existing range safety hazard areas.

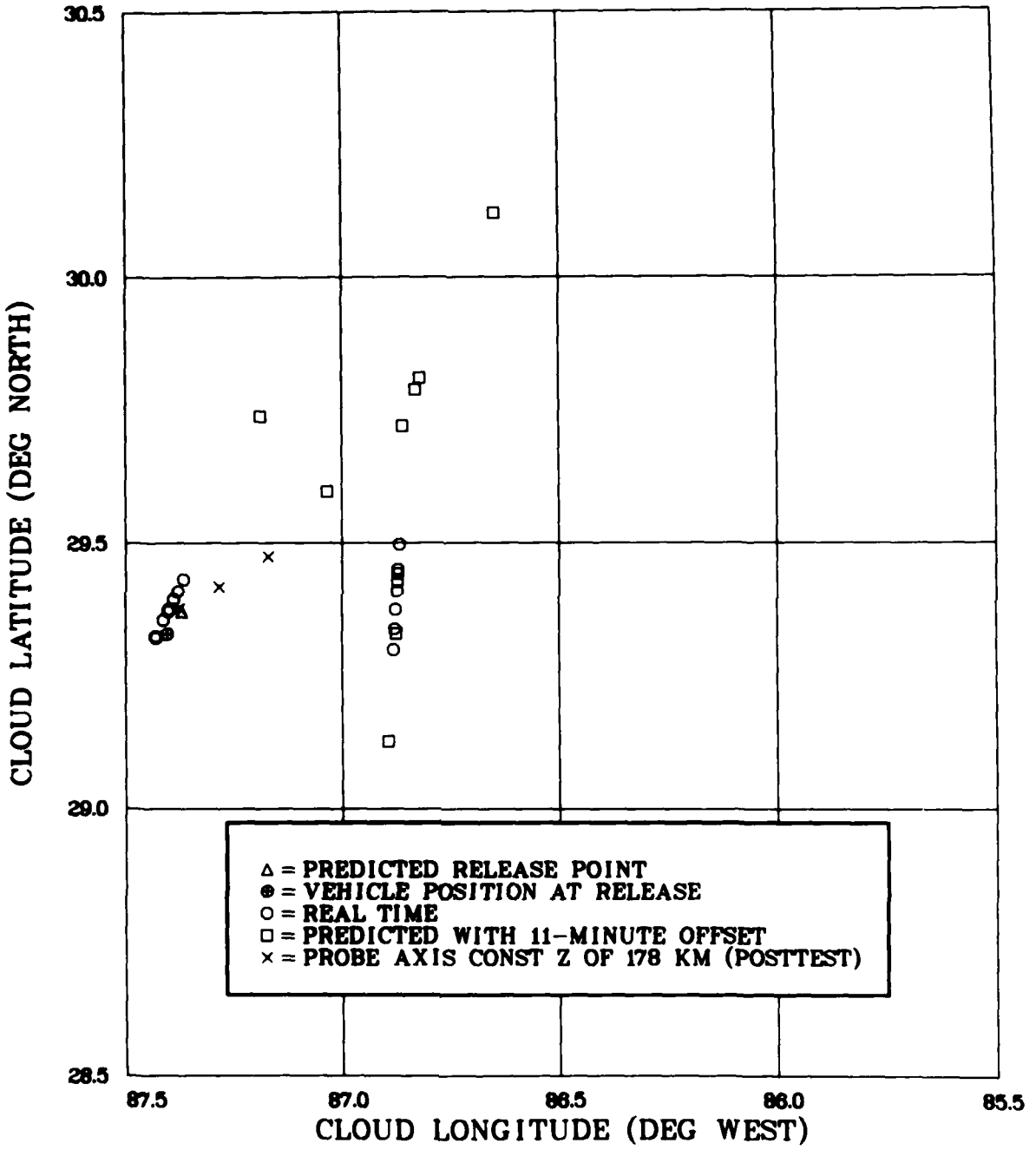

FIGURE 2 TV TRACK SOLUTION OF GAIL RELEASE, 4 DECEMBER 1980, BEACON AXIS-PROBE PLANE, CLOUD LATITUDE vs CLOUD LONGITUDE

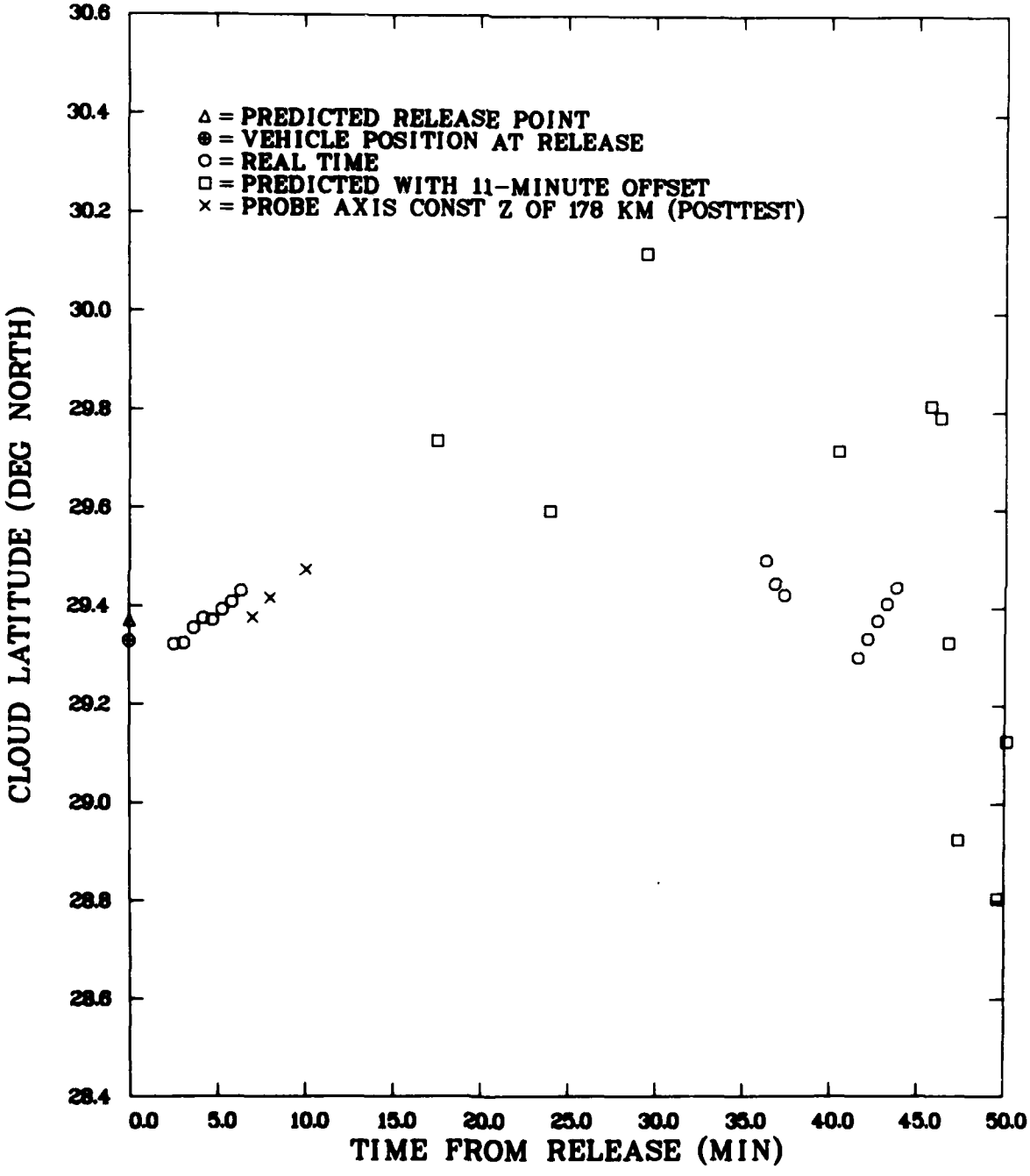

FIGURE 3 TV TRACK SOLUTION OF GAIL RELEASE, 4 DECEMBER 1980, BEACON AXIS-PROBE PLANE, CLOUD LATITUDE vs TIME FROM RELEASE

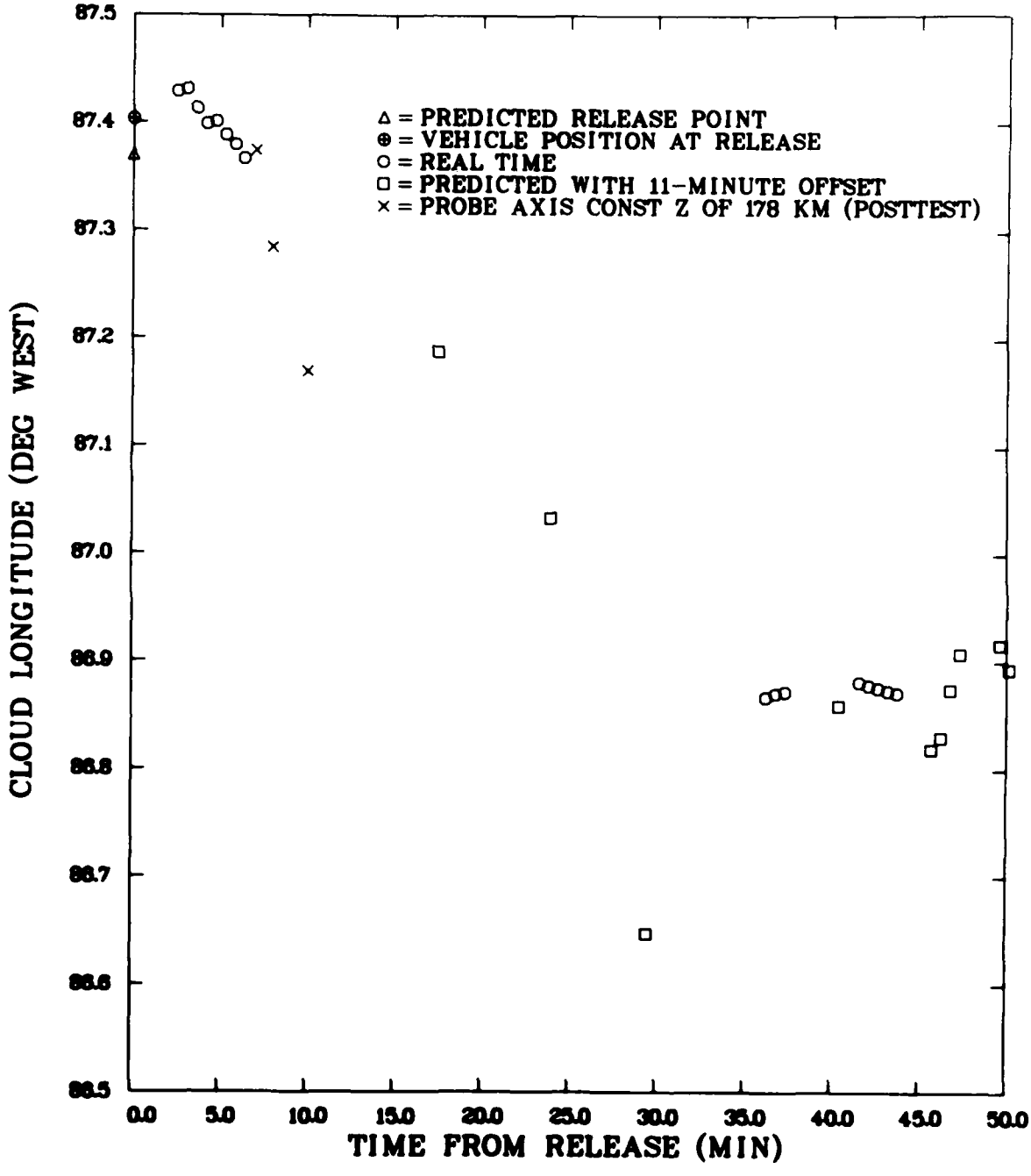

FIGURE 4 TV TRACK SOLUTION OF GAIL RELEASE, 4 DECEMBER 1980, BEACON AXIS-PROBE PLANE, CLOUD LONGITUDE vs TIME FROM RELEASE

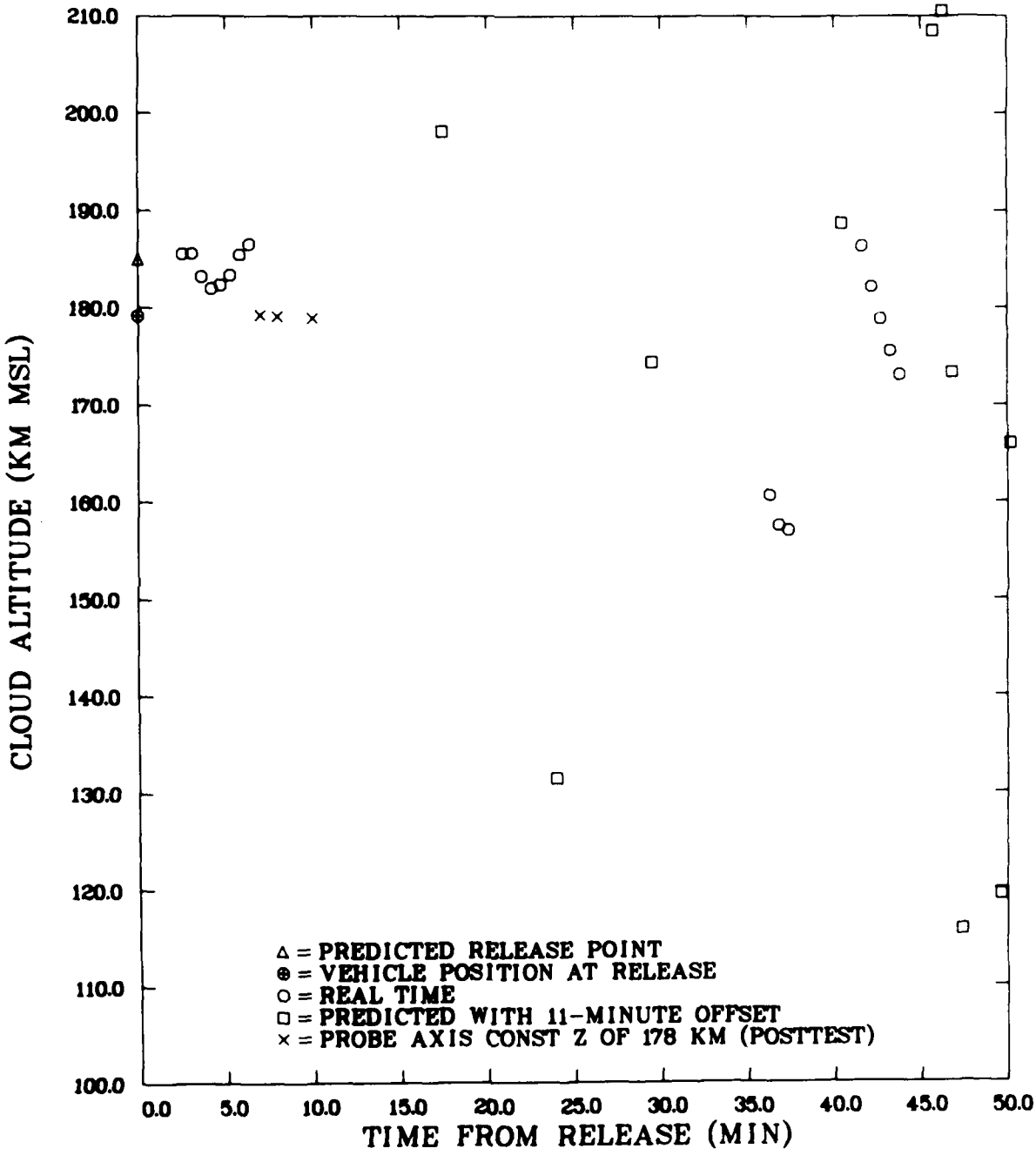

FIGURE 5 TV TRACK SOLUTION OF GAIL RELEASE, 4 DECEMBER 1980, BEACON AXIS-PROBE PLANE, CLOUD ALTITUDE vs TIME FROM RELEASE

B. Event HOPE

Several operational changes were made prior to the Event HOPE release. The companion vehicle targeting was to be exclusively based on the look-line or pointing vector from the probe TV tracker. The intersection of this line with an empirical height plane was to provide the real-time ion cloud position. This plane was to be generated using an empirical height variation based on the STRESS Event ANNE and an initial elevation from the C-band barium vehicle radar track at the nominal barium release time. This operational change was made because of the apparent difficulty in seeing the ion cloud striations from the beacon TV tracker site, especially prior to R + 15 min. The second operational change was that of moving the barium release point to the east (0.4° of longitude) and south (0.1° of latitude) from the nominal Event GAIL release point. This change was made primarily to allow for a greater azimuthal dispersion of the cloud track than that allowing a probe vehicle launch if the beacon vehicle target points were such that a beacon vehicle could not be launched because of range safety or if the beacon could not be launched because of an operational problem exclusive to the beacon vehicle.

The barium for Event HOPE was released on 6 December 1980 at an altitude of 180.9 km. The time of release was 2307:37.9Z. A smooth real-time ion cloud track was obtained from R + 8-1/2 min using the probe TV tracker look-line and the empirical height variation mentioned above (see Figures 7, 8, and 9). Predicted cloud positions for beacon vehicle target were also computed beginning at R + 8-1/2 min. The beacon target positions began to show a consistent trend with small scatter by R + 30 min. However, since the ion cloud track direction was initially west, then north, and never east of an azimuth of 15°T (see Figure 6), no beacon vehicle target point was computed such that the impact would satisfy range safety requirements.

A series of six targeting computations for the probe vehicle were made over the time period of R + 27-1/2 min to R + 37-1/2 min. However, the predicted probe vehicle payload impacts were concentrated in an area

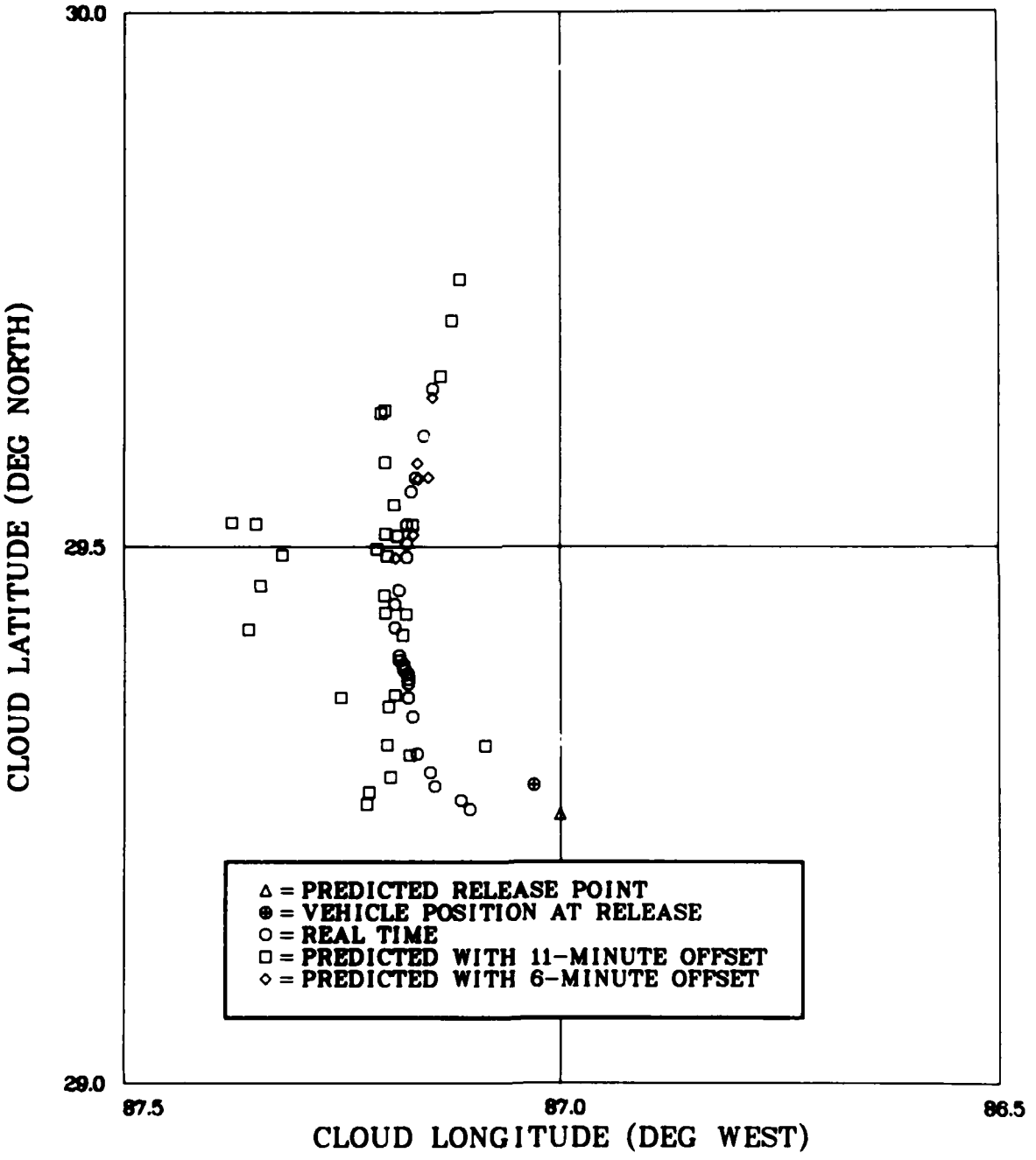

FIGURE 6 TV TRACK SOLUTION OF HOPE RELEASE, 6 DECEMBER 1980, PROBE AXIS-EMPIRICAL HEIGHT, CLOUD LATITUDE vs CLOUD LONGITUDE

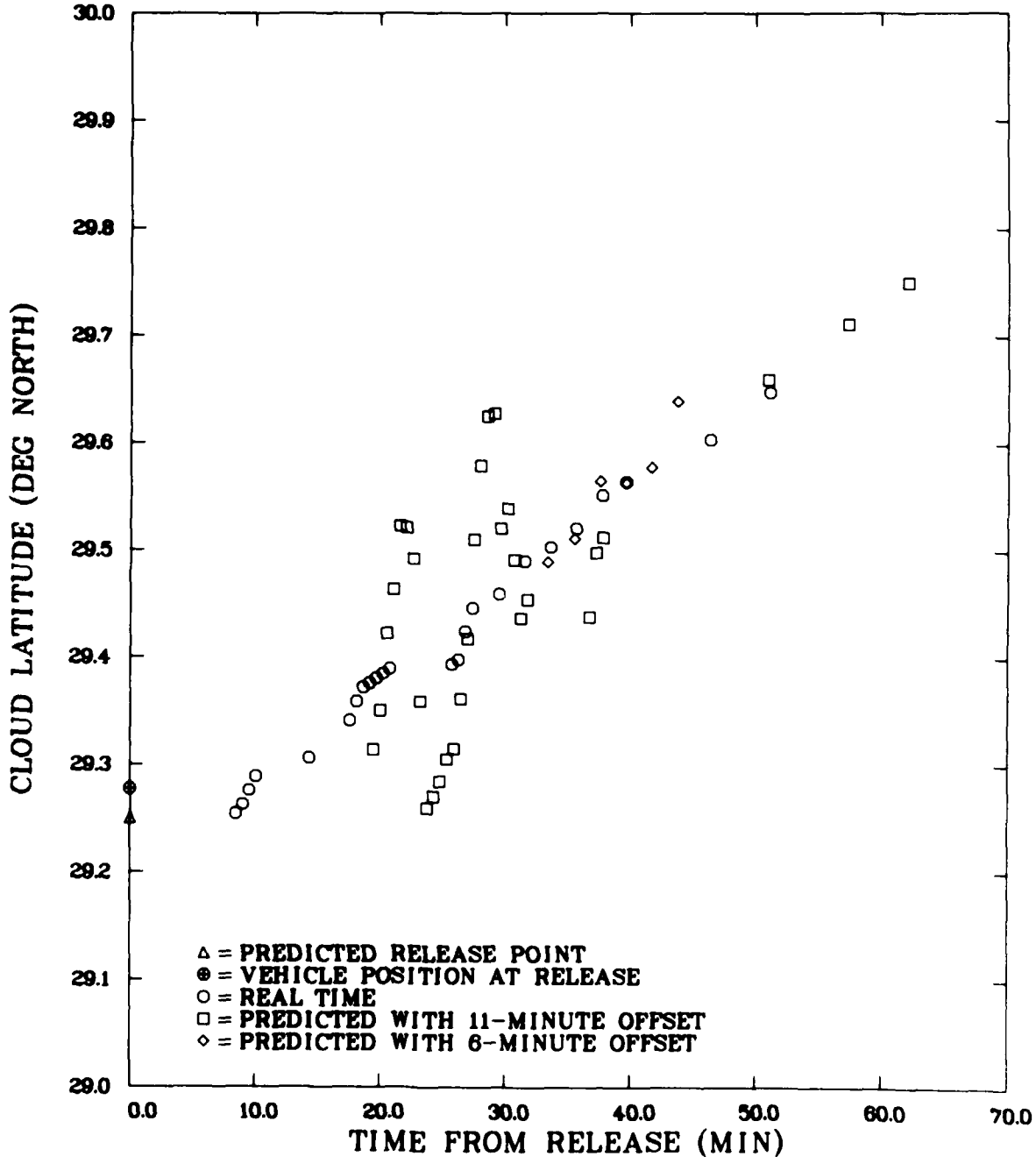

FIGURE 7 TV TRACK SOLUTION OF HOPE RELEASE, 6 DECEMBER 1980, PROBE AXIS-EMPIRICAL HEIGHT, CLOUD LATITUDE vs TIME FROM RELEASE

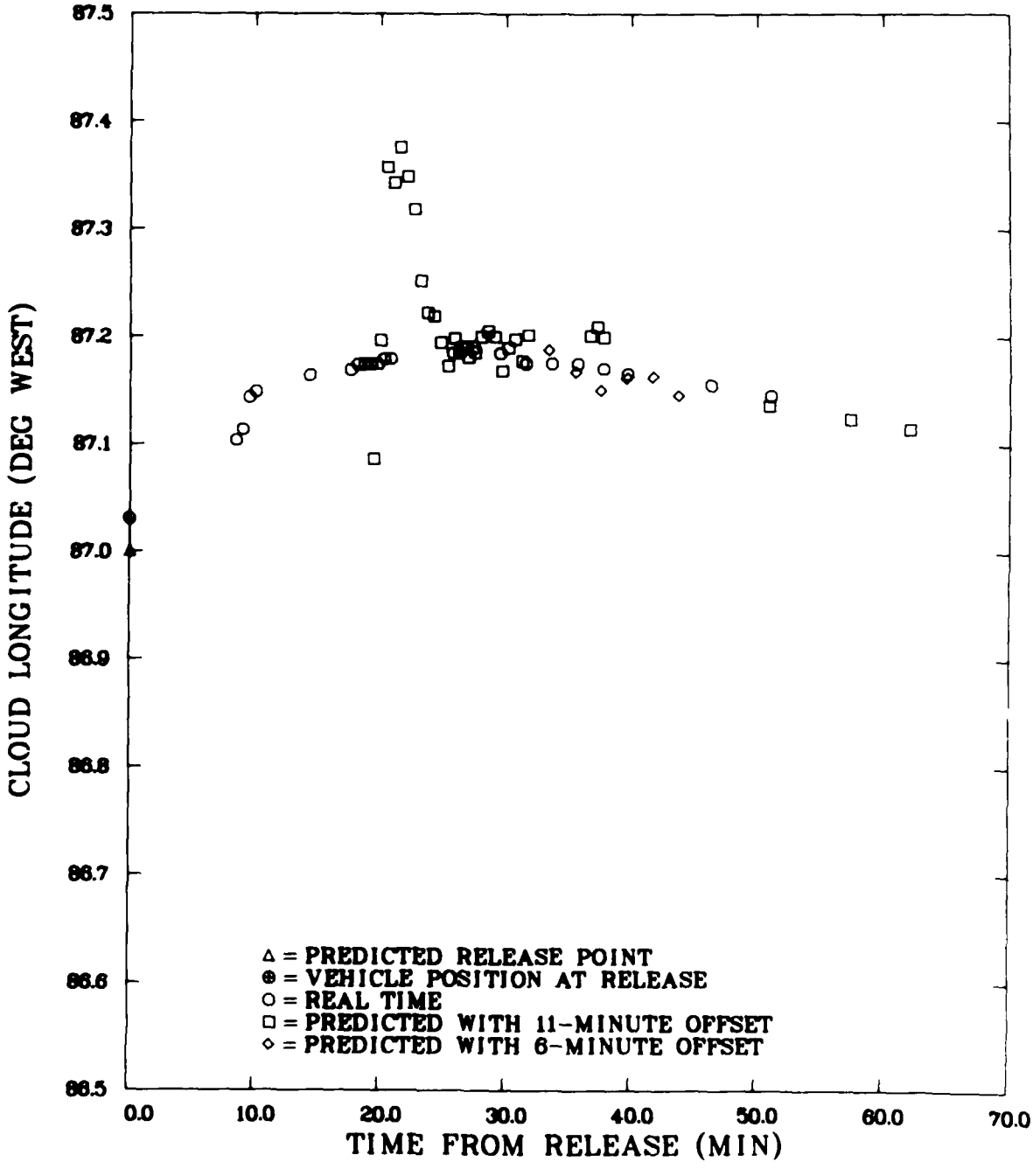

FIGURE 8 TV TRACK SOLUTION OF HOPE RELEASE, 6 DECEMBER 1980, PROBE AXIS-EMPIRICAL HEIGHT, CLOUD LONGITUDE vs TIME FROM RELEASE

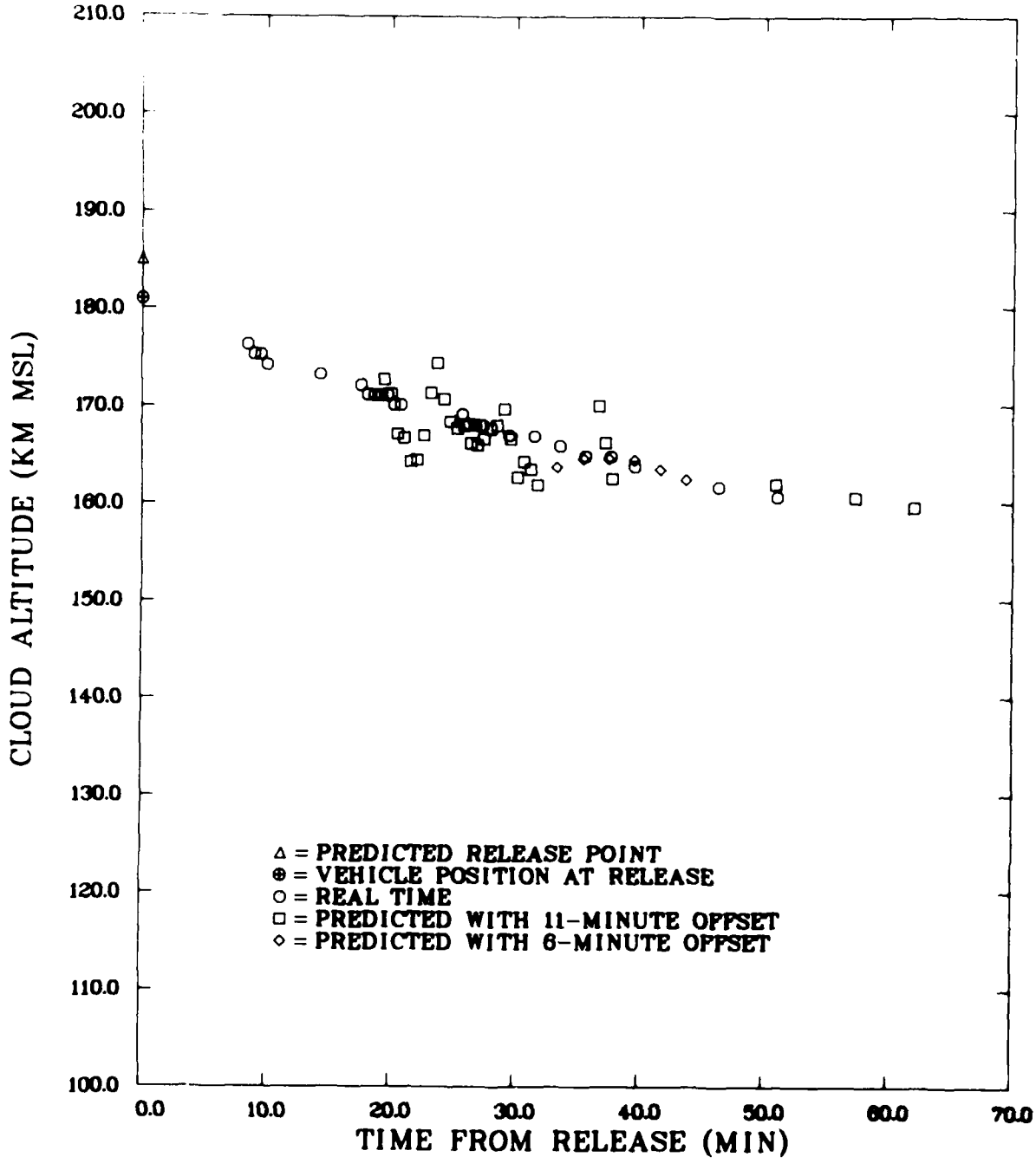

FIGURE 9 TV TRACK SOLUTION OF HOPE RELEASE, 6 DECEMBER 1980, PROBE AXIS-EMPIRICAL HEIGHT, CLOUD ALTITUDE vs TIME FROM RELEASE

of reported high-density shipping, which prevented the probe vehicle launch because of the apparent range safety hazard. Therefore, no beacon or probe companion vehicles were launched with the developed HOPE barium ion cloud.

C. Event IRIS

Several additional operational changes were made prior to the Event IRIS release. Since no companion vehicles had been launched in conjunction with the first two PLACES barium events, and since the beacon occultation experiment was of the highest program priority, two beacon vehicles were planned for launch after the IRIS barium release. No probe vehicles were planned because only three launchers were available. The IRIS event nominal release point was moved well south (approximately 0.5° of latitude) and slightly west (approximately 0.2° of longitude) of the HOPE nominal release point. This release point allowed for extensive northerly cloud movement during development, and southerly movement would not prohibit targeting with the following occultation geometry change. Prior to the PLACES operation, the distance from the striated ion cloud to the beacon vehicle during occultation was requested to be 100 km. After the HOPE barium event, a 40-km option for this distance was included in the beacon targeting computation procedure to allow for cloud positions such as the HOPE ion cloud track, and to alleviate the range safety problems. Also, this option was to be exercised if the IRIS ion cloud track was in a southerly or southeasterly direction after 40 km of drift. This was to be done because of vehicle performance limitations imposed by the downleg occultation requirement in combination with such extreme cloud ground range distances. The nominal barium release altitude was changed to 190 km in an attempt to obtain ion cloud development in less time and less drift distance. The nominal release time was changed from 6° SDA minus 5 min to 6° SDA in an attempt to obtain an ion cloud track sooner after release than had been obtained after the first two PLACES releases.

The targeting computation scheme was to include the continuous real-time monitoring of two separate cloud target position solutions. The beacon TV tracker axis with the probe TV tracker plane solution and the

probe TV tracker axis with the empirical height solution were both to be considered valid for targeting the two prospective beacon vehicle launches after the IRIS barium release. An empirical height variation obtained from L. Linson (SAI), which differed only slightly (up to -3 km at R + 40 min) from that used previously during the HOPE cloud track was to be applied during the IRIS operation.

The barium for Event IRIS was released on 8 December 1980 at an altitude of 179.6 km. The time of release was 2313:07.3Z. An off-nominal second-stage ignition time (normal staging coast time of 12 s was extended to 16 s), apparently caused by an abnormal Tomahawk ignition sequence, contributed to the inaccuracy of the barium release altitude (10 km lower than planned).

The IRIS ion cloud was tracked by the TV trackers from approximately R + 2 min. The first predicted cloud position for a beacon vehicle targeting was determined at R + 8-1/2 min after a trend of actual tracked positions had been established. The IRIS ion cloud track was generally in a southeast direction (see Figures 10 and 11), and was soon (approximately R + 15 min) beyond the range limit line, which required exercise of the occultation geometry option for targeting the beacon vehicles at 40 km behind the cloud as seen by the beacon receiver sites. Considerable data scatter was obtained in the predicted cloud positions to be used for beacon vehicle targeting from both of the TV track solution sources (see Figures 12 through 17). A target was selected in real time to help assure that the expected occultations would occur. The target cloud positions were being predicted 11 min in the future to allow time for computation of the nominal beacon vehicle trajectory to the target point behind the predicted cloud position, time for correcting the nominal launch angles for atmosphere wind effects, time for obtaining a "green-range" and a short (one min) terminal countdown, and time for the vehicle flight to the target (usually in excess of 7 min).

The beacon-axis, probe plane TV tracker solution was used for targeting the first beacon vehicle (targeted for the predicted position of the striated ion cloud at R + 32-1/2 min). The probe-axis, empirical height

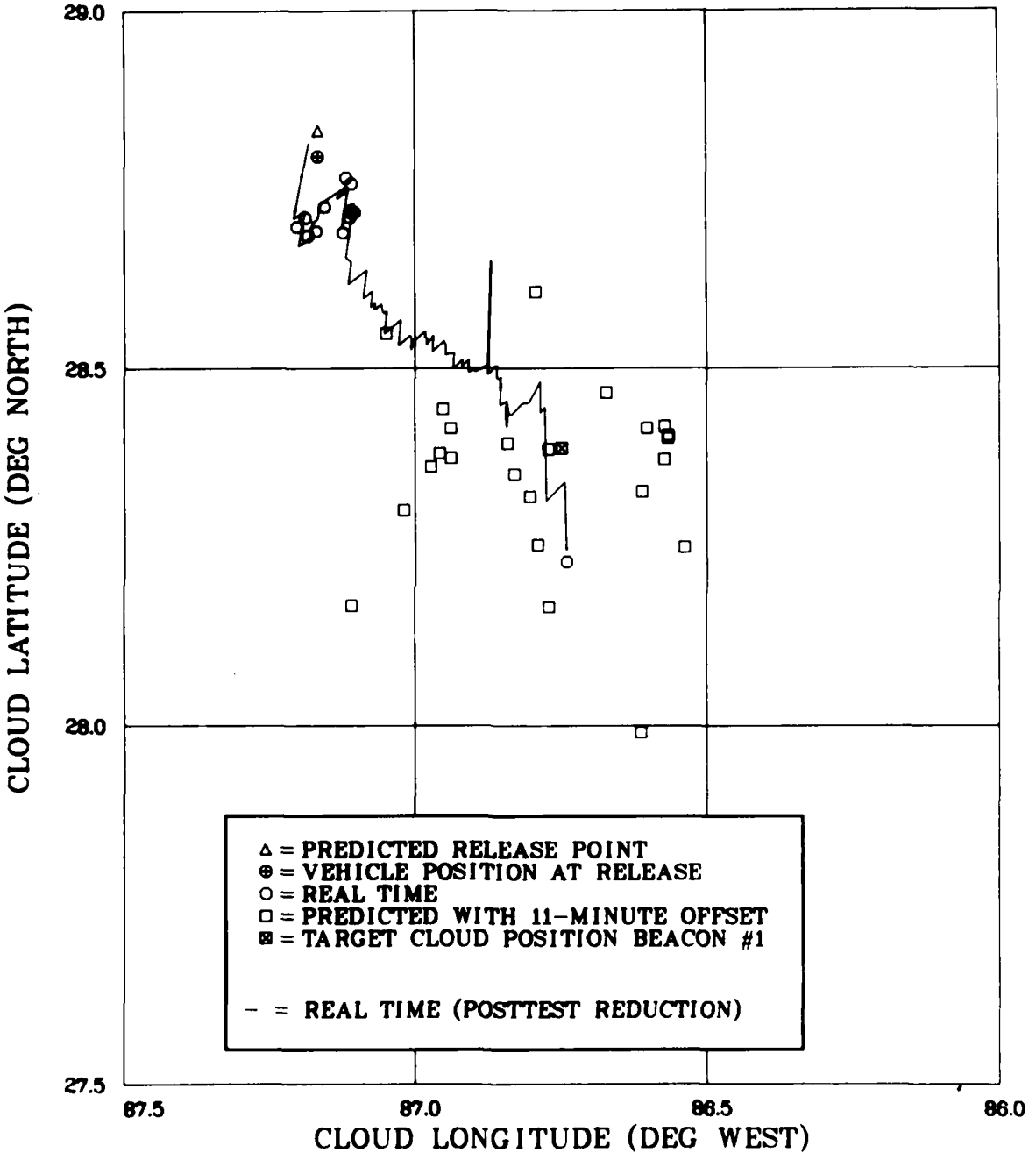

FIGURE 10 TV TRACK SOLUTION OF IRIS RELEASE, 8 DECEMBER 1980, BEACON AXIS-PROBE PLANE, CLOUD LATITUDE vs CLOUD LONGITUDE

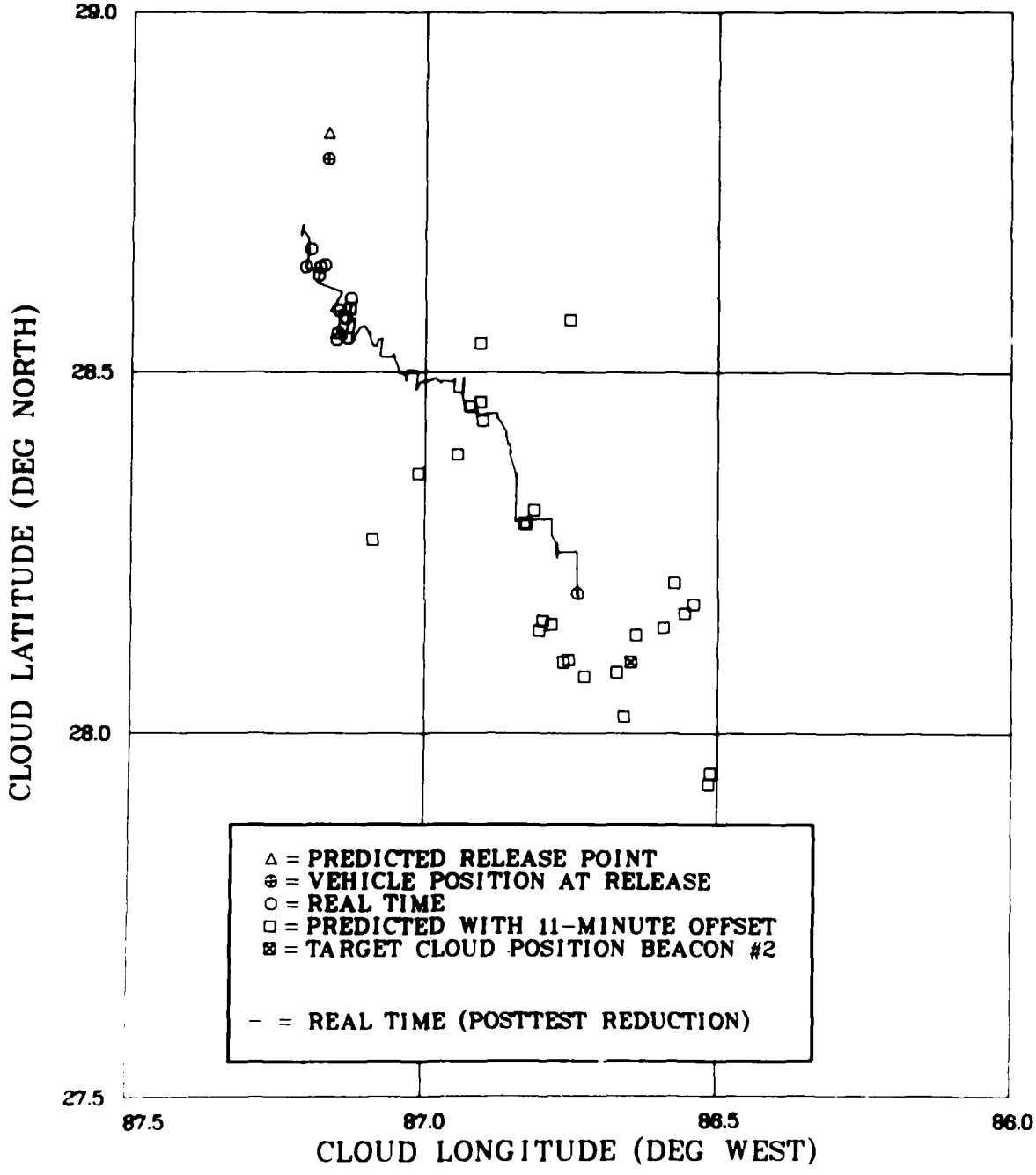

FIGURE 11 TV TRACK SOLUTION OF IRIS RELEASE, 8 DECEMBER 1980, PROBE AXIS-EMPIRICAL HEIGHT, CLOUD LATITUDE vs CLOUD LONGITUDE

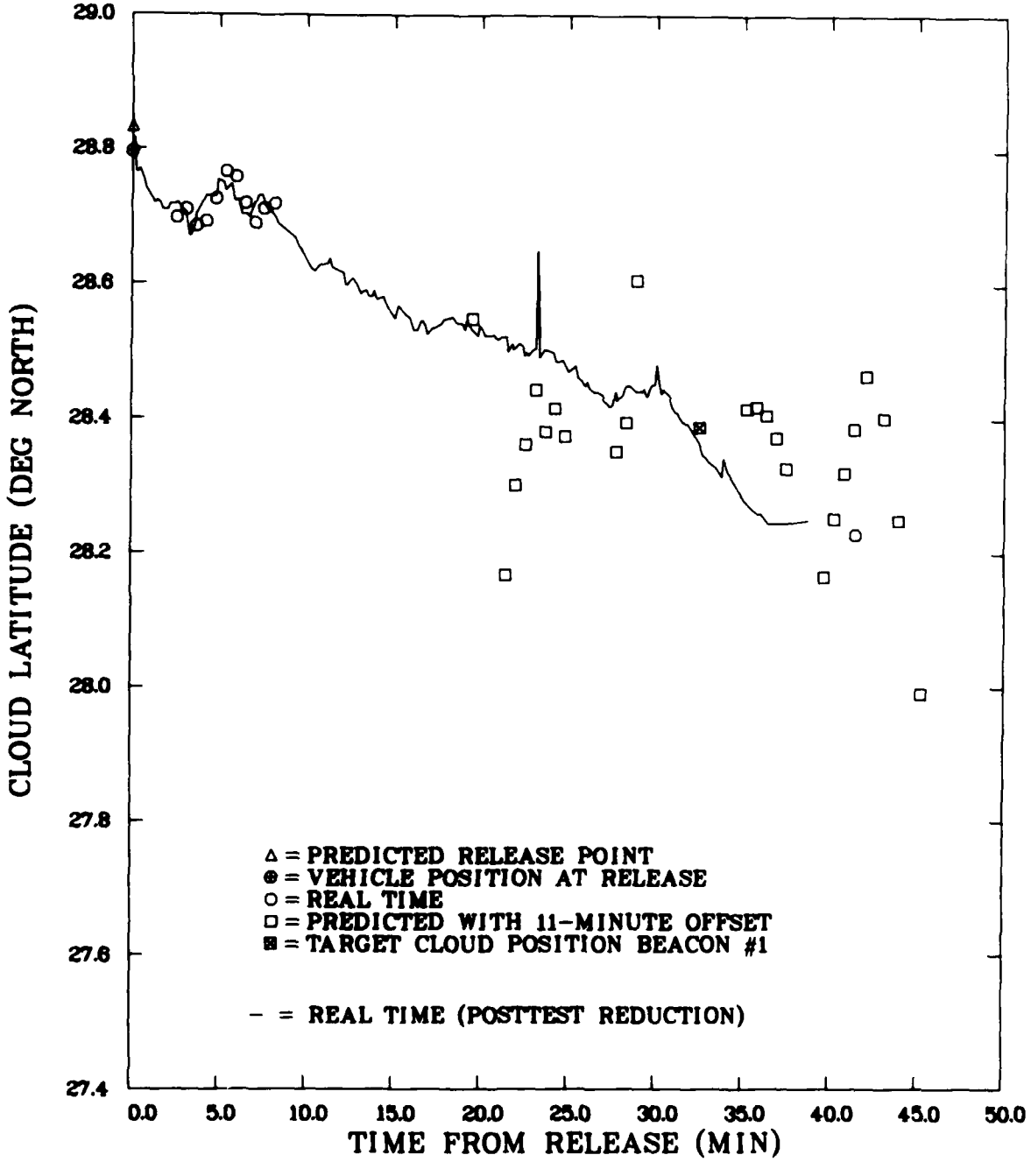

FIGURE 12 TV TRACK SOLUTION OF IRIS RELEASE, 8 DECEMBER 1980, BEACON AXIS-PROBE PLANE, CLOUD LATITUDE vs TIME FROM RELEASE

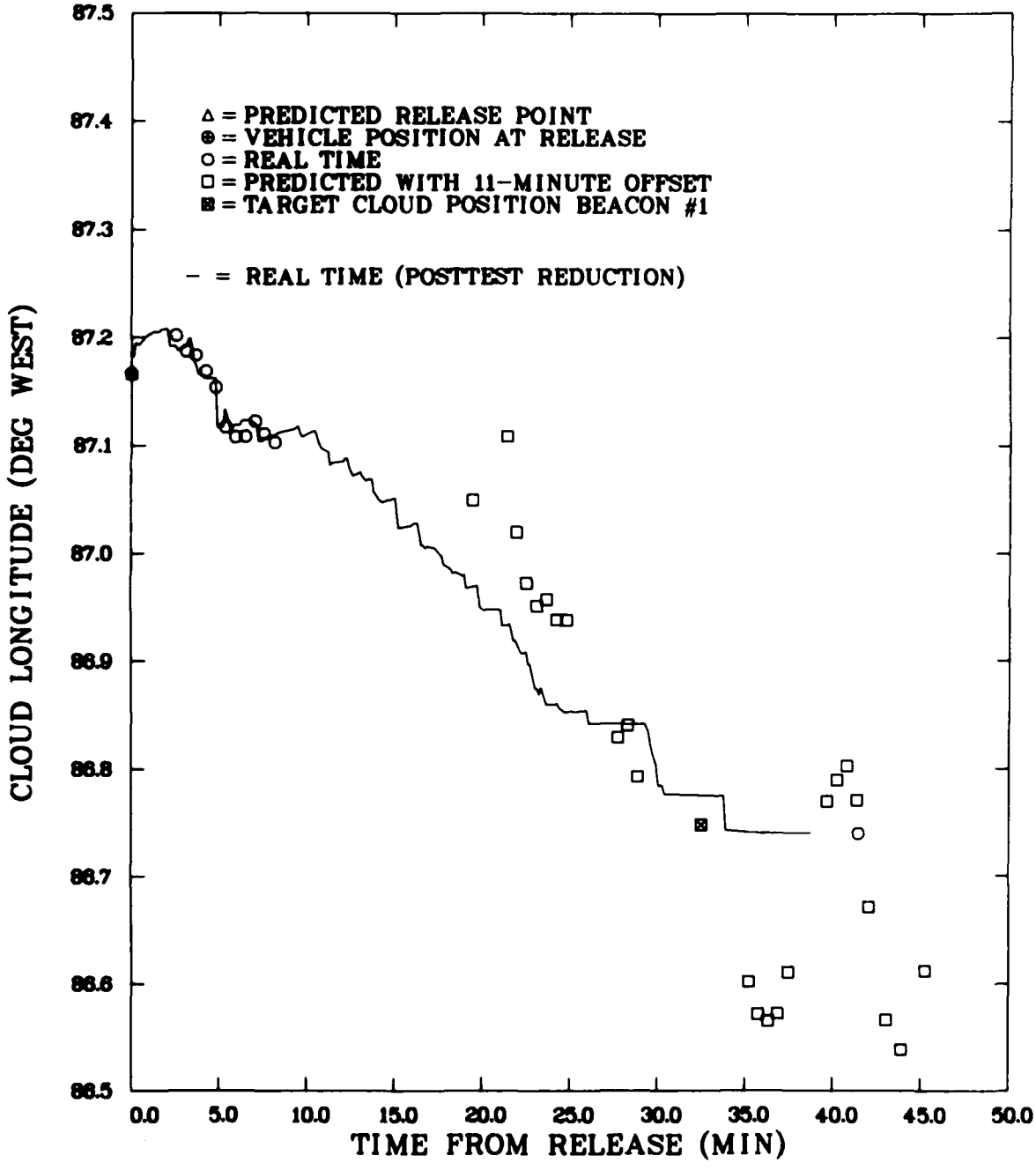

FIGURE 13 TV TRACK SOLUTION OF IRIS RELEASE, 8 DECEMBER 1980, BEACON AXIS-PROBE PLANE, CLOUD LONGITUDE vs TIME FROM RELEASE

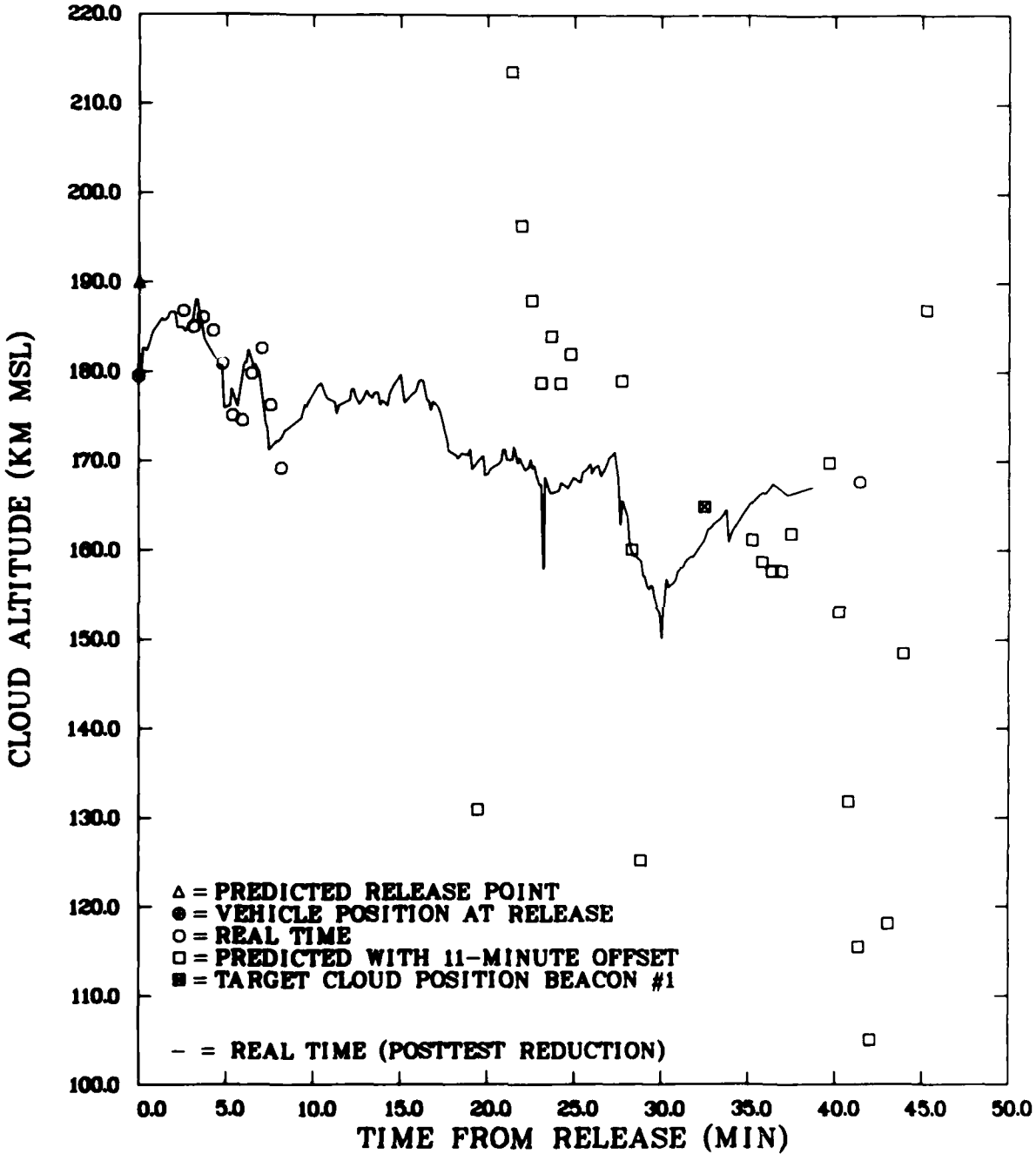

FIGURE 14 TV TRACK SOLUTION OF IRIS RELEASE, 8 DECEMBER 1980, BEACON AXIS-PROBE PLANE, CLOUD ALTITUDE vs TIME FROM RELEASE

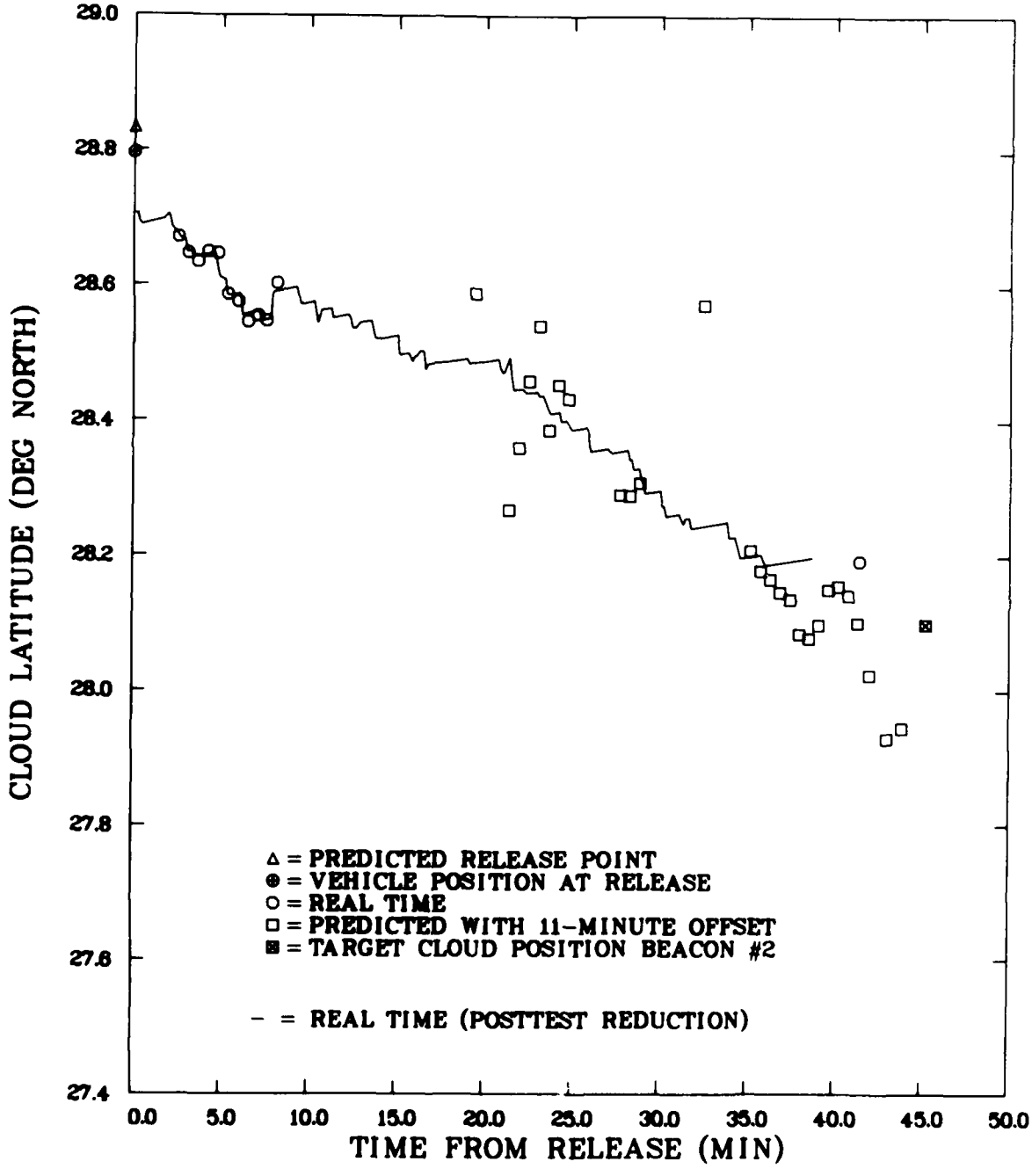

FIGURE 15 TV TRACK SOLUTION OF IRIS RELEASE, 8 DECEMBER 1980, PROBE AXIS-EMPIRICAL HEIGHT, CLOUD LATITUDE vs TIME FROM RELEASE

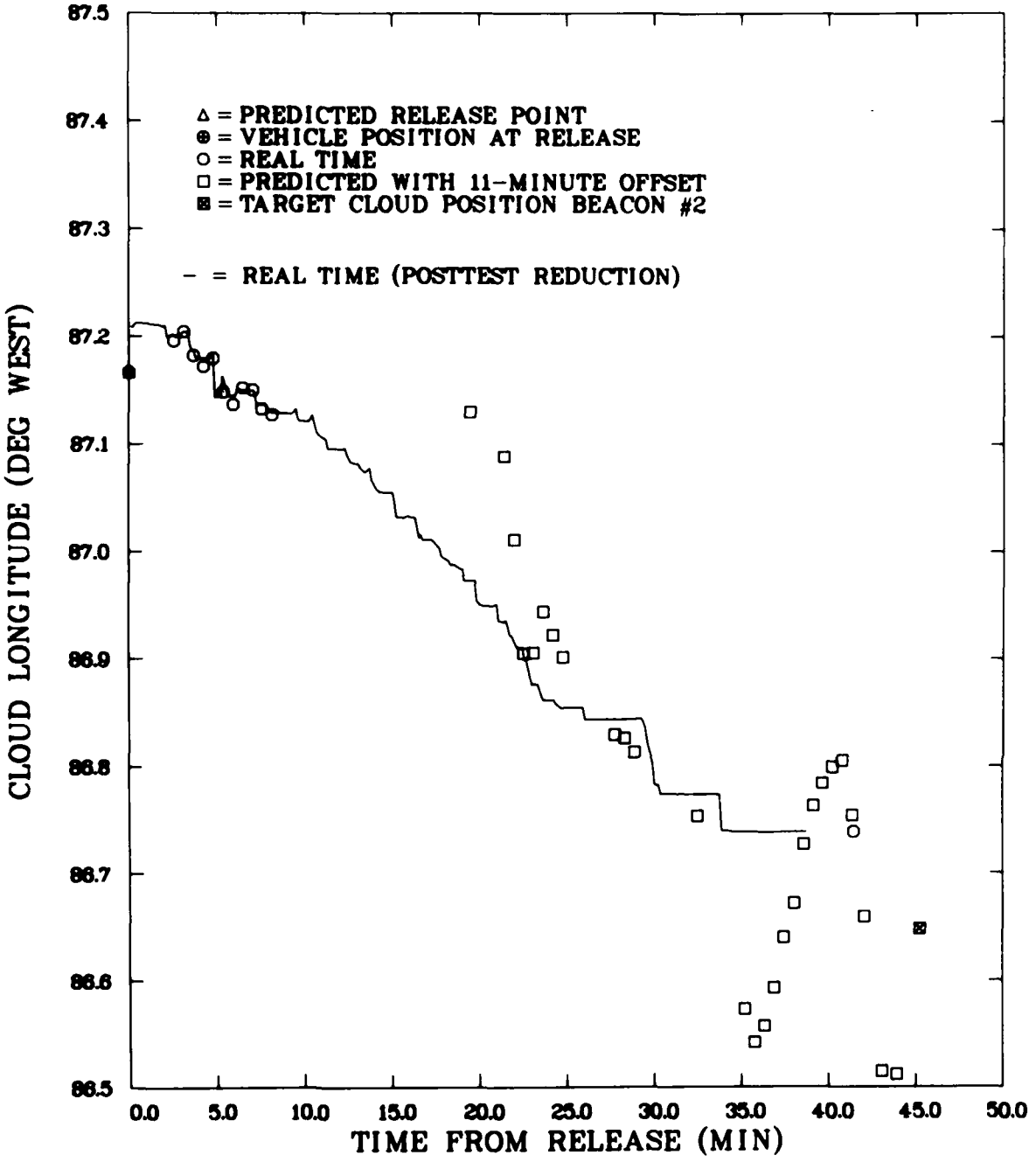

FIGURE 16 TV TRACK SOLUTION OF IRIS RELEASE, 8 DECEMBER 1980, PROBE AXIS-EMPIRICAL HEIGHT, CLOUD LONGITUDE vs TIME FROM RELEASE

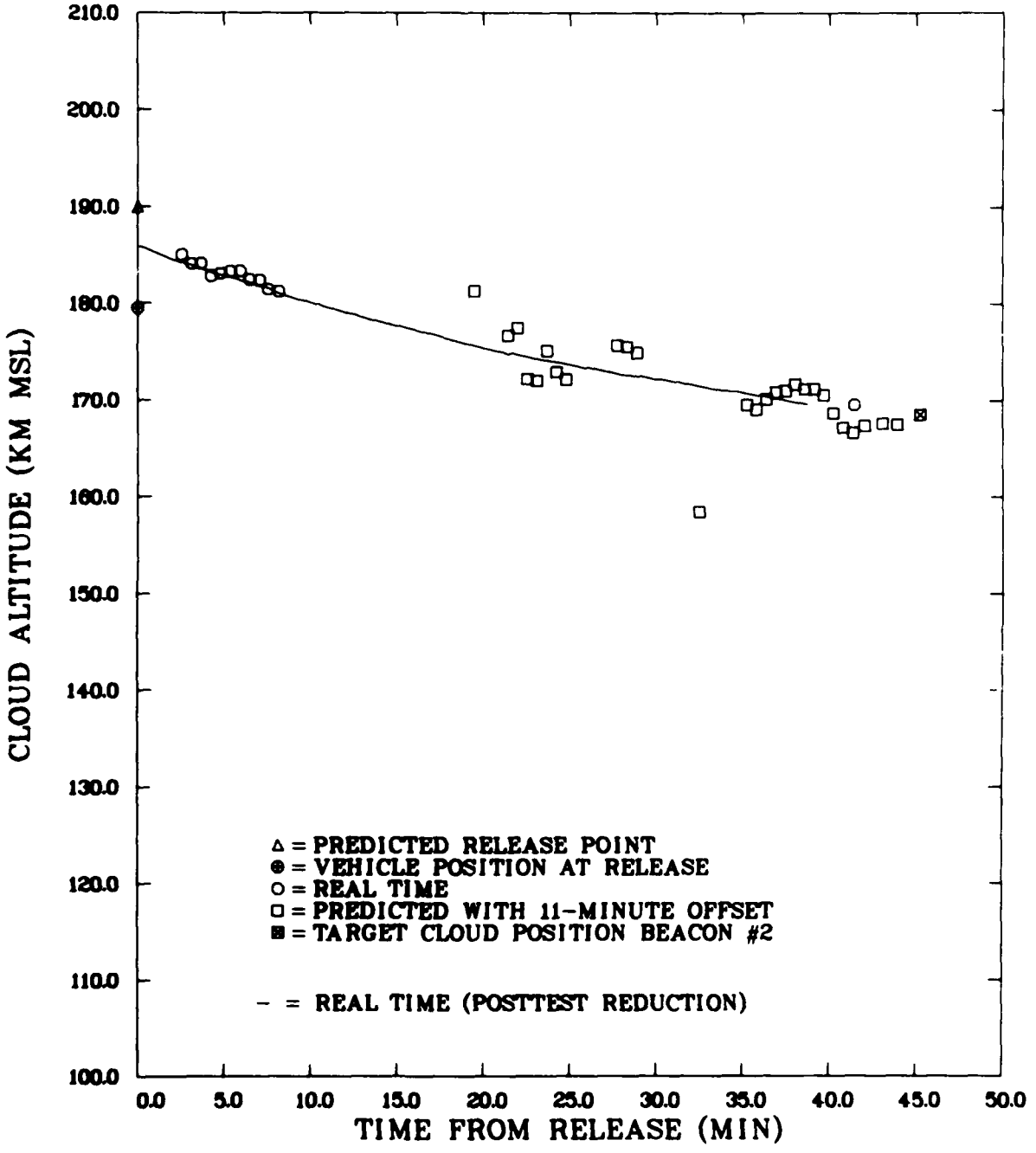

FIGURE 17 TV TRACK SOLUTION OF IRIS RELEASE, 8 DECEMBER 1980, PROBE AXIS-EMPIRICAL HEIGHT, CLOUD ALTITUDE vs TIME FROM RELEASE

TV tracker solution was used to target the second beacon vehicle (targeted for the predicted position of the striated ion cloud at R + 45-1/4 min). The particular solution selection for each vehicle was based on the predicted cloud position, which gave a better extrapolation of the real-time track than that of the other solution.

Both beacon vehicles were occulted by the striated ion cloud as viewed by both receiver sites (Cape San Blas and St. George Island) according to the received data.

D. Event JAN

A beacon and a probe vehicle were planned for launch with the developed JAN ion cloud. The nominal Event JAN release point was near that of Event HOPE (south by 0.08° latitude and east by 0.08° longitude). This release point was selected to allow either a northerly cloud track (limited by beacon vehicle range safety limits--alleviated to an extent by the 40-km cloud-to-vehicle distance option), or a southerly cloud track (limited by probe vehicle elevation launch angle less than 60°). Nominal release height and SDA were to be the same as that for Event IRIS. Companion vehicle targeting was to be based on either of the two solutions described in the case of Event IRIS for the beacon vehicle and based on the probe-axis and empirical height solution for the probe vehicle.

The barium for Event JAN was released on 12 December 1980 at an altitude of 182.5 km. The time of release was 2313:41.6Z. The JAN ion cloud was tracked with the TV trackers from approximately R + 8 min. The track was in the NNE direction (azimuth of 18°T), which caused the primary concern to be for the beacon vehicle and the range safety aspects of the payload impact (see Figures 18 and 19). The beacon vehicle was first targeted at R + 12-1/2 min (see Figures 20 through 25), with the occultation vehicle-to-cloud distance set at 100 km because this distance had been the original requirement and was still desired by the experimenters. Also, a relaxation of the range safety hazard limit line (by 1 to 1-1/2 σ) had been negotiated because of the near nominal impacts (approximately 1σ average) of the previous PLACES vehicles launched. The predicted beacon payload impact was at approximately 1/2 of the payload 3σ

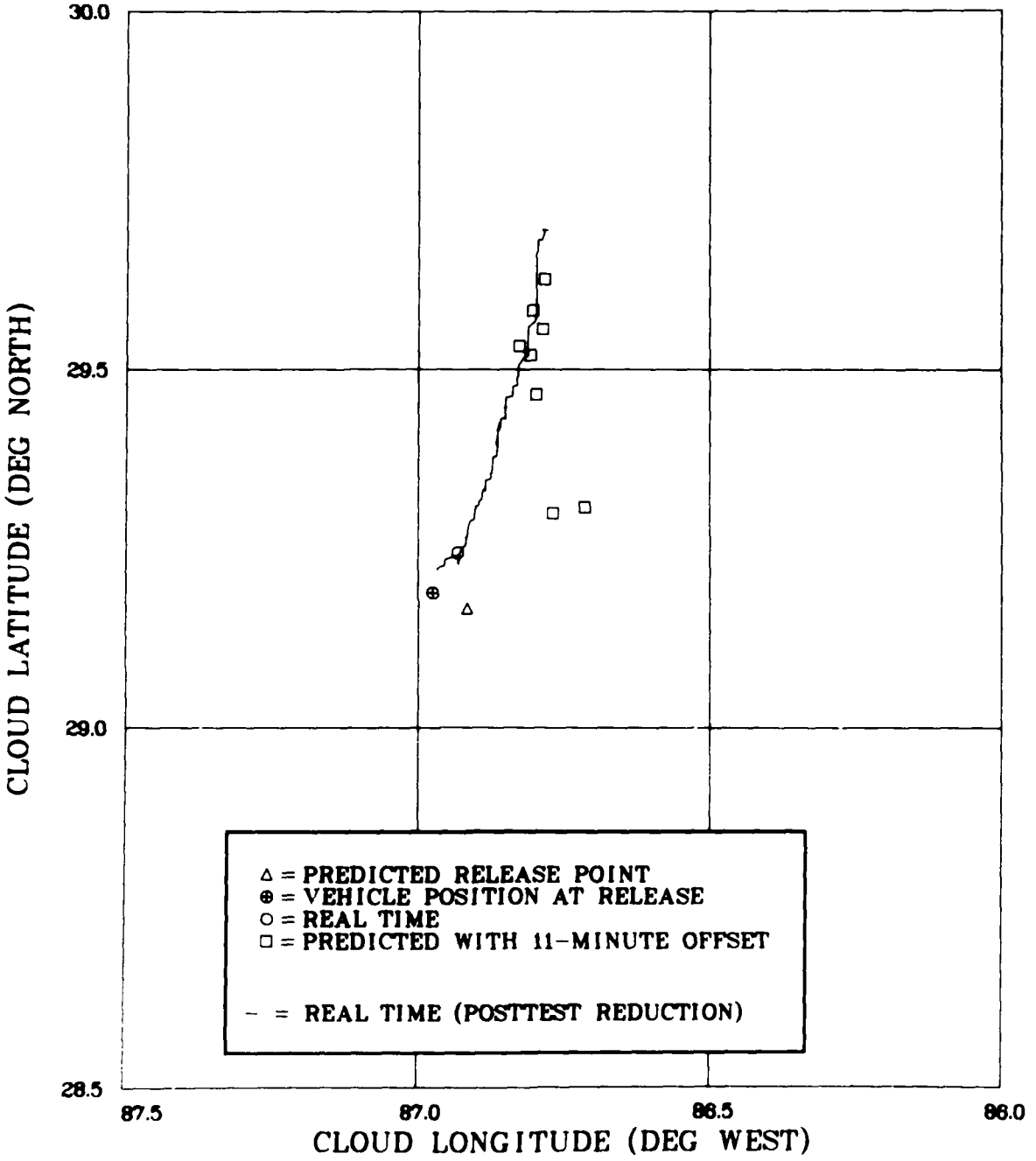

FIGURE 18 TV TRACK SOLUTION OF JAN RELEASE, 12 DECEMBER 1980, BEACON AXIS-PROBE PLANE, CLOUD LATITUDE vs CLOUD LONGITUDE

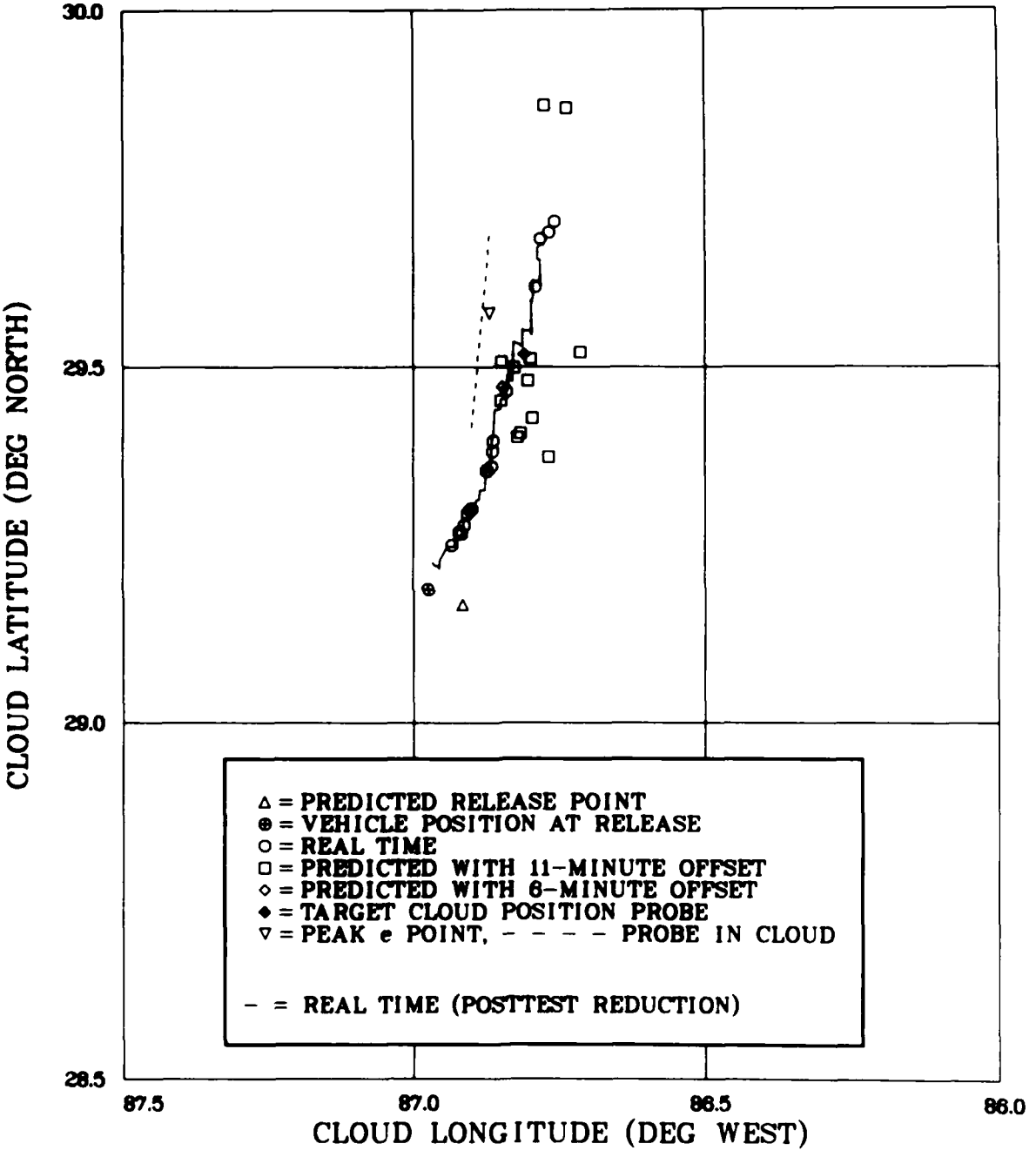

FIGURE 19 TV TRACK SOLUTION OF JAN RELEASE, 12 DECEMBER 1980, PROBE AXIS-EMPIRICAL HEIGHT, CLOUD LATITUDE vs CLOUD LONGITUDE

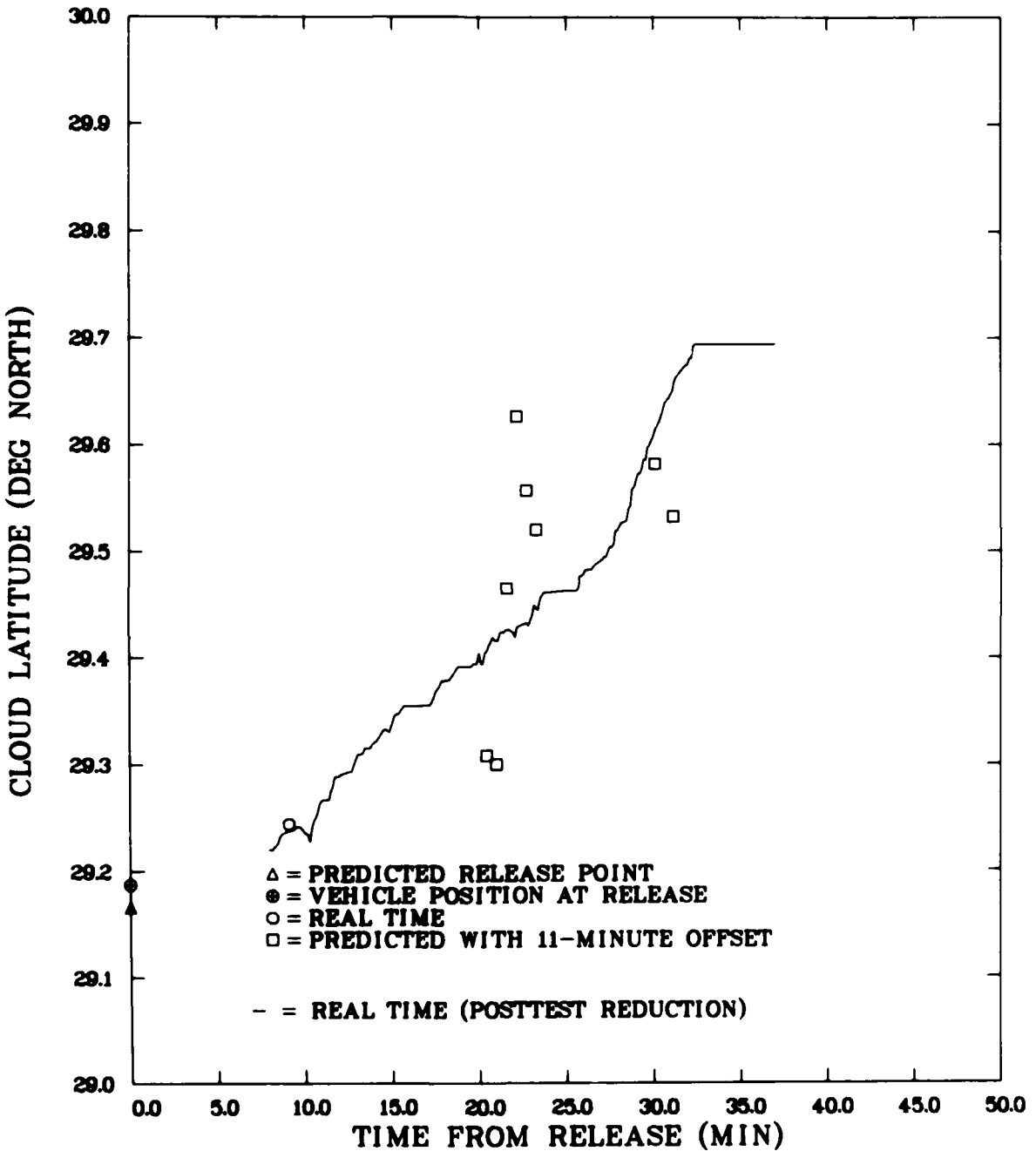

FIGURE 20 TV TRACK SOLUTION OF JAN RELEASE, 12 DECEMBER 1980, BEACON AXIS-PROBE PLANE, CLOUD LATITUDE vs TIME FROM RELEASE

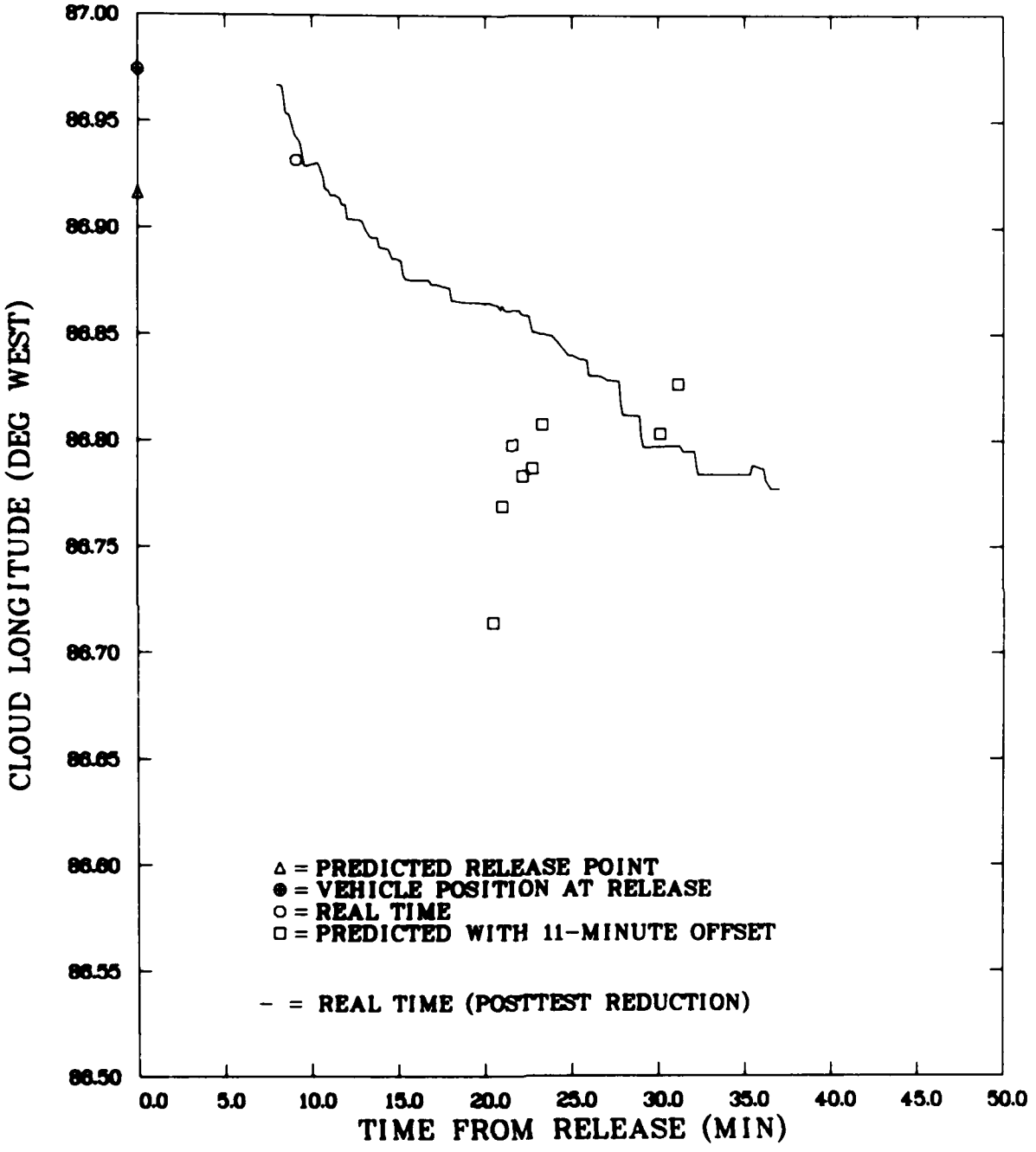

FIGURE 21 TV TRACK SOLUTION OF JAN RELEASE, 12 DECEMBER 1980, BEACON AXIS-PROBE PLANE, CLOUD LONGITUDE vs TIME FROM RELEASE

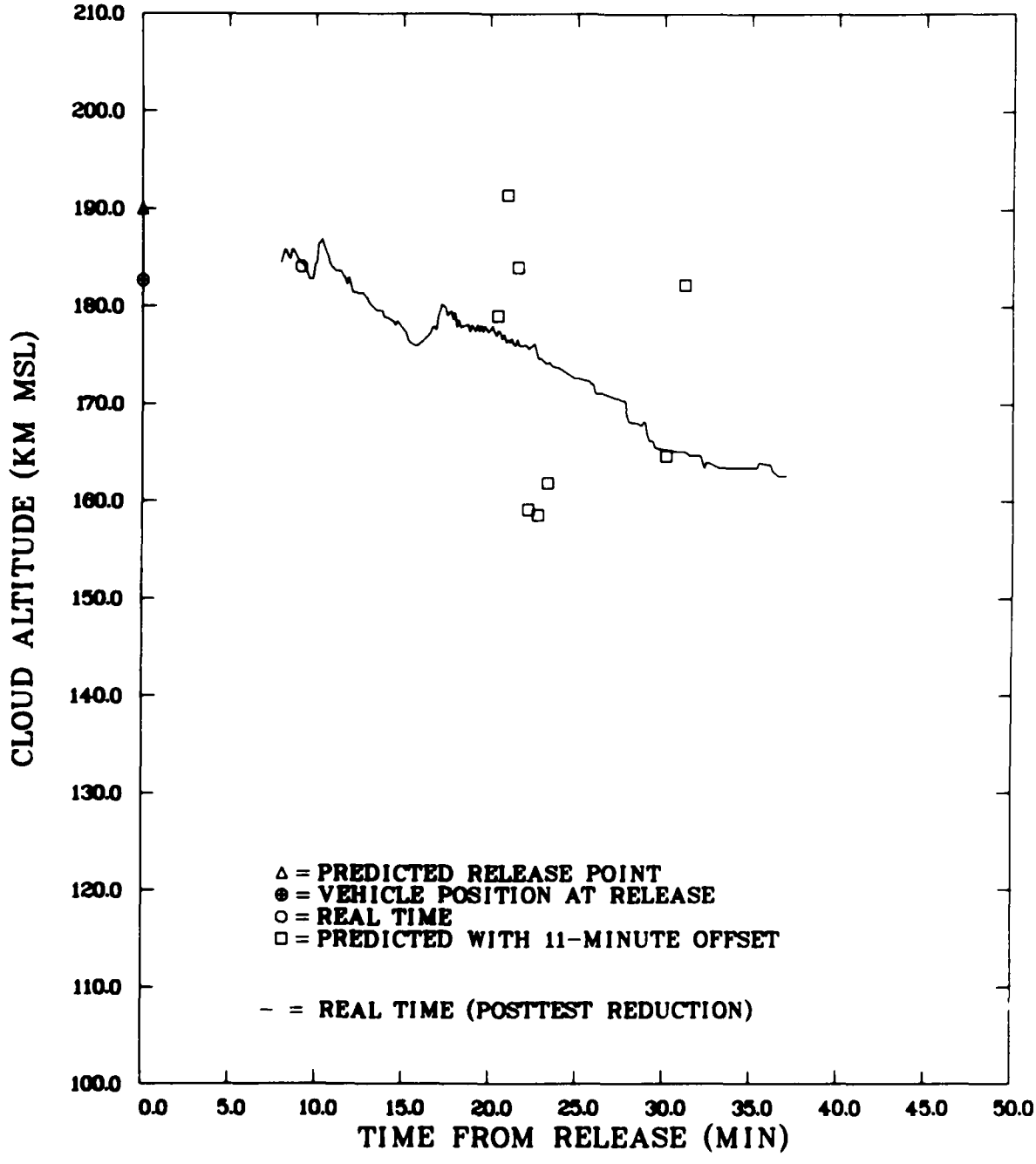

FIGURE 22 TV TRACK SOLUTION OF JAN RELEASE, 12 DECEMBER 1980, BEACON AXIS-PROBE PLANE, CLOUD ALTITUDE vs TIME FROM RELEASE

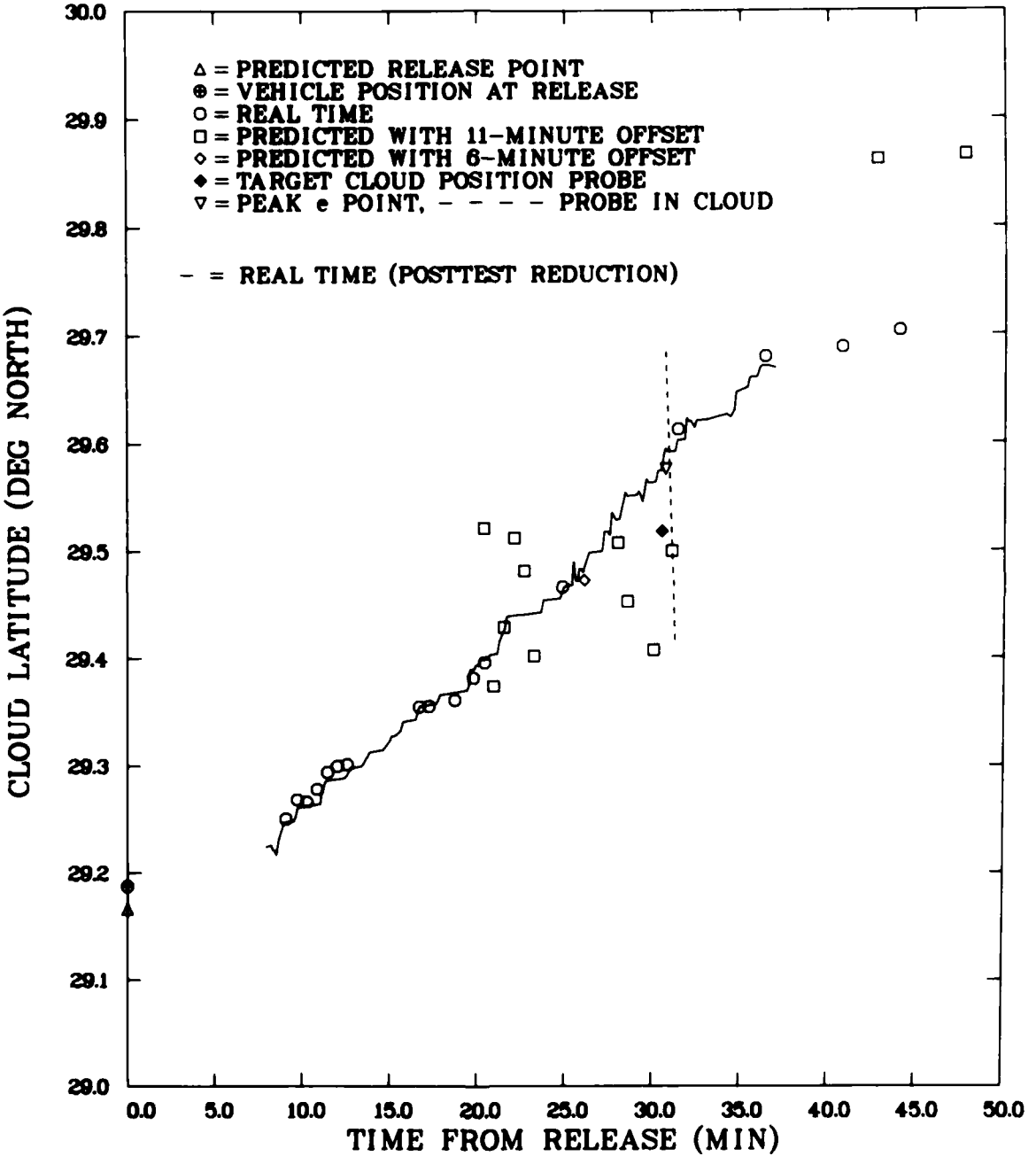

FIGURE 23 TV TRACK SOLUTION OF JAN RELEASE, 12 DECEMBER 1980, PROBE AXIS-EMPIRICAL HEIGHT, CLOUD LATITUDE vs TIME FROM RELEASE

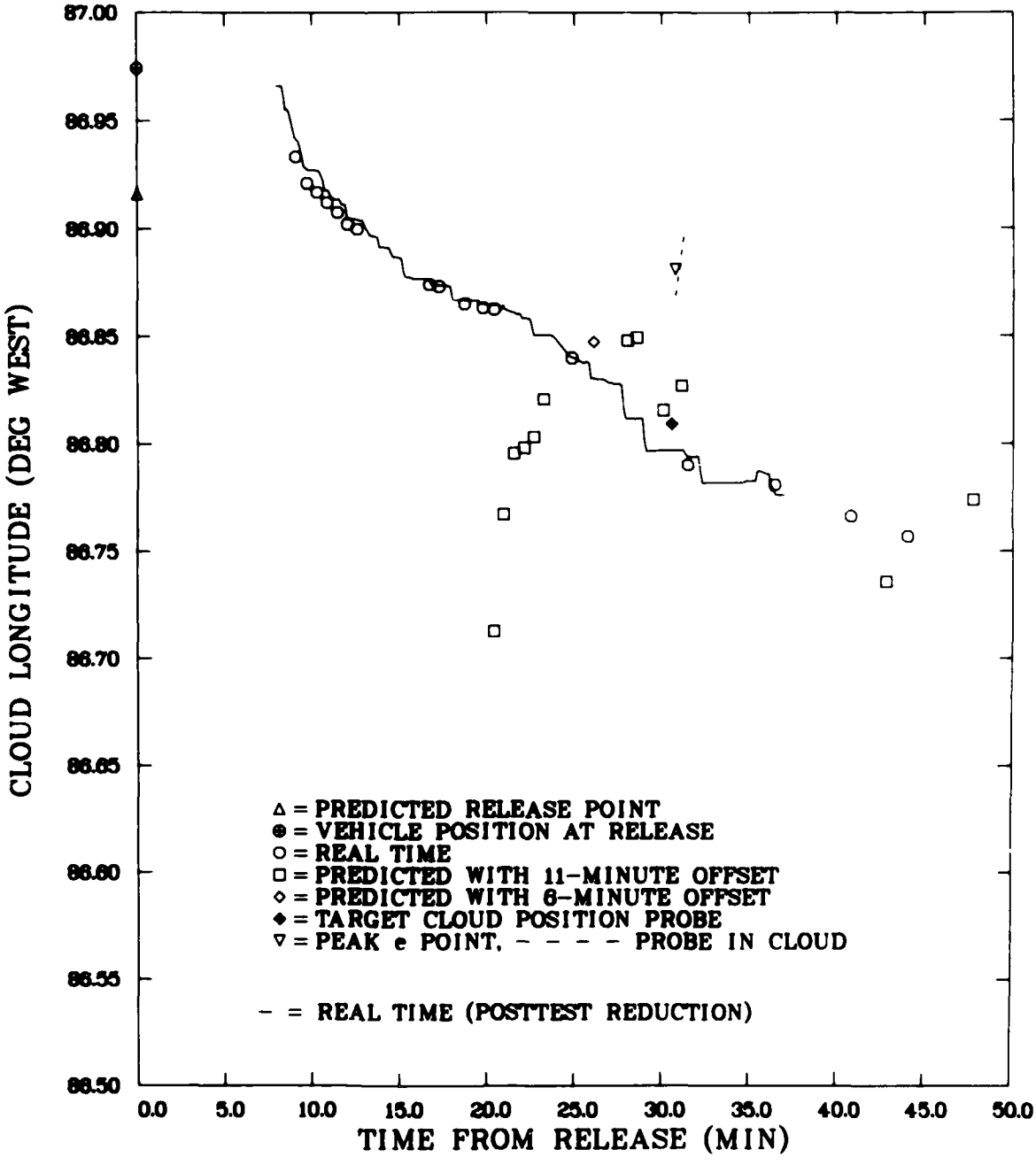

FIGURE 24 TV TRACK SOLUTION OF JAN RELEASE, 12 DECEMBER 1980, PROBE AXIS-EMPIRICAL HEIGHT, CLOUD LONGITUDE vs TIME FROM RELEASE

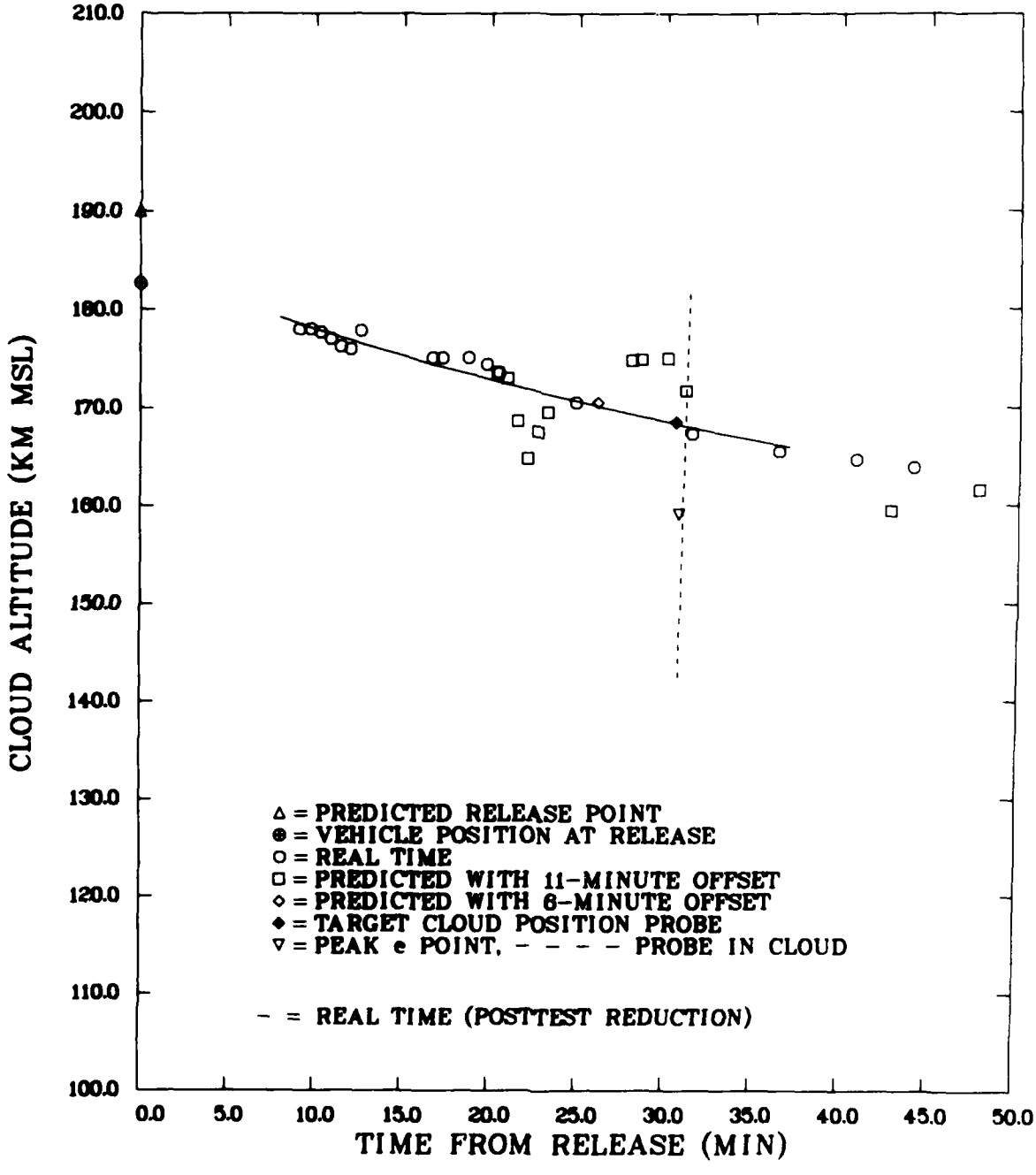

FIGURE 25 TV TRACK SOLUTION OF JAN RELEASE, 12 DECEMBER 1980, PROBE AXIS-EMPIRICAL HEIGHT, CLOUD ALTITUDE vs TIME FROM RELEASE

dispersion distance, which might have been approved. However, heavy shipping traffic in the area of this predicted impact precluded any decision based on the modified range safety criteria.

An immediate targeting computation was then started with the 40-km distance option exercised. However, difficulty with the field computer, which determined the vehicle nominal launch angles for a given target and the corrections required because of the atmosphere winds, precluded any additional vehicle targeting computations until R + 48 min. The cloud was then too far north to be targeted for the beacon at either 40 km or 100 km.

The predicted cloud positions for beacon vehicle targeting (an 11-min offset time was used) and for probe vehicle targeting (a 6-min time offset was used) and the real-time cloud track (based on the probe axis and empirical height solution) continued to be available. The probe vehicle was targeted from a set of parametric, targeting hand plots, which had been prepared prior to the test series, using the predicted cloud position for R + 30-1/2 min and launch angle corrections similar to those applied for the JAN barium vehicle. The launch time was requested to be as soon as range safety was cleared and a terminal countdown could be made. The real time was approximately R + 26 min. Because of a short range safety hold, the launch did not occur until approximately R + 29 min.

The probe vehicle penetrated the cloud (see Figures 23, 24, and 25) and the peak electron density occurred at R + 31 min.

A PLACES ion cloud track summary plot is presented in Figure 26. The expected or "allowed" cloud track dispersion area is also outlined in this figure. The plot illustrates the difficulties encountered in targeting the beacon vehicles with the GAIL, HOPE, and JAN events. The difficulties arose because predicted beacon payload impacts are within range safety hazard areas for predicted ion cloud positions near a 70°T azimuth direction, or less than 40 km drift distance from the nominal Event GAIL release point (apex of the dispersion area quadrant).

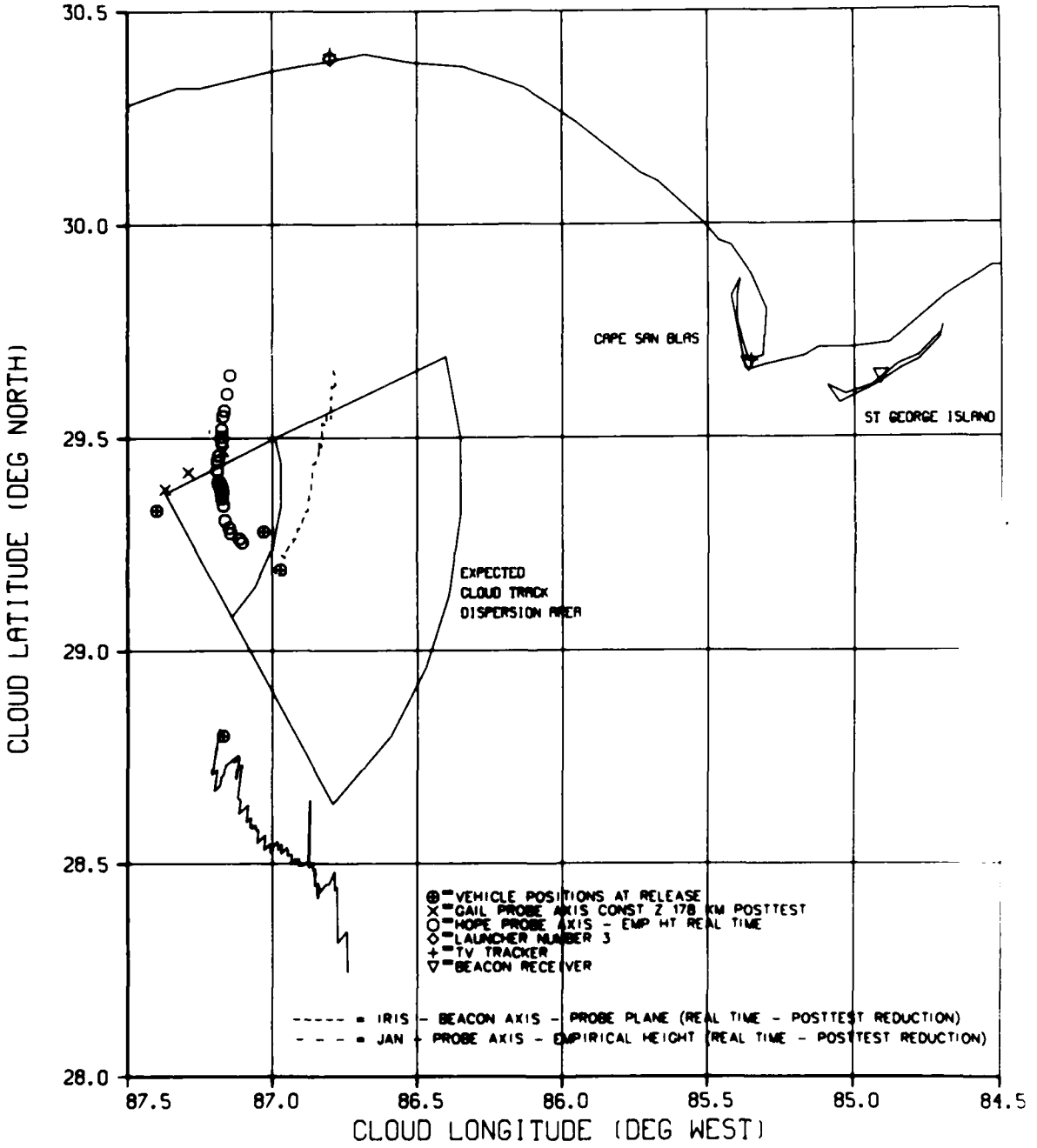

FIGURE 26 PLACES CLOUD TRACK SUMMARY

IV ROCKET SYSTEM BALLISTIC PERFORMANCE

A summary of the ballistic accuracy of the PLACES rocket systems is presented in Table 5. The nominal and actual target coordinates are presented for comparison. The nominal positions for the barium carrier vehicles are the respective nominal release points, which were different for each release. The nominal positions for the beacon vehicles and the probe vehicle are the occultation points and the penetration point, respectively, which correspond to the predicted ion cloud positions. The actual positions were determined from the vehicle C-band radar tracking data. The actual positions for the barium vehicles correspond to the vehicle radar track at the times that the barium releases were initiated. The actual position for a beacon vehicle corresponds to the vehicle radar track at the average of the midpoints of the two time intervals of occultation at the receiver sites. The actual position for the probe vehicle corresponds to the vehicle radar track at the point of peak electron density measured during ion cloud penetration.

The coordinate system applied for this ballistic accuracy assessment is an orthogonal, tangent plane system with the origin at the rocket launcher with x south, y east, and z up.

Small dispersion in x and y was realized on all flight tests. A 5-to-6-km low bias in z is apparent at the barium release points (an additional error occurred for the IRIS release because of an abnormal second-stage ignition time delay). This altitude was primarily caused by first-stage motor burn times that averaged 25% longer than expected, and actual second-stage vehicle inert weights that averaged 10 lb heavier than expected.

The ballistic error for the beacon vehicles was produced by both the vehicle dispersion and variation from the predicted ion cloud position at the nominal occultation time by the actual ion cloud track. Both beacon vehicles appeared to be slightly short (2 to 3% of range) and low at occultation. This performance degradation probably relates to that mentioned

Table 5

BALLISTIC ACCURACY SUMMARY OF PLACES ROCKET SYSTEMS

Launch Time (Z)	Time of Flight (s) Launch to Event	Release/ Vehicle	Time of Event (Z)	Target Points/Tangent Plane Coordinates								
				Actual Position (km)			Nominal Position (km)			Error (km)		
				x	y	z	x	y	z	Δx	Δy	Δz
2304:59.87	155.94	GAIL/Ba	2307:35.8	119.92	-59.65	177.39	115.93	-56.61	183.73	3.99	-3.04	-6.34
2305:00.25	157.60	HOPE/Ba	2307:37.9	126.45	-22.80	179.62	129.74	-19.67	183.68	-3.29	-3.13	-4.06
2309:59.91	187.40	IRIS/Ba	2313:07.3	181.65	-36.55	177.01	177.35	-36.51	187.49	4.30	-0.04	-10.48
2311:00.03	161.57	JAN/Ba	2313:41.6	136.41	-17.01	181.01	139.36	-11.35	188.50	-2.95	-5.66	-7.49
2338:36.9	402.40	IRIS/Be No. 1	2345:19.3	242.85	-23.03	174.64	249.11	-17.56	185.18	-6.26	-5.47	-10.54
2351:36.26	403.50	IRIS/Be No. 2	2358:19.8	279.31	-17.69	166.05	285.58	-4.78	186.59	-6.57	-12.91	-20.54
≈2342:50	110.0	JAN/Pr	2344:40	91.29	-7.61	157.27	98.95	-0.58	167.73	-7.66	-7.03	-10.46

for the barium carriers above. Also, the ion cloud track appeared to be dropping lower than the predicted positions for beacon vehicle targeting. This was especially true for the second beacon, which was targeted using the empirical height variation.

The track of the probe vehicle during its transit of the ion cloud is shown in Figures 23, 24, and 25. The ballistic accuracy of the probe vehicle does not carry the same meaning as that for the other vehicles, because the nominal launcher setting was obtained using a hand plot and the launch angle corrections due to atmospheric winds were only estimated. The short ground range to the ion cloud (approximately 100 km) helped make the probe penetration possible.

BLANK PAGE

DNA/PLACES BARIUM EVENT JAN

E. P. Szuszczewicz, J. C. Holmes, C. S. Lin,
and M. Swinney

I INTRODUCTION

At 2311:00 (GMT) on 12 December 1980, a 48-kg barium payload was launched from the A-15 Site of Eglin/Santa Rosa Island Test Range. The barium was released in the F_1-region of the ionosphere at 2313:42.1 and at an altitude of 182.7 km.

At 2342:50.8 a second rocket was launched, carrying a plasma diagnostic complement that included a pair of pulsed-plasma probes and an ion mass spectrometer for direct measurements of electron density, N_e, temperature, T_e, density fluctuation, δN_e, associated density fluctuation power spectra, $P_n(k)$, and ion composition, M_i. The probe payload penetrated the highest density region (i.e., the highest density observed along the payload's trajectory) of the barium ion cloud at 2344:40.8, a time defined as R + 31 min. The barium release and all associated measurements have been designated by code name Event JAN.

This report presents quick-look field analyses of the pulsed-plasma-probe data. A brief description will be given on the probe instrumentation, vehicle/payload performance, and "in situ" observations of plasma densities and structure in the ambient ionosphere and throughout the intense barium ion cloud structure.

II PROBE INSTRUMENTATION, PAYLOAD CONFIGURATION, AND OVERALL SYSTEM PERFORMANCE

A pair of pulsed-plasma probes were diametrically deployed from the forward-most lateral surface of the payload. The payload's attitude

control system (ACS) was designed to maintain the vehicle axis parallel to the geomagnetic field throughout flight--a condition that optimized data integrity from points of view focused on magnetic-field and vehicle aspect perturbations. Initial results indicate that the ACS functioned according to design. Table 1 lists timer functions and altitudes related to the plasma instrumentation on the probe payload, while Figure 1 presents the payload trajectory (altitude versus time), as determined by a single-station radar solution. The figure was constructed from the trajectory data listed in Table 2.

The pulsed-plasma probe[1-4]* is a specially designed Langmuir technique that eliminates distortions of the measurement procedure known to degrade the conventional approach to Langmuir probe measurements. In addition, the pulsed-probe technique makes possible the determination of absolute electron density under fluctuating plasma conditions, and simultaneously determines the electron density, N_e, temperature, T_e, density fluctuations, δN_e, associated power spectra, $P_n(k)$, and mean ion mass $\langle M_i \rangle$. The probe's highest resolution capability in Event JAN involved δN_e, with resolution down to scale sizes equal to 0.5 m at a 1-km/s payload velocity.

III ELECTRON DENSITY PROFILES

The relative electron density profile observed "in situ" by the pulsed probe measurement of baseline electron current, I_B^e (see, e.g., Ref. 1 or 2) is presented in Figure 2. The abscissa is expressed as seconds-after-launch, extending over the domain $t_o + 75 \leq [s] \leq t_o + 373$; while the ordinate is log (I_B^e). The barium ion cloud was encountered on the upleg portion of the trajectory at $t \approx 99.5$ s (altitude $\approx$ 145 km). Peak densities within the cloud were observed at $t \approx 110$ s (altitude $\approx$ 155 km). For $t > 135$ s the probe continued relative density measurements within the undisturbed background ionosphere to an apogee of 241 km (t =

*References are listed at the end of this paper.

Table 1

TIMER EVENTS RELATED TO THE PLASMA INSTRUMENTATION ON THE PROBE PAYLOAD

Time	Event	Altitude, Nominal (km)
t_o = 2342:50.8	Launch	0
t_o + 66	Nose cone separation Probe door deploy	90
t_o + 76	Payload separation ACS on Mass spec RF on	105
t_o + 78	Yo-Yo despin	110
t_o + 80	Probe deploy	112
t_o + 93	Mass spec HV on	120
t_o + 108	ACS deactivate	152
t_o + 166	ACS reactivate	213

245 s). (That I_B^e is a reasonable representation of relative electron density without major distortions from aspect sensitivities and/or vehicle potential effects has been verified by a simultaneous measurement of baseline ion saturation currents, I_B^i, shown in Figure 3. For discussions relative to this point, see References 4 and 5.)

To establish initial estimates of absolute electron densities, I-V characteristics generated by the pulsed sweep currents (see, e.g., Ref. 3) were hand analyzed at three positions within the cloud. The results indicated a simple I_B^e to N_e conversion according to

$$N_e(cm^{-3}) = 5.62\ (10^{10})\ I_B^e\ (amps) \quad ,$$

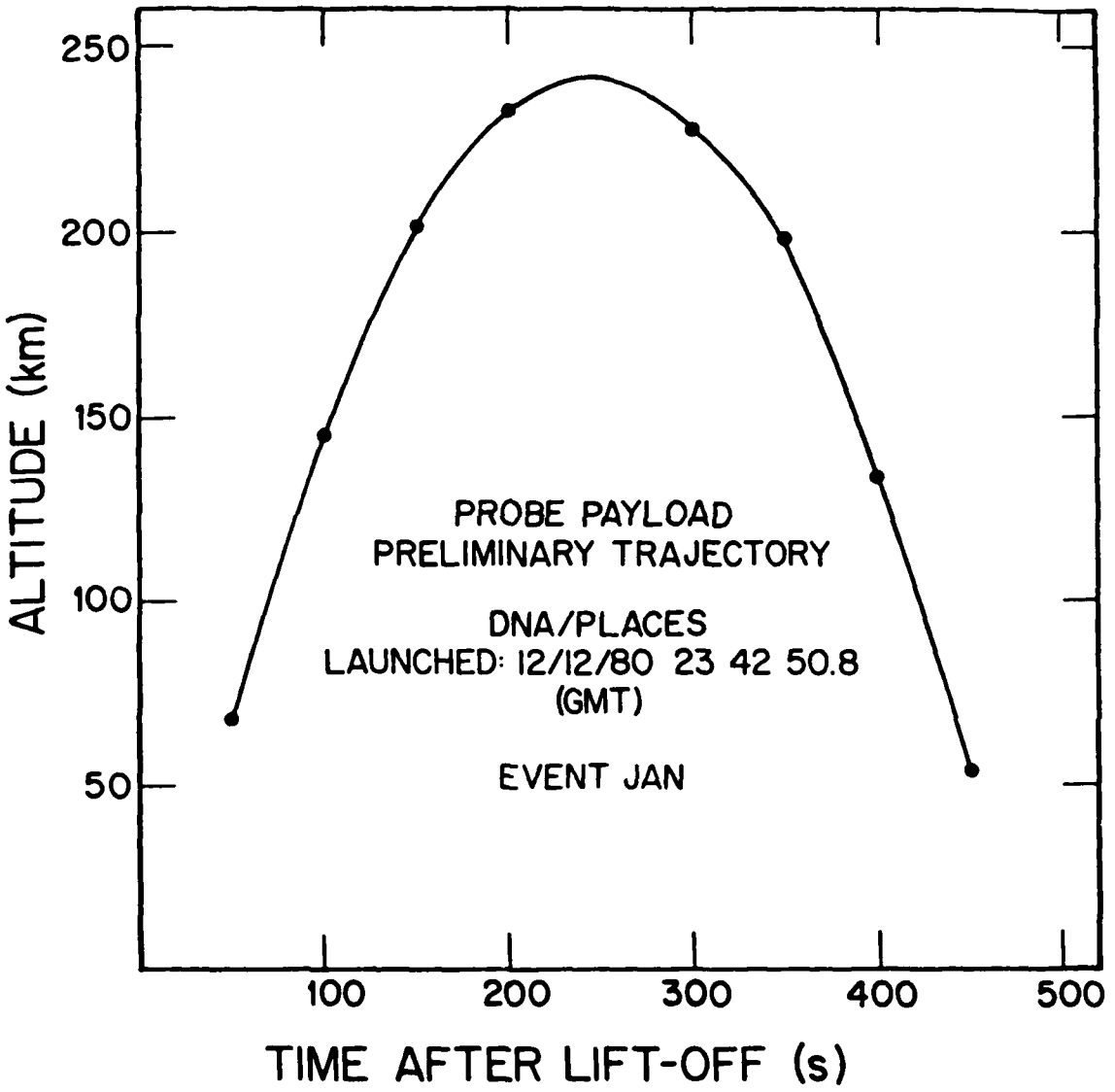

FIGURE 1 PROBE PAYLOAD TRAJECTORY FROM SINGLE RADAR STATION SOLUTION (SEE TABLE 2)

Table 2

EVENT JAN PROBE PAYLOAD TRAJECTORY INFORMATION EXCERPTED
FROM A SINGLE-STATION RADAR SOLUTION PRIOR TO SMOOTHING

Time After Lift-Off (s)	Time (GMT)	Altitude		Range		Latitude	Longitude	Velocity	
		ft	km	ft	km			ft/s	km/s
50	2343:40.8	225,862	68.83	251,479	76.64	30.0855	86.8274	6721	2.05
100	2344:30.8	479,240	146.05	549,004	167.31	29.6615	86.8717	5401	1.65
150	2345:20.8	658,330	200.63	783,270	238.71	29.2428	86.9211	4245	1.29
200	2346:10.8	761,631	232.11	956,354	291.46	28.8321	86.9735	3407	1.04
245.3	2346:56.1	791,530	241.22	1,067,348	325.28	28.464	87.0227	3100	0.94
250	2347:0.8	791,208	241.13	1,076,545	328.09	28.4265	87.0277	3100	0.94
300	2347:50.8	747,856	227.91	1,115,627	352.19	28.0193	87.0830	3452	1.05
350	2348:40.8	650,406	198.22	1,209,267	368.53	27.6732	87.3808		
400	2349:30.8	437,197	133.24	1,260,127	384.03	27.1886	87.1935	5505	1.68
448	2350:18.7	178,136	54.29	1,336,673	407.36	26.7800	87.2469	7577	2.31

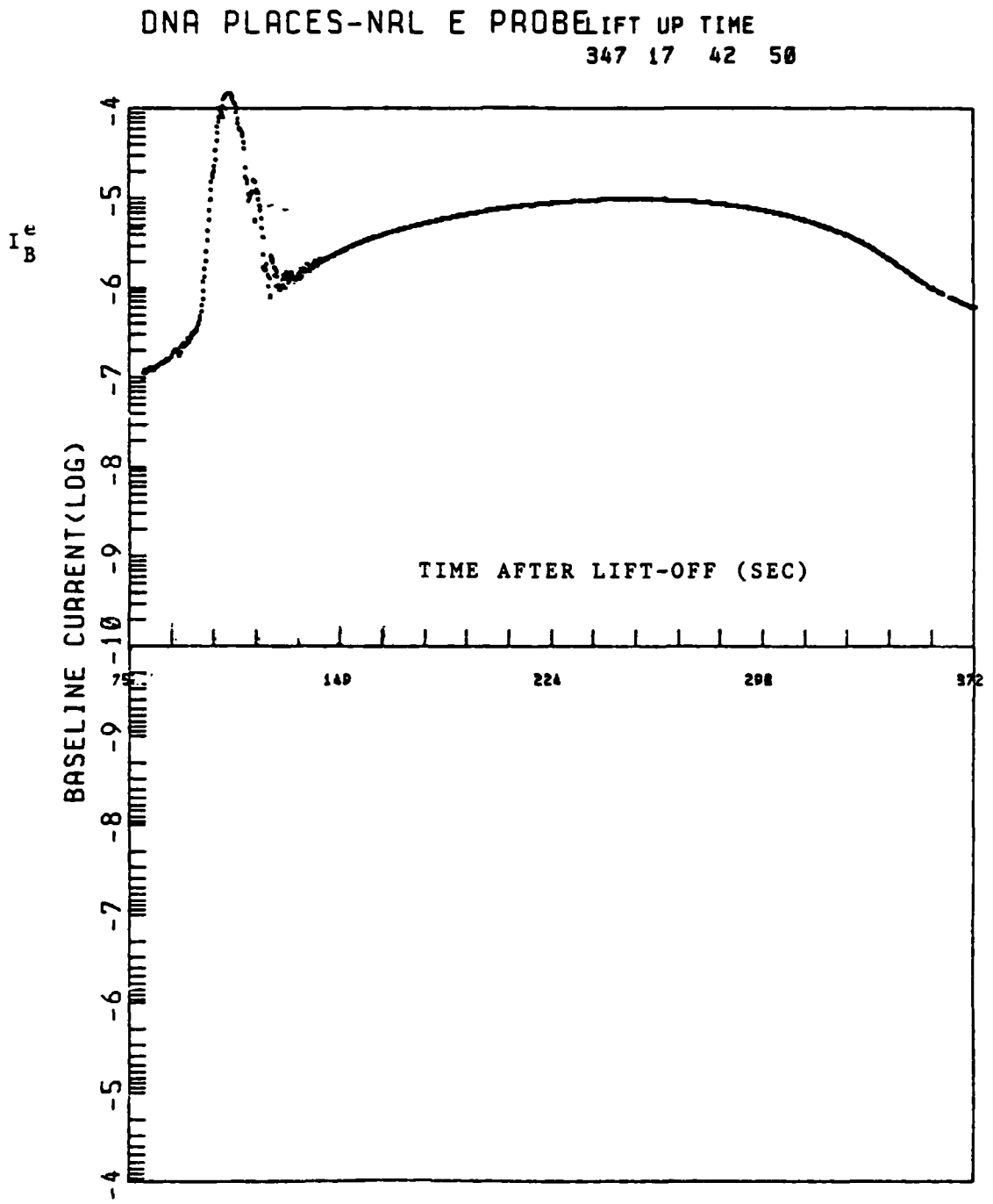

FIGURE 2 RELATIVE ELECTRON DENSITY PROFILE AS MEASURED BY BASELINE ELECTRON CURRENT I_B^e AS A FUNCTION OF SECONDS AFTER LAUNCH. Absolute electron densities can be estimated from the conversion N_e [cm^{-3}] = 5.62 (10^{10}) I_B^e[amps]. See text for statement of accuracy.

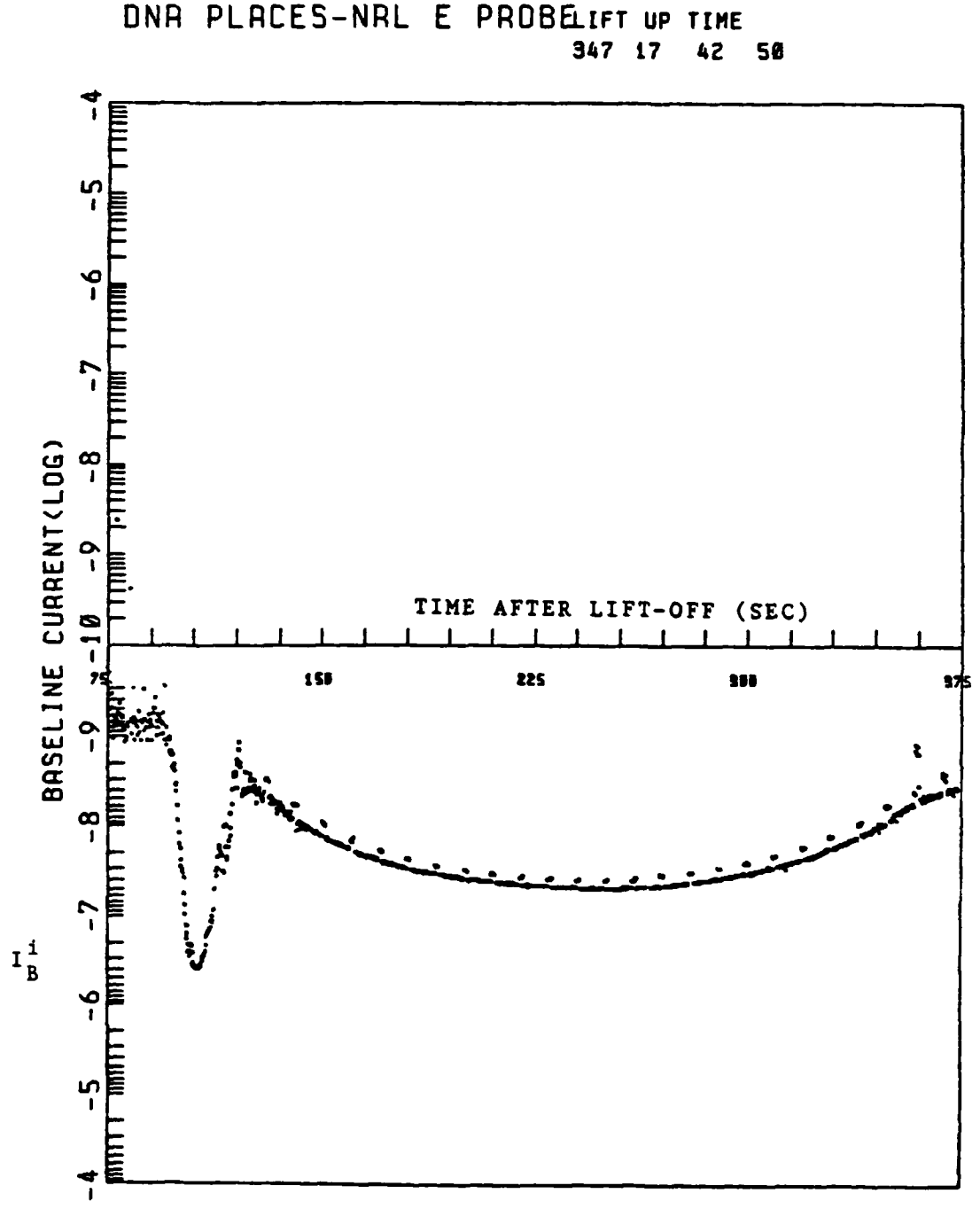

FIGURE 3 RELATIVE ELECTRON DENSITY PROFILE AS MEASURED BY BASELINE ION CURRENT I_B^i AS A FUNCTION OF SECONDS AFTER LAUNCH. Note that ion current increases downward. Agreement between Figures 2 and 3 establishes credibility in the I_B^e measurements as a reasonable representation of relative density. (See text.)

with an estimated accuracy of ± 32%. More exact analyses will result in absolute density determinations with a better than 10% accuracy. This conversion has been applied to Figure 2, resulting in initial estimates of peak barium ion densities ($t \approx 110$ s, altitude = 155 km) of $7.3(10^6)$ cm^{-3}. This value represents an enhancement of 300 over ambient ionospheric conditions at that altitude. An expanded view of the ion cloud domain [$95 < t$ (s) ≤ 135] is shown in Figure 4, while Table 3 lists densities, altitudes, and coordinates of specific observations relevant to a first-order view of the ion cloud and the background ionosphere.

REFERENCES

1. Holmes, J. C., and E. P. Szuszczewicz, "A Versatile Plasma Probe," Rev. Sci. Instr., 46, 592 (1975).

2. Szuszczewicz, E. P., and J. C. Holmes, "Surface Contamination of Active Electrodes in Plasmas: Distortion of Conventional Langmuir Probes," J. Appl. Phys., 46, 5134 (1975).

3. Szuszczewicz, E. P., and J. C. Holmes, "Observations of Electron Temperature Gradients in Mid-Latitude E_s Layers," J. Geophys. Res., 82, 5073 (1977).

4. Szuszczewicz, E. P., R. T. Tsunoda, R. Narcisi, and J. C. Holmes, "Coincident Radar and Rocket Observations of Equatorial Spread-F," Geo. Res. Lett., 7 (1980).

5. Szuszczewicz, E. P., and P. Z. Takacs, "Magnetosheat Effects on Cylindrical Langmuir Probes," Phys. Fluids, 22, 2424 (1979).

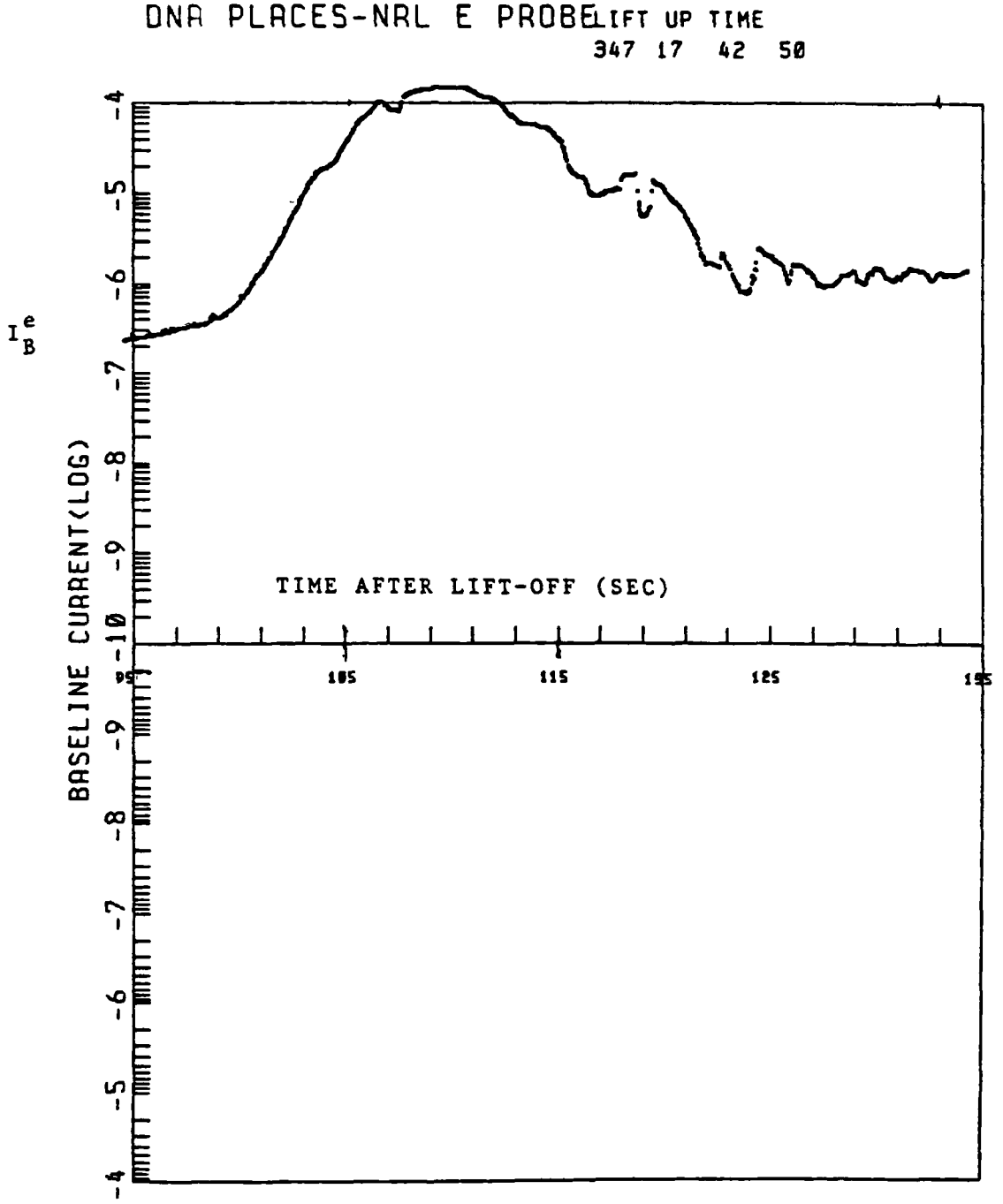

FIGURE 4 **AN EXPANDED VIEW OF THE BARIUM ION CLOUD DENSITY PROFILE AS MEASURED BY BASELINE ELECTRON CURRENTS. Absolute electron densities can be estimated within an accuracy of ± 32% (detailed analyses will yield ± 10% or better) by the conversion N_e [cm^{-3}] = 5.62 (10^{10}) I_B^e [amps].**

Table 3

SUMMARY OF RELEVANT PLASMA DENSITIES AND COORDINATES

Point of Interest	Sec After Launch	Electron Density		Altitude (km)	Latitude	Longitude
		Ionosphere	Barium			
Cloud Entry	99.5	$1.7(10^4)$	at 10^3	145	29.67°	86.87°
Cloud Peak	110	$2.4(10^4)$	$7.3(10^6)$	155	29.58°	86.88°
Cloud Exit	135	$5.6(10^4)$	at 10^2	185	29.41°	86.9°
Apogee	245	$5.6(10^5)$	0	241	28.468	87.022

DISTRIBUTION LIST

DEPARTMENT OF DEFENSE

Assistant Secretary of Defense
Comm, Cmd, Cont & Intell
ATTN: Dir of Intelligence Sys, J. Babcock

Command & Control Technical Center
ATTN: C-650, G. Jones
ATTN: C-312, R. Mason
3 cy ATTN: C-650, W. Heidig

Defense Communications Agency
ATTN: Code 480
ATTN: Code 205
ATTN: Code 101B
ATTN: Code 480, F. Dieter

Defense Communications Engineer Center
ATTN: Code R410, N. Jones
ATTN: Code R123

Defense Intelligence Agency
ATTN: Dir
ATTN: DB-4C, E. O'Farrell
ATTN: DB, A. Wise
ATTN: DT-1B
ATTN: DC-7B

Defense Nuclear Agency
ATTN: NAFD
ATTN: STNA
ATTN: RAEE
ATTN: NATD
3 cy ATTN: RAAE
4 cy ATTN: TITL

Defense Technical Information Center
12 cy ATTN: DD

Field Command
Defense Nuclear Agency
ATTN: FCP, J. T. McDaniel

Field Command
Defense Nuclear Agency
Livermore Branch
ATTN: FCPRL

Interservice Nuclear Weapons School
ATTN: TTV

Joint Strat Tgt Planning Staff
ATTN: JLA
ATTN: JLTW-2

National Security Agency
ATTN: W-32, O. Bartlett
ATTN: B-3, F. Leonard
ATTN: R-52, J. Skillman

Under Secretary of Defense for Rsch & Engrg
ATTN: Strategic & Space Sys (OS)

WWMCCS System Engineering Org
ATTN: J. Hoff

DEPARTMENT OF DEFENSE (Continued)

Joint Chiefs of Staff
ATTN: C3S
ATTN: C3S, Evaluation Office

DEPARTMENT OF THE ARMY

Assistant Chief of Staff for Automation & Comm
Department of the Army
ATTN: DAAC-ZT, P. Kenny

Atmospheric Sciences Laboratory
U.S. Army Electronics R&D Command
ATTN: DELAS-EO, F. Niles

BMD Advanced Technology Center
Department of the Army
ATTN: ATC-T, M. Capps
ATTN: ATC-O, W. Davies

BMD Systems Command
Department of the Army
2 cy ATTN: BMDSC-HW

Deputy Chief of Staff for Ops & Plans
Department of the Army
ATTN: DAMO-RQC

Harry Diamond Laboratories
Department of the Army
ATTN: DELHD-N-RB, R. Williams
ATTN: Chief, Div 20,000
ATTN: DELHD-I-TL, M. Weiner

U.S. Army Chemical School
ATTN: ATZN-CM-CS

U.S. Army Comm-Elec Engrg Instal Agency
ATTN: CCC-EMEO-PED, G. Lane
ATTN: CCC-CED-CCO, W. Neuendorf

U.S. Army Communications Command
ATTN: CC-OPS-W
ATTN: CC-OPS-WR, H. Wilson

U.S. Army Communications R&D Command
ATTN: DRDCO-COM-RY, W. Kesselman

U.S. Army Foreign Science & Tech Ctr
ATTN: DRXST-SD

U.S. Army Materiel Dev & Readiness Cmd
ATTN: DRCLDC, J. Bender

U.S. Army Missile Intelligence Agency
ATTN: YSE, J. Gamble

U.S. Army Nuclear & Chemical Agency
ATTN: Library

U.S. Army Satellite Comm Agency
ATTN: Document Control

DEPARTMENT OF THE ARMY (Continued)

U.S. Army TRADOC Sys Analysis Actvy
ATTN: ATAA-TDC
ATTN: ATAA-PL
ATTN: ATAA-TCC, F. Payan, Jr

DEPARTMENT OF THE NAVY

COMSPTEVFOR
Department of the Navy
ATTN: Code 605, R. Berg

Joint Cruise Missiles Project Ofc
Department of the Navy
ATTN: JCMG-707

Naval Air Development Center
ATTN: Code 6091, M. Setz

Naval Air Systems Command
ATTN: PMA 271

Naval Electronic Systems Command
ATTN: PME 106-4, S. Kearney
ATTN: PME 117-2013, G. Burnhart
ATTN: PME 117-211, B. Kruger
ATTN: Code 3101, T. Hughes
ATTN: PME 106-13, T. Griffin
ATTN: PME 117-20
ATTN: Code 501A

Naval Intelligence Support Ctr
ATTN: NISC-50

Naval Ocean Systems Center
ATTN: Code 532, R. Pappert
ATTN: Code 532, J. Bickel
ATTN: Code 5322, M. Paulson
3 cy ATTN: Code 5323, J. Ferguson

Naval Research Laboratory
ATTN: Code 7550, J. Davis
ATTN: Code 4187
ATTN: Code 7500, B. Wald
ATTN: Code 4700, T. Coffey
ATTN: Code 7950, J. Goodman
ATTN: Code 4780, S. Ossakow

Naval Space Surveillance System
ATTN: J. Burton

Naval Surface Weapons Center
ATTN: Code F31

Naval Telecommunications Command
ATTN: Code 341

Office of Naval Research
ATTN: Code 465
ATTN: Code 421
ATTN: Code 420

Office of the Chief of Naval Operations
ATTN: OP 65
ATTN: OP 941D
ATTN: OP 981N

DEPARTMENT OF THE NAVY (Continued)

Strategic Systems Project Office
Department of the Navy
ATTN: NSP-43
ATTN: NSP-2722, F. Wimberly
ATTN: NSP-2141

DEPARTMENT OF THE AIR FORCE

Aerospace Defense Command
Department of the Air Force
ATTN: DC, T. Long

Air Force Geophysics Laboratory
ATTN: OPR, H. Gardiner
ATTN: OPR-1
ATTN: LKB, K. Champion
ATTN: OPR, A. Stair
ATTN: S. Basu
ATTN: PHP
ATTN: PHI, J. Buchau
ATTN: R. Thompson

Air Force Weapons Laboratory
Air Force Systems Command
ATTN: SUL
ATTN: NTYC
ATTN: NTN

Air Force Wright Aeronautical Lab
ATTN: W. Hunt
ATTN: A. Johnson

Air Logistics Command
Department of the Air Force
ATTN: OO-ALC/MM

Air University Library
Department of the Air Force
ATTN: AUL-LSE

Air Weather Service, MAC
Department of the Air Force
ATTN: DNXP, R. Babcock

Assistant Chief of Staff
Studies & Analyses
Department of the Air Force
ATTN: AF/SASC, C. Rightmeyer
ATTN: AF/SASC, W. Keaus

Ballistic Missile Office
Air Force Systems Command
ATTN: ENSN, J. Allen

Deputy Chief of Staff
Operations Plans and Readiness
Department of the Air Force
ATTN: AFXOKS
ATTN: AFXOXFD
ATTN: AFXOKT
ATTN: AFXOKCD

Headquarters Space Division
Air Force Systems Command
ATTN: E. Butt

DEPARTMENT OF THE AIR FORCE (Continued)

Deputy Chief of Staff
Research, Development, & Acq
Department of the Air Force
ATTN: AFRDS
ATTN: AFRDSS
ATTN: AFRDSP

Electronic Systems Division
Department of the Air Force
ATTN: DCKC, J. Clark

Electronic Systems Division
Department of the Air Force
ATTN: OCT-4, J. Deas

Electronic Systems Division
Department of the Air Force
ATTN: YSEA
ATTN: YSM, J. Kobelski

Foreign Technology Division
Air Force Systems Command
ATTN: TQTD, B. Ballard
ATTN: NIIS, Library

Headquarters Space Division
Air Force Systems Command
ATTN: SKA, D. Bolin
ATTN: SKY, C. Kennedy

Space Division/YG
Department of the Air Force
ATTN: YGJB, W. Mercer

Rome Air Development Center
Air Force Sytems Command
ATTN: OCS, V. Coyne
ATTN: TSLD

Rome Air Development Center
Air Force Systems Command
ATTN: EEP

Strategic Air Command
Department of the Air Force
ATTN: DCXT
ATTN: DCXR, T. Jorgensen
ATTN: NRT
ATTN: XPFS
ATTN: DCX

OTHER GOVERNMENT AGENCIES

Central Intelligence Agency
ATTN: OSWR/NED

Department of Commerce
National Bureau of Standards
ATTN: Sec Ofc for R. Moore

Department of Commerce
National Oceanic & Atmospheric Admin
ATTN: R. Grubb

Institute for Telecommunications Sciences
National Telecommunications & Info Admin
ATTN: W. Utlaut
ATTN: A. Jean
ATTN: L. Berry

DEPARTMENT OF ENERGY CONTRACTORS

EG&G, Inc
Los Alamos Division
ATTN: D. Wright
ATTN: J. Colvin

Lawrence Livermore National Lab
ATTN: L-389, R. Ott
ATTN: L-31, R. Hager
ATTN: Technical Info Dept, Library

Los Alamos National Laboratory
ATTN: MS 664, J. Zinn
ATTN: D. Simons
ATTN: P. Keaton
ATTN: C. Westervelt
ATTN: E. Jones
ATTN: R. Taschek
ATTN: MS 670, J. Hopkins

Sandia National Laboratories
Livermore Laboratory
ATTN: T. Cook
ATTN: B. Murphey

Sandia National Lab
ATTN: Org 4241, T. Wright
ATTN: D. Thornbrough
ATTN: 3141
ATTN: D. Dahlgren
ATTN: Space Project Div
ATTN: Org 1250, W. Brown

DEPARTMENT OF DEFENSE CONTRACTORS

Aerospace Corp
ATTN: I. Garfunkel
ATTN: R. Slaughter
ATTN: D. Olsen
ATTN: J. Straus
ATTN: T. Salmi
ATTN: V. Josephson
ATTN: S. Bower
ATTN: N. Stockwell

University of Alaska
ATTN: N. Brown
ATTN: T. Davis
ATTN: Technical Library

Analytical Systems Engineering Corp
ATTN: Radio Sciences

Analytical Systems Engineering Corp
ATTN: Security

Barry Research Corporation
ATTN: J. McLaughlin

BDM Corp
ATTN: L. Jacobs
ATTN: T. Neighbors

Berkeley Research Associates, Inc
ATTN: J. Workman

Betac
ATTN: J. Hirsch

DEPARTMENT OF DEFENSE CONTRACTORS (Continued)

Boeing Co
ATTN: M/S 42-33, J. Kennedy
ATTN: G. Hall
ATTN: S. Tashird

Booz-Allen & Hamilton, Inc
ATTN: B. Wilkinson

University of California at San Diego
ATTN: H. Booker

Charles Stark Draper Lab, Inc
ATTN: J. Gilmore
ATTN: D. Cox

Communications Satellite Corp
ATTN: D. Fang

Computer Sciences Corp
ATTN: F. Eisenbarth

Comsat Labs
ATTN: G. Hyde
ATTN: R. Taur

Cornell University
ATTN: M. Kelly
ATTN: D. Farley, Jr

E-Systems, Inc
ATTN: R. Berezdivin

Electrospace Systems, Inc
ATTN: H. Logston

ESL, Inc
ATTN: J. Marshall

General Electric Co
ATTN: A. Harcar

General Electric Co
ATTN: A. Steinmayer
ATTN: C. Zierdt

General Electric Co
ATTN: F. Reibert

General Electric Co
ATTN: G. Millman

General Research Corp
ATTN: J. Ise, Jr
ATTN: J. Garbarino

Harris Corp
ATTN: E. Knick

Horizons Technology, Inc
ATTN: R. Kruger

HSS, Inc
ATTN: D. Hansen

IBM Corp
ATTN: F. Ricci

University of Illinois
ATTN: K. Yeh

DEPARTMENT OF DEFENSE CONTRACTORS (Continued)

Institute for Defense Analyses
ATTN: H. Wolfhard
ATTN: J. Aein
ATTN: E. Bauer

International Tel & Telegraph Corp
ATTN: G. Wetmore
ATTN: Technical Library

JAYCOR
ATTN: J. Sperling

JAYCOR
ATTN: J. Doncarlos

Johns Hopkins University
ATTN: T. Potemra
ATTN: J. Phillips
ATTN: T. Evans
ATTN: J. Newland
ATTN: P. Komiske

Kaman Tempo
ATTN: W. Knapp
ATTN: DASIAC
ATTN: T. Stephens
ATTN: W. McNamara

Linkabit Corp
ATTN: I. Jacobs

Litton Systems, Inc
ATTN: R. Grasty

Lockheed Missiles & Space Co, Inc
ATTN: W. Imhof
ATTN: R. Johnson
ATTN: M. Walt

Lockheed Missiles & Space Co, Inc
ATTN: D. Churchill
ATTN: Dept 60-12
ATTN: C. Old

M.I.T. Lincoln Lab
ATTN: D. Towle

Martin Marietta Corp
ATTN: R. Heffner

McDonnell Douglas Corp
ATTN: W. Olson
ATTN: J. Moule
ATTN: G. Mroz
ATTN: N. Harris
ATTN: R. Halprin

Meteor Communications Consultants
ATTN: R. Leader

Mission Research Corp
ATTN: R. Hendrick
ATTN: F. Fajen
ATTN: Tech Library
ATTN: R. Bogusch
ATTN: R. Kilb
ATTN: D. Sappenfield
ATTN: S. Gutsche

DEPARTMENT OF DEFENSE CONTRACTORS (Continued)

Mitre Corp
ATTN: G. Harding
ATTN: A. Kymmel
ATTN: C. Callahan
ATTN: B. Adams

Mitre Corp
ATTN: M. Horrocks
ATTN: W. Foster
ATTN: J. Wheeler
ATTN: W. Hall

Pacific-Sierra Research Corp
ATTN: E. Field, Jr
ATTN: F. Thomas
ATTN: H. Brode

Pennsylvania State University
ATTN: Ionospheric Research Lab

Photometrics, Inc
ATTN: I. Kofsky

Physical Dynamics, Inc
ATTN: E. Fremouw

Physical Research, Inc
ATTN: R. Deliberis

R & D Associates
ATTN: R. Lelevier
ATTN: R. Turco
ATTN: B. Gabbard
ATTN: M. Gantsweg
ATTN: W. Wright
ATTN: F. Gilmore
ATTN: C. Greifinger
ATTN: H. Ory
ATTN: W. Karzas
ATTN: P. Haas

R & D Associates
ATTN: B. Yoon

Rand Corp
ATTN: C. Crain
ATTN: E. Bedrozian

Riverside Research Institute
ATTN: V. Trapani

Rockwell International Corp
ATTN: R. Buckner

Rockwell International Corp
ATTN: S. Quilici

DEPARTMENT OF DEFENSE CONTRACTORS (Continued)

Santa Fe Corp
ATTN: D. Paolucci

Science Applications, Inc
ATTN: E. Straker
ATTN: C. Smith
ATTN: L. Linson
ATTN: D. Hamlin

Science Applications, Inc
ATTN: SZ

Science Applications, Inc
ATTN: J. Cockayne

SRI International
ATTN: W. Jaye
ATTN: R. Leadabrand
ATTN: D. Neilson
ATTN: J. Petrickes
ATTN: W. Chesnut
ATTN: R. Livingston
ATTN: R. Tsunoda
ATTN: G. Price
ATTN: C. Rino
ATTN: A. Burns
ATTN: G. Smith
ATTN: M. Baron
4 cy ATTN: D. McDaniel

Sylvania Systems Group
ATTN: I. Kohlberg
ATTN: R. Steinhoff

Technology International Corp
ATTN: W. Boquist

Tri-Com, Inc
ATTN: D. Murray

TRW Defense & Space Sys Group
ATTN: R. Plebuch
ATTN: D. Dee

Utah State University
ATTN: K. Baker
ATTN: L. Jensen
ATTN: J. Dupnik

Visidyne, Inc
ATTN: C. Humphrey
ATTN: J. Carpenter

BLANK PAGE